The Role Of The Blood-Brain Barrier During Pneumococcal Meningitis

Stavros Panagiotou

This thesis is submitted for the degree of Doctor of Philosophy

Clinical Infection, Microbiology and Immunology, University of Liverpool

December 2015

0.0 Declarations

The work described in this thesis is the result of my own effort. This work was carried out at the Institute of Infection and Global Health, University of Liverpool UK during the period October 2011 – December 2015 under the supervision of Dr. Adjanie Patabendige, Dr. Michael J. Griffiths, Prof. Aras Kadioglu and Prof. Tom Solomon.

This thesis does not include anything that is the outcome of work done in collaboration nor has been submitted, in whole or in part, for any other degree, diploma or qualification at another institution. For this thesis I have pursued to properly reference any findings, which are not my own.

This thesis is dedicated to my Mother, Chryso Karakosta my Grandfather, Kallis Karakosta, my Sister, Margarita Panagiotou and my wife Ourania to which I owe my past, present and future.

“Γιοκκαρούιν μου εν να έρτει μια μέρα που θα τα θυμάσαι και θα γελάς. Να δείς ότι θα περάσουν ούλλα.’’

Παππού μου. Έννεν πισσούριν πλέον.

0.1 Acknowledgments

I would like to thank my supervisors Dr. Adjanie Patabendige, Dr. Michael J. Griffiths, Prof. Aras Kadioglu and Prof. Tom Solomon for their support and for giving me the space to become an independent scientist. I would also like to thank all the Brain Infection Group members as well as the Kadioglu Group members for their constant support throughout this thesis.

From my family I would like to thank:

- My mother. Mom if it wasn't for you I would be lost. For the moments we lived and the moments we will live. Your efforts mean 2 kids with PhDs in 2016. Είσαι ο φάρος μου.
- My grandfather. I know you loved school and that you didn't get the chance to go to university. With you I share my knowledge. I love you.
- My sister. We have been walking side by side since I can remember helping me see things as they are. In every path you'll walk, I'll walk by your side. Χέρι-χέρι.
- My grandmother Margarita. Life was hard on you. For all you've done I thank you and I will always cherish you. ''Κοντά μου όταν είσαι τον πόνο μου ξεχνώ''.
- My father Costas. Your way of seeing life without any black in it makes me remember how lucky I am that you chose me to be your son. Παπά μου αγαπώ σε.
- My brother Joao (Kkeloui). There is always another way according to you. According to me there is always more love to be given to you from all of us. Stay long enough and you'll see.

- Last but not least my beautiful wife. Ουρανία (the word ‘’Sky’’ in Greek). You have been the roof of my world for the last 9 years. The reason I believe in fairytales, and my happily ever after. Never let go. Yo te quiero tal y como estas.

From my friends I would like to thank:

- Dan. For everything we both have been through. For making me part of your life and your family. Your happiness is mine. And I will always aim for it.
- Laura. For a nice summer coffee in Costa and everything that came out of it. Giving 110% for the people you love; I am honored to be part of your life. Every time you ask for my help I will be there. If not, I will still.
- Aras. For believing in me. Sen benim arkadaşım ve akıl hocam oldun bu uzun yolda. Birgün Instanbul’da bu yolculuğa devam edeceğiz beraber. Senin sayende memleketim yakındı bana. Teşekkürler.
- Jon’s. For caring so much about me and for your appreciation in my quality jokes. Love you too.
- Laura Bricio. For the day we sat in McDonald’s and looked like 50-year-old people. For the day that snow fell in Liverpool. And for saying things as they are.
- Elaine. For a lovely backgammon game at the docks. For making me feel appreciated and loved with your gifts, comments and support. My yessie.
- Suzanne. For showing me that your desire for chocolate meets no boundaries. I shall provide you with more now that I have the time!
- Emma. Dearest of them all. For introducing me to Yorkshire tea. For your unique ability to smile 25/8! For your support and positive energy. The day you will stop smiling the world will end.

- Gosia. For your ability to care whilst being extremely sarcastic! You are unique and when you care for someone there is no way back from it. Never change.
- Fiona. For suppressing my Mediterranean genes by keeping me calm and in the "reason zone". Nostalgic about our Chester night.
- Kevin. For reminding me what humans need, in order to keep themselves in the real world. The truth will always accompany you.
- Thanos. Επειδή ότι τζαι αν σου πώ στα κυπριακά σούζεις την κκελλέ σου. Τζαι επειδή ξέρω ότι αγαπάς με ρε σιηλλόπελλε. Life is simple. People aren't. Thank you for reminding me.
- The Big dog association (BDA) and its members for the moral support, and constant coffee boosting. Magnus canis congrecandi in aeternum.

0.2 Thesis Summary

Background: Pneumococcal meningitis remains the main cause of severe bacterial meningitis in children and adults (1); in February, 2010, a new 13-valent pneumococcal conjugate vaccine (PCV13) was approved by the FDA, which was presented as a successor to the 7-valent conjugate vaccine (PCV7) (2). Nonetheless, no vaccine provides protection against more than 90 serotypes of *Streptococcus pneumoniae*. In 2013, 2.8 million children died before completing one month of being born because of the pneumococcus.

Methods: Pneumococcal survival, adherence and invasion were assessed using human brain cells and an entirely human Blood-Brain Barrier model. Additionally, the role of pneumolysin during infection was investigated. Having access to a broad library of genes, host responses against pneumococcal infection were investigated.

Results: Pneumolysin enhances pneumococcal survival, and increases adherence and invasiveness. Toxin pore formation leads to tight junctions disruption and impaired cytoskeletal functions. Pneumolysin concentration was in accordance to serotype virulence. Serotype 6B exhibited high CFUs during infection in the Blood-brain barrier. Its pneumolysin concentrations suggest that *Streptococcus pneumoniae* uses multiple pathways to traverse to the abluminal side. Host immune responses contributed further to tight junction dissociation, revealing synergism between the host and the pathogen during pathogenesis progression.

0.3 Abbreviations

AIDS	acquired immune deficiency syndrome
APC	antigen presenting cell
BCR	B cell receptor
BM	Bacterial Meningitis
BBB	Blood-Brain Barrier
BBMECs	bovine microvessel endothelial cells
BSA	Bovine Serum Albumin
BAB	Blood Agar base
BHI	Brain Heart Infusion
BgaA	betagalactosidase A
ChoP	phosporylcholine
CbpA	choline-binding protein
Cav	Caveolin family protein
CNS	central nervous system
CFU	colony-forming unit
CD	cluster of differentiation

CPD	population-doubling rate
^{o}C	Celsius
CXCL	chemokine (C-X-C motif) ligand
cRNA	complementary RNA
cDNA	complementary DNA
CSF	Cerebrospinal Fluid
D39	serotype-2 lab strain
DALYs	disability-adjusted life years
ddH_2O	double distilled water
Dlg1	Drosophila disc tumor suppressor
DMEM	Dulbecco's Modified Eagle's Medium
DAPI	2-(4-amidinophenyl)-1H -indole-6-carboxamidine
ELISA	enzyme-linked immunosorbent assay
ECM	extracellular matrix
FBS	foetal bovine serum
FITC	fluorescein isothiocyanate
g	G-force

HIV	Human Immunodeficiency Virus
HRP	horseradish peroxidase
HSV	Herpes Simplex Virus
HBECs	Human Brain Endothelial Cells
HA	Human Astrocytes
IFN	interferon
Ig	immunoglobulin
IL	interleukin
IRAK-4	Interleukin-1 receptor-associated kinase 4
JEV	Japanese Encephalitis Virus
JAM	Junction Adhesion Molecules
kDa	Kilodalton
LPS	lipopolysaccharide
MIF	macrophage inflammatory factor
MMPs	Matrix metalloproteinases
MTT	3-(4,5-Dimethylthiazol-2-yl)-2,5-diphenyltetrazolium bromide
μm	micrometer

ml	milliliter
mM	micromolar
M	molar
µl	microliter
MAP	Mitogen-Activated Protein
mAb	monoclonal antibody
MHC	major histocompatability complex
mRNA	messenger RNA
nm	nanometer
ng	nanogram
NanA	beta-*N*-acetylglucosaminidase, neuraminidase A
Nod1	nucleotide oligomerization domain 1
NLR	Nod-like receptor
NF-kB	nuclear factor kappa-light-chain-enhancer of activated B cells
OD_x	optical density at wavelength x nm
PLY	pneumolysin
PBS	phosphate buffered saline
PCR	polymerase chain reaction

pIgR	polymeric immunoglobulin receptor
PAF	platelet activating factor
PCN	population doubling number
PdB	genetically detoxified variant of pneumolysin
PLN-A	pneumolysin-negative serotype-2 strain D39
p.i.	post-infection
PRR	pattern recognition receptor
r	recombinant
R	receptor
ROS	reactive oxygen species
rpm	revolutions per minute
sIgA	secretory immunoglobulin A
SEM	standard error of the mean
STAT	signal transducer and activator of transcription
SDS	sodium dodecyl sulphate
SAM	significant analysis of microarray
ST	sequence type

S1	serotype 1
TEER	Trans-Endothelial Electrical Resistance
TCR	T cell receptor
TGF	transforming growth factor
Th	T helper
TLR	Toll-like receptor
TNF	tumour necrosis factor
Treg	T regulatory
TIMPs	tissue inhibitors of metalloproteinases
Tween20	polyoxyethylene(20)sorbitan monolaurate
WHO	World Health Organization
Ω/cm^2	Ohms per square centimeter
ZO	Zonula Occludens Protein

Table of Contents

CHAPTER 1.

Introduction

1.1.0 Infectious Diseases

Infectious diseases account to approximately a quarter of deaths worldwide, more than 13 million deaths each year [1]. The top 5 causes of death due to infectious disease are lower respiratory tract infections (4 million), HIV (2.8 million), diarrheal diseases (1.8 million), tuberculosis (1.6 million) and malaria (1.3 million). A quarter of the world's morbidity is also due to infectious diseases as measured by disability-adjusted life years (DALYs).

The emergence of new pathogens in the developing and developed countries is a threat dealt in different ways (figure 1). In poorer countries the burden of infectious diseases is much greater than in wealthier countries. The greatest sufferers of this threat are children; 11 million children die every year, of which half are lost to pneumonia, diarrhea, malaria, HIV/AIDS and measles [1]. Mortality rates increase due to exogenous factors such as malnutrition, poverty, poor education and gender inequality.

In the developed countries, less mortality is observed due to infectious diseases; nevertheless, infectious diseases in the United Kingdom account to 10% of deaths. Additionally, mortality and treatment because of infectious diseases is a great financial burden. The cost of treating human infectious diseases in England was estimated to £6 billion per year (10% of the UK National Health Service budget). Out of the £6 billion, £900 million were spent on hospital admissions alone [2].

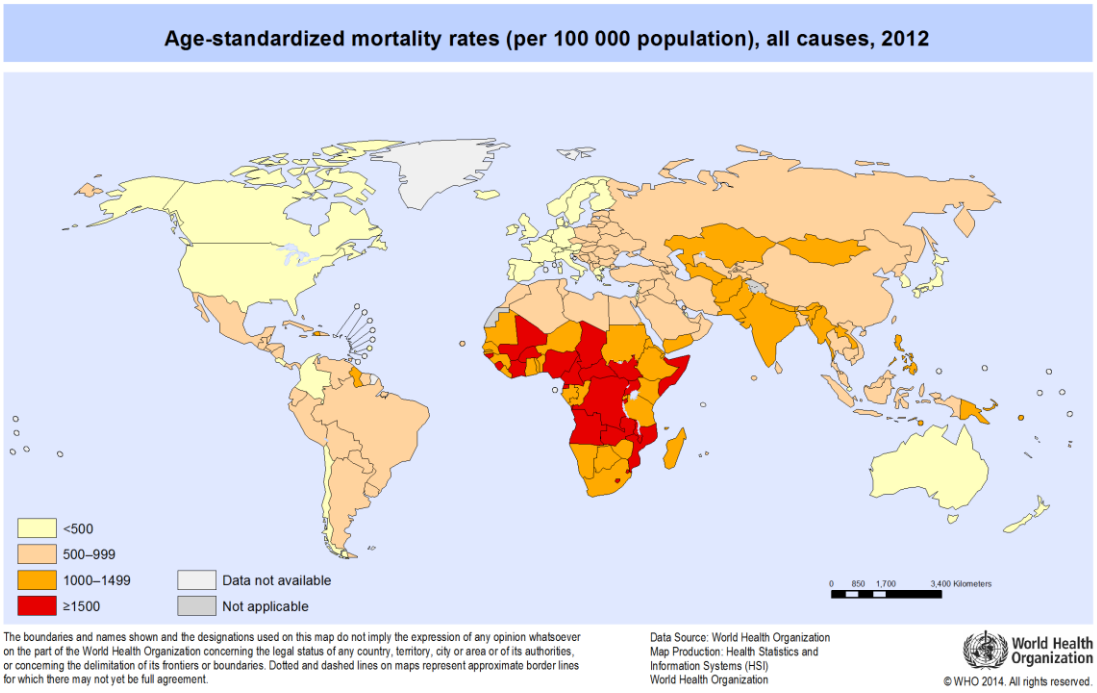

Figure 1| Burden of disease across the globe Less than 500,000 people lose their life in the developed countries whereas in the developing nations the incidents are doubled or trebled. The image was adopted from the World Health Organization [3].

Viral and bacterial infections are both significant causes of infection and there are noteworthy infectious diseases where our understanding of their development and pathogenesis is not complete, such as Japanese Encephalitis (JE) [4], HSV Encephalitis (HSE) [5], HIV-Encephalopathy [6], Bacterial Meningitis (BM) [7, 8], septic encephalopathy, pneumonia, bacteremia for example. This project is focused on pneumococcal meningitis and in particular on the interaction of bacterial and host factors during infection, as well as the host immune response during infection of the blood-brain barrier.

1.1.0 The Blood-Brain Barrier and Brain Endothelial Cells – Discovery of a system within a system

The blood-brain barrier (BBB) is the protective barrier that prevents the entry of pathogens (e.g. viruses, bacteria, parasites) and toxins into the brain. It is responsible for preserving homeostasis in the brain as well as supplying the brain with the necessary nutrients and disposing toxins and waste [9]. The endothelial cells are connected by complex tight junctions and form the BBB. These tight junctions restrict the entry of molecules through the junctional complex. Astrocytes and pericytes help maintain the BBB features of the endothelial cells (figure 2). The brain's functional stability is widely thought to be dependent on a series of brain cellular interactions (microglia, astrocytes, oligodendrocytes, neurons, endothelial cells, pericytes and smooth muscle cells). These are the cells, which form the neurovascular unit [10, 11].

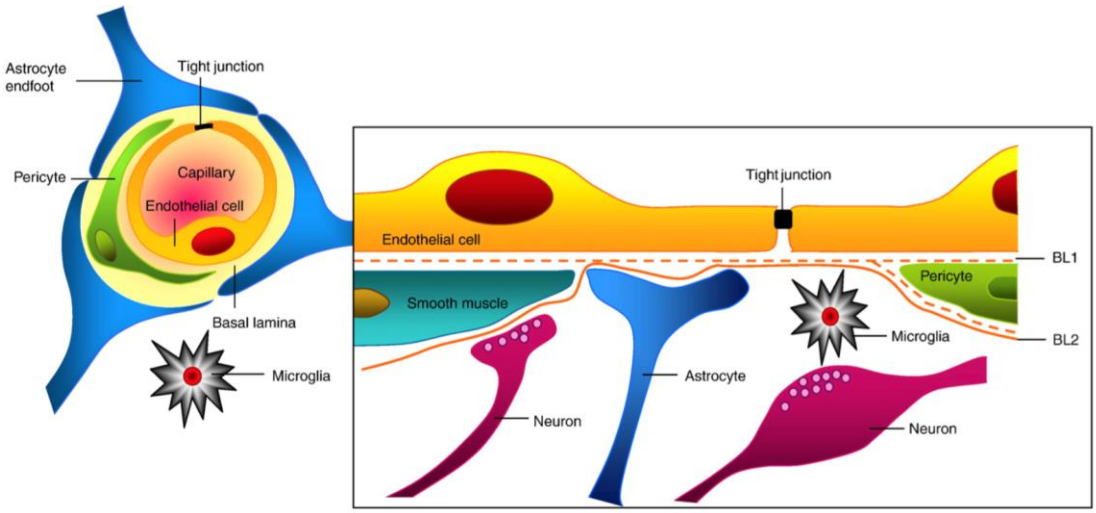

Figure 2| The structure of the blood-brain barrier Although the main constituent of the BBB is the endothelial cells, other brain cells have a crucial role in maintaining the phenotypic characteristics of the barrier. Cells such as pericytes, and astrocytes support the endothelial cells, which are surrounded by basal lamina (BL1 and BL2 on the image). The endothelial cells form tight junctions, which restrict the entry of molecules through the paracellular route. Image adopted from [9].

Although not officially discovered until 1885, the "tightness of blood vessels" is mentioned for the first time by Humphrey Ridley in his book "The Anatomy of the Brain" in 1695 [12]. Specifically, Humphrey Ridley states:

'... I have offer'd nothing but Matter of Fact, and have taken all possible care to avoid being impos'd upon my self [sic], by making Experiments in pro- portion to my Doubts. Some of them have been upon Subjects in their natural, some in their morbid [state], some upon those of Untimely Death; and on those last sometimes whist the natural Fluids remained in their proper Vessels, though after a pre- ternatural manner occasion'd by Strangulation; sometimes when in the room thereof, other Bodies have been introduc'd by Injection, as Tinged Wax and Mercury, the first of which by its consistence chiefly, the other by its permanent nature and col- our, contribute mightily towards bringing to view the most minute ramifications of Vessels, and secretes recesses of Nature.'

There is a clear reference to the vessels' impermeability and it is the first recorded discovery that relates to brain barriers (figure 3).

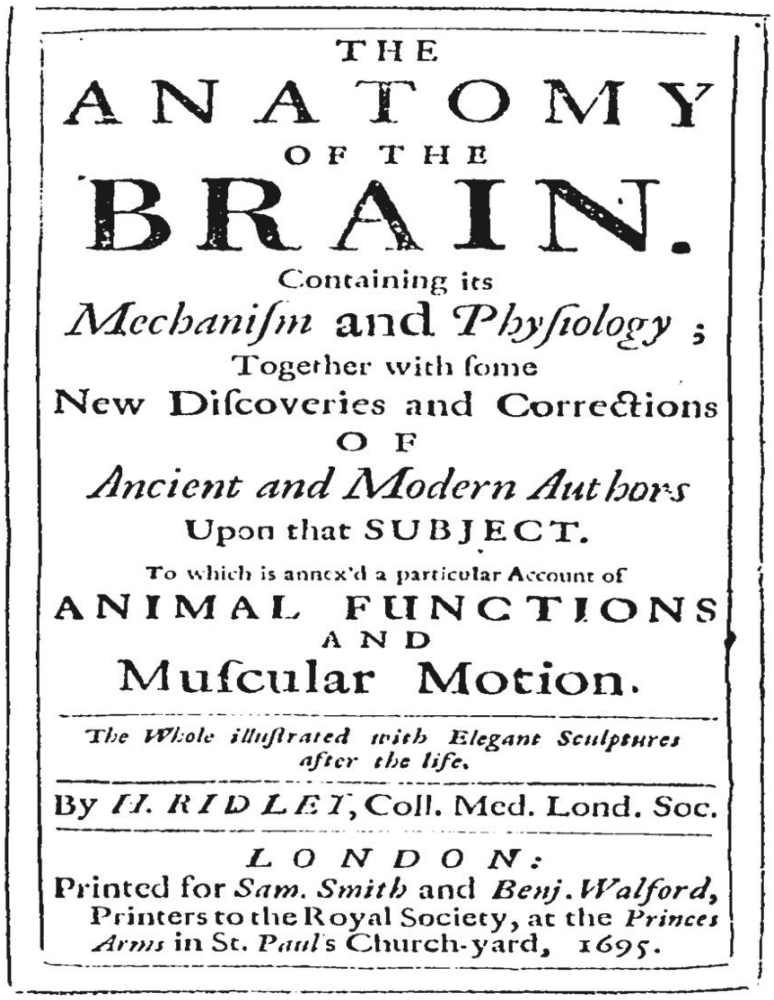

THE
ANATOMY
OF THE
BRAIN.
Containing its
Mechaniſm and *Phyſiology*;
Together with ſome
New Diſcoveries and Corrections
OF
Ancient and Modern Authors
Upon that SUBJECT.
To which is annex'd a particular Account of
ANIMAL FUNCTIONS
AND
Muſcular Motion.
The Whole illuſtrated with Elegant Sculptures after the life.
By *H. RIDLEY*, Coll. Med. Lond. Soc.
LONDON:
Printed for *Sam. Smith* and *Benj. Walford*,
Printers to the Royal Society, at the *Princes Arms* in St. *Paul's* Church-yard, 1695.

Figure 3| Front cover of Humphrey Ridley's book "The Anatomy of The Brain" The first reference of barrier tightness and permeability was by Humphrey Ridley in 1695 when he injected a substance to the bloodstream. Image adopted from [12].

Brain endothelial cells are the cells responsible for the formation of the BBB. The realisation of its existence came along when the physician/scientist Paul Ehrlich (figure 4A) injected mice with cerulean-s-sulphate intravenously and observed that all the organs of the rodent were stained blue except of its brain (figure 4B). Further investigations confirmed Paul Ehrlich's results and the term ''blood-brain barrier'' was born [13].

Figure 4| Paul Ehrlich and the exclusion experiment A) Paul Ehrlich on a German 200 marks banknote (https://www.bundesbank.de). Besides putting the blood-brain barrier on the map of CNS sciences, the Nobel Laureate was also responsible for the invention of arsphenamine, the first effective drug against syphilis. B) A trypan blue injection experiment performed by Edwin E. Goldmann (assistant of Ehrlich's), shows the blue stain of in vital organs of the murine model, except the brain justifying Ehrlich's first experiments. The image was adopted from [14].

Continuous research thereafter revealed the transportive properties of the endothelial cells, and the biochemical, anatomical and physiological mechanisms, involved in the exchange process of blood and the cerebrospinal fluid (CSF).

Brain endothelial cells share a great deal of the characteristics with the endothelia that are not part of the neurovascular unit (i.e. adhesion molecules, integrin receptors,

glycoproteins). The main differences however, are the reduced density of the lipid raft of the vessel (*caveolae*) and the tight junctions between endothelial cells. These lipid rafts are vesicles bound within the cell and are found in different cell types, including the endothelial cells. They can also be found in any endothelial type moving freely in the cell cytoplasm [15]. Most of them have a spherical shape and they have an approximate diameter of 70 nm (figure 5).

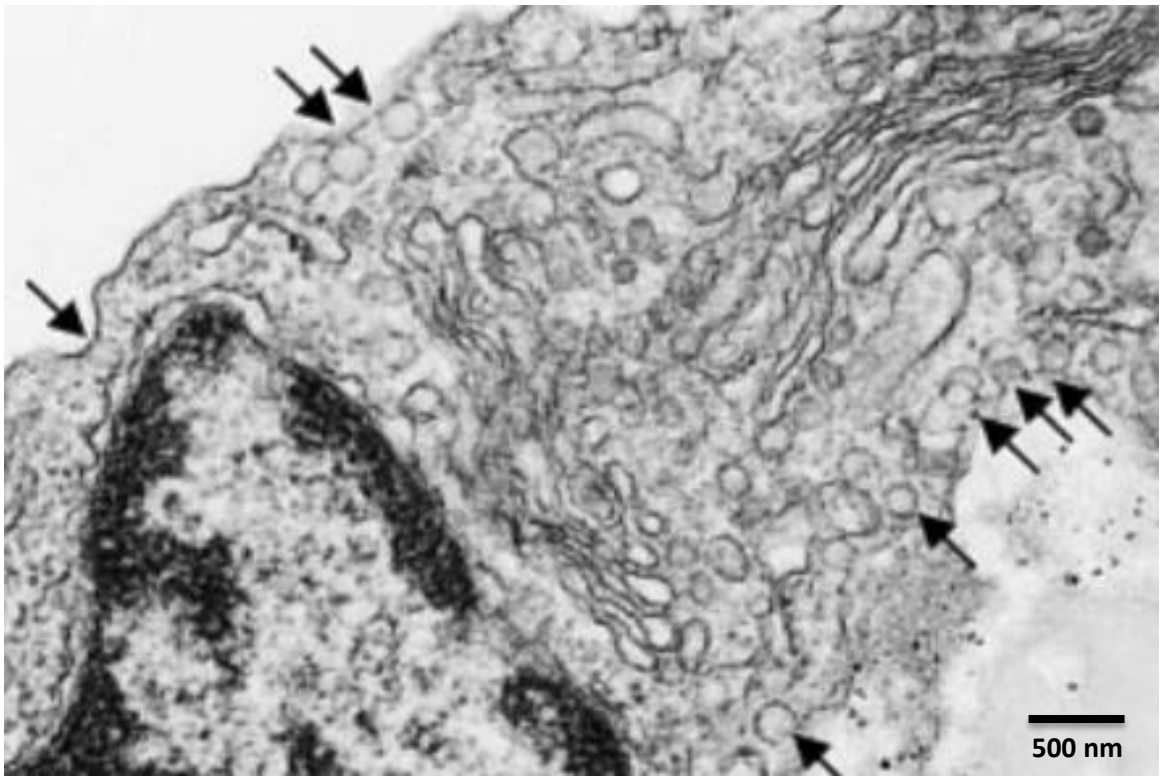

Figure 5| Image of *caveolae* from aortic endothelial cells Caveolae is shown in x1.5 magnification (black arrows). The image was taken with an electron microscope and the bar scale is 500nm. Image adopted from [15].

Studies have revealed thin protein barriers, which are anchored in the caveolae's region. These barriers seem to be linked to the inner part of the cells but their functions are unknown. Caveolae seemed to be related to the tightness of endothelial cells. Cerebral

endothelial cells have 14-fold fewer vesicles in comparison to non-brain endothelial cells [16]. Thus,, capillaries lacking a BBB system are relatively easy to penetrate and have a higher number of caveolae.

The membrane of the caveolae contains cholesterol and sphingolipids. Sphingolipids are scaffolds for the synthesis of ceramides (messengers within the cell) [17] and cholesterol is responsible for the shape of the caveolae.

Going even further in the analysis of the elements that consist of the caveolae, proteins found in the coat of these lipid rafts are called caveolin family proteins (Cav). Proteins of this family are Cav-1, Cav-2 and Cav-3. Despite the fact that all three caveolin proteins belong to the same family, Cav-3 is mainly expressed in astrocytes, while Cav-1 and Cav-2 are mostly expressed in endothelial cells [18-21]. Caveolin proteins 1 and 2 are highly dependent on each other and are co-expressed, which indicates an indistinguishable regulatory pathway [22].

1.1.1 Endothelial Junctions

The tight junctions of endothelial cells are found in the apical end of the interendothelial space and are closely linked with and rely on the cadherin based adherens junctions, which are found closely to the basolateral side of the interendothelial space. Horseradish peroxidase (HPR), which is extensively used to enhance biochemical signals, is incapable of passing though the barrier; this is due to a pentalaminar structure, which is created by the adjacent plasma membranes of the endothelial cells [23]. When the junctions are formed, small channels are also formed which allow small hydrophilic molecules to go through the barrier (mostly ion molecules – e.g. hydrogen or sodium). The literature

suggests that brain endothelium junctions are made of continuous fiber-like strands, which expand down the length of the blood vessel with more strands that openly communicate (anastomotically) [24]. Just to understand how tight these junctions are, a comparison between different junction-type cells can be made: Leaky epithelial cells also form junctions but when the electrical resistance for their tightness is measured, the values will range between 100 to 200 Ω/cm^2 whereas the blood- brain barrier's electrical resistance *in vivo* can reach values between 4000 to 8000 Ω/cm^2 [25, 26]. The BBB is formed by cerebral endothelial cells but is highly dependent on cells and other factors that surround it. Such crucial elements include astrocyte cells, e.g. in experimental co-culture models, the electrical resistance of brain endothelial cells (a measure of integrity of the barrier) drops up to 100-fold when not co-cultured with astrocytes [27]. Major components of the endothelial junctions are the junction adhesion molecules (JAMs), zonula occludens (ZO-1, ZO-2, ZO3), occludin, claudin 3, and claudin 5. The tight junctions remain intact with the help of cadherins, which form the adherens junctions (figure 6).

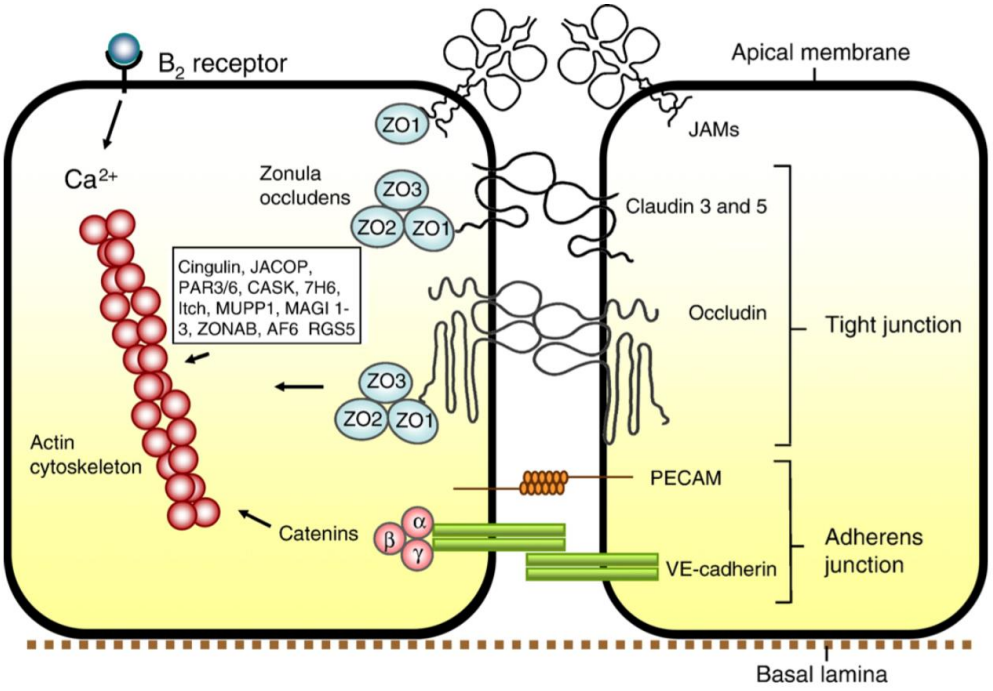

Figure 6| The tight junctions formed by brain endothelial cells The tight junctions are formed by many junctional proteins. The zonula occludens complex along with occludin, claudin 3 and claudin 5 form the tight junctions. In order for the tight junctions to remain intact the adherens junctions are in place. Adherens junctions consist of cadherins, platelet endothelial cell adhesion molecule (PECAM) and catenins. Image adopted from [9].

1.1.2 Claudins

Claudin proteins are crucial elements for the tightness of the barrier. There are 24 members in both humans and mice, and there are distinctive patterns in how they are expressed both in cells and in tissue [28-31]. The size of claudin proteins ranges from between 18-27 kDa, and they are tetraspan proteins with short N-terminus loops, which extend to the outer site of the cell membrane. Additionally a carboxylic terminus is also present that ends with the amino acid valine. This non-polar amino acid attracts a domain of proteins, which consists of the postsynaptic density protein (PSD95), the Drosophila disc tumor suppressor (Dlg1) and zonula occludens-1 protein. These three proteins form the PDZ

domain. Further proteins of the domain were found to be strongly attracted to valine such as zo-2 and zo-3 but also the maguk protein-PALS1, multi-PDZ protein 1 (MUPP1) and pals1 associated tight junction protein (PATJ) [32]. All of these interactions are considered important when tight junctions are constructed. Claudins are very important structural "machinery'' for the membrane as mentioned before [33], as they interact with occludin at the junctions. Research has shown that mice lacking occludin can still form interendothelial junctions with the proper morphology and function [34], whereas mice that lack of claudin are incapable of remaining alive [35]. The part of claudins' loops that lies on the outer part of the membranes creates pores that have analogous properties to the properties of the ion channels (charge selectivity, antagonism of permeative molecules, permeability which is dependent on ion concentrations). These aqueous pores allow diffusion preferably to ions with positive charge rather than ones with a negative one [31, 36].

1.1.3 Occludin

Occludin is a protein that is related to the intramembrane strands (where tight junctions are) and is not a vital element to the formation of the junctions. When there is increased electrical resistance on the BBB and low paracellular activity in regards to transportation, occludin is found in excess [37]. Occludin has a size of 60 kDa and is also a tetraspan membrane with two loops that have a part on the outer side of the membrane, a short twist on the inner part, and N/C-terminal domains [38]. The N-terminal domain is responsible for the transmigration of molecules such as neutrophils where the C-terminal is responsible for molecules that are small in size and also show high hydrophilicity [39].

TGF-β, Raf1 and Ras homolog (Rho) signaling as well as MAP-kinase-depended pathways are also closely related to occludin [40, 41].

1.1.4 Junction Adhesion Molecules (JAMs)

Junction adhesion molecules (JAMs) are single-span transmembrane proteins and belong to the immunoglobulin superfamily. JAMs are also under the Cortical Thymocyte marker that is found in the way of antigen-specific receptors and adhesion molecules [42]. There are five JAMs (JAM-4, JAM-A-C, and JAM-L). These can arbitrate a same type cell-cell adhesion. The only JAM protein related to the tight junctions of the brain is JAM-A. The rest of the identified JAM proteins can be found around endothelium, which unrelated to the nervous system [43]. JAM-A is a glycoprotein of 32-kDa. It has two immunoglobulin loops on its extracellular domain, a transmembrane domain and a cytoplasmic tail which end like the PDZ domain-binding sequence (classical type II). JAM-A was found to be involved in the construction of the tight junctions, activation of platelets, angiogenesis, reovirus binding, and transmigration of leukocytes [44-51]. JAMs are responsible for the polarity of cells and by interacting with the protease-activated receptor complex 3/6 (PAR3/6) and phosphoenolpyruvate carboxykinase (PCK) [52-54].

Since junctions are formed due to the interaction between endothelial cells, it would be important to mention that microtubules, microfilaments and intermediate filaments are the scaffold to form the cytoskeleton of the brain endothelial cells [55]. Claudin, ZO proteins and occludin have binding sites that can tether actin, which is found in the endothelium plasma [56]. Between the tight junction membrane and the cytoskeleton, a cytoplasmic plaque is found and is important in processes such as transmissions of signals from the

junction to the inner part of the cell in order to regulate gene expression and migration. Adhesion and paracellular permeability are also processes that the cytoplasmic plaque is involved in. The cytoplasmic plaque is also responsible for gathering phosphatases and kinases which have the role of signaling components, and proteins that are found on the junctions or even the nucleus; that is a way for the tight junctions to control gene expression [57-59]. As mentioned before ZO proteins are closely related to the tight junctions. ZO1-3 have domains that bind to adherens and tight junctions, and they are important in signal transduction but also in attaching the cytoskeleton to the tight junction proteins [60]. ZO-1 and ZO-2 bind directly to the C-terminal of occludin [61-63]. When occludin amino acid tyrosine is phosphorylated, all interactions between occludin and ZO protein stop [64]. Tight junctions are also involved in signal transcription and proliferation, cytoskeletal dynamics, and vesicle targeting [65-67].

1.2.0 Bacterial Infections

Streptococcus pneumoniae, *Neisseria meningitidis* and *Haemophilus influenzae* are the top 3 causes for brain infections for all age categories except newborns. Brain infections caused in newborns derive from Group B streptococcus (GBS) *Escherichia coli* or *Listeria monocytogenes* [3, 68, 69].

1.2.1 *Streptococcus pneumoniae*

Streptococcus pneumoniae are Gram-positive alpha-hemolytic and facultative anaerobes. The bacteria can appear alone, paired (diplococcoid) or in chains and they are protected by a capsule formed by composite polysaccharides (figure 7A+B) [70].

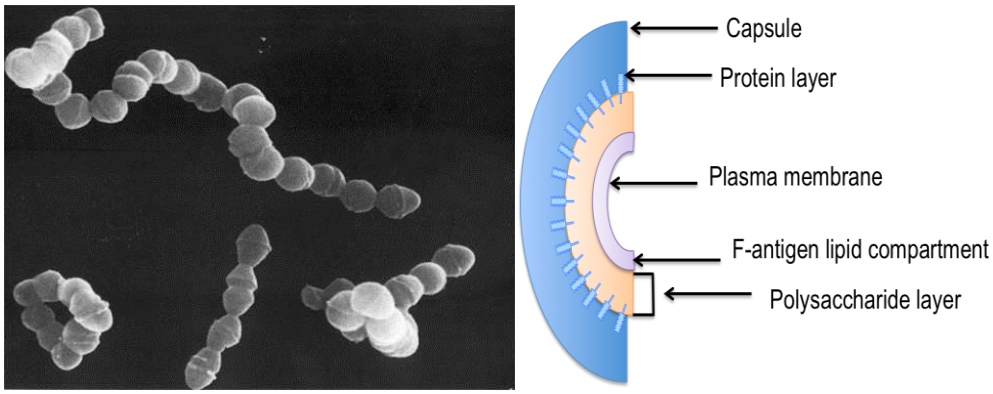

Figure 7| Streptococcus pneumoniae characteristics A) The bacteria can be found as single isolates, as a pair (diplococcoid) or as a chain. B) The bacteria are protected by a capsule, which consists from the protein layer, polysaccharide layer, a lipid compartment and the plasma membrane. Image 7a was adopted from [71].

Polysaccharides, which contribute to capsule formation, are usually associated with pathogenicity. These polysaccharides are recognized by the immune system (i.e. they are antigenic) and are the basis of the classification of pneumococcal serotypes; it is estimated that there are more than 95 different serotypes [72].

1.2.2 Pneumolysin

Pneumococci produce a toxin called pneumolysin, which was first mentioned 110 years ago by Libman who observed a "peculiar'' type of hemolysis [73]. Although pneumolysin

was first characterized as a thiol-activated toxin, it has now been reclassified as a cholesterol-binding cytolysin [74]. The toxin was successfully purified in the early 1970s [75, 76] and through continuous studies it was observed that is released during bacterial cell death caused by antibiotics or even autolysis caused by LytA (autolysin) [77-79].

Pneumolysin exists as a polypeptide and consists of 53 kilo Daltons (kDa) (471 amino acids) [80]. It has been proven difficult to crystalize pneumolysin until very recently where a 3 dimensional structure of the toxin was achieved (figure 8) [81, 82].

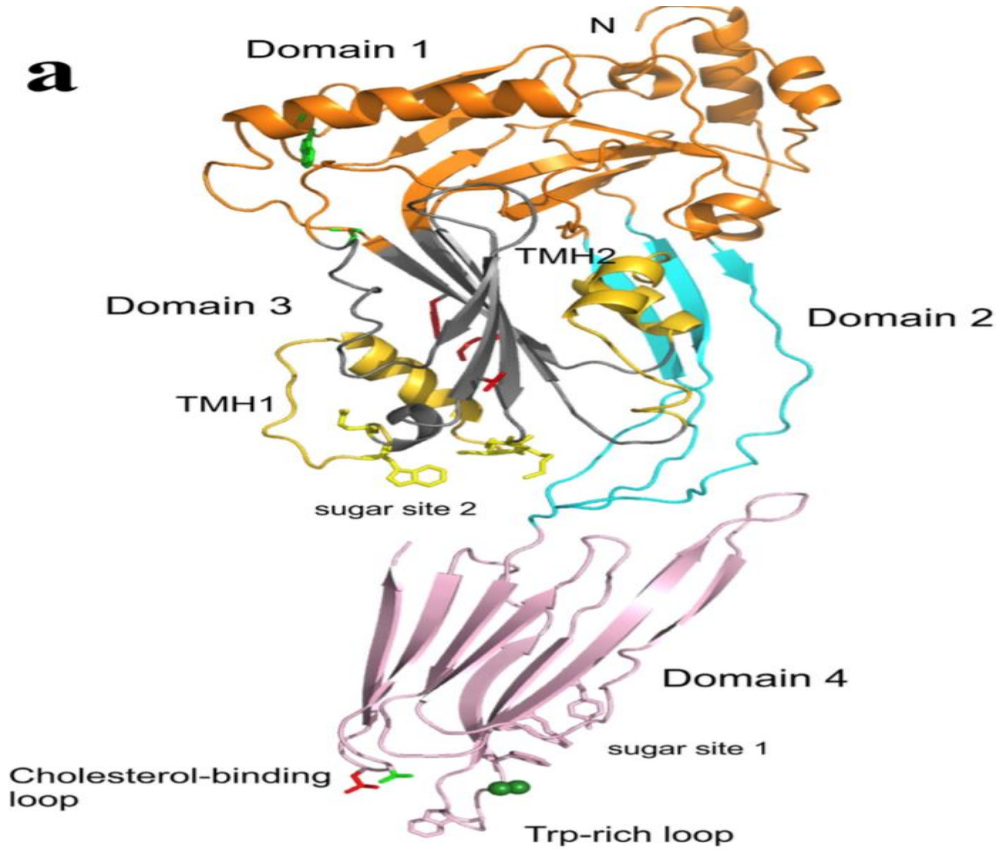

Figure 8| 3 Dimensional representation of pneumolysin The toxin consists of 4 domains. In the ribbon form of the toxin, domain 1 is colored orange, domain 2 colored cyan, domain 3 is colored grey and domain 4 is colored pink. Domain 4 is responsible for the binding of the toxin on cell membranes. The membrane-sensing loops of domain 4 (Trp-rich loop and cholesterol-binding loop) are displayed below domain 4 in the image. Section "a" of this image was adopted from Lawrence et al. [82].

Pneumolysin consists of 4 domains with domain-4 being responsible for the binding of the toxin to cell membranes. In high concentrations, pneumolysin is capable of forming pores as well as arc structures on cellular membranes [83]. It has been previously demonstrated that upon pore formation instability of calcium levels occurs in the cell cytoplasm. Additionally the actin cytoskeleton of the cells is affected, thus, the cell morphology of the cells are altered due to the toxin [84]. Endothelial cells interacting with pneumolysin have been characterized with hyper-permeability through the modulation of VE-cadherin, a key protein to the formation of adherens junctions in endothelial cells [85, 86]. Pneumolysin has been associated with virulence in numerous publications [79, 87-89]. Absence of the toxin has been associated with reduced infection in the lung [90-92] and with reduced nasopharyngeal colonization [93] while high levels of toxin in CSF during meningitis correlates with poor patient outcome and high mortality [94].

1.2.3 History of pneumococcal infection

Streptococcus pneumoniae causes many different infections. The ‘’pneumococcus’’ -as it is also called- was first isolated and identified by Sternberg and Pasteur in 1881. Sternberg collected specimens from his own saliva whereas Pasteur collect saliva from a child suffering with rabies [95, 96]. Pneumonia was first mentioned in1883 by Friedlander and Talamon whereas the association of *Streptococcus pneumoniae* with pneumonia was shown by Sternberg [97]. In a period that lasted 30 years (1915-1945), the scientists of the time, identified the chemical structure of the bacteria, the type of antibodies, which are activated when exposed to different polysaccharides, and the invasiveness of each serotype. These capsular polysaccharides consist of repeating oligosaccharide elements

and the majority of them have been chemically characterized [98]. The chemical resemblance of capsular polysaccharides can determine the degree of cross-reactivity. Pneumococcal serotypes 6A and 6B differ only in one of the bonds between two sugars, thus, the degree of cross-reactivity is high [99, 100]. In contrast, types such as 19F and 19A differ in more than one sugar bond, which results in a lower degree of cross-reactivity. By the end of 1940 more than 80 different serotypes of pneumococci were characterized [101], and in total more than 90 serotypes were described [70].

1.2.4.0 Epidemiology

Streptococcus pneumoniae is a significant pathogen as it causes, endemic pneumococcal disease globally. The most common cause of acute otitis media, sinusitis, and pneumonia is *Streptococcus pneumoniae* and its recurrence to cause the diseases mentioned above have been recorded for more than a century. *Streptococcus pneumoniae* is also one of the most important pathogens that cause bacterial meningitis [102, 103]. Approximately 14.5 million episodes of acute pneumococcal disease were reported in 2000 alone, resulting in about 826,000 deaths in children of age 1–59 months. It is important to mention that over half of the cases, which resulted in death, were recorded in the African continent and in South East Asian countries.

For the developing countries, pneumonia is cause for serious disease, especially in children; it is estimated that more than 1 million children below the age of 5 die from pneumococcal pneumonia annually [104]. Before the introduction of vaccines in the UK, the pneumococci was found to colonise 45% of children examined, in comparison to only 2% of people examined and were above the age of 18 [105]. Approximately 5800

hospitalisations occurred due to *Streptococcus pneumoniae* in England and Wales only. For the same setting, almost 40 000 cases were recorded as lobar pneumonia and over 15 000 recorded as otitis media cases. Additionally, cases deriving recorded by general practitioners showed an additional 70 000 for pneumococcal related community acquire pneumonia and 630000 for otitis media [106]. A significant number of both hospitalisations and GP consultations for pneumococcal disease related to high- risk groups. Out of 100,000 cases, 15 are pneumococcal meningitis cases [106].

Annually, the total number for incidences relating to pneumonia in Western populations reaches approximately 1 %. *Streptococcus pneumoniae* is responsible for almost half of the cases of community-acquired pneumonia [107-111]. This is translated, as 5 persons out of 1000 will acquire pneumococcal pneumonia every year, with the number significantly increased when the cases involve the very young and the elderly [108, 112, 113]. Pneumococcal pneumonia is the main cause of bacteremia. Pneumococcal disease cases usually increase during the winter months since viral infections are predisposed to pneumococcal infections in the winter [114-116]. Outbreaks of pneumococcal disease may occur if a new strain is introduced in a closed setting, such as Schools, military camps, nursing homes, or jails are possible settings for pneumococcal outbreaks due to the surrounding environment [102, 117, 118].

Since pneumococci are a naturally transformable pathogen, it can exchange its genetic material with different strains. [119-121]. Transformation was firstly described in 1928 [102] and it is, a considerably common incident in nature [121-123]. When isolating samples from patients with invasive pneumococcal disease, up to 77 different serotypes were identified [113, 124, 125]. Serogroups 6, 14, 18, 19, and 23 are more prevalent in

children because these serotypes are less immunogenic than other types [126]. In previous studies, it was observed that 9 out of 10 patients found with pneumococci in their nasopharynx were young children [105, 127, 128].

1.2.4.1 Bacterial meningitis and *Streptococcus pneumoniae*

Bacterial meningitis is a significant problem in the developing countries. In Senegal, the average incidence of bacterial meningitis was 50 cases per 100,000 people during the decade of 1970. From these cases 1 in 250 children would develop bacterial meningitis during the first year of theirs life [129]. *Streptococcus pneumoniae* is the leading cause for bacterial meningitis in Africa for individuals infected with human immunodeficiency virus (HIV). Pneumococcal meningitis in Africa has been associated with high mortality [130, 131]. Sub-Saharan Africa, also referred to as the meningitis belt (figure 9), is known for epidemics of bacterial meningitis, with 101 cases per 100,000 population in Niger and 40 cases per 100,000 in Burkina Faso until 1996 [132, 133].

In the developed countries, *Streptococcus pneumoniae* is the most common aetiology of bacterial meningitis with 61% of the cases being recorded in the United States and 39% in Europe [134-136]. Vaccination strategies are already underway in an effort to reduce pneumococcal meningitis cases. Initial studies demonstrated that 74-90% of the serotypes identified from patient CSF, accounted to serotypes included in the 23-valent-polysaccharide vaccine [137, 138]. Severe diseases can emerge due to bacterial infection, and each disease is classified according to the type of infection but also its stage (table 1).

Table 1 Bacterial Organisms that cause Infection of the Central Nervous System

Bacterial Organism	Type of Disease	Age Categories
Streptococcus pneumoniae	Bacterial meningitis (Acute)	Adult
Streptococcus agalactiae (Group B)	Bacterial meningitis (Acute or subacute)	Newborns/Elderly
Listeria monocytogenes	Bacterial meningitis (Acute)	Infants
Staphylococcus epidermidis	Bacterial meningitis (Subacute)	After neurosurgury
Staphylococcus aureous	Bacterial meningitis (Acute)	Any age category
Neisseria meningitidis	Bacterial meningitis (Acute)	Adolescent
Streptococcus milleri group	Brain abscess	Any age category
Hemophilus influenzae type B	Bacterial meningitis (Acute)	Children
Mycobacterium tuberculosis	Meningitis/Brain & Epidural abscess	Severe in children
Treponema pallidum	Neurosyphilis	Any age category
Mycobacterium avium	Meningitis/Encephalitis/Peripheral neurop.	Any age category

Table 1| Bacterial pathogens responsible for infections in the central nervous system The etiology for CNS infections can vary according to the age of the patient, the condition that the patient is in (accident or surgery) as well as the pathogen causing the infection. The information of table 1 was acquired from [139-142].

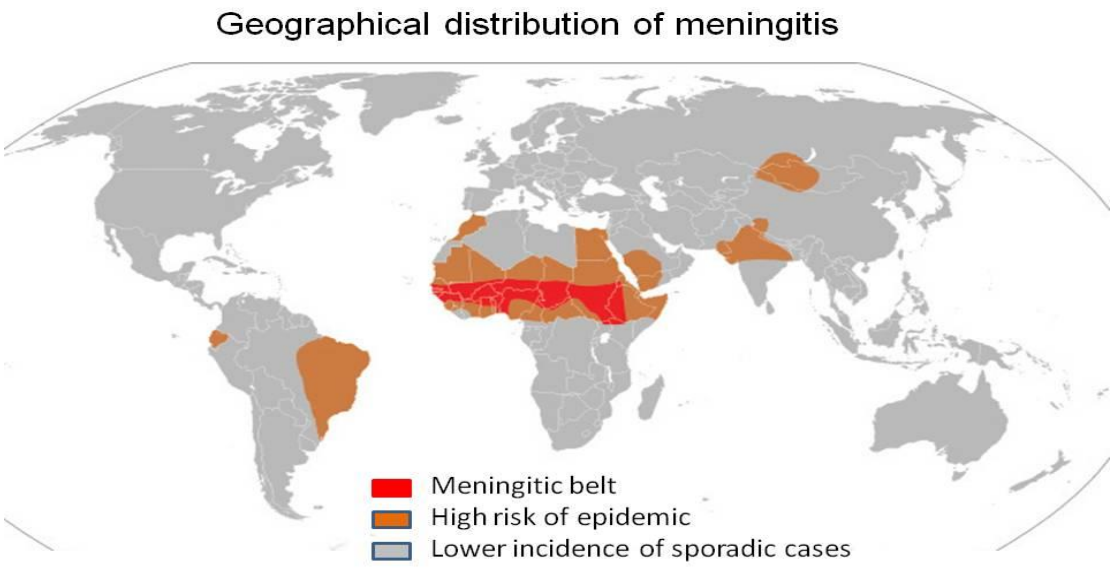

Figure 9| Bacterial meningitis incidents across the globe The annual incidents of acute bacterial meningitis in the developed world reach is 0.005% per 100,000 whereas in the developing nations the incidents increase 10-fold. *Streptococcus pneumoniae* is one of the main causes of bacterial meningitis along with *Neisseria meningitides*, and *Haemophilus influenzae*, which was estimated to 75%-80% of the cases in newborns. The image was adopted from http://encephalitisindia.org/abm.html.

1.2.4.2 Vaccines

Conjugate vaccines to prevent infection against pneumococci have been used for the last 15 years. In an effort to include as many serotypes as possible in one vaccine, a polysaccharide vaccine was designed (PPV23), which targets 23 different serotypes. It has been demonstrated that conjugation of bacteria in a vaccine is more efficient since the immune response is greater upon vaccination (figure 10) [143]. The first conjugate vaccine targeted pneumococcal serotypes 4, 6B, 9V, 14, 18C, 19F, and 23F (heptavalent vaccine - PCV7). Further production of conjugate vaccines came out, such as PCV10 and then, PCV13, which target 10 and 13 different serotypes accordingly.

Figure 10| Vaccines against Streptococcus pneumoniae Synflorix® and Pneumo23 are some of the vaccines available against the pneumococci. Synflorix® is a 10valent conjugate vaccine whereas Pneumo23 is a 23valent polysaccharide vaccine. Although Pneumo23 covers more serotypes, a conjugate vaccine was shown to be more effective against the pneumococci. Images adopted from GSK and Sanofi Pasteur.

Within a few years following the introduction of PCV7 vaccine, vaccine-covered serotypes were replaced by non-vaccine serotypes prevalent in the community i.e. serotype replacement [144-148]. The thirteen-covalent vaccine PCV13 targets six additional serotypes (1, 3, 5, 6A, 7F, and 19A) to the ones the PCV7 had; despite the success rates from the use of vaccines, serotype replacement is an issue, which may rise

rapidly, and thus, constant screening for serotype replacement must be performed. Very recently serotype replacement was observed for serotypes covered both by PCV7 and PCV 13 [149]. New efforts are made to increase serotype coverage of vaccines and new generations of vaccines based on conserved protein antigens are also in development such as the pneumococcal pneumolysin toxoid recently introduced in clinical phase I trials as a vaccine candidate against pneumococcal infections [150].

Despite knowledge that has been acquired in the last 20 years around bacterial meningitis, the vaccination programs, or medical administrations (antibiotics) to prevent the disease or provide treatment, bacterial meningitis remains the leading cause of meningitis in adults around the world [7, 8, 135, 136, 151-156]. The bacteria, which appear to be causing BM in the majority of cases, are *Neisseria meningitidis* and *Streptococcus pneumoniae*, with the last one being the cause of almost 70% of the cases that occur in the United States and also Europe [134, 136]. Focal neurological deficits, hearing loss, cognitive impairments are some of the results of the disease which can affect 30 to 50% of the patients suffering from bacterial meningitis where the other 15 to 37% of patients are likely to face death [136, 157-159]. The exact steps that pneumococci follow so that BM can develop remain unclear. However, here follows an effort to put steps of the disease in order based on the best available evidence; starting from colonization of the pathogen up to the point that the central nervous system (CNS) is compromised leading eventually to bacterial meningitis.

This information reveals the severity of meningitis as a disease and the significance in studying it. Additionally thorough investigation could be significant in achieving protection against disease and increase the efficacy of different vaccines. Diseases that are caused by invasive pneumococcal infections include bacteremia, pneumonia and

meningitis in figure 11 [3].

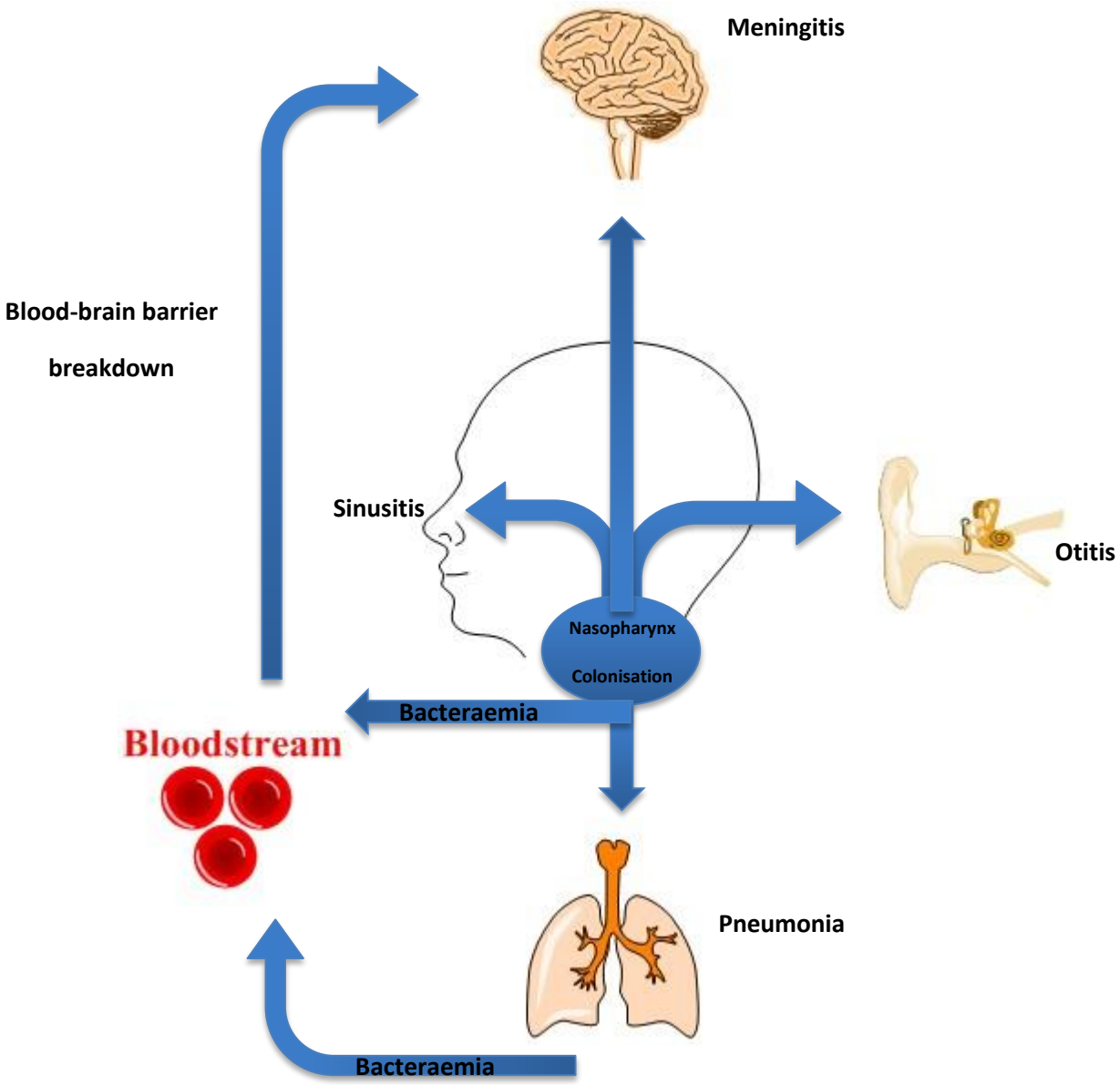

Figure 11| Infectious diseases caused by Streptococcus pneumoniae In the majority of cases when the host comes in contact with the bacteria colonization in the nasopharynx occurs. Many of us carry the bacteria without a burden in our immune system. When infection occurs the bacteria can move through different routes causing pneumonia, bacteraemia, meningitis and other diseases. Direct infection of the pathogen to specific organs could occur on extreme circumstances such as cranial injury or surgery.

1.3.0 Host defenses against the pneumococci

Respiratory mucus is the first barrier defense against pneumococcal colonisation and prevents binding onto mucosal surfaces [160-162].

As soon as the bacteria reach the nasopharyngeal mucosal site, the innate immune system of the host is activated and the pneumococcus is confronted by antibodies such as secretory immunoglobulin A (sIgA) and the lactoferrin protein; with further support derived from mechanisms of the innate immune system (complement system) [163-165]. sIgA prevents pneumococci from binding to nasopharyngeal mucosal sites by attaching to it and activating opsonisation, which leads to the activation of phagocytes such as neutrophils and antigen-presenting cells such as macrophages [163, 166, 167]. Lactoferrin is a protein, which targets the iron that pneumococci need in order to keep an active bacterial metabolism. Once the iron is depleted, bacteria can be cleared. Lactoferrin can be found in nasal secretions, saliva and other body fluids, enhancing the immune system of the host [168]. Contribution from the innate immune system leads to multiple actions which involves leukocyte recruitment, opsonisation and phagocytosis [169].

1.4.0 Bacterial defense mechanisms

Pneumococci have developed various mechanisms to avoid the host's immune system, and achieve their adherence on the epithelium. Pneumococcal capsule acts as a shield against mucus entrapment, by promoting its negative charge against the negative charge of the sialic acid that exists in mucus [161]. Pneumococci alter their capsule according to the level of immunity surrounding them. This process is called phase variation [170-172].

Through this process, pneumococcal capsule can go from transparent (very thin layer of capsule) to opaque (thick capsule layer) and that is achieved by alternations of polysaccharides forming the capsule [172]. When the pneumococci reaches the epithelium of the nasopharynx, the opaque capsule of the pathogen can shift to a transparent one, allowing various adhesion molecules to bind the epithelium layer of the host [170, 172]. Capsule switch occurs through altered gene expression and when in the bloodstream capsule thickness increases [173]. Whilst in colonization phase, opaque bacteria can avoid factors such as sIgA and mucus; hence avoid opsonisation and phagocytosis [161, 174-176].

Another way for the pneumococci to be protected is the liquefaction of mucus (reduction of mucus viscosity) by the deglycosylation of mucus glycoconjugates (achieved by pneumococci's exoglycosidases beta-*N*-acetylglucosaminidase, neuraminidase A (NanA) and betagalactosidase A (BgaA)) [177-179]. Additionally pneumococci prevents its removal by mucus by using its pore forming toxin pneumolysin, which causes reduction and stoppage of ciliary activity on epithelial cells, allowing them to progress on the epithelial cell layer without being removed [180, 181].

It has been previously demonstrated that the pneumococci is able to express an IgA1 protease, which may tamper with the ability of this Ig subclass to prevent pneumococcal adherence. Specifically, it was shown that even with the use of IgA1 protease antibodies, there was increased adherence by the pneumococci, which occurred due to the cleavage of the antibodies. The production of positively charged fragments inhibited the negatively charged capsule, allowing for better adhesion on epithelial cells [182].

1.6.0 Colonisation

During colonisation of the human nasopharynx, many different bacterial species are found to be colonising at the same time. Often there can be up to 700 different species [183, 184]. Due to the amount of organisms that can be found simultaneously in the nasopharynx, interactions between different organisms can occur [185]. If there are more than one type of bacteria colonizing the nasopharynx, genetic material can be exchanged. There are also cases where competition or synergism can occur between different bacteria [186, 187]. When bacteria compete, reinforcement of one strain against others occurs. For example *S. pneumoniae* is capable of combining DNA from species of the same Streptococcal family in order to gain significant advantage against other competitive organisms [188].

1.7.0 Invading Host Endothelial and Epithelial Cells

When it comes to invading endothelial cells and epithelial cells, pneumococci use endocytosis and transcytosis through phosporylcholine (ChoP), which binds to the platelet activating factor receptor (PAF receptor) of these cells [170]. When pneumococci bind to the PAF receptor, the pathogen is allowed to follow the receptor recycling pathway which gives the opportunity to the pneumococci to be transported to the basal membrane of the cell, leading to disease [189, 190]. The pneumococci can also invade the host using the choline-binding protein (CbpA). CbpA binds to the cell's polymeric immunoglobulin receptor (pIgR) [166, 191]. As in the case of the PAF receptor, pneumococci use the pIgR

recycling pathway in order to be transported in the apical and basal membrane of the cell [166, 192].

1.8.0 Bloodstream survival - Complement System

Whilst in the bloodstream capsule thickness increases in order to avoid phagocytosis or complement deposition [79, 193]. Further protection to the pathogen is provided by the binding of pneumococcal surface proteins (CbpA and CbpC) or by the use of pneumolysin, which derives from bacterial autolysis. Once pneumolysin is released, it binds to the Fc portion of immunoglobulin G (IgG), hence activating the complement pathway, and increasing the virulence of the pathogen by significantly reducing complement factors that are trying to clear bacteria form the blood [194].

1.9.0 Recognition by the Host Immune System

The host immune system is capable of recognizing possible threats in order to prevent progression of the disease. APCs can identify bacteria by receptors that are considered vital to the pathogen in order to remain viable. Toll-like receptors (TLRs) are recognition receptors that can detect pneumococci and the main receptors are TLR2, TLR4, TLR9 and nucleotide oligomerization domain 1 (Nod1) [195-203]. Upon activation of these receptors, APCs create a flow of inflammatory reactions, by releasing specific cytokines; this cytokines are capable of eliminating the pathogen but also increase immune response with using neutrophils recruited by these cytokines [169]. The cytokines, which seem to be most important during pneumococci recognition, are interleukin-1 (IL-1), IL-6 and tumor necrosis factor alpha (TNF-α) [204]. In order to reinforce the response of the

immune system around the infected area, IL-1 and TNF-α increase vascular permeability of local vascular endothelial cells. Up-regulation of adhesion molecules occurs (P-selectin, E-selectin vascular cell adhesion molecule 1 [VCAM-1]), which further allows the presence of more neutrophils and various lymphocytes to the infected area through the bloodstream [205, 206].

1.10.0 Central Nervous System infections

The very own ability of the CNS to be so selective and isolated sometimes works against itself. That is due to the absence of mechanisms [207] to defend the CNS (the blood-brain barrier restricts the presence of immune cells to the CNS). Also the comparably low levels of immune cells such as phagocytes, complement proteins and immunoglobulin, make the CNS environment a perfect conditioned media for the pathogen to replicate and further infect the host.

The pathogens that are mostly found to cause infection in the CNS are viruses and bacteria, and the route that they follow to reach the CNS is either through the bloodstream (indirect pathway), neighboring tissues (exposed parts due to surgery or neighboring routes to the CNS like the sinus), or spread up through the nerves from the peripheral nervous system (e.g. rabies).

Hippocrates first mentioned meningitis 2300 years ago. Once the CNS is infected, several symptoms can indicate infection, such as intracranial pressure, local pain around the spinal cord, or pressure on the nerve root [208]. The same pathogen can sometimes cause different diseases. For example in the case of meningitis, infection is found in the subarachnoid space [209] whereas when in the ventricular system, ventriculitis or

ependymitis may appear [209]. Lumbar puncture, magnetic resonance imaging, computed tomography were and still are key tools used to expand knowledge around the CNS but also evaluate and further take action on an ongoing infection [208].

CNS infections and specifically pneumococcal meningitis is a life-threatening condition. Even though the discovery of antibiotics and vaccines has contributed significantly in the battle against infection, the outcome is still often poor (bacterial infections are greatly dependent on time of diagnosis but even if caught early permanent damage might be left with the patient). The main reason that bacterial infections in the CNS remain high in numbers is the inability to fully comprehend the way that disease develops.

Almost 70% of deaths related to bacterial meningitis, are due to CNS complications or breakdown [210] and the remaining 30% due to more complicated and systemic events [211]. This reveals how important immune responses are in regulating inflammation. Table 2 shows the most important pneumococcal diseases in the CNS [212].

Table 2 Infection of the Central Nervous System due to bacterial pathogens

Type of Disease	Infection's information
Bacterial meningitis	Infection of the meninges affecting pia, arachnoid and subarachnoid space/Can lead up to septic shock.
Brain abscess	Infection within the brain parenchyma which leads to central core necrosis, accumulation of inflammatory molecules and edema.
Epidural abscess	Infection between the inner skull surface and the dura. Can only occur if injury occurs or operation on the cranium is performed.
Subdural empyema	Collection of pus between dura and arachnoid membranes. Often epidural empyema is associated with the subdural. Venous cortical infection can also occur.
Ventriculitis	Infection of the brain ventricular system. Meningitis can cause it due to complications or drainage from the ventricule.
Suppurative thrombophlebitis	Bacterial meningitis , epidural abscess, or subdural empyema can create the disease which is associated with a septic venous thrombosis of cortical veins and sinuses.

Table 2| Central nervous system infections cause by Streptococcus pneumoniae The pneumococci is one of the leading causes in CNS infections and besides meningitis the pneumococci can cause abscesses in the CNS, empyema, ventriculitis as well as thrombophlebitis. The information of table 2 was acquired from [139-141].

1.10.1 Bacterial meningitis – Mechanisms and breakdown of the Blood-Brain Barrier

1.10.2 Central nervous system invasion - translocation across the Blood-Brain Barrier

To maintain an intact CNS and protect against infectious diseases, cerebral vascular endothelial cells significantly differ from endothelial cells that lie in the general vasculature. As mentioned previously the cerebral vascular endothelial cells have tight junctions between them, are abundant in mitochondria, and have reduced processes of pinocytosis [213]. As shown *in vitro*, human brain microvascular endothelial cells were used to identify mechanisms of transcytosis that the pneumococci uses, by adhering to the platelet-activating factor (PAF) receptor of the cells [214]. Again phosphorylcholine binds to the PAF receptor in order to induce transmigration to the cell's basolateral site [170, 215]. As mentioned previously, pneumococci with a thin capsule (transparent colony morphology) have increased adherent abilities [214].

Another pathway that the pneumococci can use to enter the CSF is translocation through the tight junctions of epithelial cells that form the blood-CSF barrier. The tight junctions of brain endothelial cells can also be disrupted during progression of the disease [213], and that can be due to the concurrent actions by pneumococci components (pneumolysin disrupts the epithelial cell layer of the nasopharyngeal area) or components of the host's immune system [216-218] (figure 12).

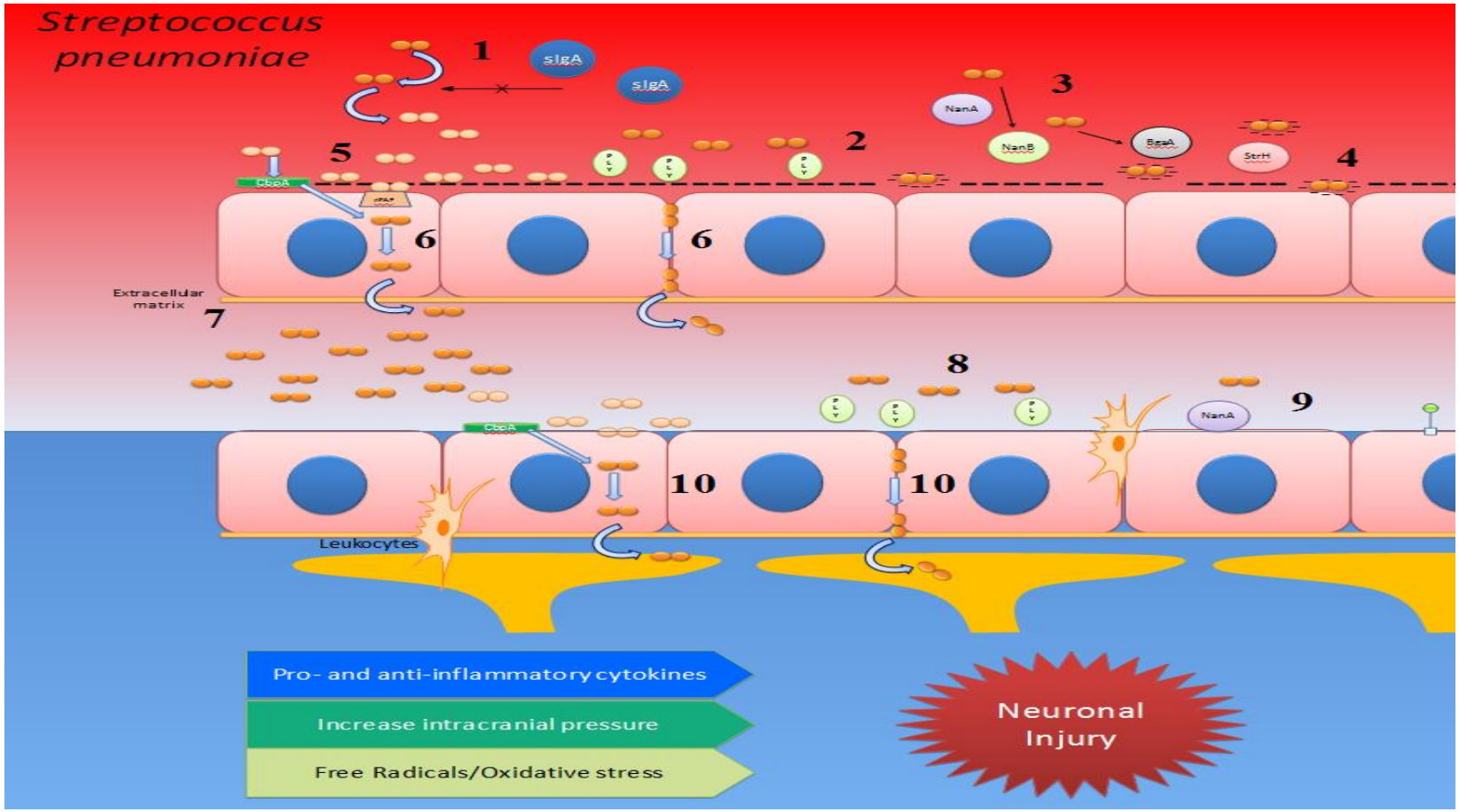

Figure 12| Mechanisms of infection and BBB breakdown Colonization by pneumococcus is achieved by various stepwise mechanisms. The opaque capsule of the bacteria prevents secretory immunoglobulin A (sIgA) to remove the bacteria from the nasopharynx (1). Release of the pneumolysin (PLY) toxin from lysed bacteria reduces ciliary contractility of the upper airway (2), whereas deglycosylation of the mucus reduces further cilia activity (3). The negative charge surrounding the capsule, opposes the negative charge of the sialic acid found in mucus (4). Additionally the phase variation of the capsule from opaque to transparent enables adhesion molecules to bind to the epithelium (5). Invasion of pneumococci into the bloodstream is achieved by transcytotic or paracellular mechanisms (6) and degradation of the cells' extracellular matrix (7). The pneumococci then enter the nervous system by following similar mechanistic pathways in the upper airway (8, 9, and 10).

1.10.3 Central nervous system immune response – activation of the immune system

Pneumococcal multiplication and lysis (when the immune system is activated) is an event that happens both simultaneously and continuously coming to a point that autolysis and multiplication have a ratio of 1:1 [219]. Pneumococcal components, which are released due to lysis, can create a very strong immune response that may cause further damage and breakdown of the BBB [220]. Some of the pneumococcal components are capable of inducing a proinflammatory response. This was demonstrated by purified pneumococcal cell wall, lipoteichoic acid, or peptidoglycan from the pneumococcal cell wall [220] When all these components were incubated in rabbits, no disease was observed suggesting that they do not activate immunity in the CSF [220]. Additionally a pneumolysin-deficient strain was used in a murine model and exhibited decreased CFUs as well as increased survival of the host. Nevertheless tissue from the murine model showed similar results as the wilt-type pneumococci in inflammatory changes [221]. Antibiotics used to induce bacterial autolysis, thus, pneumolysin release which could also create a stressful environment leading again in a strong immune response hence a more severe disease and possible BBB breakdown.

1.10.4 Anatomical Localization of Blood-Brain Barrier - Invasion by Leukocytes

In order to deal with possible threats in the CNS, leukocytes can migrate to the perivascular space, which connects with the subarachnoid space. Due to the spaces neighboring to the CSF (corpus callosum, periventricular space or the meninges), neutrophils can also gain access to the brain [222]. When neutrophils phagocytose

bacteria, oxygen and nitric components are released, which create a bacteria-like environment around the neutrophils, making them hazardous for the surrounding tissue, and possible candidate for the damage that is caused in neurons in bacterial meningitis cases. Whilst in the brain, microglia act as macrophages, secrete pro-inflammatory factors to increase microglial presence and initiate T-cell response [223, 224].

1.10.5 Pattern Recognition Receptors

It was previously mentioned that APCs are activated during bacterial opsonisation in order to clear bacterial pathogens. Antigen-presenting cells can be found in the CSF, the meninges, perivascular space, choroid plexus, and brain parenchyma (microglial and astrocyte cells) [225-227]. Toll-like receptors 2, 4, 9 and Nod-like receptors are some of the pattern recognition receptors involved in sensing threats such as pneumococci in the CNS [228-231]. Specifically, when *Streptococcus pneumoniae* is found in the CNS, TLR2 and Nod2 are activated. Although a component of the pneumococci, pneumolysin **does not** activate TLR-4 [88]. Absence of TLR2 and TLR4 in a mouse model, showed reduction of inflammatory molecules and increased of pneumococcal CFUs in the CNS [232]. TLR9 is responsible for the activation of peripheral macrophages and interleukin-8 (IL-8) induction [197, 202]. Absence of TLR9 showed reduced immunity against the pneumococci and increased CFUs in the nasopharynx [202]. Nod-like receptors (NLRs) are a secondary group of pattern recognition receptors. Once activated, the nuclear factor kappa-light-chain-enhancer of activated B cells (NF-kB) and the mitogen-activated protein kinase (MAPK) pathways are activated [233].

1.10.6 Downstream signaling molecules and inflammatory molecules release

There is a wide range of proinflammatory or anti-inflammatory cytokines, which are released upon infection; chemokines, matrix metalloproteinases, and other chemoattractants are some of them. Leukocyte migration adhesion molecules and the complement system, not only help clear pneumococci, but also induce cytotoxicity, which can further cause a breakdown of important sites in the central nervous system such as the blood-CSF barrier and the BBB. Interleukin-1 receptor-associated kinase 4 (IRAK-4) is a signaling protein involved in pneumococcal disease [234]. IRAK-4 is an adaptor protein and one of the links in the TLR- and IL-1 receptor (IL-1R)-induced activation of MyD88 and NF-kB. This activation will eventually lead to cytokine production [235, 236]. IRAK-4 deficiency leads to increased susceptibility in invasive pneumococcal disease, but also increase of recurrent events with high mortality [237]. Deficiencies in IRAK-4 and MyD88 show unresponsive agonists for TLR1, -2, -5, -6, -7, -8, -9, and IL-1R [238-240]. The TLR3 signaling pathway is not affected, whereas the TLR4 pathway is partially affected. These 2 pathways can still initiate the signaling cascade for cytokine production [239].

1.10.7 Proinflammatory cytokines

Sensing of pneumococci and production of proinflammatory cytokines can derive from endothelial cells, astrocytes, macrophages of the meninges, as well as microglia [216, 241-245]. As soon as the pneumococci is recognized in the CNS, IL-1, TNF-α, IFN-γ and IL6, are produced [246, 247].

TNF-α is an important proinflammatory cytokine, and it was shown in elevated concentrations in the CSF of patients suffering from pneumococcal meningitis [217, 248-251]. In a study with 48 patients suffering from pneumococcal meningitis, levels of TNF-α were associated to severity of blood-brain barrier disruption, disease, and neurologic sequelae. Once the patients were administered with antibiotics, the TNF-α levels decreased [217]. In animal models of pneumococcal meningitis, production of TNF-α was observed within the first 6 to 24 h of the immune response [252, 253]. Increased levels of TNF-α are important for a rapid response during infection [254]. Thus, on the first 4-6 hours TNF-α is crucial, even though increased levels of the cytokine may promote BBB disossiation [255].

IL-1β is a proinflammatory cytokine and is produced [241]by perivascular and meningeal macrophages (557). Increased levels of IL-1β were observed during the first 18 hours of pneumococcal infection [256]. Pro-IL-1β is cleaved by caspase-1, which is regulated the inflammasome [257]. Although present, IL-1β does not seem to be associated with BBB breakdown in meningitis sufferers [217]. Absence of caspase-1 in a mouse model showed decreased levels of IL-1β and decreased intracranial pressure (ICP), leukocyte recruitment, and brain edema compared to the wild-type mice [258]. In a rabbit meningitis model, IL-1β was administered intrathecally and showed no CSF pleocytosis or brain edema [259]. Mice lacking the IL-1α and IL-1β receptor (IL-1R) had reduced survival rates and decreased cytokine responses [260]. Nonetheless CSF pleocytosis was not affected, suggesting that cytokines which are cleaved by caspase-1 might (551). Thus,, although IL-1 did not influence CSF pleocytosis lack of capsase-1 may be responsible for reduced pleocytosis in mice lacking the enzyme.

IL-6 can also act as anti-inflammatory cytokine and has been associated with disease severity [261]. Decreased cerebral edema intracranial pressure and blood- brain barrier disruption in an IL-6 knockout mouse model [262]. Additionally, IL-6 was shown to suppress pro- and anti-inflammatory cytokines in a pneumonia model suggesting that IL-6 constricts leukocyte recruitment [263].

Gamma interferon (IFN-γ) is part of the T-helper 1 (Th1) pathway and showed increased concentrations in patients suffering with pneumococcal meningitis [264, 265]. IFN-γ was also present in an animal model of pneumococcal meningitis[266] The exact role of IFN- in pneumococcal meningitis remains unclear. Significant stimulus to IFN-γ production is the cytokine interleukin 12 (IL12p70). This cytokine was detected both in patients as well as animal models of pnemococcal meningitis [265, 266] During the course of pneumococcal meningitis in patients, macrophage inflammatory factor (MIF) exhibited increased concentrations in the CSF and was also associated with disease severity [267].

1.10.8 Anti-inflammatory Cytokines

Two important anti-inflammatory cytokines involved in meningitis are IL10 and TGF- β. IL10 can have a downstream effect on proinflammatory cytokines and macrophages [268, 269]. Depleting the cytokine showed no differences in bacterial loads [270], yet its considered to be an important factor in determining sepsis outcome. Over-expression of the cytokine showed decreased levels of neuronal damage when the host suffered from pneumococcal meningitis [271]. Administration of the cytokine to the host showed less efficacy in comparison to the systemic release of the cytokine [272].

TGF- β is another anti-inflammatory cytokine and has a major role in maintaining T-regulatory cells as well differentiating them [273]. TGF-β is a suppressor of proinflammatory cytokines, since IL-1β and IL6 were reduced upon its activation [274, 275]. Reduction of the cytokine may have positive effects in patient outcome since its absence showed increased survival, less bacteria counts in the host, and minimal disruption of the BBB [276]. As in the case of IL10, systemic production of the cytokine showed reduce severity in meningitis cases [277]. Many other cytokines and chemokines fight infection better when produced systemically rather than when overexpressed or administered. In example, IL8 (CXCL8) is a chemokine responsible for neutrophil chemotaxis [278]. When IL8 was systemically produced, it showed better pleocytosis in the CSF, as in the case of IL10 and TGF- β mentioned earlier [279].

1.10.9 Matrix metalloproteinases (MMPs)

Matrix metalloproteinases are enzymes which are responsible for the remodelling of the extracellular matrix (ECM) throught degradation processes. These enzymes are associated with cations such as calcium and zinc, and can degrade laminin, fibronectin, collagen (of various types) as well as proteoglycans [280, 281]. It was believed that MMPs had the restrictive role of degrading the ECM for leukocyte migration to occur, until recent studies showed that MMPs might be driving inflammation [282, 283]. The most recognised MMPs associated with meningitis are MMP-8 and MMP-9 [249]. Specifically, neurological sequelae such as impaired hearing was observed when levels of MMP-9 were significantly elevated [249].

1.11.0 Bacterial meningitis and oxidative stress

During bacterial infection in the meninges, reactive oxygen species (ROS) are released. Hydrogen peroxide (H_2O_2), the anion form of oxygen (O_2^-) and anything with an unpaired electron (radicals) are classified as ROS. These components are abundantly produced once the brain immune cells are activated, either due to stroke or bacterial infections [284]. The bacteria themselves are capable of producing H_2O_2, which can accelerate the process of oxidative stress due to the exposure of the tissue to ROS [284]. The interaction of H_2O_2 with nitric oxide (NO) results in the creation of peroxynitrite, a highly reactive ROS that has a direct effect in the leptomeninges of the patients [285]. Previous studies have shown that ROS have a huge part in the generation of brain edema, intracranial pressure and other neurological deficits [285-287].

1.12.0 Blood-brain barrier models

Research on CNS systems were relatively rare until the mid-1980s where models based on cell lines made their first appearance in the scientific community, having as a goal to understand how the blood-brain barrier functions, how the barrier is designed, its pathophysiology and pharmacology [288].

There are numerous monoculture-derived BBB models that were developed; brain endothelial cells from different species were used (human, porcine, bovine or rodent cells), both primary (cells that are harvested without any genetic modification) and immortalized cell lines. The creation of models *in vitro* allowed to scientists to study characteristics of the BBB that occur *in vivo* without the need of blood-related techniques

or complicated procedures. At the beginning it was believed that the BBB was a static barrier, but further understanding of the barrier revealed that the BBB functions as a dynamic neurovascular unit (brain endothelial cells supported by astrocytes pericytes and neurons) [289-293]. This understanding also contributed to the upgrade of BBB models, introducing besides monoculture systems, co-culture and multi-culture systems, which enhanced the studies around the BBB [294].

Despite the availability that exists in BBB models nowadays, the majority of the existing models lacks of realistic facts (i.e. most of the models present the brain endothelial cells as a layer where in reality the microvascular cells are connected in a cylindrical shape.). That affects the BBB models in aspects such as permeability, tightness of junctions, transporters, polarity and transendothelial electrical resistance (TEER). Until now none of the existing *in vitro* models was able to illustrate the exact functions of the BBB that occur *in vivo*.

Since Joo and Karnushina introduced the methodology on brain microvessel harvesting in 1973 [295], a great amount of data has since been generated around the BBB, involving cell biology and microbiology. Methodologies in brain endothelial cells isolation were modernized, to better isolate, and purify brain endothelial cells [296-299].

Among brain endothelial cells from different species, bovine microvessel endothelial cells (BBMEC) preserve many properties of the *in vivo* BBB both morphologically, and biochemically. Some of these properties are adhesion molecules, marker enzymes, polarity and TEER values which can range between 160-200 Ω x cm^2. BBMECs were

used for drug permeability studies [300], investigations for endo- and transcytotic mechanisms, as well as nutrient/ion transporters of endothelial cells [301-305].

1.12.1 Primary endothelial cells vs. Immortalized cell lines

To preserve the phenotype of primary brain endothelial cells, co-culture of the cells with astrocytes or astrocyte-conditioned medium can be used [306]. Primary astrocytes in co-culture with endothelial cells were shown in various studies [307-309] and can increase BBB phenotypic characteristics in respect to primary brain endothelial cells. Serum-free media, which can decrease permeability, and increase the TEER values can also be used to better mimic the BBB [310-313].

While primary brain endothelial cells approach better the *in vivo* BBB, their phenotype is lost after a few passages. There are also specific procedures in order to isolate primary brain endothelial cells, which are time-consuming, and in situations like primary human brain endothelial cells, ethical issues and approvals arise. These artifacts are dealt by immortalized brain endothelial cell lines, which were created and concern various species. Immortalized cell lines can be passaged up to 4-5 times more in comparison to primary cells. Where cell lines provide ease in regards to time management and utilization, they lack in characteristics such as tightness of junctions. Like in the case of BBMECs the rat cell line RBE4 was extensively used in studies about cell markers or drug transport due to the many similarities that the cell line shares with primary cells. RBE4 have a strong phenotypical response when co-cultured with factors deriving from astroglial cells [314-316].

Brain cells that derive from the same species have the advantage of carrying exactly the same genetic background when the species are in the same age; hence co-culture BBB models of this kind make studies more reliable [317]. Along with animal immortalized cell lines there are also human brain endothelial cell lines such as SV-HCEC, HBEC-51, BB19, and TY08 [318-323].

1.12.2 Type of BBB models

Inserts are used to seed brain endothelial cells (regardless of the species). The membrane consists of small pores, which permit to a liquid agent to go through, establishing biochemical communication between the two chambers. When the system is used for co-culturing, astrocytes or pericytes can be grown either on the other side of the membrane or even at the bottom of a standard well, which supports the insert. Three different cell types can be cultured in a single system. Co-culture with astrocytes increases the BBB phenotype and TEER increases (figure 12-ex2) [324].

The use of Matrigel (a gel structured component) allows the cells to take their natural shape (brain endothelial cells form tube-like structures) whereas astrocytes and pericytes, can interact with brain endothelial cells (figure 12-ex3) [325].

Considering that brain endothelial cells exist in a tubular form (figure 12-ex5), there is a significant advantage of the Matrigel as an *in vitro* BBB model, which is also a 3 dimensional model (figure 12-ex3). Other types of 3 dimensional models have been used [326]. Previous studies showed that having a constant flow of cell culture media through brain endothelial cells could increase TEER by approximately 1000-fold (standard model

values are can reach up to ~75 Ωcm^2 whereas a 3D flow model with the same cell type can reach 1200 Ωcm^2) (figure 12-ex4) [327].

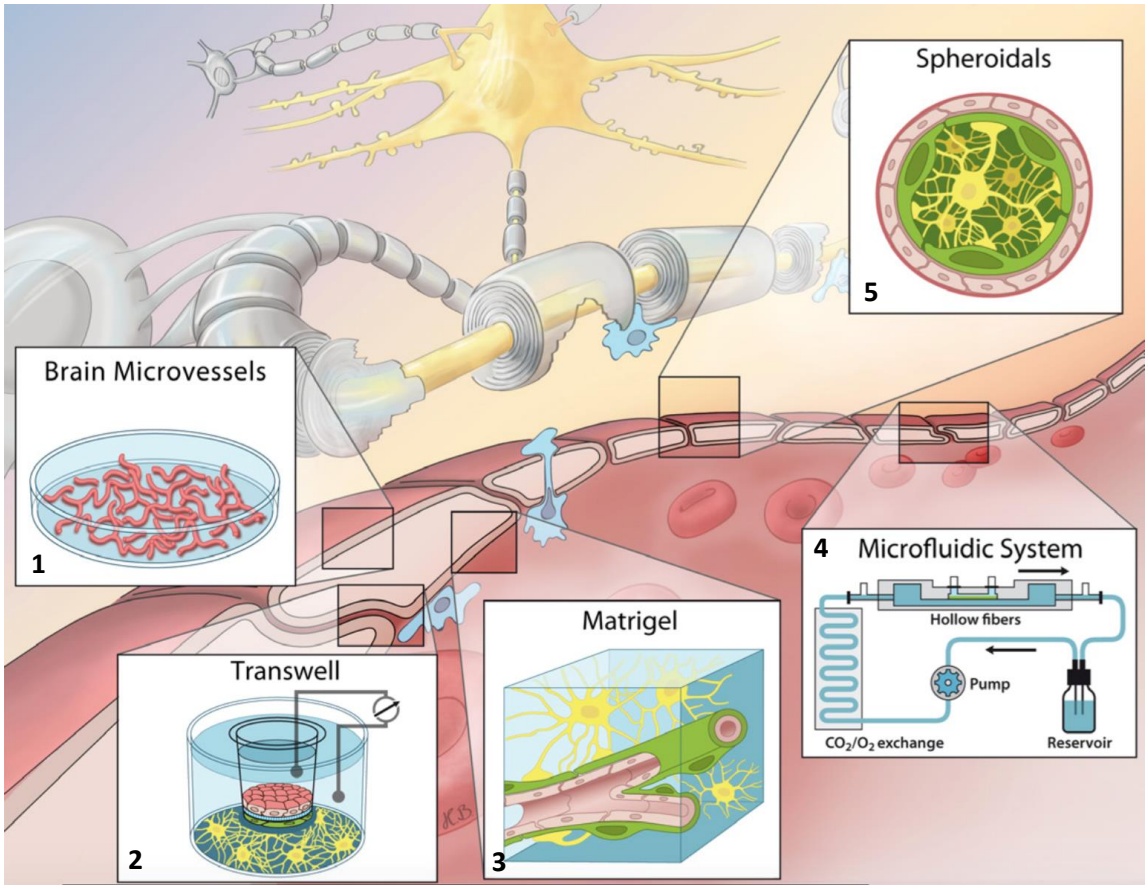

Figure 12-ex| Type of *in vitro* Blood Brain Barrier models There are various BBB models that can be used in an *in vitro* setting. The simplest way to investigate some of the features of the BBB would be to seed brain endothelial cells in monoculture (1). More complex models include the co-culture of brain endothelial cells with BBB cell components (such as astrocytes or pericytes) (2). A more realistic approach to the physical BBB is the Matrigel model (3) and the microfluidic system (4) (DIV model) due to the fact that they allow the cells to take their natural occurring form (5) as well as allow flow of nutrients using a reservoir powered by a pump. The image was adopted from [328].

1.13.0 The importance of studying pneumococcal interactions with the Blood-Brain Barrier

Although extensive research has been done on pneumococcal pneumonia, and meningitis, the specific interactions of the pneumococcus with the blood-brain barrier are still under represented and we still have significant gaps in our knowledge on the pathophysiology of this disease process. It is evident that pneumococcal meningitis is a disease occurring

from a series of events and not from a single point. New research methods are available where basic principle experiments can be combined with the genomic components of the BBB [329]. Thus,, the work in this thesis, sought to elucidate and provide specific information around the interactions of the pneumococcus and the BBB, providing insight into both pneumococcal and host factors that contribute to virulence and protection respectively.

1.13.1 Research questions on the blood-brain barrier and bacterial meningitis

Gathering the information found in the literature in regards to research done previously around pneumococcal meningitis, the following questions were raised:

a) How much better different pneumococcal serotypes can adhere and invade the blood-brain barrier?
b) Can a better *in vitro* human blood-brain barrier be developed that would allow reliable experiments with the pneumococci?
c) Are there any differences between infecting a BBB model or cells in a conventional well?
d) Does pneumococcal infection in the BBB affect the tight junctions, and if so is there a different junctional response of the cells towards different pneumococcal serotypes?
e) What is the impact of the toxin pneumolysin during pneumococcal infection in the BBB?
f) What are the immune responses of the BBB during pneumococcal meningitis and do they show variance when different serotypes are used?

1.13.2 Aims and objectives of this PhD thesis – Addressing the research questions

Gathering all the questions raised previously I decided that the aims and objectives of this project should be:

a) To investigate the ability of various pneumococcal serotypes to adhere and invade the cells consisting of the BBB model. This will be achieved by using two clinical isolates (serotype 1 sequence type 217, a bacteremia isolate and serotype 6B, a meningitis isolate), a lab derived serotype 2 strain (D39) and its pneumolysin knockout mutant PLN-A. The cells used during infection will be immortalised human brain endothelial cells (the cells forming the BBB), and primary human astrocyte cells (which enhance the BBB features by communicating with endothelial cells using their end-feet). Pneumococcal survival, adherence and invasion would be investigated for the various serotypes used.

b) To establish a BBB model consisting exclusively from human cells, and show that the pneumococci are able to traverse through the endothelial cell monolayer to the other side of the model. This will be achieved by using the cells mentioned in section a. Brain endothelial cells will be seeded on a semi-permeable membrane with pores large enough to allow free passage of the pneumococci. To enhance the BBB features of this model, primary human astrocytes will be seeded on the bottom of the well supporting the semi-permeable membrane. The model will be monitored by constant TEER readings and supplementation of nutrients.

c) To use the same serotypes as in monoculture in order to observe differences between the two conditions. This will be achieved by infecting the model from the

topside at the exact same dose previously used in monoculture. Hourly monitoring of pneumococcal survival adhesion and invasion as well as possible pneumococcal traversal to the lower compartment of the model will be recorded.

d) To acquire the TEER values hourly in order to assess the integrity of the tight junctions during pneumococcal infection of the BBB model. These values will be compared according to the different serotypes used in order to assess their impact on the BBB model and the tight junctions.

e) To use the pneumococcal toxin pneumolysin in order to see how it affects cell viability and junctional integrity. Firstly, a dose response curve of the toxin will be created in order to decide for a dose that is not jeopardising the viability of the cells but has an impact in a molecular level. This will be achieved by performing a series of viability assays on both brain endothelial cells as well as astrocytes. Further on the optimum dose will be used individually or in co-culture with the pneumococci in the BBB model. Pneumococcal survival, adherence and invasion will be hourly monitored. Junctional integrity will be assessed by acquiring the TEER values before, during and post infection.

f) To perform a series of molecular and immunological experiments in order to see the host responses against the toxin and the different pneumococcal serotypes used. This will be achieved by isolating the RNA from the brain endothelial cells and by performing a two-colour gene expression microarray. Dr. Mike Griffiths will kindly provide a custom designed array slide, with over 60,000 transcripts that relate to brain endothelial cells. To make comparisons with the array findings, the supernatant from the BBB model will be isolated and used in enzyme-linked immunosorbent assays (ELISAs). Additionally imaging of the endothelial cells

during infection will increase our understanding around pneumococcal/toxin infection and tight junction breakdown.

CHAPTER 2.

Materials & Methods

2.0 Cell culture

2.1.0 Immortalised Human Brain Endothelial Cells – Tissue culture flask preparation

Cell culture flasks with an area of $75cm^2$ (Corning®) were coated with 2ml of 15% collagen type I solution (300µg/ml – Sigma Aldrich®). The coating solution was evenly spread over the whole surface of the flask and left for incubation at 37ºC / 5% CO_2 for minimum 3 hours. Excess amounts of collagen solution in the flask were aspirated before use of the flask.

2.1.1 Immortalised Human Brain Endothelial Cells - cell line establishment

Dr. Adjanie Patabendige kindly provided an immortalised cell line of Human Brain Endothelial Cells. Cells from liquid nitrogen were brought gradually to 37 ºC. The contents of the tube were collected using a Pasteur pipette and added **dropwise** into a 15ml centrifuge tube containing 10ml of HBEC conditioned media (Gibco™). The suspension was gently mixed and transferred to a T-75 collagen-coated flask. The flask was lightly tilted to ensure the suspension occupied the total coated surface and was transferred to a tissue culture incubator at 37 ºC with 5% CO_2. The cells were allowed to adhere on the flask's surface for 24 hours and they were then re-supplied with 10ml of fresh HBEC media.

2.1.2 Immortalised Human Brain Endothelial Cells - cell line splitting/preservation

When the HBECs reached 100% confluency, the supernatant was removed and the cells were washed with 1x PBS solution (OXOID). The PBS solution was discarded and 2ml of the serine protease Trypsin (Sigma Aldrich®) was added and evenly spread over the surface in order to initiate cell detachment. The Trypsin solution was left in the flask at 37 ^{o}C with 5% CO_2 for 1 minute, and then 8ml of fresh HBEC media were added in order to quench enzyme effects. The cells were pelleted at 1250 rpm for 4 minutes. The supernatant was removed and the cell-pellet was re-suspended in 10ml of HBEC media, and gently mixed with a pipette until a homogenous solution was observed. The cell concentration was determined using a hemocytometer chamber (see thesis' appendix A for cell counting calculations). The population-doubling rate (CPD) of the HBECs was acquired by calculating the population doubling number (PCN) of cells as previously described [330]. The PCN of HBECs usually ranges from 3.90 - 4.32 and $1x10^6$ cells/ml is sufficient to preserve the cell line. The cells reach confluency and the desired PCN within 3 - 4 days of culture. The HBECs were washed with 6ml of 1x PBS and resupplied with fresh HBEC media every 48 hours in order to keep the cells in optimal growth conditions.

2.2.0 Primary Human Astrocytes – Tissue culture flask preparation

Cell culture flasks with an area of 75cm^2 (Corning®) were coated with 2ml of 0.005% Poly-D-lysine hydrobromide solution (50μg/ml – Sigma Aldrich®). The coating solution was evenly spread to the whole surface of the flask and left for incubation at room temperature for 1-hour minimum. Excess amounts of Poly-D-lysine hydrobromide

solution were aspirated from the flask prior to use. The flask surface was rinsed with 2ml of graded tissue culture water to remove any Poly-D-lysine hydrobromide residues.

2.2.1 Primary Human Astrocytes - cell establishment

Primary Human Astrocytes (HA) were purchased from ScienCell™. Cell aliquots from liquid nitrogen were brought gradually to 37 ºC. Tube contents were collected using a Pasteur pipette and were re-suspended **dropwise** in a 50ml centrifuge tube containing 15ml of HA conditioned media (F12 DMEM - Sigma Aldrich®). The suspension was gently mixed and transferred to a T-75 coated with Poly-D-lysine hydrobromide. The flask was lightly tilted in order for the suspension to occupy the total coated surface and it was transferred to a tissue culture incubator at 37 ºC / 5% CO_2. The cells were allowed to adhere on the flask's surface for 24 hours and they were then re-supplied with 15ml of fresh HA media.

2.2.2 Primary Human Astrocytes (HA) - cell splitting/preservation

When the HA reached 100% confluency, the supernatant was removed and the cells were washed with 1x PBS solution. The PBS solution was discarded and 2ml of the serine protease Trypsin were added in the flask and evenly spread on the surface in order to initiate cell detachment. The trypsin solution was left in the flask at 37 ºC / 5% CO_2 for 2 minutes, and then 8ml of fresh HA media were added in order to quench enzyme action. The cells were pelleted at 1250rpm for 4 minutes, supernatant was removed and the cell-pellet was re-suspended in 10ml of HA media and gently mixed with a pipette until a homogenous solution was observed. The cell concentration was determined by using a

hemocytometer chamber. The PCN of HA usually ranges between 3.58-3.90, and $1x10^6$ cells/ml is sufficient in order to preserve the cell line. The cells reach confluency and the desired PCN in 7-8 days of culture. The cells were allowed to secrete their growth factors for 48 hours and half of the supernatant was removed from the flask in order to resupply the cells with fresh HA media.

2.2.3 Long-term storage of HBEC and HA in liquid nitrogen

To create stock aliquots of the cell line, 2ml cryovial tubes (Corning®) were used, and $1x10^6$ cells in 90% HBEC or HA media and 10% Dimethyl Sulfoxide (Sigma Aldrich®) were added to each tube (total volume of 1ml / cryovial). The stock tubes were transferred for cryo-storage in cell-storage containers containing Liquid Nitrogen (LN) at ~ -195ºC.

2.3.0 Cell Counting using a Hemocytometer chamber

200 µl of cell suspension was transferred into a 1.5 ml microcentrifuge tube and 500 µl of 1x PBS was added to the cell suspension, along with 300µl of 0.4% Trypan Blue Solution (Sigma Aldrich®) (1ml total volume). 10µl of the mix was injected into each side of the hemocytometer chamber and placed under a phase contrast microscope at 4x magnification. Cells were counted within the central 5 x 5 grid (figure 13A+B).

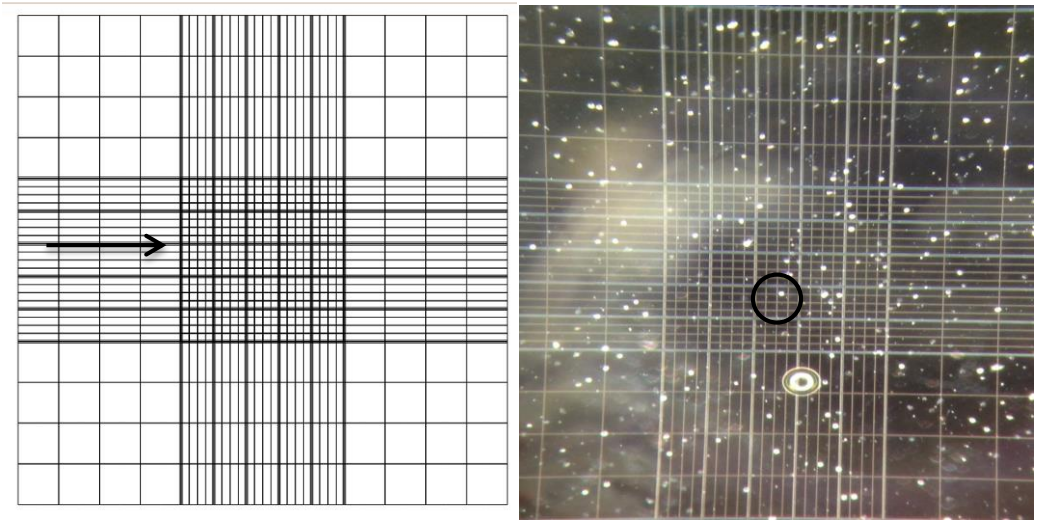

Figure 13| Cell counting using a hemocytometer A) All viable cells were counted from the corner squares and the middle square as seen in the figure (arrows). B) The hemocytometer shows the cells as white-blue dots scattering the light of the microscope (circle).

The same approach was taken for the other side of the hemocytometer chamber and the amount of cells per ml was calculated according to the following equation:

$$\frac{Cells}{ml} = (\text{Average } value\ of\ cells\ counted\ in\ 5\ squares\ on\ both\ chambers\ x\ Dilution\ Factor)\ \text{x}10^4$$

2.4.0 Cell seeding on a Transwell® system (BBB model setup)

The 12-well inserts (Transwells® - Corning®) contained $2x10^6$ pores per cm^2. The pore size was 3.0 μm and the membrane type was polyester [331]. Before using the Transwells®, the membrane was coated with 200 μl of 15% collagen type I solution (300μg/ml – Sigma Aldrich®) for 3 hours. Then the membrane was equilibrated with 1xPBS for 5 minutes at room temperature. The PBS was aspirated from the inserts and $1x10^5$ HBECs were seeded **per insert**, in 150 μl antibiotic free cell culture media. The cells were incubated for 3 hours at 37ºC / 5% CO^2. Post incubation of the cells, additional media was added to each insert in order to reach a final volume of 500 μl/insert. On the

same day, primary human astrocytes were also seeded in a seperate 12-well plate (conventional cell culture plate) at the same cell density ($1x10^5$ HA **per well** in a total volume of 1.5 ml per well). Both cell lines were incubated at 37ºC / 5% CO^2 for 24h and then the inserts were added to the plate containing the HAs. The system was supplumented with HBEC and HA media on the the second, fourth and sixth days of culture (figure 14).

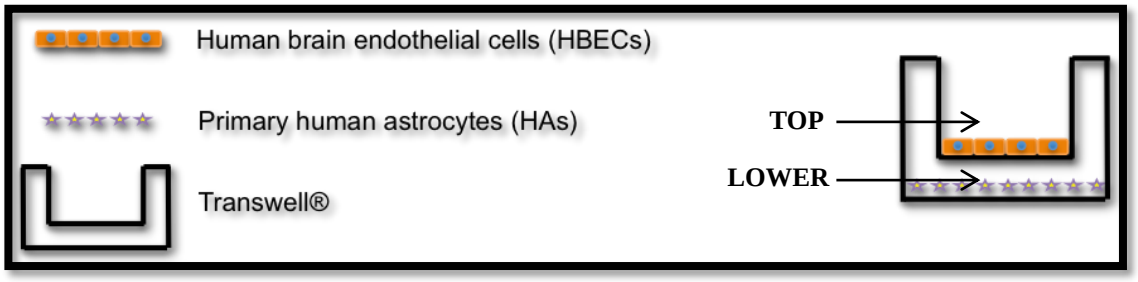

Figure 14| Blood-brain barrier model setup HBECs were seeded on the top compartment of the system (in the Transwell® membrane), whereas HA were seeded on the lower compartment of the system (conventional 12-well plate). The model was constantly kept at 37ºC/5% CO_2 and supplemented with HBEC/HA media every other day.

2.4.1 Trans-endothelial electrical resistance

Monolayer integrity of the BBB model was assessed by measurement of the resistance generated between the tight junctions of neighbouring cells. Both the STX2 electrodes and the $EVOM^2$ voltohmmeter were purchased from World Precision Instruments [332]. The SXT2 electrodes were sterilized in 100% ethyl alchohol for 5 minutes and then connected to the voltohmmeter. The $EVOM^2$ was set to ‘’Ohms’’ and the electrodes were immersed in cell culture media until the value on the $EVOM^2$ reached ‘’0’’. Then the

SXT2 electrodes were immersed in the BBB system with the shorter part of the electrode found in the insert and the longer part of the electrode immersed in the well (figure 15).

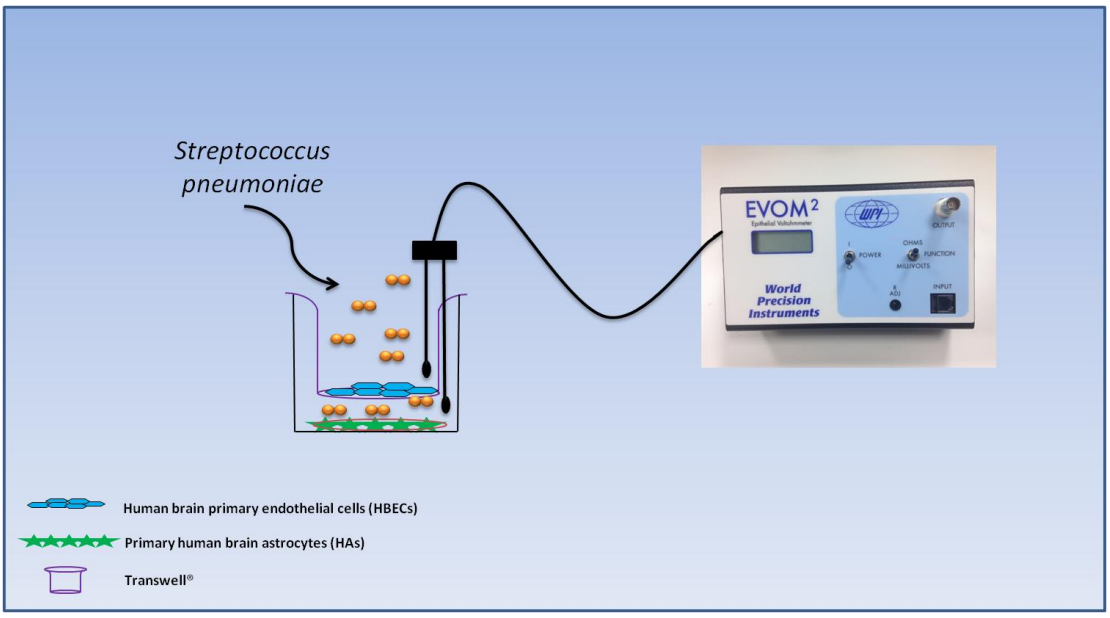

Figure 15: Graphic representation of the bacterial Blood-Brain Barrier model used in this project A Transwell® insert will rest in a 12-well plate, which has been previously seeded with human astrocytes. The membrane of the insert will be supplied with Human Brain Endothelial Cells; cell resistance through the use of an EVOM2 voltohmmeter will assess monolayer integrity. Upon completion of the model's setup, the system will be infected with pneumococci and monitor bacteria for survival adherence and invasion.

The first reading taken was from the insert/well that contained no cells (blank). Two additional readings were taken, and the average value of the blank was multiplied by the surface area of the insert (the surface area for a 3.0 μm pore insert was 0.33 cm^2). Then the blank value was subtracted from the values generated from experimental inserts.

2.5.0 Cell viability assays

Prior to the assay, 96-well flat-bottomed micro-plates were coated with 15% collagen type I solution, and seeded with $5x10^4$ cells / well (total cell media volume of 200µl/well). The micro-plates were incubated at 37°C / 5% CO_2 for 24 hours. The supernatant was carefully removed and the cells were washed with 100µl 1xPBS. The cells were re-suspended in 200µl of 1% antibiotic-free cell media for 2 hours.

2.5.1 (3-(4,5-Dimethylthiazol-2-yl)-2,5-diphenyltetrazolium bromide) assay

The MTT assay measures the reduction of MTT (3-(4,5-Dimethylthiazol-2-yl)-2,5-diphenyltetrazolium bromide) to formazan within living cells. Formazan production is associated with a quantifiable colour change that linearly correlates with levels of intracellular enzyme activity [333]. MTT solution was prepared by the addition of 1 mg MTT (Sigma Aldrich®) to 1 ml of phenol red-free media (Gibco®).

Cell culture media was removed and wells were washed with 100 µl PBS followed by the addition of 100 µl MTT to each well. The assay was protected from light by covering plates with aluminium foil. The plate supplemented with MTT was incubated at 37°C / 5% CO_2 for 4 hours. Following incubation, light microscopy was used to observe whether formazan crystals had formed within the cells. Then the supernatant was removed by aspiration and 100 µl of isopropanol were added to the wells to dissolve the crystals formed. Colour change was assessed by absorbance at 560nm using a ThermoScientific Multiskan plate-reader with the SkanIt (Research Edition) for Multiskan Spectrum 2.2 software.

2.5.2 Bicinchoninic Acid Protein Assay

The bicinchoninic acid (BCA) assay is used to quantifiably detect the amount of protein in a sample [334]. Data acquired from the BCA assay was combined with the MTT data to give a ratio of absorbance/mg of protein.

Cell culture media was removed and the cells were lysed with 100 µl of 1% Triton (in PBS) and then incubated for 30 minutes at 37°C. The albumin standards and BCA working reagent (50:1 ratio of Reagent A to Reagent B) were prepared during the incubation period. Standards were loaded on the plate and BCA working reagent was added to all wells. The plate was then incubated for 30 minutes at 37°C and the readings were taken by ThermoScientific Multiskan plate-reader SkanIt (Research Edition) for Multiskan Spectrum 2.2 software at 562 nm.

2.6.0 Microbiology

For this project, Streptococcus pneumoniae serotypes 1 (ST217), 2 (D39 and PLN-A) and 6B were used and were kindly provided from the stock glycerol bead collection from Prof. Kadioglu.

2.6.1 Pneumococcal Culture

Streptococcus pneumoniae collected from bitstocks was plated on a 90 mm Blood Agar base (BAB) plate (OXOID) and incubated overnight at 37ºC for 24 hours under anaerobic conditions. Single colonies were collected (figure 16) and re-suspended in 10 ml brain Heart Infusion (BHI) (OXOID) solution for 16-18 hours.

Figure 16| Streaking of *Streptococcus pneumoniae* on BAB culture plates The circle shows a single colony picked for liquid culture. The pneumococci were tested for optochin susceptibility (arrow).

When the Optical Density (OD_{500}) of the culture reached 1.4-1.6, pneumococci were pelleted at 1500g (~3000rpm) for 15 minutes. The pellet formed was re-suspended in 1 ml of 4:1 brain-heart infusion : fetal bovine serum (BHI : FBS) and 700µl of the suspension were transferred into a new universal tube containing 10ml of 4:1 BHI:FBS. The OD_{500} was evaluated and further bacteria or media added to obtain an OD_{500}: ~0.7. The bacteria were incubated statically at 37^{o}C for approximately 5 hours or until the OD_{500} value reached 1.4-1.6. The bacteria were transferred into 500µl aliquots and stored at -80 ^{o}C. The colony-forming unit per ml (CFU/ml) was determined after at least 47 hours at -80 ^{o}C.

2.6.2 Viable Count (Miles and Misra Method)

Blood-Agar plates were divided into 6 equal sectors in order to distinguish the differences in dilutions (figure 17).

The inoculum was serially diluted in 1x PBS (range 1:10 – 1:1,000,000) and the dilutions where then delivered as 60µl drops on BAB (3 x 20µl per dilution). The plates were left to dry in a sterile environment (Bunsen Burner or Bacterial Cabinet) and incubated at 37^{o}C for 24 hours under anaerobic conditions. Bacteria were enumerated on the sector containing 30-300 colonies (figure 17) [335].

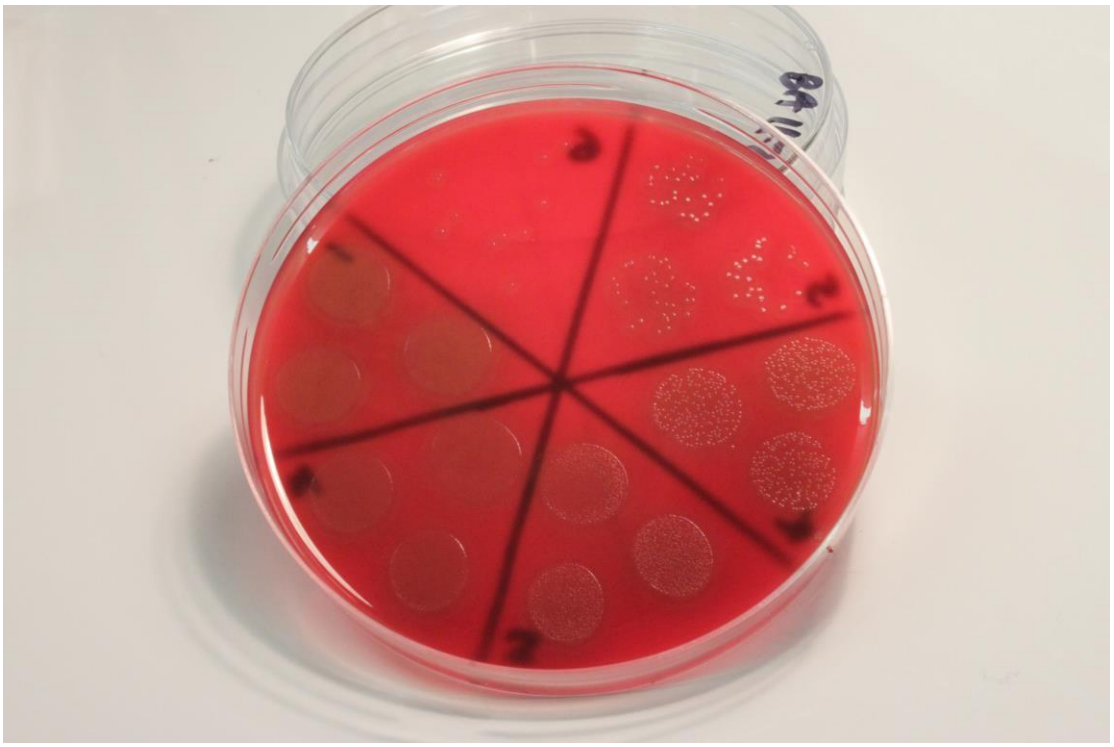

Figure 17| Miles and Misra This technique involves a series of dilutions where the density of pneumococcal colonies is reduced. The suitable dilution for counting is the one where 30-300 colonies can be counted.

The CFU/ml was calculated using the formula below:

$$CFU / ml = \left[\left((Droplet1 + Droplet2 + Droplet3) \, \mathrm{x} \, (Dilution\,Factor) \right) x \left(\frac{1000}{60} \right) \right]$$

The Miles and Misra formula was used a previously described [335].

2.7.0 Purification and isolation of the toxin pneumolysin and the genetically detoxified variant of pneumolysin PdB

Pneumolysin isolation purification and assessment was kindly instructed by Mr. Hesham Malak, PhD candidate at the University of Liverpool.

Recombinant pneumolysin and the genetically detoxified variant of pneumolysin PdB were expressed in *E. coli* and purified as described previously [88, 336] [337]. Briefly, recombinant pneumolysin was expressed in Escherichia coli (*E. coli*) strain MC1061 harboring plasmid pJW208 (which has an IPTG-inducible promoter and carries resistance to kanamycin and ampicillin). MC1061 was grown overnight in 8 L of Luria-Bertani (Sigma) broth supplemented with 100μg/ml ampicillin (Sigma Aldrich®). Bacterial cells were collected by centrifugation (14000xg for 20 minutes at 4 °C) and washed once in Equilibration buffer (Equilibration buffer (PH7); 10 mM $NaPO_3$, 250 mM NaCl). Cells were re-suspended in 30 ml of Equilibration buffer and disrupted by sonication (Cole-Parmer). The extract supernatants were clarified by centrifugation and stored at -20 °C until further use. Pneumolysin was purified from cell extracts supernatants using the high-performance affinity chromatography system (GE healthcare). Then 50 ml of the supernatants were loaded onto the purification column and the column was washed with 5 column volumes of 10 mM equilibration buffer, 10 mM Imidazole, 20 mM Imidazole

and 100mM Imidazole. Proteins were detected by Bradford assay using the kit supplied (Bio-Rad). Pneumolysin concentrations were measured using the NanoDrop ND-1000 UV-VIS Spectrophotometer at 280 nm. Then the toxin was passed 3 times through an EndoTrap endotoxin removal column (Profos AG, Germany) after which LPS was undetectable using the PyroGene Recombinant Factor C assay (Lonza; detection limit 0.01 EU/ml) and pneumolysin purity was > 97% as determined by SDS-PAGE gel stained with Coomassie brilliant blue R250 (Sigma Aldrich®). Purified pneumolysin was filter sterilized and stored at -80°C. **Molecular weight confirmation and characterization was kindly assessed by Mr. Hesham Malak, PhD candidate at the University of Liverpool using SDS –PAGE and Western blot**.

2.7.1 Hemolytic assay

Mr. Hesham Malak, PhD candidate at the University of Liverpool, kindly instructed hemolytic assay.

To determine the hemolytic activity of the toxin, 50 µl of sample was serially diluted (2-fold dilutions) in 1x PBS along one row of a 96-well plate. Then 50 µl of 1% (v/v) sheep erythrocyte (OXOID) suspension was added to each well, and the plate was incubated at 37°C / 5% CO_2 for 30 min. Then the plate was centrifuged at 3,000 x g for 5 minutes to remove red blood cells that were did not undergo lysis. Lysis was assessed by absorbance at 540 nm using a ThermoScientific Multiskan plate-reader with the SkanIt (Research Edition) for Multiskan Spectrum 2.2 software.

The percentage of erythrocytes lysed was plotted against the dilutions of the toxin (figure 19), and the pneumolysin activity of the sample was defined as the reciprocal of the

estimated dilution at which 50% of the erythrocytes would have lysed. The highest dilution of each sample resulting in at least 50% hemolysis was then estimated visually. This activity was expressed as hemolytic units (HU) per milliliter.

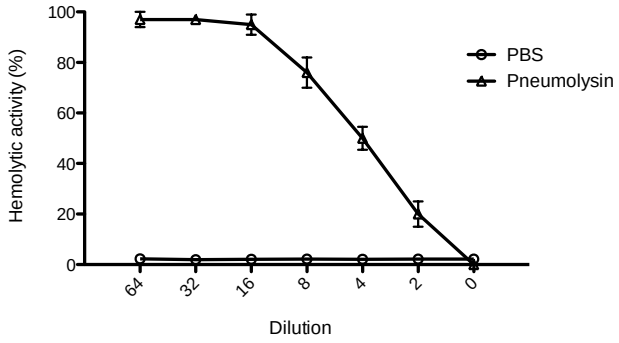

Figure 19| Graphical representation fro the determination of pneumolysin's hemolytic activity against 1% (vol/vol) sheep red blood erythrocytes The image was kindly provided by Mr. Hesham Malak – PhD candidate at the University of Liverpool.

2.8.0 Pneumococcal adhesion/invasion assays

2.8.1 Monoculture Adhesion/Invasion Assays

The adhesion assays were performed under the same conditions (cell growth, cell nutrient supplementation) for both cell lines used in this project (HBECs/HA). The infection dose used ranged between 10^3 – 10^7 CFU/ml (MOI: 0.01 – 100) and the incubation period was 1-6 hours.

One day prior to infection, the cells were washed with 1ml 1xPBS 3 times and re-supplemented with 1% HBEC antibiotic-free media. On the infection day half of the total

volume of the cell culture media was removed and was replaced with cell culture media containing the desired bacterial load. The experiment was monitored hourly and samples were collected from the supernatant to determine pneumococcal growth. Then the cells were washed with 1ml 1xPBS 3 times and treated with 200 µl of 0.05% Triton™ X-100 solution (Sigma Aldrich®). The saponin was allowed to deplete the cell wall for 1 minute and then Triton™ X-100 activity was quenched with 800 µl of media. The suspension was collected into a 1.5 ml microcentrifuge tube vortexed briefly to ensure complete cell lysis and release of adherent bacteria from the cell surface and the intracellular compartment. The suspension was then used to perform serial dilution and a Miles & Misra assay was performed. The blood agar plates were incubated for 24 hours at 37ºC under anaerobic conditions. Post incubation the colonies on the plates were counted in order to determine the CFU/ml of the adherent and invaded pneumococci.

To determine the invaded pneumococci (excluding adherent bacteria), the cells were washed with 1ml 1xPBS 3 times and re-supplemented 1% HBEC media containing 10µg/ml penicillin-G (Sigma Aldrich®). The cells were incubated further for 1 hour in order to eliminate extracellular bacteria. The process to release the bacteria form the cellular compartment was then performed as described above. The final number of adherent pneumococci was calculated after the invasion assays were performed where the invaded pneumococci were subtracted from the total CFU of adherent + invaded pneumococci.

2.8.2 Adhesion Assays in the Blood Brain Barrier Model

The infection dose was 10^7 CFU/ml (MOI: 100) and the incubation period was 3 hour. One day prior to infection, cells were washed separately with 0.5ml (top compartment) or 1.5 ml (lower compartment) 1xPBS 3 times and re-supplemented with 1% HBEC antibiotic-free media. On the infection day, half of the total volume of the cell culture media in the top compartment was removed and replaced with cell culture media containing 10^7 CFU/ml. The experiment was monitored hourly and samples were collected from the supernatant to determine pneumococcal growth. Post incubation, inserts were separated from the 12-well plate containing the astrocytes, and were placed into a new standard 12-well plate in order to avoid cross-contamination. The cells were washed separately with 0.5ml (top compartment) or 1.5 ml (lower compartment) 1xPBS 3 times and then treated with 200 µl of 0.05% Triton™ X-100 solution (Sigma Aldrich®) in both compartments for 1 minute. Then the cells were supplemented with 300 µl of media to reach a final volume of 0.5ml. Repetitive pipetting allowed for all cells to be removed from the membrane. The rest of the adhesion and invasion assay was performed as described in Section 2.8.1 for cells grown in monoculture.

2.9.0 Endothelial Cells RNA Extraction

After incubation of the BBB model with pathogen or toxin, cells were transferred into a new 12-well plate and washed 3 times with 1ml of 1xPBS. The PBS solution was discarded and 200µl of the serine protease Trypsin (Sigma Aldrich®) were added in the insert-well and evenly spread on the surface in order to initiate cell detachment. The Trypsin solution was left in the insert-well at 37 ºC / 5% CO_2 for 2 minutes. Plates were

tapped lightly to assist cell detachment. 300µl of fresh HBEC media were added in order to quench enzyme action. A pipette tip was used to gently scrape the insert membrane to remove all remaining cells. Cells were collected into a 1.5 ml microcentrifuge tube and spun down at 1250rpm for 4 minutes. The supernatant was removed and the cell-pellet was carefully re-suspended in 1ml of PBS. Cells were lysed in 500 µl of TRI-Reagent® (Sigma Aldrich®) by repeated pipetting.

To ensure complete dissociation of nucleoprotein complexes, the samples were allowed to stand for 5 minutes at room temperature. Then 250 µl of chloroform (Sigma Aldrich®/isoamyl alcohol-free) were added to the sample and the tube was covered tightly. Samples were vigorously shaken for 15 seconds, and allowed to stand for 15 minutes at room temperature. The resulting mixture was centrifuged at 12,000 × *g* for 15 minutes at 4 °C. Centrifugation separated the mixture into 3 phases: a red organic phase (containing protein), an interphase (containing DNA), and a colorless upper aqueous phase (containing RNA). The aqueous phase was transferred to a fresh tube and 250µl of 2-propanol (Sigma Aldrich®) were added. The sample was mixed by shaking and then was transferred into a cryo-container containing acetone (Sigma Aldrich®) with dry ice (~ -78ºC). The samples underwent a freeze-thaw cycle (cycle was repeated twice) in order to increase RNA precipitation. The samples were allowed to stand for 5–10 minutes at room temperature. The samples were centrifuged at 12,000 × *g* for 20 minutes at 4 °C. The RNA precipitant formed a pellet on the side and bottom of the tube. The supernatant was carefully removed leaving the pellet untouched. The RNA pellet was washed with 1 ml 75% ethanol (Sigma Aldrich®), vortexed until the pellet was lifted into suspension, and then centrifuged at maximum speed (14,000 x g) for 15 minutes at 4 °C. The washing step

was repeated twice. The RNA pellet was dried on a heating block for 15 minutes. The pellet was not allowed to dry completely, as this greatly decreased its solubility. 20µl of RNase-free water was added mixed by repeated pipetting at 55–60 °C for 10–15 minutes in order to facilitate dissolution. Both quality and quantity of the isolated cRNA was determined with the NanoDrop ND-1000 UV-VIS Spectrophotometer (version 3.2.1). From the results the RNA absorbance ratio (260 nm/280 nm) and RNA concentration (ng/µl) were recorded. Typical yields from endothelial cells found in an insert well ranged from 100-200 ng/µl.

2.10.0 Two-Color Microarray-Based Gene Expression Analysis

Firstly all RNA content from different experimental conditions was diluted to the desired concentration of 200ng/µl of purified total RNA.

2.10.1 Preparation of Spike A Mix and Spike B

Spike A Mix and Spike B Mix solutions were vigorously mixed on a vortex mixer. The spike mixes were heated at 37°C for 5 minutes, and again mixed by vortexing. The tubes were briefly centrifuged to drive contents to the bottom of the tube prior to opening. Spike A Mix and Spike B Mix were diluted according to manufacturer's instructions. Briefly, the 200 ng sample was diluted three times to give a final dilution of 1 in 12,800.

2.10.2 Preparation for labeling reaction

In a 1.5 ml microcentrifuge tube, 1.5 µl of RNA was added to 2 µl of diluted Spike Mix. To this total volume of 3.5 µl, 1.8 µl of T7 primer was added. The template and the primer were denatured by incubation of the samples in a water bath at 65^{o}C for 10 minutes before immediate transferal to ice for 5 minutes. The samples were briefly spun to remove residue from the tube walls and lid. 4.7 µl of cDNA Master Mix (Agilent®) were added to each sample tube and mixed by pipetting up and down. Each tube now contained a total volume of 10 µl.

Samples were incubated at 40°C in a water bath for 2 hours, and then at 70°C for 15 minutes. Immediately after, the samples were put on ice for 5 minutes and then briefly spun. 6 µl of Transcription Master Mix (Agilent®) was added with either Cyanine 3-CTP (containing Spike A Mix) or Cyanine 5-CTP (containing Spike B Mix). The contents were mixed gently by pipetting, and each tube now contained a total volume of 16 µl. The samples were incubated in a water bath at 40°C for 2 hours. The procedure is represented as a schematic in figure 20.

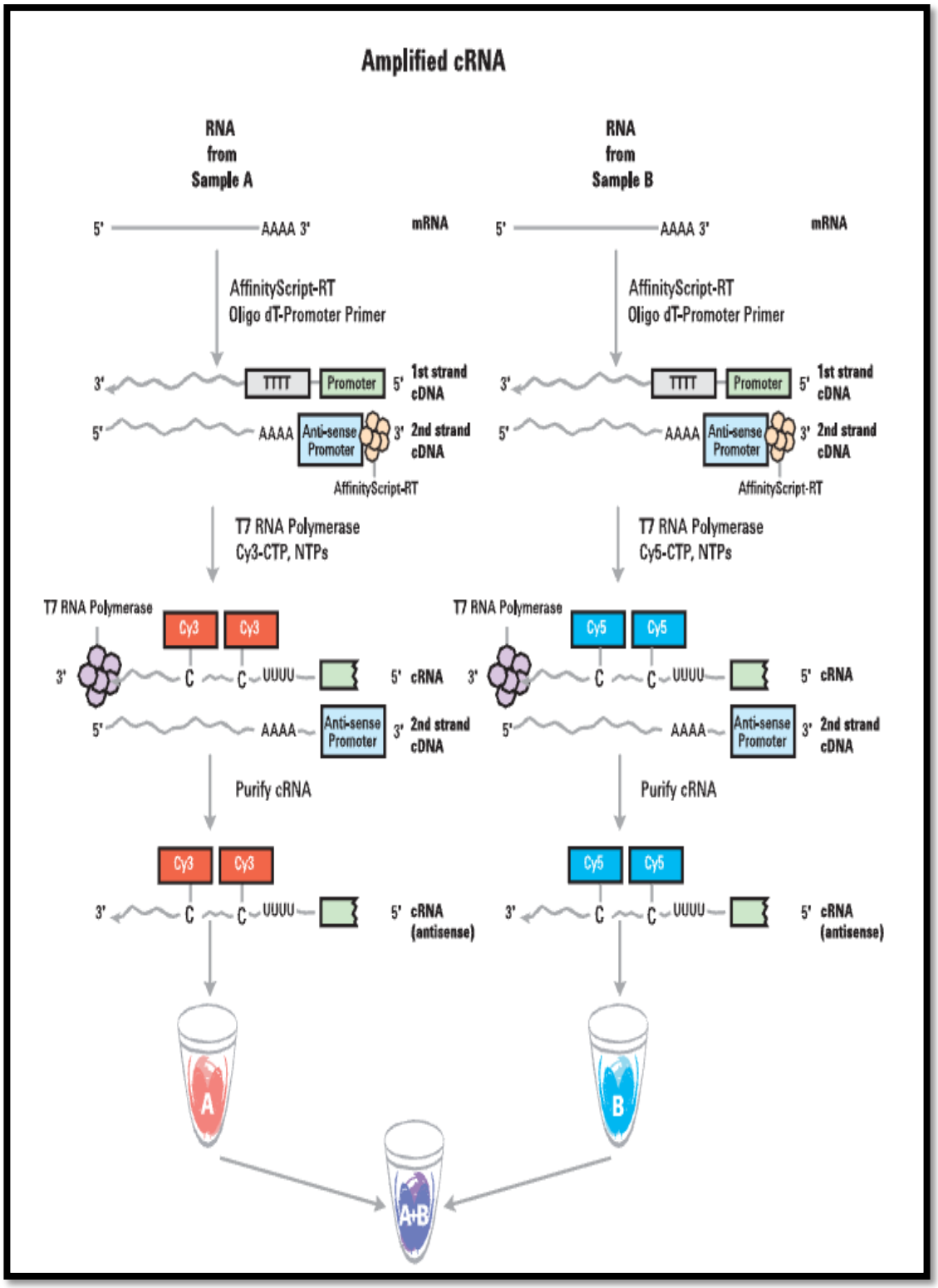

Figure 20| Schematic representation of the amplification procedure for cRNA in a two-color microarray experiment The image was adopted by Agilent Technologies (www.agilent.com).

2.10.3 Purification of the labeled/amplified RNA

After the labeling/amplification procedure, 84 μl of nuclease-free water were added to the cRNA samples. Then 350 μl of Buffer RLT and 250 μl of absolute ethanol (Sigma Aldrich®) were added and mixed well by pipetting.

Samples were transferred to an RNeasy® Mini Spin Column in a 2ml collection tube. The sample was spun at 4°C for 30 seconds at 13,000 × g. The flow-through and the collection tube were discarded and the RNeasy® column was transferred to a new 2ml collection tube.

The column was then loaded with 500 μl of Buffer RPE (containing ethanol) and the sample was spun down in a centrifuge at 4°C for 30 seconds at 13,000 × g. The flow-through was discarded and the column reloaded with another 500 μl of Buffer RPE and centrifuged at 4°C for 60 seconds at 13,000 rpm. The flow-through and the collection tube were discarded, and the cRNA eluted by adding 30 μl of RNase-free water directly onto the RNeasy® filter membrane. The column was allowed to stand for 60 seconds, and then centrifuged at 4°C for 30 seconds at 13,000 rpm. The cRNA sample containing the flow-through was collected and put on ice in order to be quantified.

2.10.4 Quantification of cRNA

To assess the quantity of the labeled/amplified cRNA, the NanoDrop ND-1000 UV-VIS Spectrophotometer was used (version 3.2.1). RNA absorbance ratio (260 nm/280 nm) and

RNA concentration (ng/µl) were recorded. The yield and specific activity of each reaction was evaluated by the calculations shown below:

The concentration of cRNA (ng/µl) was used to determine the µg cRNA yield as follows:

$$\frac{(Concentration\,of\ cRNA)x30\ \mu l(elution\,volume)}{1000} = \mu g\ of\ cRNA$$

The concentrations of cRNA (ng/µl) and cyanine 3 or cyanine 5 (pmol/µl) were used to determine the specific activity as follows:

$$\frac{Concentration\,of\ Cy3\,or\,Cy5}{Concentration\,of\ cRNA}x1000 = pmol\ of\ Cy3\,or\,Cy5\ per\ \mu g\ cRNA$$

A yield of 0.825 µg per sample and a specific activity of 6 was required in order to proceed to hybridization using an 8-pack array chip.

2.10.5 Hybridization

500 µl of nuclease-free water was added to a vial containing lyophilized 10× Gene Expression Blocking Agent supplied with the Gene Expression Hybridization Kit (Agilent®). The vial was gently mixed by pulse vortexing. To ensure that the pellet was completely dissolved, the mix was heated for 4 to 5 minutes at 37°C.

2.10.6 Preparation of hybridization samples

The sample was gently mixed and incubated in an equilibrated water bath at 60°C for 30 minutes to fragment the RNA. Immediately after the water bath incubation, the sample was cooled on ice for one minute. In order to stop the fragmentation reaction 25 µl of 2x Hi-RPM Hybridization Buffer was added to the sample.

The sample was mixed well by careful pipetting part way up and down to avoid bubble formation. The sample was spun for 1 minute at room temperature at 13,000 × g. The sample was used immediately and was loaded onto the microarray.

2.10.7 Preparation of the hybridization assembly

A clean gasket slide was loaded into the Agilent SureHyb chamber base with the label facing up and aligned with the rectangular section of the chamber base. The gasket slide was flush with the chamber base and not ajar. Slowly 40 µl of the hybridisation sample were dispensed onto the gasket well in a "drag and dispense" manner. The "active side" of the slide was slowly put down, parallel to the SureHyb gasket slide, so that the "Agilent"-labelled barcode was facing down and the numeric barcode was facing up (figure 21).

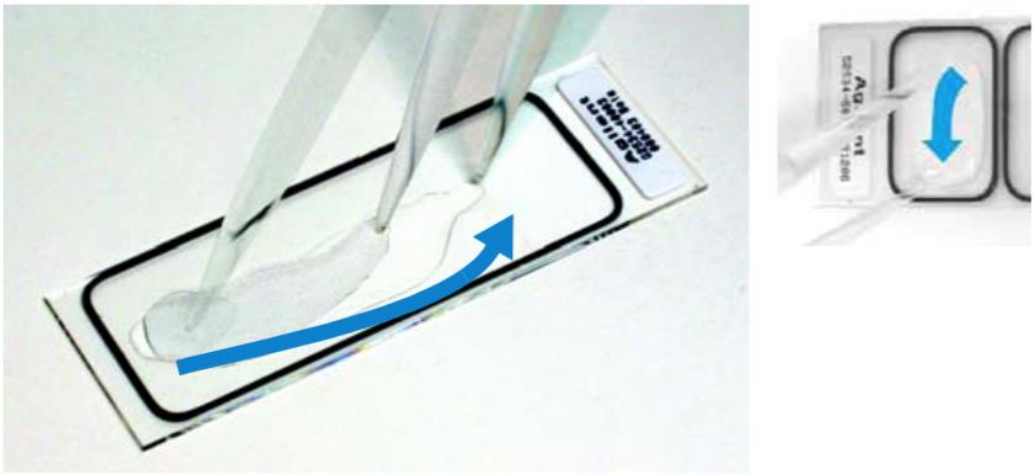

Figure 21| Preparation of the hybridization assembly: "Drag and dispense" of sample The image was adopted by Agilent Technologies (www.agilent.com).

The SureHyb chamber cover was placed onto the sandwiched slides and the clamp assembly adhered onto both pieces. The clamp was firmly hand-tightened onto the chamber (figure 22).

Figure 22| Preparation of the hybridization assembly: Placement of SureHyb onto sandwiched slides The image was adopted by Agilent Technologies (www.agilent.com).

The assembled chamber was vertically rotated to wet the gasket and assess the mobility of the bubbles. The assembly was tapped on a hard surface to move stationary bubbles (figure 23).

Figure 23| Preparation of the hybridization assembly: Wetting the gaskets, and assessment of bubble mobility The image was adopted by Agilent Technologies (www.agilent.com).

The assembled slide chamber was placed in rotisserie in a hybridization oven set to 65°C. The hybridization rotator was set to rotate at 10 × g when using 2× Hi-RPM Hybridization Buffer, and the hybridization period lasted for 17 hours (figure 24).

Figure 24| Preparation of the hybridization assembly: Placement in the hybridization oven for 17 hours The image was adopted by Agilent Technologies (www.agilent.com).

2.10.8 Microarray Wash, Scanning and Feature Extraction

The microarray wash, scanning and feature extraction were kindly executed by Mrs Lucille Rainbow at the Centre for Genomic Research (CGR) at the University of Liverpool. The custom-designed microarray glass slides (chips) were kindly provided by Dr. Michael Griffiths of the Institute of Infection and Global Health. **Each slide contains 8 square chambers and each chamber contained multiple transcripts of the same desired sequence**. The desired miRNA probes were printed on glass slides to produce the miRNA microarrays. After the RNA was isolated and labelled with a fluorescence dye, the reference DNA corresponding to a subset of miRNAs was also labelled with a different fluorescence dye. The reference DNA served to demonstrate the quality of the slide during hybridization and it was also used for data normalization. The RNA and DNA were mixed and hybridized to a microarray slide containing probes for most of the miRNAs in the database. After washing, the slide was scanned to obtain images, and intensities of the individual spots quantified. The raw signals acquired will be further processed and analysed as in correspondence to the experimental miRNAs. The control RNA was firstly loaded on the slide in order to initiate binding before binding of the experimental sample. This step contributed towards the embedment of the control as the background in the microarray assay. Further information on how these steps are executed can be found on **http://www.genomics.agilent.com/en/home.jsp** performing a search for ‘’Running a Microarray experiment’’.

2.10.9 Gene expression microarray analysis

The raw data were passed through the Collapser® software (written by Dr. Michael Griffiths as part of a Doctor of Philosophy degree) which identified replicates of the same gene, and combined the replicates of each gene to calculate an average expression value. Post calculation, the database contained only one of each gene. All genes were then loaded to the Cluster 3.0® software (developed by Michael Elsen whilst at Stanford University), which assigned each gene to a gene family. In the form of a dendrogram, the genes were further classified into specific sub-families based on known interactions (part of a specific mechanistic pathway). The outcome of the gene clustering was subject to the parameters set for the calculations. For example the gene vector removed all genes that had standard deviations of observed values less than X. If the gene vector was set at the value of 0.25 then the number of gene results returned, which had a standard deviation of 0.25 or higher, was 2513. If the gene vector was set at the value of 0.15, then the gene results returned (with a standard deviation of 0.15 or more) rose to 14482.

The significant analysis of microarray software (SAM®) was used for comparison of gene expression between the different groups (infection conditions). The computation of a statistic Xj for each gene j is the function of SAM. This computation showed how strong the relationship between the gene and the condition was. The ability of the software to use repeated permutations of the data, allowed the determination of the significance for expressed genes in relation to the condition used. The tuning parameter delta (d) determined the false positive rate. A greater delta value would reduce the rate of false positive genes whereas a reduced delta value would increase the rate of the false positive

genes. SAM® calculated the significant gene expression changes relative to the delta value. That immediately excluded genes, which mathematically may not be considered significant, but *in vita* might have contributed within a cascade of a protein-protein reactions [338].

2.10.10 Gene over representation (GO-ORA) analysis

All data acquired after SAM® were then loaded in the online software InnateDB. This software is a publicly available and has a vast library of genes, proteins, experimentally verified interactions and signaling pathways. This information is related to the innate immune response of humans as it concerns microbial infection [339]. The software clusters the user's data according to the relationship between them and their contribution to a common pathway. Next to the name of the pathway the user can find the statistical significance of the pathway (figure 25).

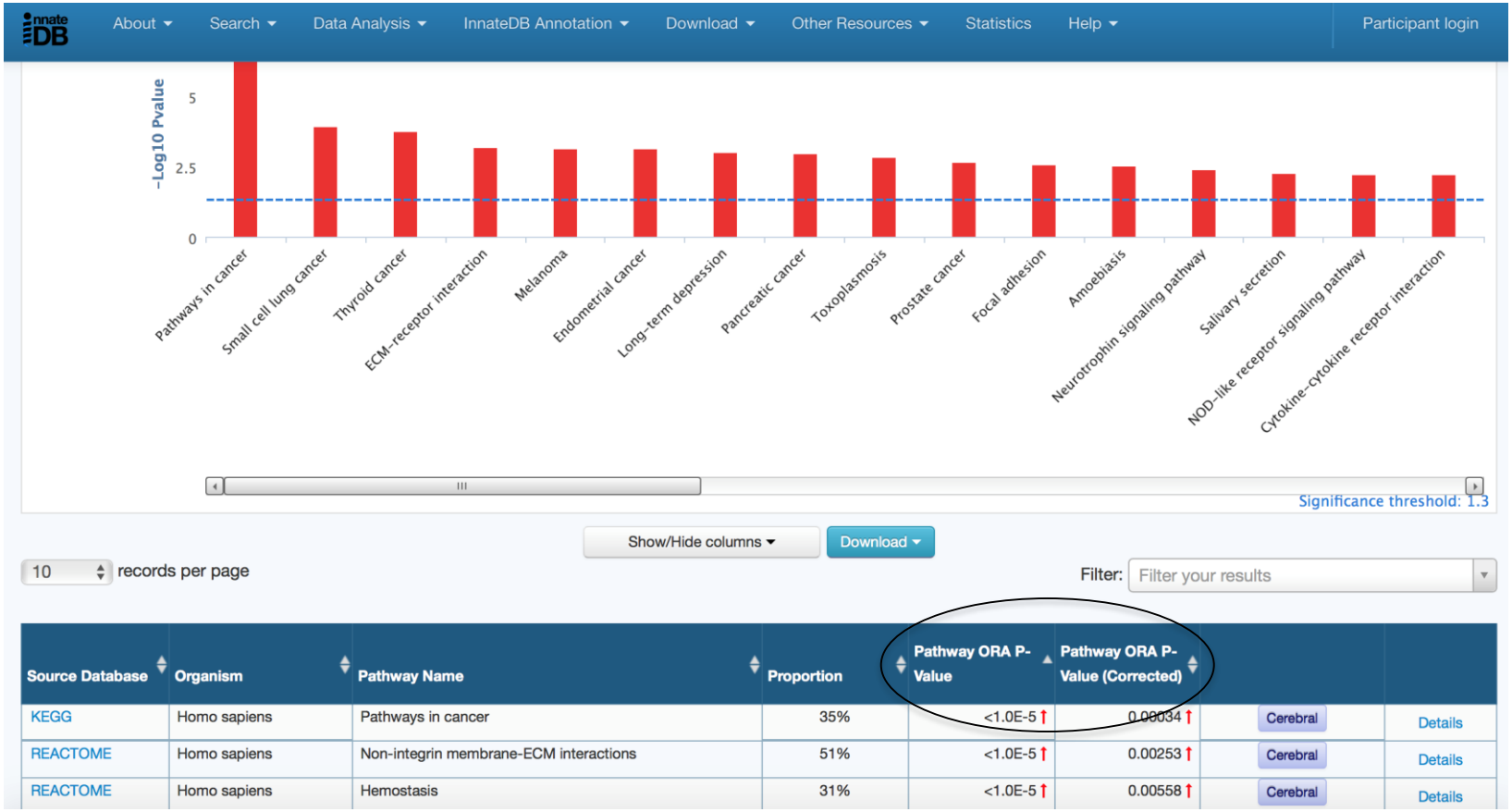

Figure 25| Analysis of microarray data with the InnateDB software The pathway over-representation analysis shows the different pathways that various genes may contribute to as red vertical bars. In the table at the bottom of the figure, the pathway browser is shown to the left (i.e. KEGG, REACTOME etc.) and the significance of the named pathway is shown to the right in the form of the p-value (circle).

2.10.11 Mapping of pathways using the microarray data

Gene interactions in a pathway were visualized using the online software REACTOME and Kyoto Encyclopedia of Genes and Genomes (KEGG). The use of different mapping software was necessary since some of the pathways were not found on both databases. Comparing the two databases, I observed that REACTOME could provide the user with a more detailed analysis [340], whereas KEGG could only highlight the genes imported without defining their statistical significance [341] (figure 26A+B).

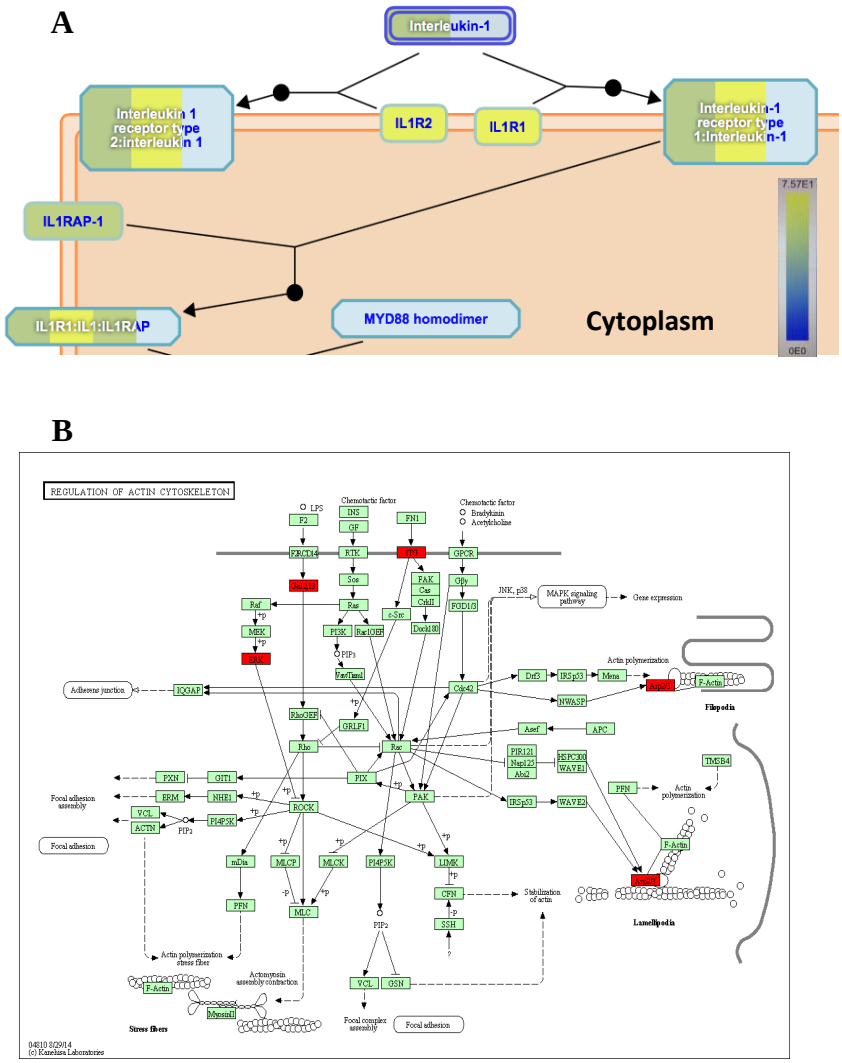

Figure 26| Examples and comparisons between different pathway databases A) When using the REACTOME database, the element to determine significance is the colored ladder which designates differences in expression in the form of the q-value (dark blue = highest expression – grey = moderate expression - yellow = least expression – light blue = gene not present for this transcript). One or more genes can contribute in the activation of a complex, and this is illustrated with different colored bars (variation in expression) inside the complex. B) KEGG does not provide the user with a significance tool. The red transcripts are genes found to be significantly up-regulated. The intense-green transcripts (not present in this pathway) show the genes, which down-regulate the transcript, whereas pale-green boxes are transcripts, which are not activated due to the absence of the relevant genes. Both databases were used to complete missing pathways from each database.

2.11.0 Enzyme-Linked Immunosorbent Assay (ELISA) of Interleukin 1β, 6 and 8

The capture antibody (polyclonal supplied by Peprotech®) was diluted with 1x PBS to a concentration of 1µg/ml and immediately, added to each ELISA plate well in quantities of 100 µl. The plate was sealed and incubated overnight at room temperature. The wells were then aspirated to remove any liquid and washed with 300 µl ELISA wash buffer (0.05% Tween-20 in PBS supplied by Peprotech®) 5 times. After the last wash the plate was inverted to remove residual buffer and blotted on paper towel. Then 300µl of blocking buffer (supplied by Peprotech®) was added to each well and incubated for 2 hour at r.t.

The plate was again aspirated and washed 5 times and the standard protein was serially diluted from 1.5 ng/ml to 2.34 x10^{-2} ng/ml in diluent (0.05% Tween-20, 0.1% BSA in PBS supplied by Peprotech®). Then 100µl of standard protein (supplied by Peprotech®) or sample were added to each well in triplicates and incubated at room temperature for at least 2 hours. The plate was again aspirated and washed 5 times and detection antibody (in diluent to a concentration of 0.5µg/ml supplied by Peprotech®) was immediately added in quantities of 100µl per well.

After 2 hours of incubation the plate was again aspirated and washed 5 times. Avidin-HRP conjugate (supplied by Peprotech®) was diluted in a ratio of 1:2000 in diluent and 100µl was added per well. The plate was incubated for 30 min at room temperature. The plate was again aspirated and washed 5 times and 100µl of substrate solution (ABTS Liquid Substrate Solution supplied by Peprotech®) was added to each well. The plate was incubated at room temperature for 5 minutes to allow color development to occur. Colour

development was assessed by absorbance at 405 nm (correction wavelength at 650 nm) using a ThermoScientific Multiskan plate-reader with the SkanIt (Research Edition) for Multiskan Spectrum 2.2 software.

Reliable standard curves were obtained when the O.D. readings did not exceed 0.2 units for the zero standard concentrations, or 1.2 units for the highest standard concentration. The plate was monitored at 5-minute intervals until desired O.D. readings were obtained. The typical range is 5-40 minutes but for every experiment performed the time frame was kept the same.

2.11.1 Enzyme-Linked Immunosorbent Assay (ELISA) of pneumolysin

A high-binding 96-well plate was coated with 1µg of IgG1- PLY4 antibody in each well and incubated overnight, at 4^{o}C. The plate was washed and then blocked for 2 hours. Then recombinant pneumolysin was added in the wells in a series of dilutions (100 to 1.56 ng/ml). The samples were also loaded and the plate was set for incubation. PLY polyclonal antibody was then added in each and the plate was incubated at room temperature. Then anti-rabbit IgG alkaline phosphatase was added in each well and the plate was incubated for 30 minutes at room temperature. To allow the colour to develop, para-Nitrophenylphosphate (PNPP - Sigma Aldrich®) was added in the wells. Colour development was assessed by absorbance at 405 nm using a ThermoScientific Multiskan plate-reader with the SkanIt (Research Edition) for Multiskan Spectrum 2.2 software.

2.12.0 Fluorescent detection assay

After an experiment with pneumococci, HBECs were washed 3 times with 1xPBS before fixation with 4% paraformaldehyde solution (Sigma Aldrich®) for 10 minutes. Then the

cells were washed 4 times with 1xPBS at 5-minute intervals per wash before permeabilisation with 0.1% Triton-X100. Then the cells were washed with 0.1% Triton-X100 for 15 minutes (5-minute intervals). Goat serum solution (3%) was added and incubated on a rocker for 1 hour at room temperature. The monoclonal and polyclonal antibodies were diluted with normal goat serum and PBS NGS/PBS solution (1:100 for ZO-1 polyclonal) and incubated with the cells overnight. Post incubation the antibody was removed and the cells were washed with 1xPBS for 15 minutes (5-minute intervals). The secondary antibody was diluted in PBS (1:1000) and incubated with the cells for 2 hours. Post incubation the cells were washed with 1xPBS for 1 hour (15 minute intervals). For microscopic visualization the cells were mounted with media containing 2-(4-amidinophenyl)-1H -indole-6-carboxamidine (DAPI), which stains the nuclei of cells.

2.13.0 Fluorescein isothiocyanate-dextran exclusion assay

To determine the capsular surface area of the pneumococci, a fluorescein isothiocyanate-dextran (Sigma Aldrich®) (FITC-dextran) exclusion assay was performed. Firstly the bacteria were cultured in BHI overnight to mid-log phase (OD_{600} = 0.5 (depending on the serotype/strain used). The bacterial culture was re-suspended in 1xPBS and then 2 µl of FITC-dextran were mixed with 10 µl of the suspension. Immediately after, 10 µl of the mixture were transferred to a glass slide (Thermo Fisher, Menzel-gläser, superfrost® plus) and a cover slip (Thermo Fisher, Menzel-gläser) was used to press the mixture on the slide in order to spread it evenly. The bacteria were visualized on a Nikon Eclipse 80i fluorescence microscope with 100x objective lens and photographed by a Hamamatsu C4742-95 camera. The determination of the capsular surface was achieved using the

ImageJ tool for analysis [342].

2.14.0 Graphical representation and statistical significance

All experiments were repeated 3 times (n=3). The standard error of mean was calculated. According to the number of variables in an experiment, one-way ANOVA or two-way ANOVA test would be used. For nonparametric tests a Mann-Whitney U test was used. All results were calculated with 95% confidence interval.

2.14.1 Advantages and disadvantages for using the Mann-Whitney U test

Advantages of the test: The Mann-Whitney U test does not require any assumptions on the distribution of the population. Thus, it is used when the shape of the distribution is not known, or there is no necessity to assume it [343].

Disadvantages: The Mann-Whitney U has a lower power than parametric tests. This means that, if there is a possible difference between two groups, the test is less likely to detect it [343].

Best Used: Because the Mann-Whitney U test is less powerful than a parametric test, and because the Central Limit Theorem allows us to assume normality in most cases (if the sample size is large), the Mann-Whitney U is best used for small data sets [343].

Materials **(Supplier if different)**	**Constituents (Supplier)**
Human Brain Endothelial Cell Media (Gibco™)	Fetal Bovine Serum (10%) (BioSera) Penicillin/Streptomycin (1%) (Sigma Aldrich®) L-Glutamine (1%) (Sigma Aldrich®) Hydrocortisone (0.01%) (Sigma Aldrich®) Endothelin growth factor 0.01% BioLabs
Human Astrocyte Media (Sigma Aldrich®)	Fetal Bovine Serum (10%) (BioSera) Penicillin/Streptomycin (1%) (Sigma Aldrich®) L-Glutamine (1%) (Sigma Aldrich®)
Collagen Type I	Collagen Solution - rat tail (Sigma Aldrich®)
Phosphate Buffer Saline	Cell washing solution (OXOID)
Trypsin (Sigma Aldrich®)	10x Trypsin Solution (Sigma Aldrich®)
Poly-D-lysine Hydrobromide	Poly-D-lysine Hydrobromide solution 0.05% (Sigma Aldrich®)
Trypan Blue	Trypan blue solution (Sigma Aldrich®)
Dimethyl Sulfoxide (DMSO)	Dimethyl Sulfoxide (Sigma Aldrich®)
Ethanol	Ethanol (Absolut) (Sigma Aldrich®)
Isopropanol	Isopropanol (99.9%) (Sigma Aldrich®)
Chloroform	Chloroform (99.9% isoamyl alcohol-free) (Sigma Aldrich®)
Trizol®	Guanidinium Isothyocyanate/Phenol (Sigma Aldrich®)
MTT	(3-(4,5-Dimethylthiazol-2-yl)-2,5-diphenyltetrazolium bromide) yellow powder (Sigma Aldrich®)
BCA	Bicinchoninic acid (ThermoFisher)
Phenol red-free media (Gibco™)	Fetal Bovine Serum (10%) (BioSera) Penicillin/Streptomycin (1%)(Sigma Aldrich®) L-Glutamine (1%) (Sigma Aldrich®)
Penicillin-G	Penicillin-G solution (10μg/ml)
Blood Agar Base	16 grams in 400ml distilled water (OXOID)
Brain-Heart Infusion	14.8 grams in 400ml of distilled water (OXOID)
Triton™ X-100 solution	Triton™ X-100 0.1% and 0.01% solutions (Sigma Aldrich®)
RNeasy®	RNA purification kit (Qiagen®)
Agilent Technologies	G3 Human Gene Expression Microarray Kit
IL-1β, IL-6, IL-8 ELISAs	Standard protein (Peprotech®) Avidin-HRP conjugate (Peprotech®) ABTS (Peprotech®) PBS (Peprotech®) Diluent (Peprotech®) Monoclonal (Mouse) and polyclonal (Rabit) antibodies for IL-1β, IL-6, IL-8 (Peprotech®)
Pneumolysin ELISA	PLY4 mouse monoclonal (abcam®) Rabbit polyclonal to PLY (abcam®) anti-rabbit IgG alkaline phosphatase (abcam®) PBS (Peprotech®) Diluent (Peprotech®)
PNPP	para-Nitrophenylphosphate (Sigma Aldrich®)

Materials (cont.)	**Constituents (cont.)**
Sodium Hydroxide (NaOH)	1 Molar NaOH solution
Mounting media with DAPI	2-(4-amidinophenyl)-1H -indole-6-carboxamidine (Sigma Aldrich®)
Tight junction protein 1	ZO-1 Rabbit polyclonal (Invitrogen™)
Normal Goat Serum	NGS (Sigma Aldrich®)
Secondary antibody	Alexa Fluor® 594 rabbit anti-goat IgG, for polyclonal antibodies (Invitrogen™)
FITC-Dextran	Fluorescein isothiocyanate with Dextran (2000 kDa) (Sigma Aldrich®)
SDS-PAGE/Western Blot	Nanopure Water (Sigma Aldrich®) 30% Acrylamide (Protogel – Gene flow) 1.5M Tris HCl pH 8.8 (Sigma Aldrich®) 1M Tris HCl pH 6.8 (Sigma Aldrich®) 10% SDS (Sigma Aldrich®) 10% Ammonium Sulphate (ThermoFisher) TEMED (Sigma Aldrich®)
Pneumolysin expression and isolation	Ampicillin (100 μg/ml) (Sigma Aldrich®) Sodium Phosphate (Sigma Aldrich®) Sodium Chloride (Sigma Aldrich®) Imidazole Reagent Plus® (Sigma Aldrich®) Brilliant Blue R250 (Sigma Aldrich®)
Hemolytic Assay	Red blood erythrocytes (OXOID)

Table of Materials used during this project Combinations of reagents for a single buffer, concentrations and suppliers are mentioned on the right column of the table.

CHAPTER 3.

Studies Of Pneumococcal Adherence And Invasion Of Human Brain Endothelial Cells And Human Astrocytes

3.0 Aims

Before establishing a bacterial Blood-Brain Barrier model (BBB), I first sought to investigate the interactions of various *Streptococcus pneumoniae* (pneumococcus) serotypes in culture with Human Brain Endothelial Cells (HBECs) and Primary Human Astrocytes (HA). At the time of undertaking this study, there were no prior studies of human brain cell interactions with pneumococci in co-culture. To reveal mechanisms of pneumococcal pathogenesis in vitro, I used HBECs and HA in monoculture to assess bacterial growth kinetics over time, adherence (attachment of bacteria on the cell surface) and invasion (bacteria found within the cell compartment).

Different pneumococcal serotypes were used in an effort to identify core bacterial processes and distinguish differences in overall virulence. The first step was to evaluate the growth of pneumococcal serotypes in co-culture with HBEC or HA.

3.1.0 *Streptococcus pneumoniae* serotype-2 interactions with Human Brain Endothelial Cells

The serotype-2, D39 strain was co-cultured with HBECs in 10-fold increasing doses from $1x10^4$ to $1x10^7$ colony forming units (CFU)/ml. Doses $1x10^6$ CFU/ml and $1x10^7$ CFU/ml were significantly higher 6 hours post incubation when compared against the other doses used ($^{\$\$}p<0.01$/$^{*}p<0.05$) as compared to $1x10^4$ CFU/ml and $1x10^5$ CFU/ml (figure 27).

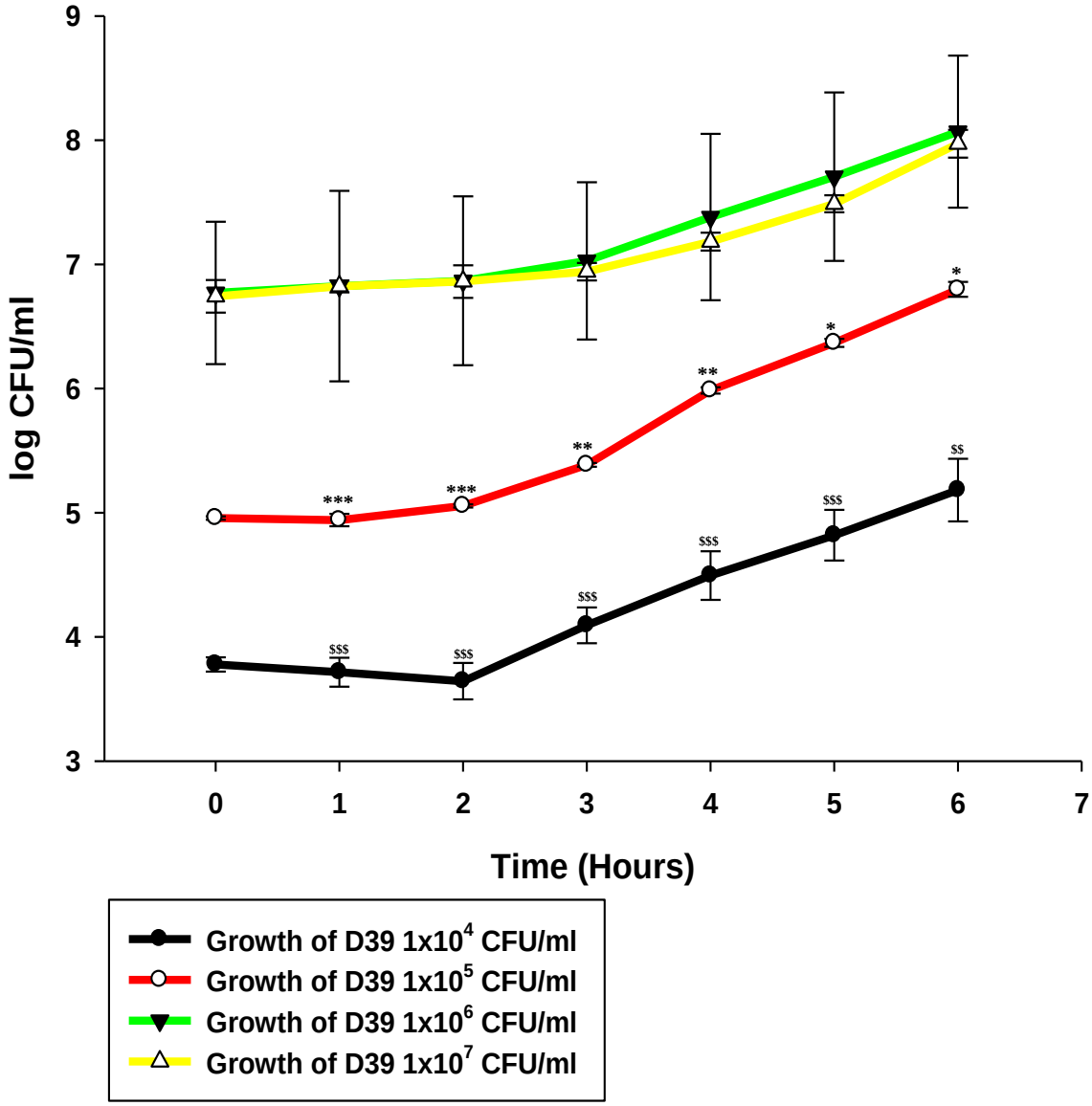

Figure 27| *Streptococcus pneumoniae* serotype-2 (strain D39) growth in co-culture with Human Brain Endothelial Cells Bacterial growth was monitored for a total of 6 hours. The experiment was repeated 3 times (n=3). The standard error of the mean was calculated (SEM). Significant differences are determined using a two-way ANOVA and relate to differences as compared to bacterial growth of $1x10^4$ CFU/ml and $1x10^5$ CFU/ml against bacteria of $1x10^6$ CFU/ml and $1x10^7$ CFU/ml. *P<0.05, **P<0.01, ***P<0.001, $^{\$\$}$P<0.01, $^{\$\$\$}$P<0.001.

Pneumococci were incubated with the HBEC for a total of 6 hours. Bacterial growth was monitored hourly by serial dilution of media onto blood agar. D39 grew successfully in

co-culture with HBECs at all doses tested (figure 1). The mean CFU varied significantly according to dose in two-way ANOVA analysis ($p<0.0001$).

3.1.1 *Streptococcus pneumoniae* serotype-2 adherence and invasion of Human Brain Endothelial Cells

D39 adherence to and invasion of HBECs was investigated at different CFU doses ($1x10^4$-$1x10^7$ CFU/ml).

Adherent pneumococci were detected only when $1x10^7$ CFU/ml were used (figure 28A). The highest CFUs of adherent pneumococci were observed 3 hours post infection, which accounts to 42% of the initial infection dose (figure 28A). No bacterial invasion was observed for any CFU used (figure 28B).

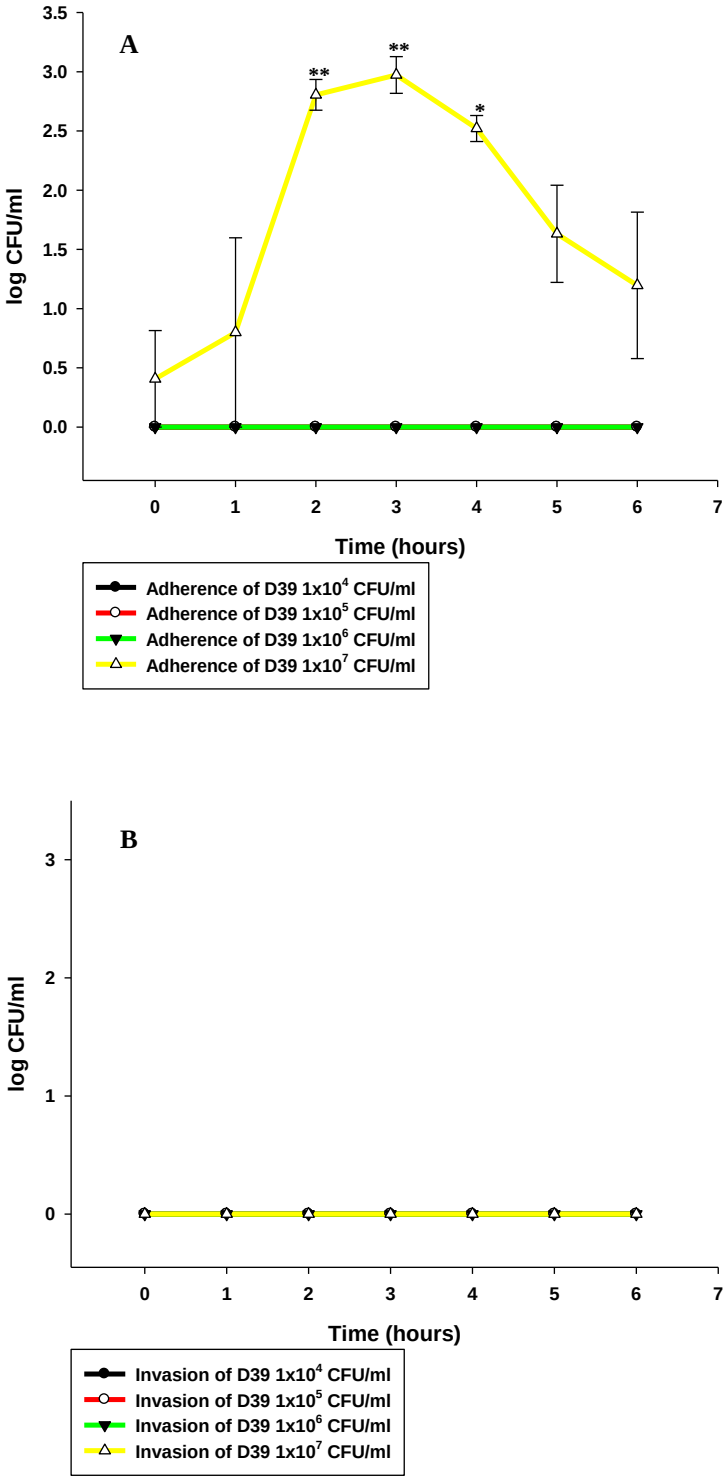

Figure 28| *Streptococcus Pneumoniae* serotype-2 (strain D39) adherence and invasion of Human Brain Endothelial Cells A) Adherence of D39 to HBECs. B) Invasion of D39 to HBECs. Bacterial adherence and invasion were monitored for a total of 6 hours. The experiment was repeated 3 times (n=3). The standard error of the mean was calculated (SEM). Significant differences are determined using a two-way ANOVA and relate to comparisons of adherent against invaded bacteria. *P<0.05, **P<0.01.

3.2.0 *Streptococcus pneumoniae* serotype-6B interactions with Human Brain Endothelial Cells

In order to identify differences between pneumococcal serotypes, a human clinical isolate from a meningitis case (serotype-6B) was used. The same conditions as with the experiment for the D39 strain were used and with doses of $1x10^6$ CFU/ml and $1x10^7$ CFU/ml.

Serotype 6 grew equally well in co-culture with HBECs when compared to D39. Bacterial numbers at 6 hours post infection were comparable for starting doses of $1x10^6$ CFU/ml and $1x10^7$ CFU/ml (figure 29).

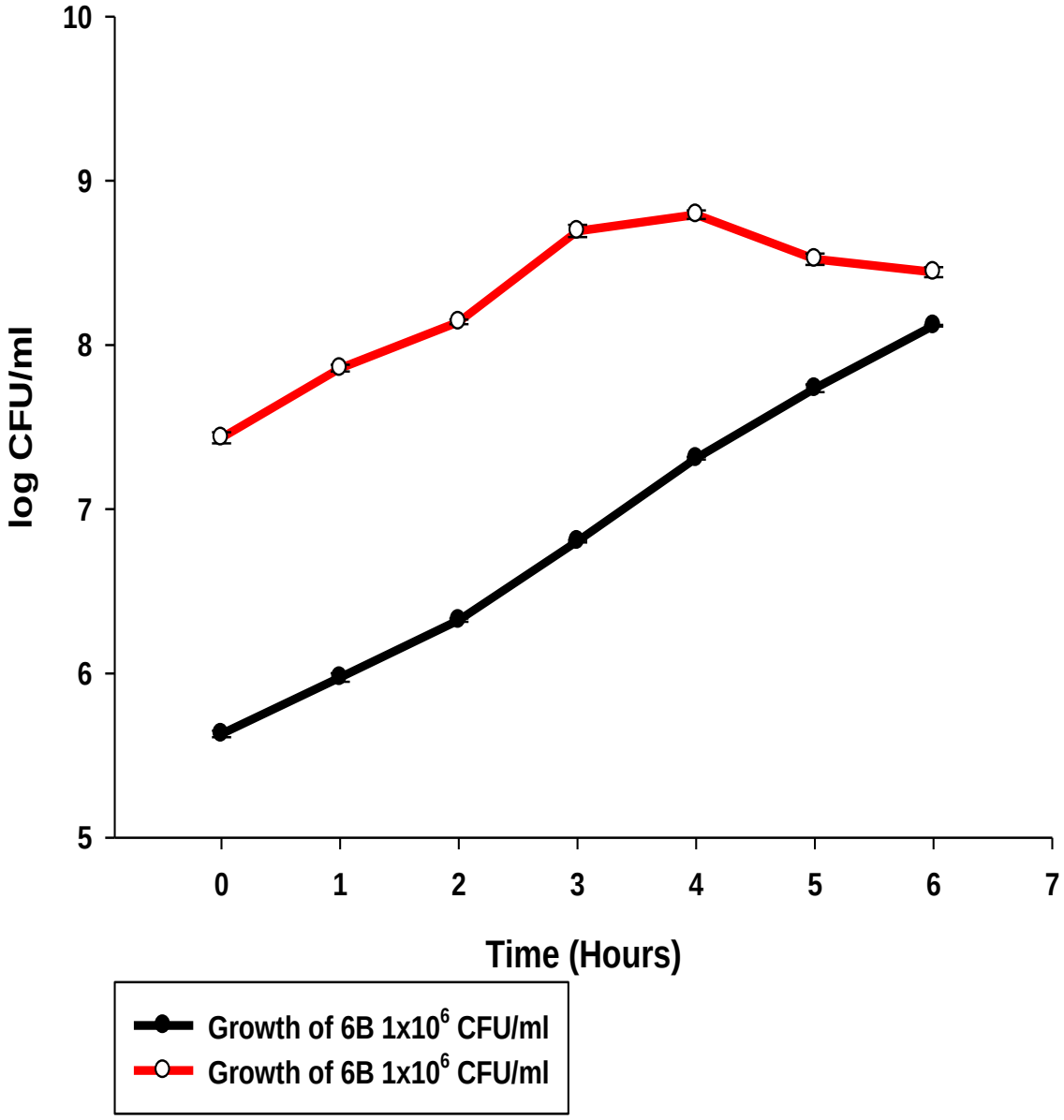

Figure 29| *Streptococcus Pneumoniae* serotype-6B growth in co-culture with Human Brain Endothelial Cells In co-culture with the cells $1x10^6$ CFU/ml and $1x10^7$ CFU/ml were used as the infective dose. Bacterial growth was monitored for a total of 6 hours. The experiment was repeated 3 times (n=3). The standard error of the mean was calculated (SEM).

The mean CFU varied significantly according to dose and duration of the experiment in two-way ANOVA analysis ($p<0.0001$ and $p<0.05$ respectively).

3.2.1 *Streptococcus pneumoniae* 6B adherence and invasion on Human Brain Endothelial Cells

There was no significant difference in pneumococcal adherence over time for any infection dose used (figure 30A). Invasion was detected with both infection doses used, but was significantly higher for $1x10^7$ CFU/ml at 5 and 6 hours post infection ($*p<0.05$ and $*p<0.01$) (figure 30B).

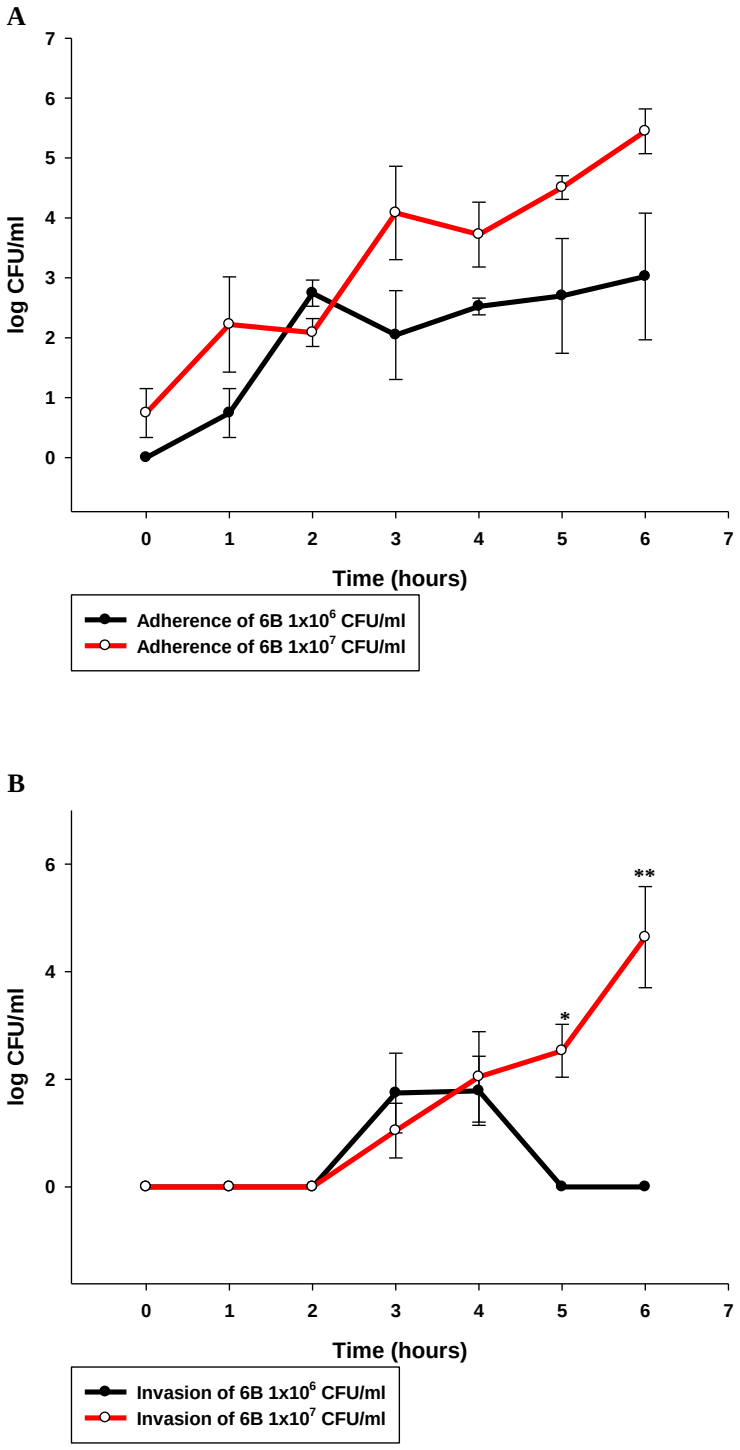

Figure 30| *Streptococcus pneumoniae* serotype-6B adherence to Human Brain Endothelial Cells A) Adherence of 6B to HBECs. B) Invasion of 6B to HBECs. Bacterial adherence and invasion were monitored for a total of 6 hours. The experiment was repeated 3 times (n=3). The standard error of the mean was calculated (SEM). Significant differences are determined using a two-way ANOVA and relate to comparisons for CFUs of adherent or invaded pneumococci from different infection doses. *P<0.05, **P<0.01.

The mean CFU varied significantly according to dose and duration of the experiment in two-way ANOVA analysis ($p<0.01$ for both variables characterized).

3.3.0 *Streptococcus pneumoniae* serotype-1 interactions with Human Brain Endothelial Cells

In an effort to include highly invasive clinical isolates from different geographical regions of the world in our study, pneumococcal serotype-1 was used. Serotype-1 is the dominant invasive disease-causing serotype across Sub-Saharan Africa and South-East Asia. The serotype-1 isolate used was recovered from a sepsis case in Malawi. Based on the results I described above, $1x10^7$ CFU/ml was chosen as the dose for the HBEC cell line.

3.3.1 *Streptococcus pneumoniae* Serotype-1 (S1) growth, adherence and invasion of Human Brain Endothelial Cells

Pneumococcal serotype-1 successfully grows when co-cultured with HBECs. Both adherence and invasion of the pneumococci was detected. Numbers of adhered and invaded bacteria were similar at 6 hours post infection (4.69 log CFU/ml for adherence and 4.19 log CFU/ml for invasion) (figure 31). Numbers of adherent bacteria outstripped those of invaded bacteria up to 4 hours post-infection (**$p<0.01$, *$p<0.05$), **$p<0.01$ and *$p<0.05$).

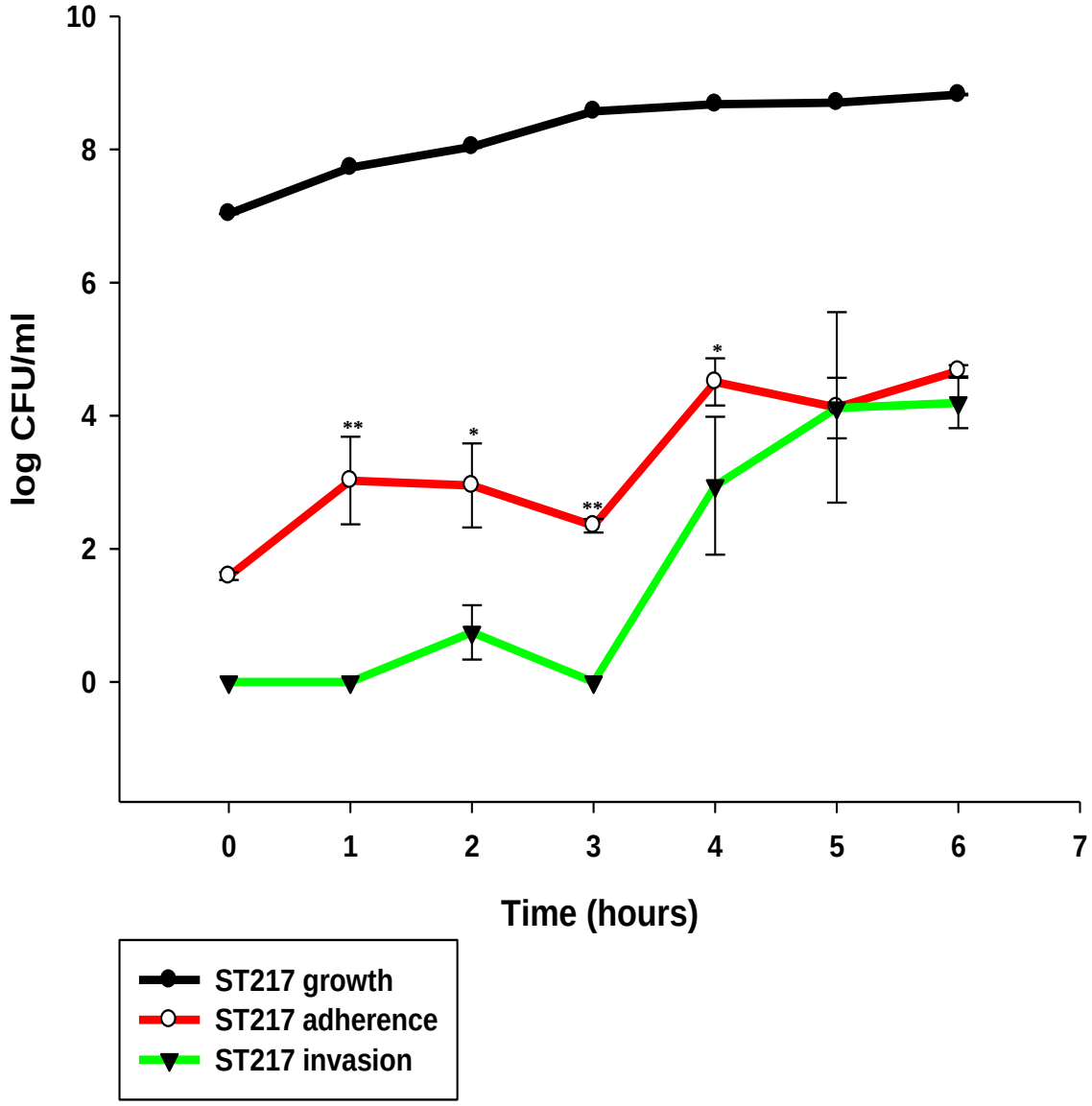

Figure 31| Growth, adherence and invasion of *Streptococcus pneumoniae* Serotype-1 (ST217) to Human Brain Endothelial Cells Bacterial growth, adherence and invasion were monitored for a total of 6 hours. The experiment was repeated 3 times (n=3). The standard error of the mean was calculated (SEM). Significant differences are determined using a two-way ANOVA and relate to differences as compared to bacteria that adhered on the cells *vs*. the bacteria which invaded the cells. *P<0.05, **P<0.01.

3.4.0 *Streptococcus pneumoniae* serotype-2 isogenic pneumolysin-deficient mutant (PLN-A) interactions with Human Brain Endothelial Cells

A pneumolysin deficient version of serotype-2 (D39) was used. The PLN-A strain was introduced in this project to determine the role of pneumolysin in adherence and invasion of pneumococci.

3.4.1 PLN-A growth, adherence and invasion of Human Brain Endothelial Cells

CFU counts for PLN-A declined over time (from log 7.23 CFU/ml at time zero to log 3.76 CFU/ml at 6hrs post-incubation). No bacteria were detected adhered to or within HBEC cells throughout this experiment (figure 32).

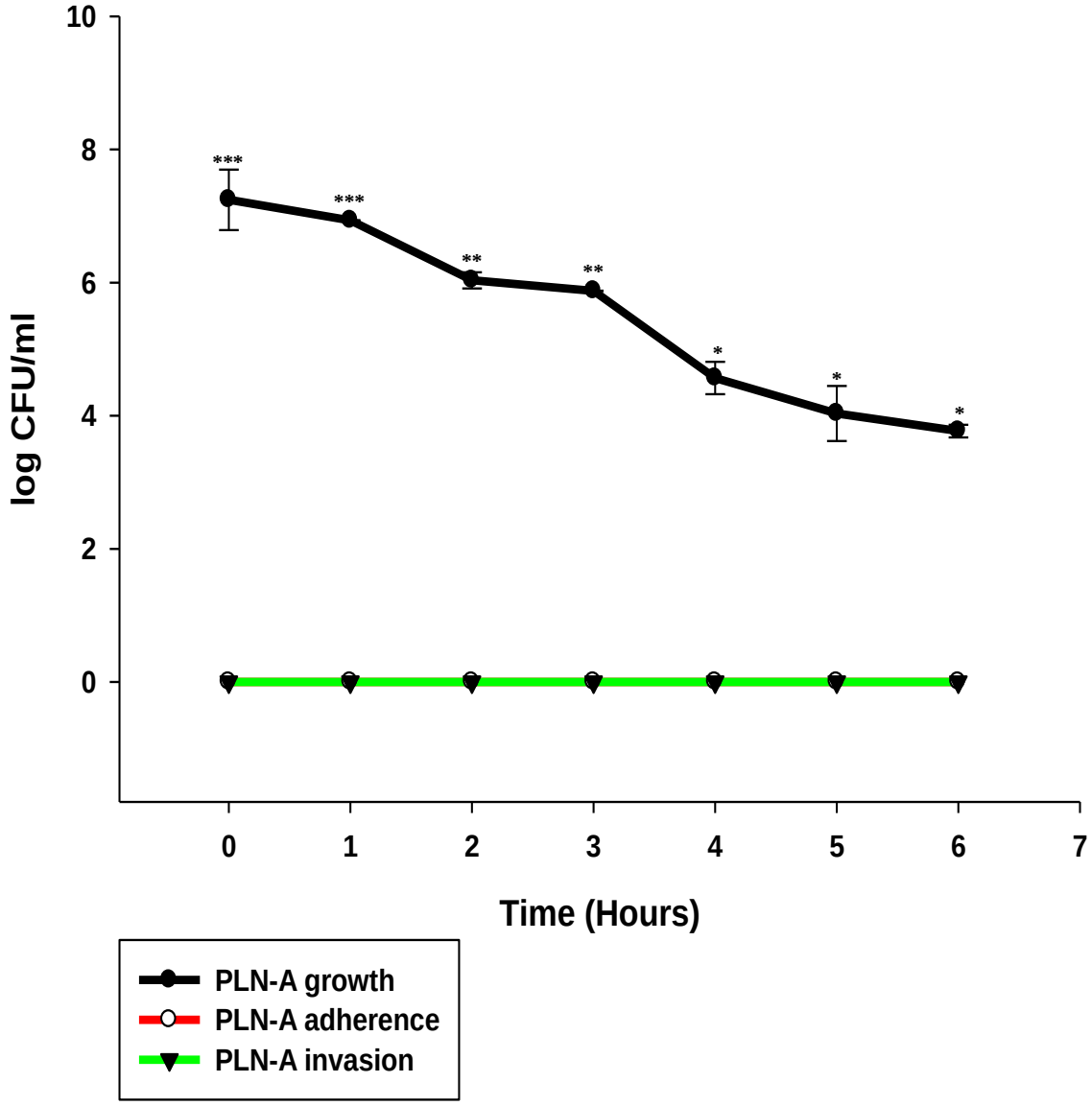

Figure 32| Growth, adherence and invasion of serotype-2 isogenic pneumolysin mutant (PLN-A) to Human Brain Endothelial Cells Bacterial growth, adherence and invasion were monitored for a total of 6 hours. The experiment was repeated 3 times (n=3). The standard error of the mean was calculated (SEM). Significant differences are determined using a two-way ANOVA and relate to differences as compared to bacterial growth against adherence or invasion. *P<0.05, **P<0.01, ***P<0.001.

3.5.0 Comparison of *Streptococcus pneumoniae* serotypes 1, 2, 6B and the pneumolysin deficient serotype-2 strain

I compared the growth, adherence and invasion characteristics of 4 different pneumococcal strains on HBECs at the optimised dose of infection ($1x10^7$ CFU/ml). Each of these pneumococcal strains was used under the same conditions (dose, detection methods, and incubation periods), for a total of 6 hours.

3.5.1 Growth (composite construct of previous experiments)

Growth over time was detected for serotypes 1 (17% by 6 hours), 2 (6%) and 6B (11%), whereas PLN-A CFU numbers declined over time (24%), despite similar counts to the other strains at time 0 (figure 33A+B). PLN-A showed a log 5 difference in bacterial numbers versus the other strains by 6 hours post infection (PLN-A vs. D39 *$p<0.05$, PLN-A vs. 6B **$p<0.01$, PLN-A vs. S1 **$p<0.01$) (figure 33A). Differences in growth were also observed between D39 and 6B as well D39 and S1 (**$p<0.01$ for both comparisons made) (figure 33A).

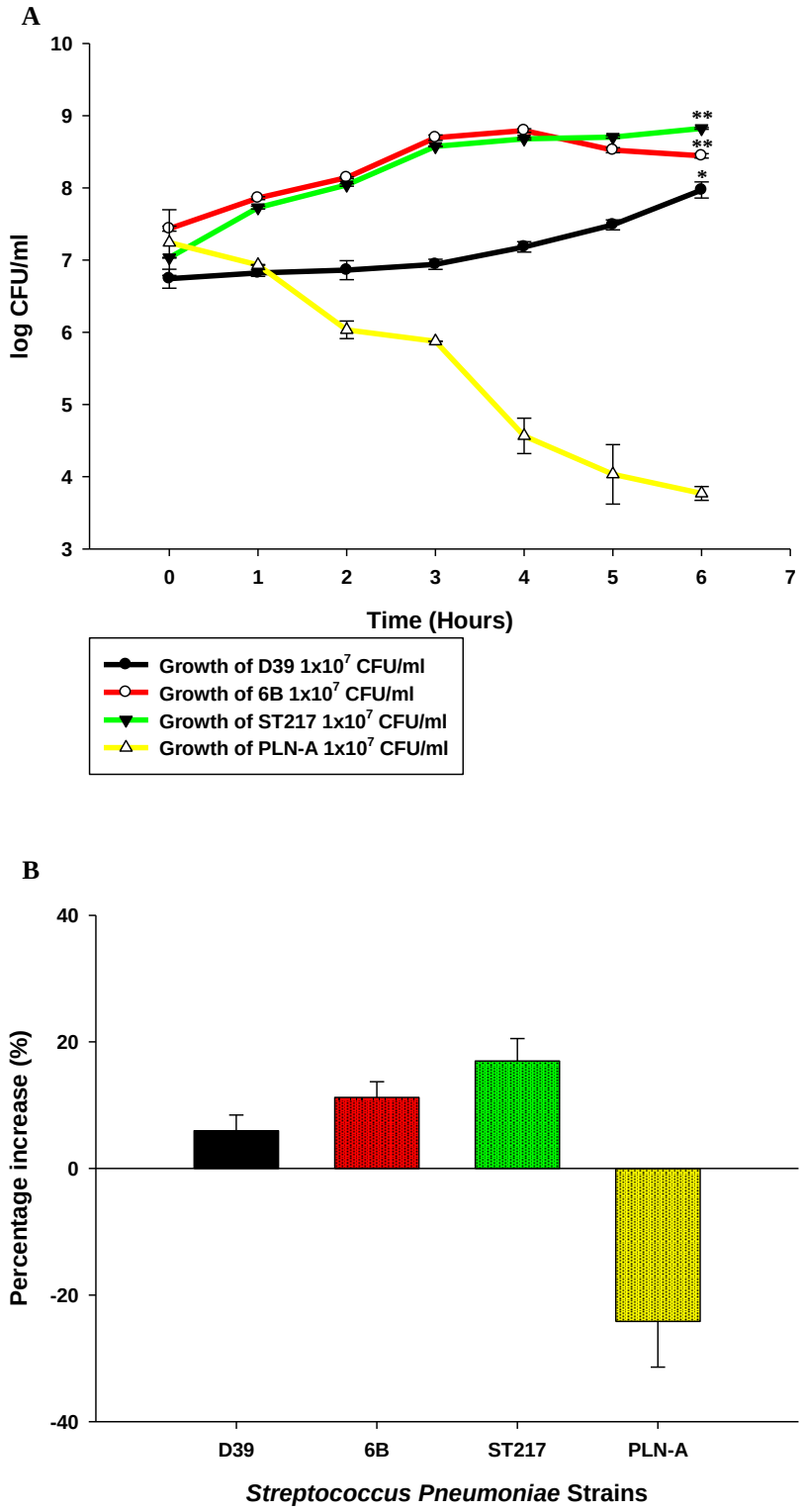

Figure 33| Growth comparisons of serotypes 1, 2, 6B on Human Brain Endothelial Cells A) Growth comparisons of the serotypes used at $1x10^7$ CFU/ml. B) Overall percentage of growth for the serotypes used. The experiment was repeated 3 times (n=3). The standard error of the mean was calculated (SEM). Significant differences are determined using a two-way ANOVA and relate to differences as compared to bacterial growth of the serotypes 1, 2, 6B against the PLN-A isogenic mutant. *P<0.05, **P<0.01.

3.5.2 Adherence (composite construct of previous experiments)

Adherence for serotypes 1 and 6B increased over time. There was a significant difference in adherence between the different serotypes used; with D39 declining in numbers three hours post infection in comparison to S1 and 6B (*$p<0.05$ for both) (figure 34A).

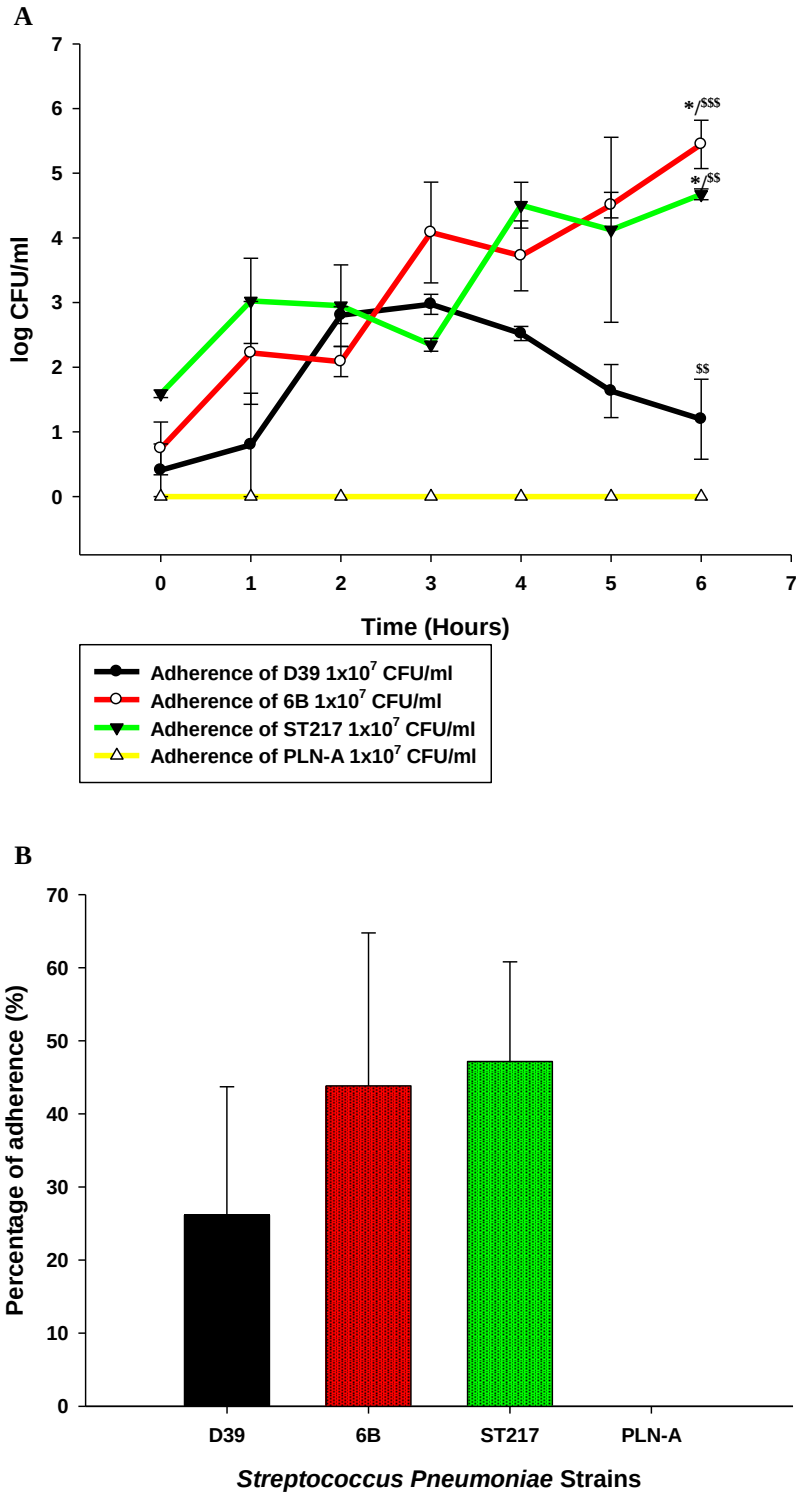

Figure 34| Adherence comparisons of serotypes 1, 2, 6B to Human Brain Endothelial Cells A) Adherence comparisons of the serotypes used at $1x10^7$ CFU/ml. B) Overall percentage of adherence for the serotypes used. The experiment was repeated 3 times (n=3). The standard error of the mean was calculated (SEM). Significant differences are determined using a two-way ANOVA and relate to differences as compared to bacterial adherence of the 6B and S1 serotypes against the D39 strain (*) and the 6B and S1 serotypes against the PLN-A isogenic mutant ($). *P<0.05, **P<0.01, ***P<0.001. $^{\$}$P<0.05, $^{\$\$}$P<0.01, $^{\$\$\$}$P<0.001.

The CFU counts for adherent D39 were significantly reduced in comparison to serotype-1 or -6B. The CFU counts for adherent S1 pneumococci reached approximately 50% of the initial dose of infection (figure 34B). The PLN-A mutant was not detected in this experiment.

3.5.3 Invasion (composite construct of previous experiments)

Similar numbers of invaded pneumococci were observed for S1 and 6B up to 4 hours post infection (figure 35A). As figure 35B shows, no invasion was detected for D39 or PLN-A.

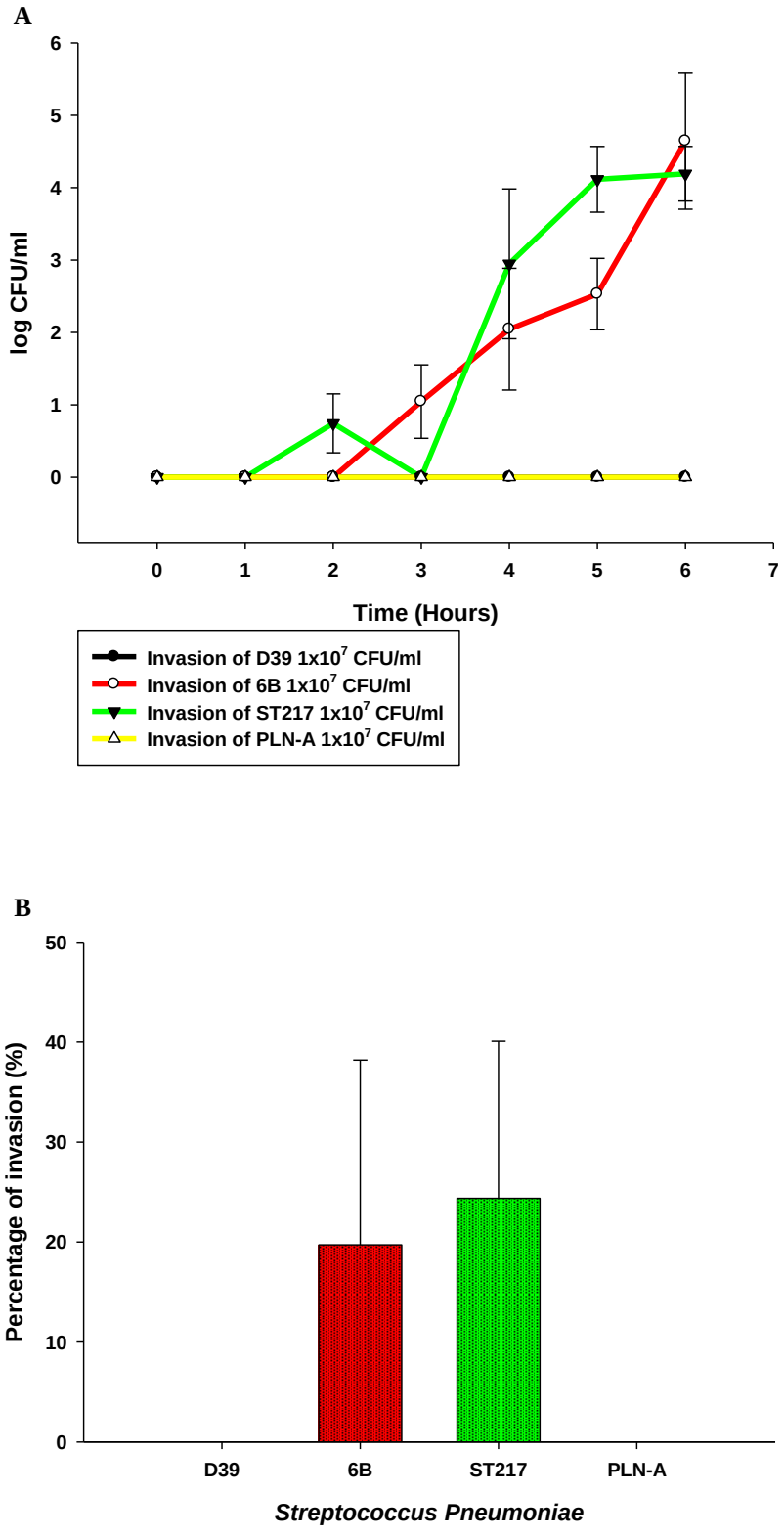

Figure 35| Invasion comparisons of serotypes 1, 2, 6B to Human Brain Endothelial Cells A) Invasion comparisons of the serotypes used at $1x10^7$ CFU/ml. B) Overall percentage of invasion for the serotypes used. The experiment was repeated 3 times (n=3). The standard error of the mean was calculated (SEM).

3.6.0 *Streptococcus pneumoniae* serotype-2 growth in primary human astrocytes

I next sought to determine whether bacterial growth, adhesion and invasion on human astrocytes (HA) differed from what I had observed with HBECs. The D39 strain was co-cultured with HA in 10-fold increasing doses of CFU from $1x10^4$ to $1x10^7$ CFU/ml.

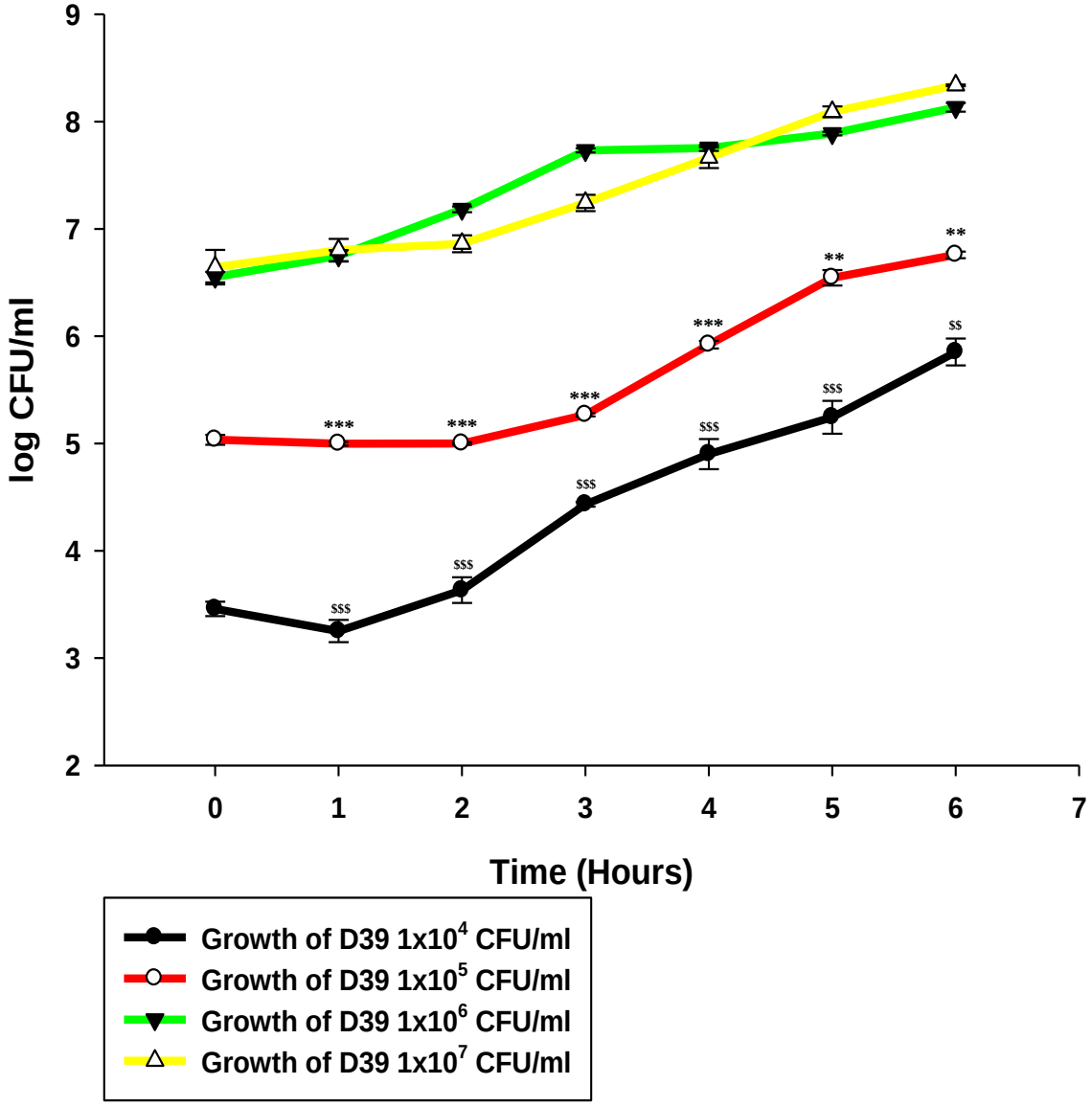

Figure 36| *Streptococcus pneumoniae* serotype-2 (strain D39) growth in co-culture with Human Astrocyte Cells Bacterial growth was monitored for a total of 6 hours. The experiment was repeated 3 times (n=3). The standard error of the mean was calculated (SEM). Significant differences are determined using a two-way ANOVA and relate to differences as compared to bacterial growth of $1x10^4$ CFU/ml and $1x10^5$ CFU/ml against bacteria of $1x10^6$ CFU/ml and $1x10^7$ CFU/ml. **P<0.01, ***P<0.001, $^{\$\$}$P<0.01, $^{\$\$\$}$P<0.001.

These experiments confirmed that D39 grew when co-cultured with HA (Figure 36). Doses $1x10^6$ CFU/ml and $1x10^7$ CFU/ml were significantly higher 6 hours post incubation when compared against the other doses used ($^{\$\$}p<0.01$/$^{**}p<0.01$).

3.6.1 *Streptococcus pneumoniae* serotype-2 adherence and invasion of primary human astrocytes

As previously, a range of pneumococcal CFUs ($1x10^4$ - $1x10^7$ CFU/ml) was tested.

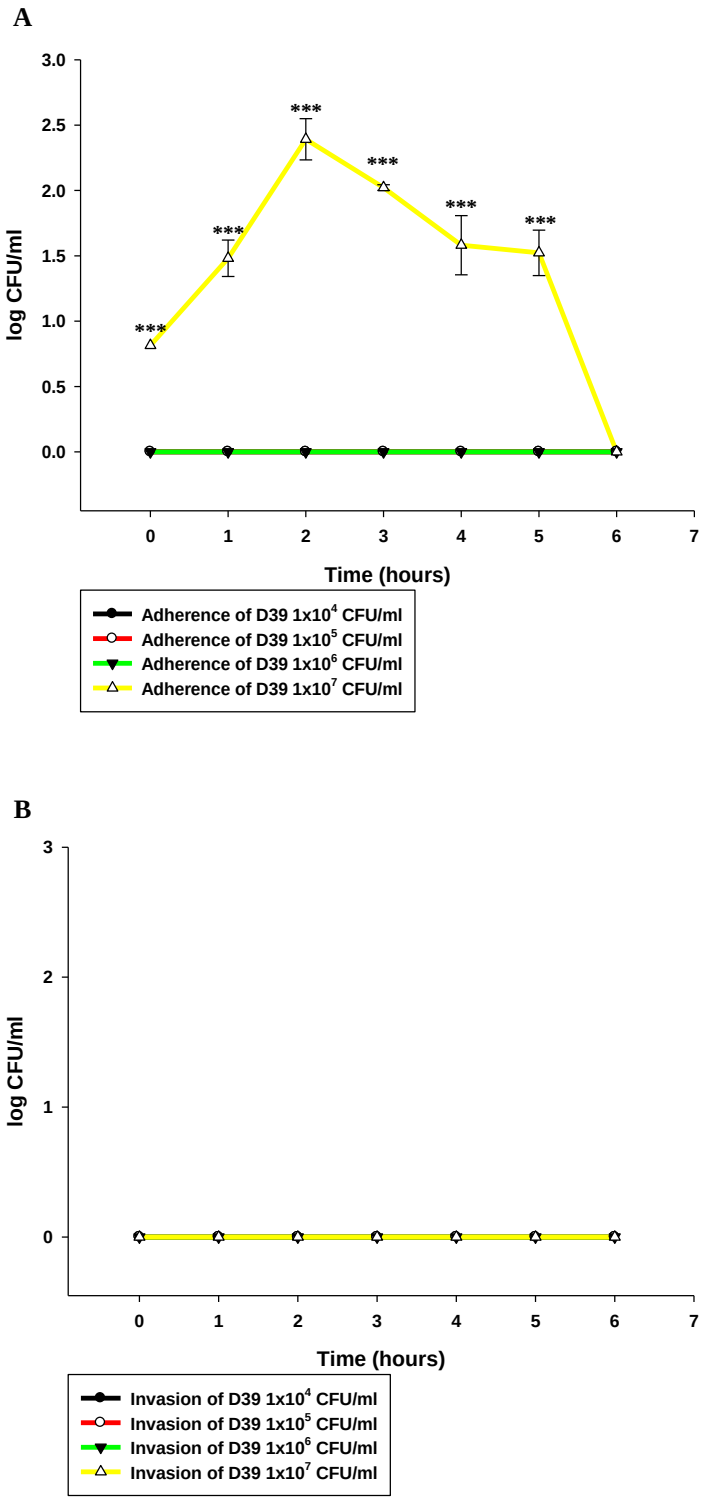

Figure 37| *Streptococcus pneumoniae* serotype-2 (strain D39) adherence and invasion on Human Astrocyte Cells
A) Adherence of D39 to HA. B) Invasion of D39 to HA. The experiment was repeated 3 times (n=3). Bacterial adherence and invasion were monitored for a total of 6 hours. The standard error of the mean was calculated (SEM). Significant differences are determined using a two-way ANOVA and relate to differences as compared to bacterial of the different doses used in this experiment. ***P<0.001.

Adherent pneumococci were detected only when $1x10^7$ CFU/ml (***$p<0.001$ for all the time points compared to other infection doses). The highest CFUs of adherent pneumococci were observed 2 hours post infection, which accounts to 32% of the initial infection dose (figure 37A). No bacterial invasion was observed for any dose used (figure 37B).

3.7.0 *Streptococcus pneumoniae* 6B growth on primary human astrocytes

Serotype-6B was successfully detected in co-culture with HA. The mean CFU varied significantly according to dose and duration of the experiment in two-way ANOVA analysis ($p<0.001$) (figure 38).

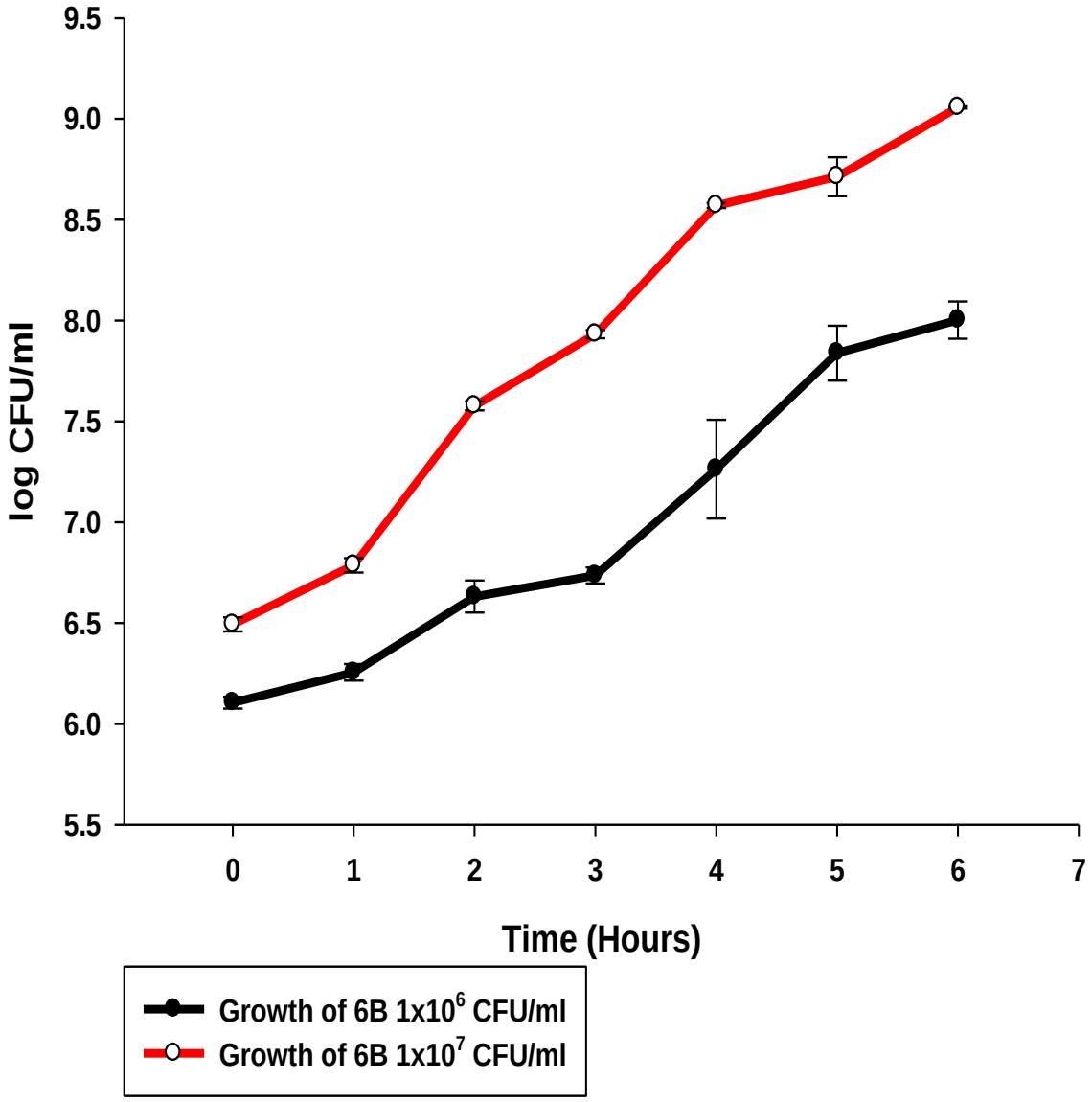

Figure 38| *Streptococcus pneumoniae* serotype-6B growth in co-culture with primary Human Astrocyte Cells Bacterial growth was monitored for a total of 6 hours. In co-culture with the cells, $1x10^6$ CFU/ml and $1x10^7$ CFU/ml were used as the infective dose. The experiment was repeated 3 times (n=3). The standard error of the mean was calculated (SEM).

3.7.1 *Streptococcus pneumoniae* 6B adherence and invasion of primary human astrocytes

Adherent pneumococci were detected within 3 hours when using $1x10^6$ CFU/ml. Adherent pneumococci were detected 1-hour post infection when $1x10^7$ CFU/ml were used. No significant differences were observed between numbers of adherent pneumococci (figure 39A). Invaded pneumococci were detected only when $1x10^7$ CFU/ml was used, at 5 and 6 hours post infection. The mean invaded CFU count varied significantly according to dose and duration of the experiment in two-way ANOVA analysis ($p<0.001$) (figure 39B).

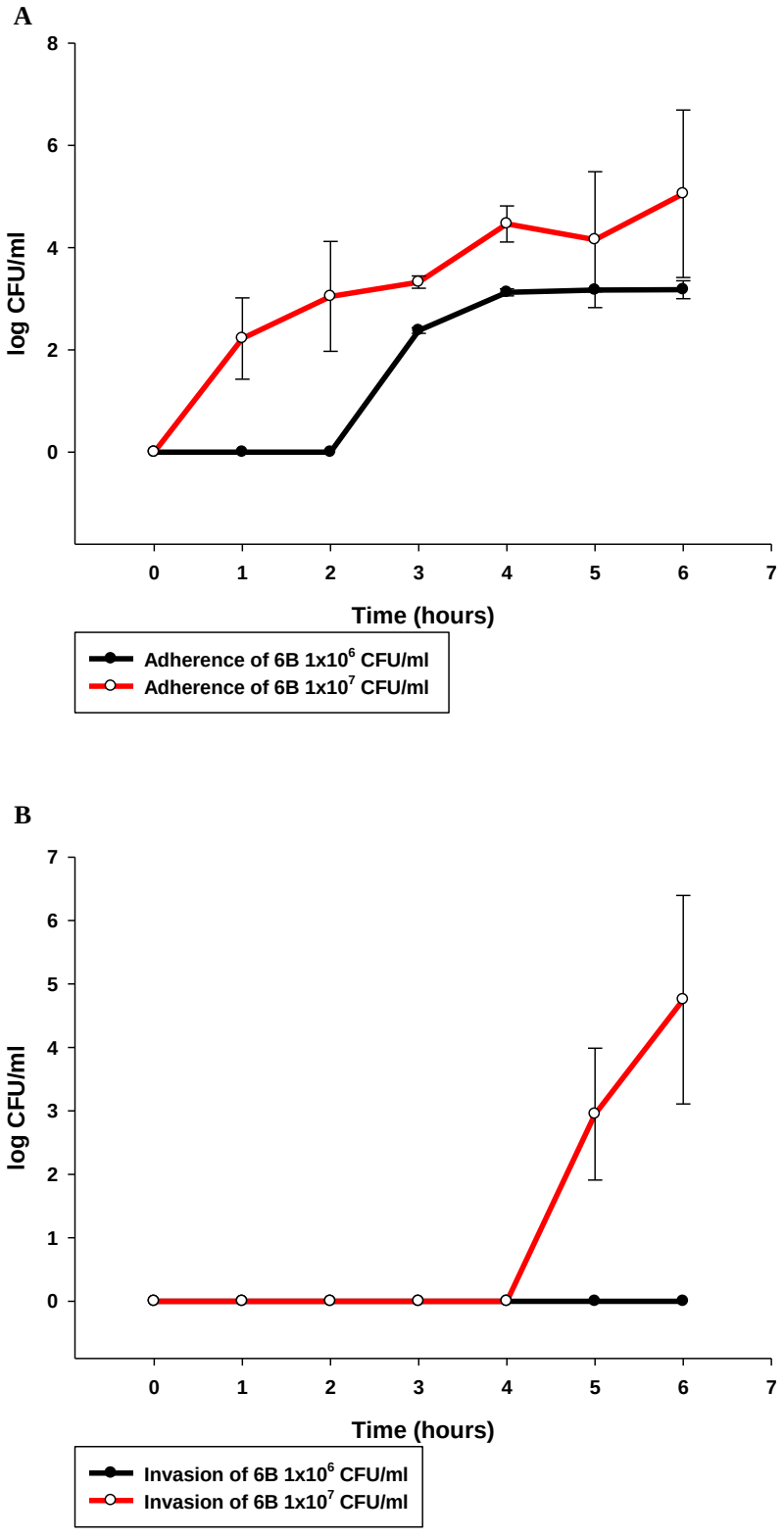

Figure 39| ***Streptococcus pneumoniae* serotype-6B adherence to primary Human Astrocyte cells** A) Adherence of 6B to HA. B) Invasion of 6B to HA. Bacterial adherence and invasion were monitored for a total of 6 hours. The experiment was repeated 3 times (n=3). The standard error of the mean was calculated (SEM).

3.8.0 *Streptococcus pneumoniae* serotype-1 growth, adherence and invasion of HA

S1 grew significantly in co-culture with HA, reaching ~$1x10^9$ CFU/ml by 6 hours post infection. Adherent pneumococci were detected throughout the experiment and invaded pneumococci were detected from 3 hours post infection. There was a 2-fold increase for adherent pneumococci 6 hours post infection in comparison to the invaded pneumococci (4.61 log CFU/ml for adherence and 2.78 log CFU/ml for invasion). There was a significant difference between growth, adherence and invasion for all compared time points (***$p<0.001$) (figure 40).

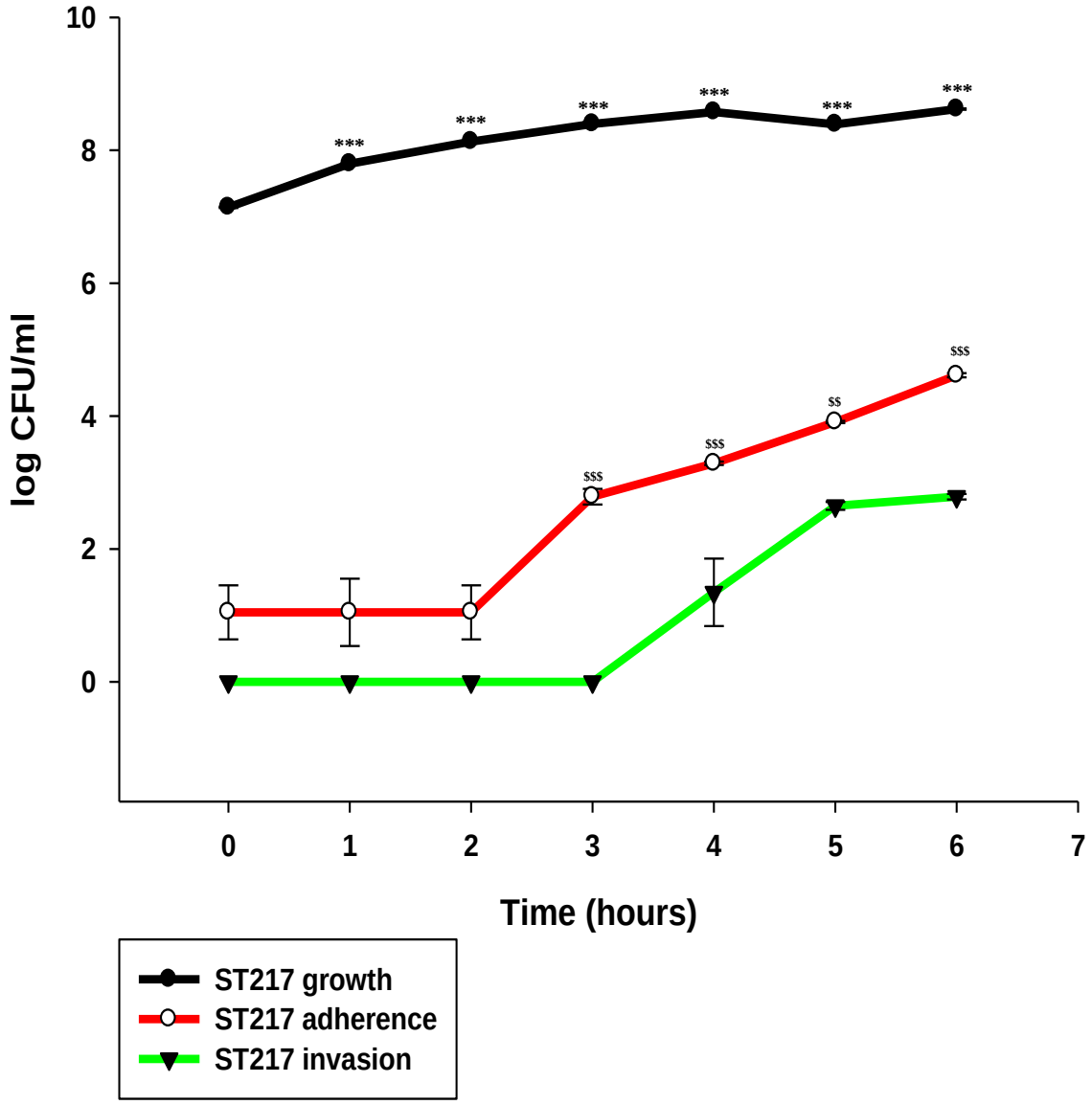

Figure 40| Growth, adherence and invasion of serotype-1 in co-culture with primary Human Astrocyte Cells Bacterial growth, adherence and invasion were monitored for a total of 6 hours. The experiment was repeated 3 times (n=3). The standard error of the mean was calculated (SEM). Significant differences are determined using a two-way ANOVA and relate to differences as compared to the process of bacterial growth against adherence or invasion (*) and adherence against invasion ($). ***P<0.001. $$P<0.01, $$$P<0.001.

3.9.0 *Streptococcus pneumoniae* serotype-2 isogenic pneumolysin negative mutant (PLN-A)

The pneumolysin deficient strain was also used in an effort to determine the role of pneumolysin in adherence and invasion.

3.9.1 PLN-A growth, adherence and invasion of HA

PLN-A CFU counts declined over time, dropping to log 2.66 CFU / ml by 6 hours post infection (figure 41). Adherent and invaded pneumococci were not detected during this experiment (figure 41).

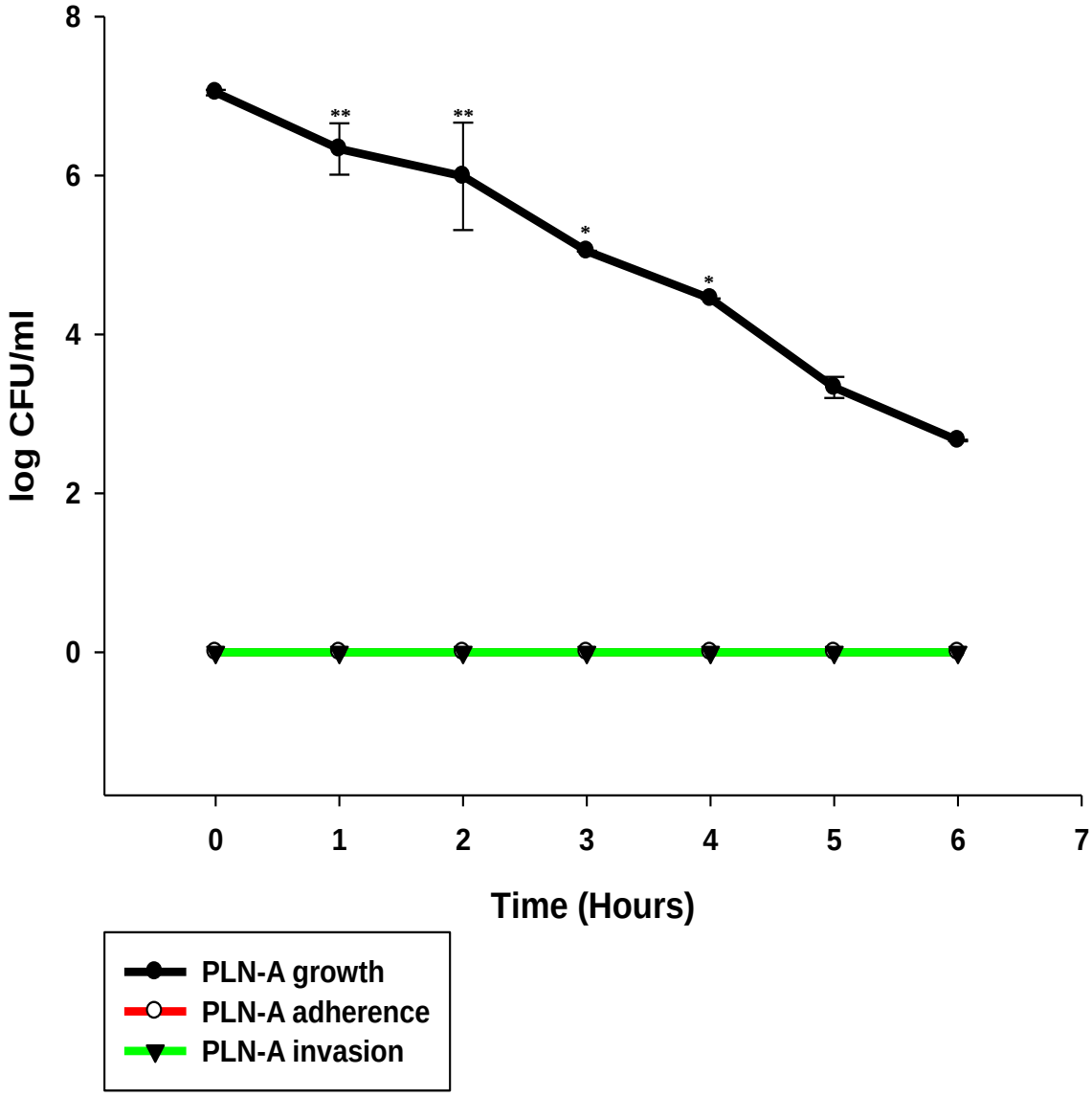

Figure 41| Growth, adherence and invasion of PLN-A to Human Astrocyte Cells Bacterial growth, adherence and invasion were monitored for a total of 6 hours. The experiment was repeated 3 times (n=3). The standard error of the mean was calculated (SEM). Significant differences are determined using a two-way ANOVA and relate to differences as compared to bacterial growth against adherence or invasion. *P<0.05, **P<0.01.

3.10.0 Comparison of *Streptococcus pneumoniae* serotypes and a pneumolysin deficient strain

I compared the growth, adherence and invasion characteristics of 4 different pneumococcal strains on HA at the optimised dose of infection ($1x10^7$ CFU/ml). Each of these pneumococcal strains was used under the same conditions (dose, detection methods, and incubation periods), for a total of 6 hours.

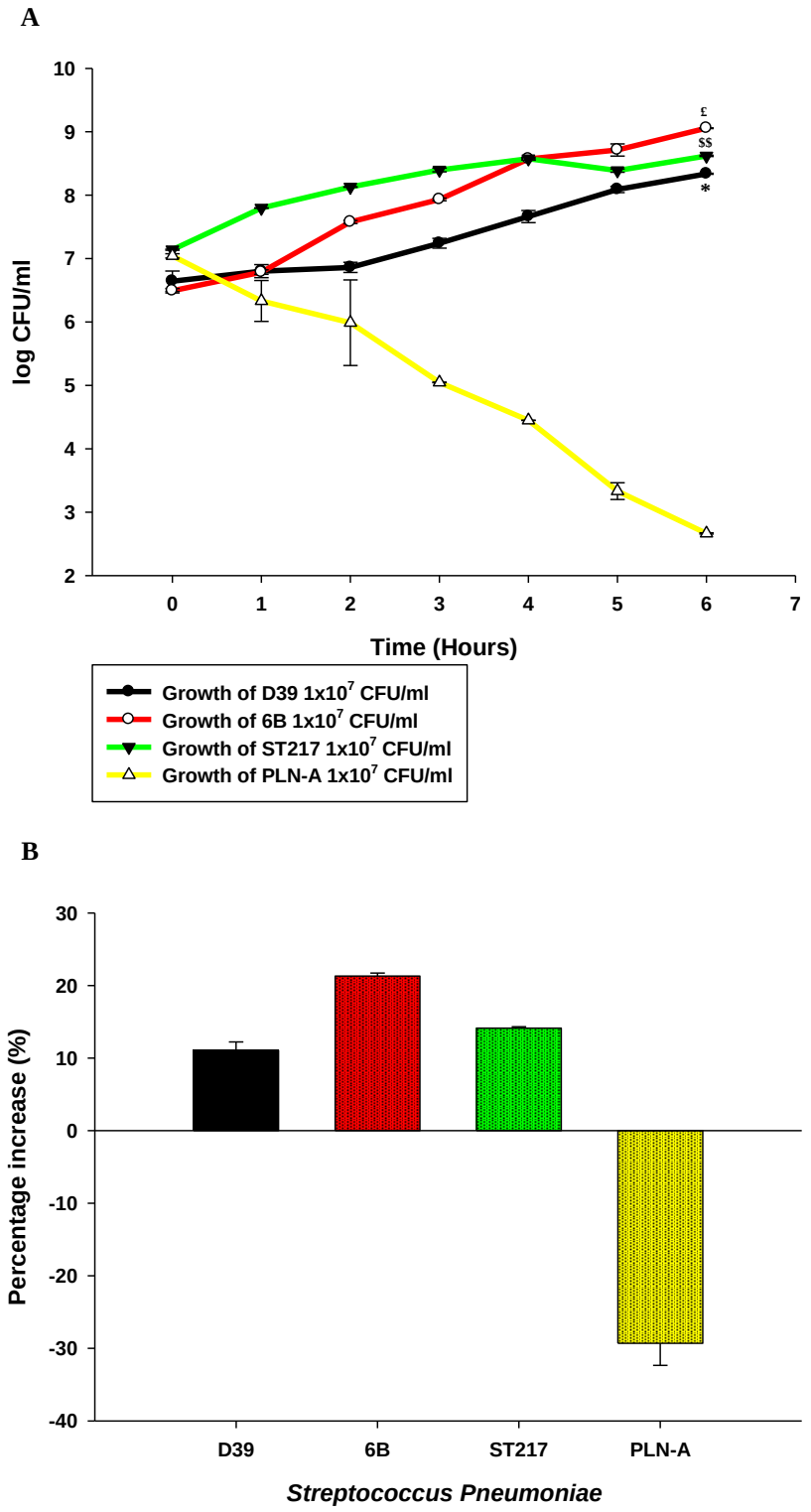

Figure 42| Growth comparisons of serotypes 1, 2, 6B to Human Astrocyte Cells A) Growth comparisons of the serotypes used at $1x10^7$ CFU/ml. B) Overall percentage of growth for the serotypes used. The experiment was repeated 3 times (n=3). The standard error of the mean was calculated (SEM). Significant differences are determined using a two-way ANOVA and relate to differences as compared to the growth of the PLN-A strain against the D39 (*), 6B ($^{\$}$) and S1 ($^{£}$). *P<0.05. $^{\$\$}$P<0.01. $^{£}$P<0.05.

3.10.1 Growth (composite construct of previous experiments)

There was an increase in CFU counts for serotypes-1 (14% by 6 hours), -2 (11%) and -6B (21%) over time, whereas PLN-A CFU counts declined (figure 42A+B). There was a significant difference of CFUs when PLN-A was compared against serotype-1 -2 and -6B at 6 hours post infection (*$p<0.05$, $^{\$\$}p<0.01$ and $^{£}p<0.05$ respectively).

3.10.2 Adherence (composite construct of previous experiments)

There was a significant increase in numbers of adherent pneumococci on HAs over time when serotype-1 and -6B were used. D39 adherent pneumococci declined over time and significantly differed from the serotype-1 and -6B adherent pneumococci (*$p<0.05$ for both comparisons) (figure 43A). No adherent pneumococci were detected for PLN-A (figure 43A+B).

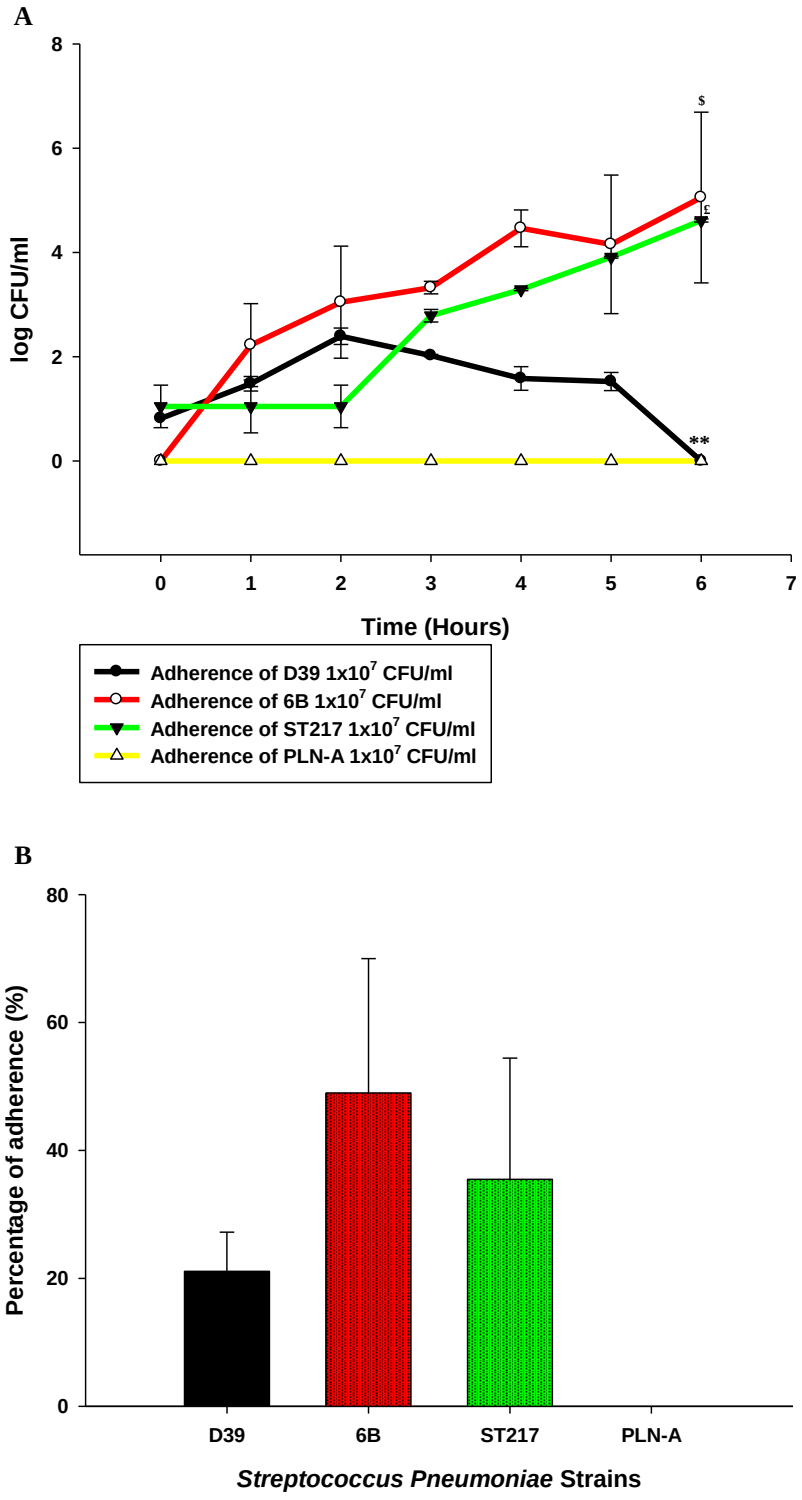

Figure 43| Adherence comparisons of serotypes 1, 2, 6B to Human Astrocyte Cells A) Adherence comparisons of the serotypes used at $1x10^7$ CFU/ml. B) Overall percentage of adherence for the serotypes used. The experiment was repeated 3 times (n=3). The standard error of the mean was calculated (SEM). Significant differences are determined using a two-way ANOVA and relate to differences as compared to the adherence of the PLN-A strain against the D39 (*), 6B ($^{\$}$) and S1 ($^{£}$). **P<0.01. $^{\$}$P<0.05. $^{£}$P<0.05.

3.10.4 Invasion (composite construct of previous experiments)

None of the serotypes used invaded cells up to 4 hours post incubation. Serotype-6B invaded HA cells by 5 hours post infection whereas S1 invaded HA cells by 4 hours. Serotype-6B had the highest number of invaded pneumococci 6 hours post infection (figure 44A). There was no evidence of pneumococcal invasion when D39 or PLN-A was used. Serotype-6B showed the highest invaded CFUs of all serotypes (figure 44B).

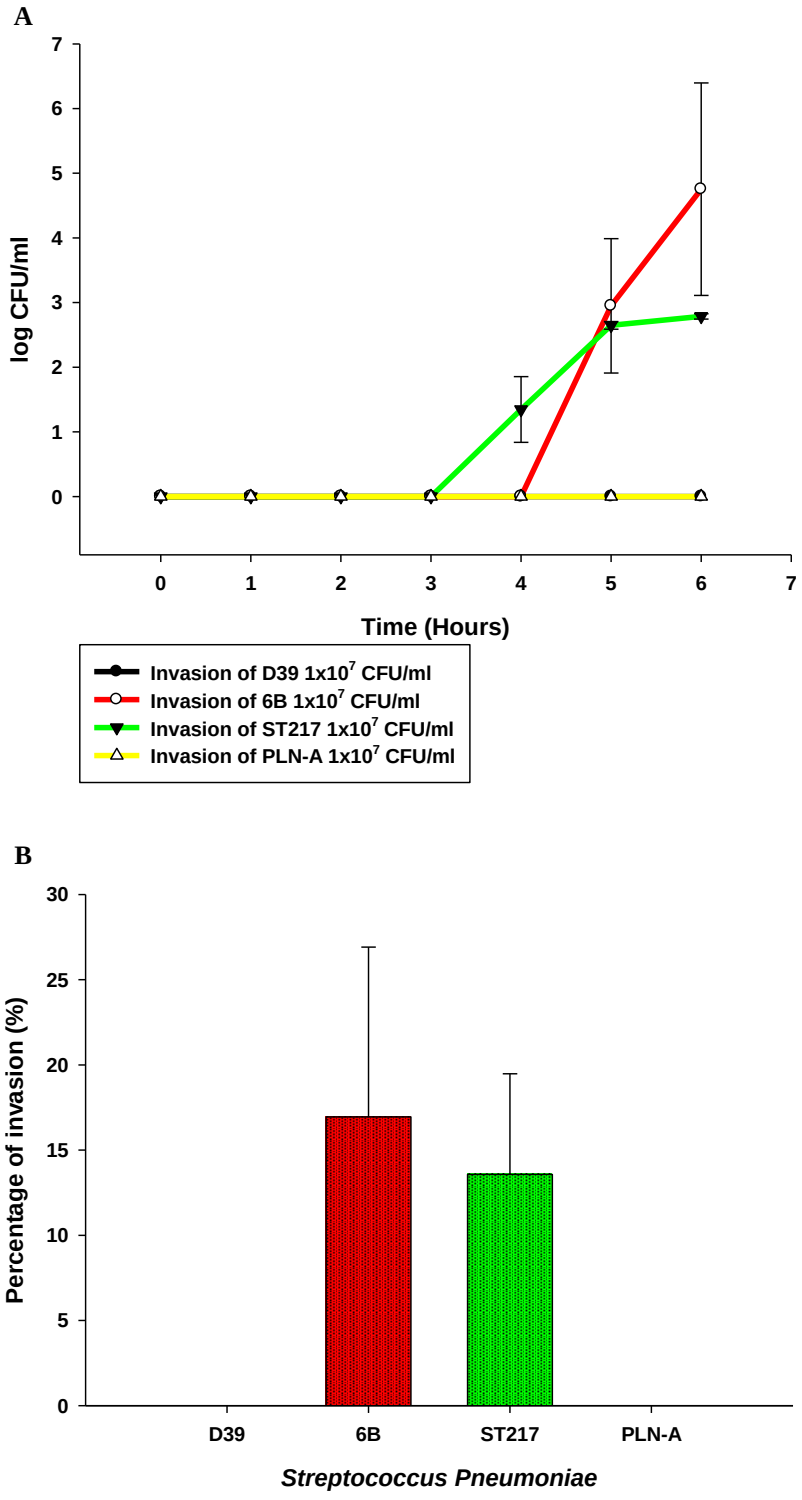

Figure 44| Invasion comparisons of serotypes 1, 2, 6B to Human Astrocyte Cells A) Invasion comparisons of the serotypes used at $1x10^7$ CFU/ml. B) Overall percentage of invasion for the serotypes used. The experiment was repeated 3 times (n=3). The standard error of the mean was calculated (SEM).

3.11.0 Discussion

During the monoculture experiments in this project, I investigated the growth, adherence and invasion of different clinical pneumococcal serotypes on HBECs and HAs, something which has not previously been published. It was evident that the most virulent strains were the serotype-1 and -6B clinical isolates. In contrast, serotype-2 exhibited little growth and its pneumolysin deficient isogenic mutant PLN-A showed significant reductions of CFUs when cultured with either cell line, suggesting that pneumolysin plays a key role in pneumococcal survival. All serotypes grew successfully (and comparably) in bacterial broth, **signifying that the declining numbers of PLN-A in co-culture with cell lines was not due to an inherent growth defect carried by the strain**. The dominant serotypes in regard to adherence were S1 and 6B. Adherence of serotype-2 pneumococci declined over time whereas PLN-A did not exhibit any levels of adherence. With serotype-6B having the highest overall levels of virulence (as determined by its ability to adhere and invade host tissues) in both cell lines, it was selected as the main isolate for experiments with the BBB model. Since pneumococci will be introduced in a system where gravitational flow is present (due to the pore membrane), serotype-2 (strains D39 and PLN-A) were also selected for use in the BBB model. The extensively investigated lab-adapted serotype 2 pneumococci (D39) (investigated for the last 100 years, [344]), will allow me to compare the general behavior of pneumococci in regards to adhesion and invasion. This will also enable me to separate common mechanisms followed by the D39 when comparing it with the clinical isolates.

Only serotype-1 and -6B were capable of invading HBECs or HA during a 6-hour experiment. Serotype 1 had a higher overall number of pneumococci, which invaded in comparison to 6B when co-cultured with HBECs whereas the opposite was observed when the comparison was made for pneumococci co-cultured with HA.

3.12.0 Conclusion

In this chapter, the growth, adherence and invasion of various *Streptococcus pneumoniae* serotypes were evaluated. Each serotype was found to behave differently during co-incubation with either HBECs or HA. The serotype-6B grew, adhered and invaded these cells in greater numbers and efficiency than the other serotypes tested. The pneumolysin deficient strain was unable to adhere to or invade HBEC or HA cells, suggesting that the toxin pneumolysin has a crucial role in pneumococcal adherence and invasion to host cells.

CHAPTER 4.

The Optimization And Characterization Of A Human *In Vitro* Blood-Brain Barrier Model

4.1.0 Aims

The infection dose for pneumococcal serotypes 1, 2, 6B were screened and optimized; Bacterial growth, adherence and invasion were determined during infection. Establishment of a Blood-Brain Barrier model (BBB) would reveal more in regards to these processes. The literature displays several *in vitro* BBB models used for studying bacterial adherence and invasion, but at the time there no support by the literature for studies of pneumococcal adherence and invasion in a model, which consists of HBECs with HA in co-culture.

4.1.1 Selection of the appropriate Transwells® and optimization of the BBB model

With various pore-membrane types and sizes commercially available, I decided to select a membrane that would be easy to visualise under a phase microscope, but also a membrane that would carry pores of at least 3.0μm in diameter. Individual pneumococci usually range between 0.5 – 1.25 μm in diameter; assuming that pneumococci is predominantly found in diplococcoid or multi-coccoid form, the diameter could immediately change to 1.0 – 1.50 μm or higher. Having in mind the tendency of cells to migrate, it was decided to use the 3.0-μm pore size membrane, in order to assure a firm monolayer which would enable us to acquire high Trans-Endothelial Electrical resistance (TEER) readings, but also allow the pneumococci to migrate to the lower compartment.

4.1.2 Duration of the experiment performed with the BBB model

As seen in monoculture experiments, both HBECs and HA exhibited deterioration of their monolayer; detachment of cells from the well was also observed. An intact monolayer is necessary to acquire reliable TEER values when using Transwells® (figure 15).

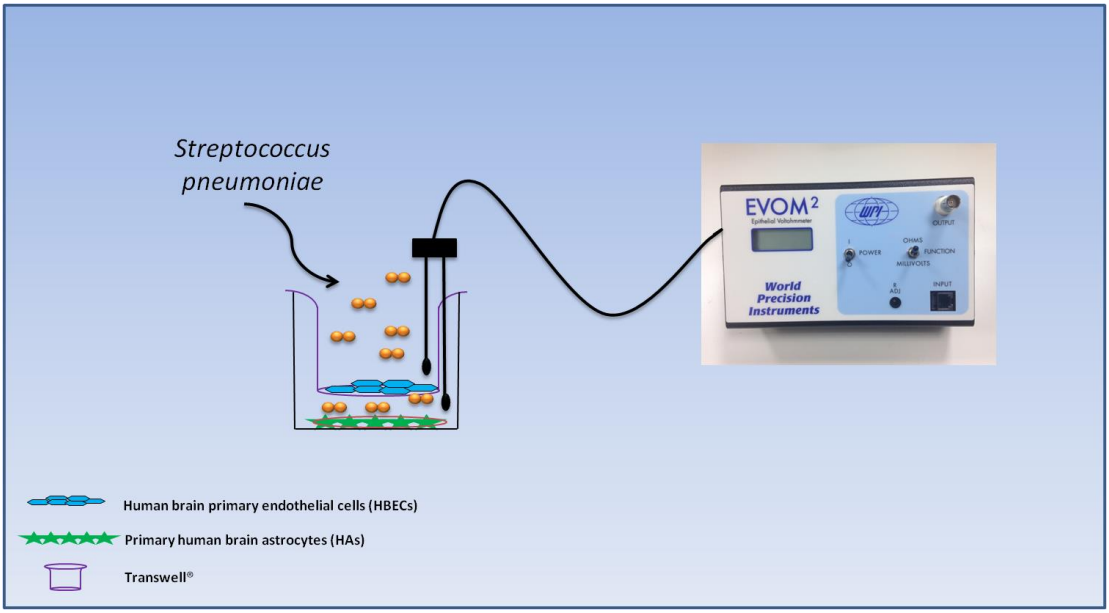

Figure 15| Graphic representation of the bacterial Blood-Brain Barrier model used in this project A Transwell® insert will rest in a 12-well plate, which has been previously seeded with human astrocytes. The membrane of the insert will be supplied with Human Brain Endothelial Cells; cell resistance through the use of an EVOM2 voltohmmeter will assess monolayer integrity. Upon completion of the model's setup, the system will be infected with pneumococci and monitor bacteria for survival adherence and invasion.

As seen in previous experiments, co-incubation of pneumococci with cells for 6 hours resulted in cell deterioration. On the contrary in every experiment where pneumococcal serotypes with either HBECs or HA were used, no cell death or disruption of the cell monolayer was observed 3 hours post infection. To increase the potential of the BBB and allow pneumococci to grow adhere and invade cells, a total of 3 hours was decided to be the time frame for experiments in the BBB model.

4.2.0 Testing serotype 6B in Transwells®

As reported in the methodology chapter (section 2.4.0), surfaces seeded with endothelial cells were coated with type-IV collagen, and surfaces seeded with human astrocytes were coated with poly-d-lysine hydrobromide.

4.2.1 *Streptococcus Pneumoniae* 6B (Serotype 6) in Transwells® (no cells)

The high adherence and invasiveness exhibited by the pneumococcal serotype 6B in my monoculture experiments drove me to select this serotype for evaluation of pneumococcal presence in the BBB model.

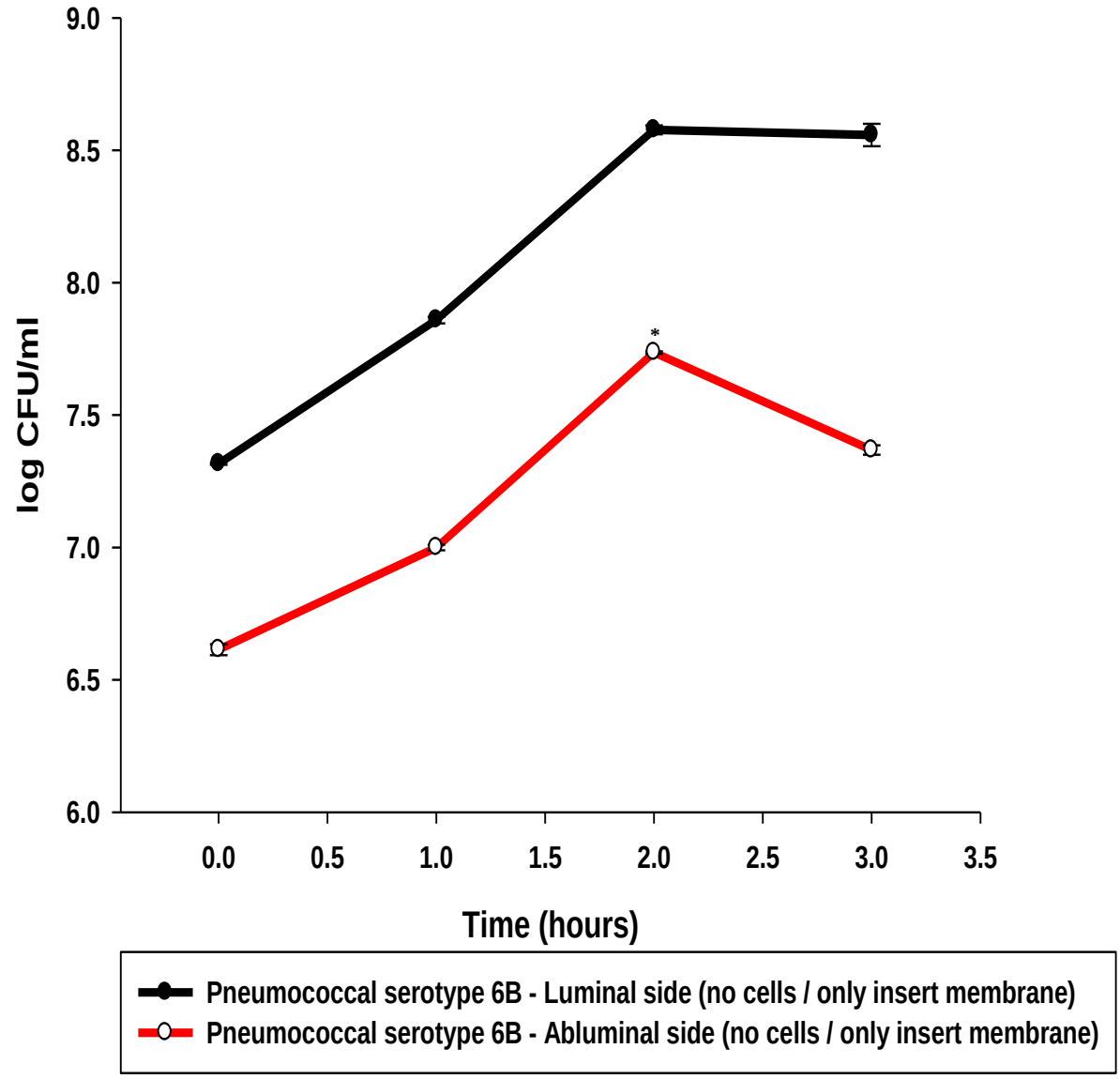

Figure 45| *Streptococcus Pneumoniae* serotype 6B in a Transwell® system It was important to detect bacteria crossing from the top compartment of the model to the lower compartment. Pneumococci were detected in both sides over time. Significant differences are determined using a two-way ANOVA and relate to differences as compared to pneumococci found in the top compartment of the model (luminal) *vs*. the bacteria found in the lower compartment (abluminal). *P<0.05.

As figure 45 shows, the pneumococci successfully crossed the insert membrane and carried on growing in both sides of the model. From the very addition of the pneumococci (~$1x10^7$ CFU/ml) there was successful crossing to the lower compartment of the model (at t = 0 hours 6B is ~7.3 log CFU/ml on the top compartment of the model and 6.6 log CFU/ml on the lower compartment of the model). The CFUs in the top compartment were significantly higher in comparison to the CFUs of the lower compartment 2 hours post incubation (*$p<0.05$).

4.3.0 Use of Human Brain Endothelial Cells in a Transwell® system

In order to keep the cells adhered on the membrane I sought to assess whether the cells were involved in cell migration processes. The cells spread out in an approximate diameter of 159μm, when attached on a coated surface, thus, no immediate concerns were raised for cell migration to the lower compartment of the system; even when cells are in a spherical form cells have average size in sphere shape of ~ 41.72 μm much larger than the pore size of the membrane. According to the already optimized protocols found in the literature [324] $1x10^5$ cells per insert were usually seeded in a total volume of 500 μl. In the lower compartment of the system, 1.5 ml of HBECs culture media was added without the presence of astrocytes. This would allow monitoring any cells migrating to the lower compartment, and avoid mixed cultures of endothelial cells with astrocytes.

Firstly, the cells were passaged using the same methodology as in monocultures and $1x10^5$ cells were seeded in each insert in a total volume of 500 μl of HBECs media. The Transwell® system was incubated at 37ºC/CO_2 5% for 24 hours in order to allow the cells to adhere on the insert's membrane. After the designated incubation period, the system

was transferred under a phase microscope to monitor adherence of the cells on the membrane.

4.3.1 Human Brain Endothelial cell migration to the lower compartment of the Transwell® system

The endothelial cells used to form the monolayer on the membrane were unable to maintain their total cell population in the top compartment of the system, allowing some cells to migrate through to the other compartment. The cells that were found in the lower compartment were collected and counted with the use of trypan blue exclusion assay.

The results showed that the amount of cells migrating across the insert membrane reached approximately 32% of the initial cell concentration. During the trypan blue exclusion assay approximately 11% of the cells that migrated to the lower compartment were stained positive revealing that 20% of the migrating cells remained viable (figure 46).

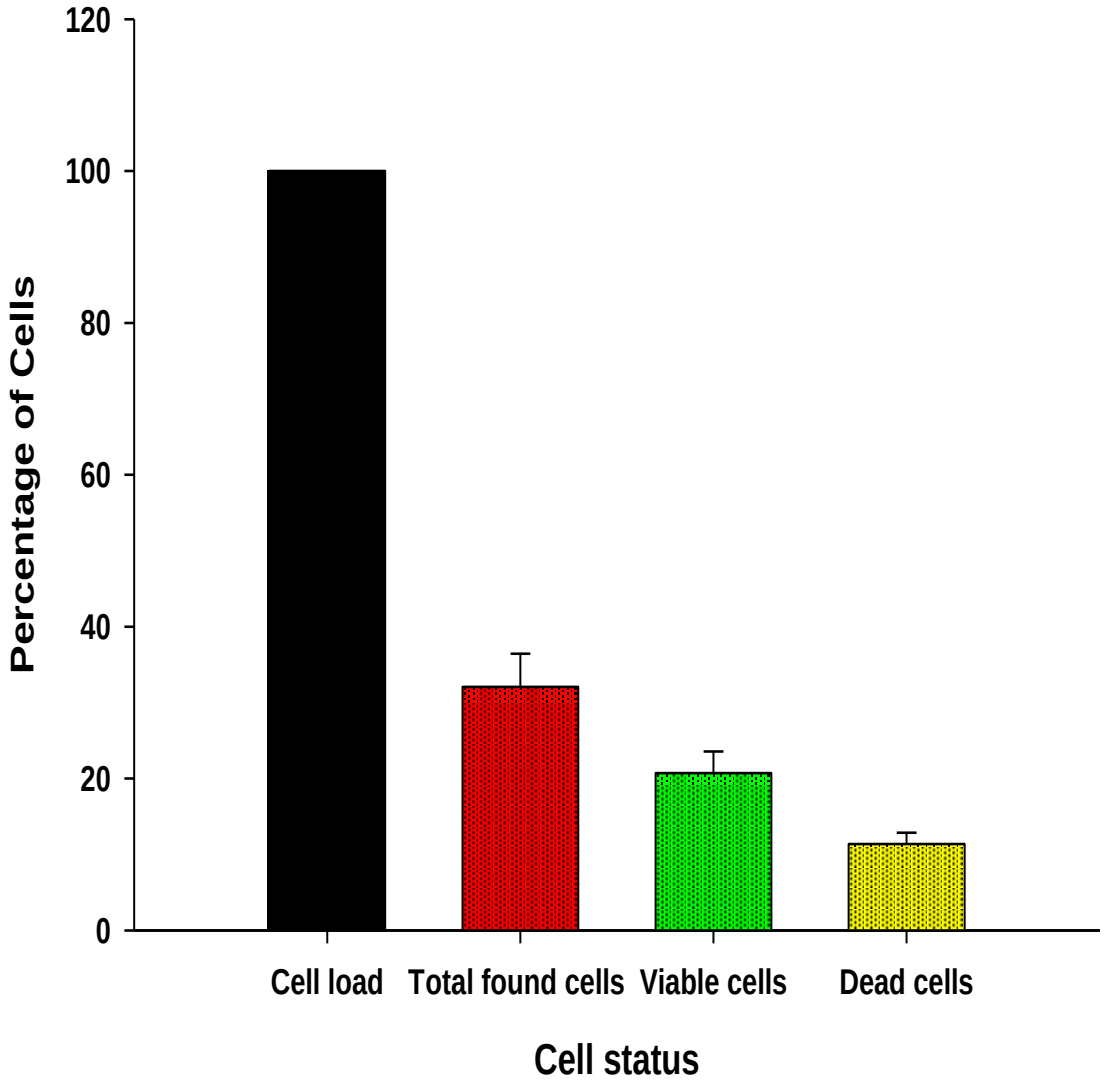

Figure 46| Human brain endothelial cell migration to the lower compartment of the Transwell system The cells that migrated across the lower compartment accounted to 32% of the total cell amount used to form the cell monolayer.

Since a percentage of cells can migrate to the lower compartment, the question of how many cells remained on the membrane and how many crossed to the lower compartment was raised. Even if the difference in the amount of cells that migrate was not vast, it would

jeopardize the consistency of factors such as time that the cells need in order to reach confluency, TEER, bacterial growth, adherence and/or invasion.

The conditions for setting up a BBB model needed further optimizations. The amount of cells seeded was one of the parameters, which could help resolving the problem of cells migration. Altering this parameter would generate other complications, such as the uneven numbers in cells occupying both compartments ($1x10^5$ cells/well is a concentration used both for HBECs and HA cultured in the system). Another important parameter that could assist in reducing cell migration was the total volume that the cells were seeded in. In a standard protocol for a static *in vitro* BBB model, the volume that the cells are is 500μl.

4.4.0 Terminal Velocity in creeping flow changes according to the cell media volume

An object's terminal velocity is the speed of the object when forces such as the drag force (F_d), buoyancy and gravity are acting upon the object [345]. When an object is at its terminal velocity (fluid dynamics) it means that the object has a constant speed due to the restraining force applied by the fluid that the object is found in, while the object moves.

The drag force applied on the object allows it to accelerate until the gravitational pull on the object will equalize this force. This equalization sets the object into a constant speed called terminal velocity (figure 47).

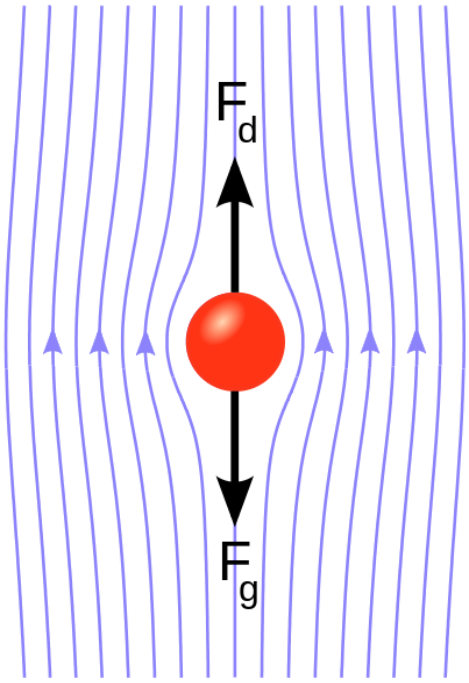

Figure 47| Terminal velocity of a particle in fluid The drag force applied on the object (F_d) allows the particle to accelerate until the gravitational pull (F_g) on the object will equalize this force. This equalization sets the object into a constant speed called terminal velocity whilst creeping flow is moving is going past the particle (blue lines). The image was adopted by [345].

For cells seeded in 500 μl of cell media, the terminal velocity in creeping flow was $9.978x10^{-5}$ m/s whereas the cells seeded in a total volume of 150 μl, the terminal velocity in creeping flow was $2.254x10^{-5}$ m/s.

4.4.1 Pore diameter of the insert's membrane affects flow rate

During the BBB model optimization I observed that when the cell culture media was added in a 3.0μm insert without the presence of media in the lower compartment, the majority of the cell media would instantly flow to the lower compartment whereas this phenomenon was not observed when a 0.4 μm insert was used. Darcy's law describes the kinetics of fluid flow through a porous membrane in relation to the driving force as well as the permeability of the media [345].

In order to show that pore size is an important parameter, the flow rate for endothelial cell media found in 3.0 μm and 0.4 μm pore inserts was calculated. For media found in a 3.0 μm pore insert the flow rate was $1.835x10^{-4}$ m^3/s, whereas for media found in inserts of 0.4 μm pores the flow rate was $3.262x10^{-6}$ m^3/s. Extending my calculations to the amount of mass flowing between compartments, I observed that the mass/flow rate for media found in a 3.0 μm pore insert was $9.102x10^{-2}$ Kg/s whereas the mass/flow rate of media found in inserts of 0.4 μm pores was $4.854x10^{-4}$ Kg/s.

4.4.2 Endothelial Cell adherence on the Transwell® membrane

After evaluating the results acquired for terminal velocity, flow and mass-flow rate, I decided that the time of incubation for endothelial cells was also important in order to increase the potential of this model. Culturing the cells for different incubation periods would enable me to decide how long the cells needed with the minimum volume of 150 μl of cell culture media in order to adhere on the membrane. This would also reveal whether $1x10^5$ cells would be able to survive in this volume.

The incubation temperature (37ºC) was also one of the variables under evaluation, since any temperature above 25ºC reduces the time of evaporation of a fluid. Having the cells in 150 μl could jeopardise cell viability since a few hours of incubation would be enough to force the fluid into evaporation, leaving the cells without any nutrient supplement.

I decided to monitor cell adherence for 1, 2 and 3 hours of incubation. After seeding inserts with $1x10^5$ cells in 150 μl, the inserts were incubated for the selected periods of time. Post incubation, each insert was supplemented with additional media in order to reach a final volume of 500 μl. The inserts were then transferred in a pre-incubated 12-well plate, which contained 1.5 ml of astrocyte culture media in each well. The system was incubated at 37ºC/5% CO_2 for 24 hours. Post incubation, TEER values was assessed (Day 1 - without the presence of astrocytes) and the inserts were transferred in a 12-well plate containing primary human astrocytes which were seeded on the same day as the endothelial cells also at cell $1x10^5$ density. The model was further incubated for 48 hours and then the TEER was assessed in order to monitor whether any differences would occur between different stages. The model was then supplemented with fresh media and incubated for an

additional 48 hours. Final TEER was evaluated to identify the integrity of the monolayer 5 days post cell seeding.

When comparing all 3 incubation periods of the experiment, I observed that the cells were viable during all incubation periods, capable of adhering, and forming a monolayer (evaluated by TEER) (figure 48).

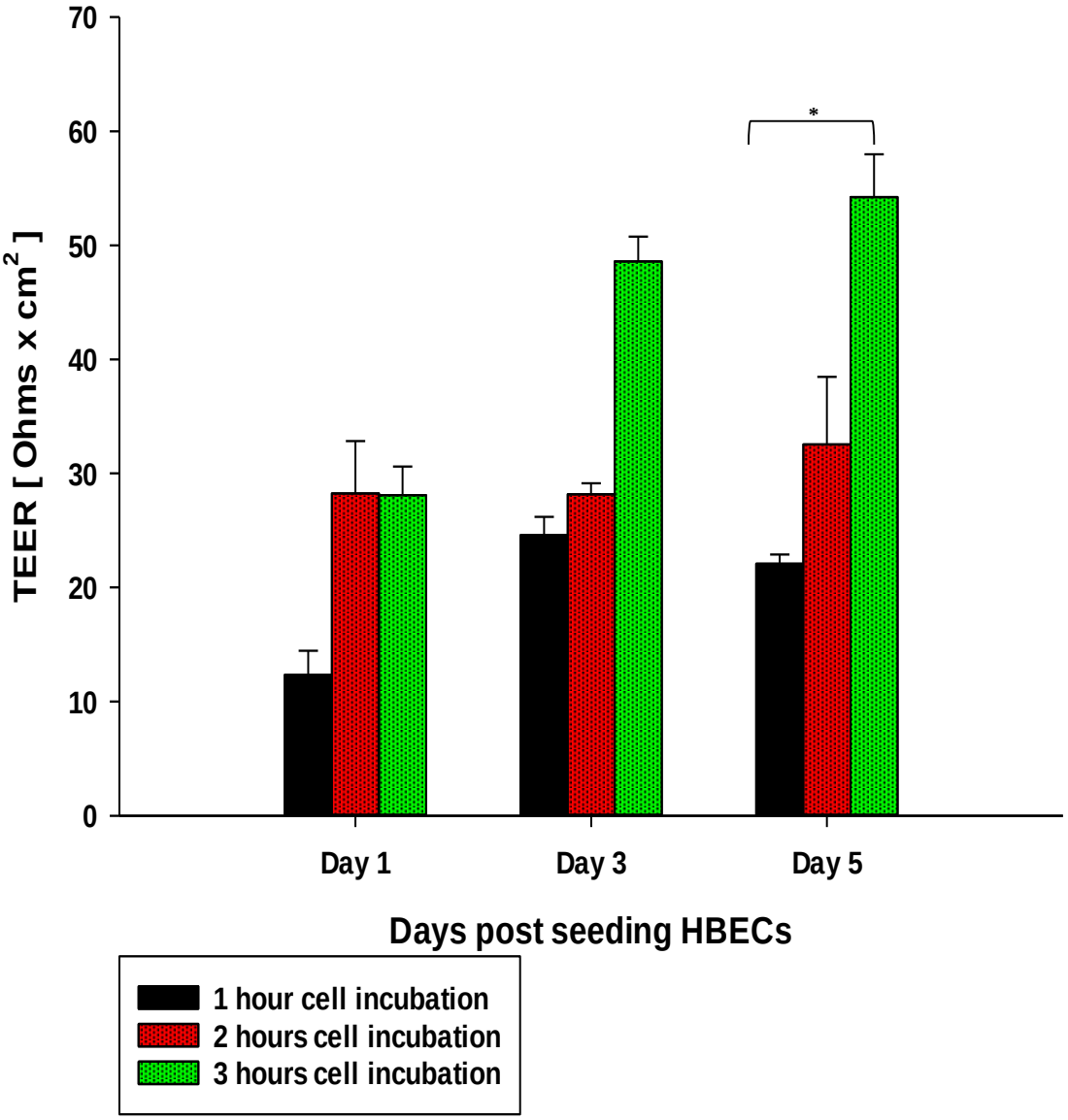

Figure 48| Incubation periods of HBECs seeded on inserts Incubation for 1 hour showed the lowest TEER, whereas inserts incubated for 2 or 3 hours presented exhibited higher TEER. The highest TEER was observed with cells incubated for 3 hours. Thus, the 3-hour incubation period was selected as the appropriate period to set up the model in this project. Statistical significance of the results was evaluated by the use of a Mann-Whitney U test and relate to comparisons made between cell resistances in different days. *P<0.05.

The TEER from inserts incubated for 1 hour did not exceed 30 Ω x cm^2, revealing that 1 hour is not enough for cells to adhere and form a reliable monolayer. Cells left for 2 or 3 hours exhibited higher TEER with increased resistance as the model progressed through the days of the optimization. At the end of the experiment, the 2-hour incubation inserts showed a resistance of 48 Ω x cm^2 and the 3-hour incubation inserts showed a resistance of 54 Ω x cm^2 which was significantly higher than day 1 TEER (*$p<0.05$). A two-way ANOVA test showed that the mean TEER value significantly affected the time of incubation ($p<0.05$), and experiment duration (day 1-5) ($p<0.05$).

4.5.0 Adjustment of the optimized BBB model to a pneumococcal environment

The current model was setup using DMEM cell media supplemented with 10% FBS, 1% penicillin/streptomycin and 1% L-Glutamine. In monoculture experiments, both cell lines were used for infection experiments using a DMEM containing only 1% of FBS without antibiotics.

The BBB model was adjusted as presented in table 3, where growth of the cell lines up to Day 4, was carried out with a 10% DMEM cell media carrying no antibiotics. After the fourth day, the whole system was supplemented with 1% antibiotic-free DMEM media; due to the lower amounts of FBS, the growth period of the model was extended to 6 days (one additional day in comparison to the current model). After the setup of this antibiotic-free BBB model TEER was assessed on days 2, 4 and 6. The model exhibited a steady increase of TEER over the days of the setup, with the highest value taken on the last day of the setup (infection day). The highest value was 63 Ω x cm^2 almost 10 Ω x cm^2 higher than the "Day-5" model (Figure 49). This setup was selected for use in this project.

Table 3 Adjustments of the Blood-Brain Barrier model into an antibiotic-free model

Days of setup	Process	Incubation Period
Day 0	Seeding HBECs on 3.0um inserts/Seeding HA in a 12-well plate 10% Ab-free HBECs media / 10% Ab-free HA media	24 hours
Day 1	Transfering of inserts in the HA 12-well plate and left to stand	24 hours
Day 2	Measuring TEER and Feeding both compartments	24 hours
Day 3	The BBB model is left to stand	24 hours
Day 4	Measuring TEER and supplementing both compartments with 1% Ab-free HBECs/HA media	24 hours
Day 5	The BBB model is left to stand	24 hours
Day 6	Measuring TEER and using the plate for an experiment	0 hours

Table 3| Adjustments of the Blood-Brain Barrier model to an antibiotic-free environment The model was constantly supplied with 10% antibiotic-free media for the first 4 days of the setup and then both compartments were supplemented with 1% of antibiotic-free media until the last day of the setup.

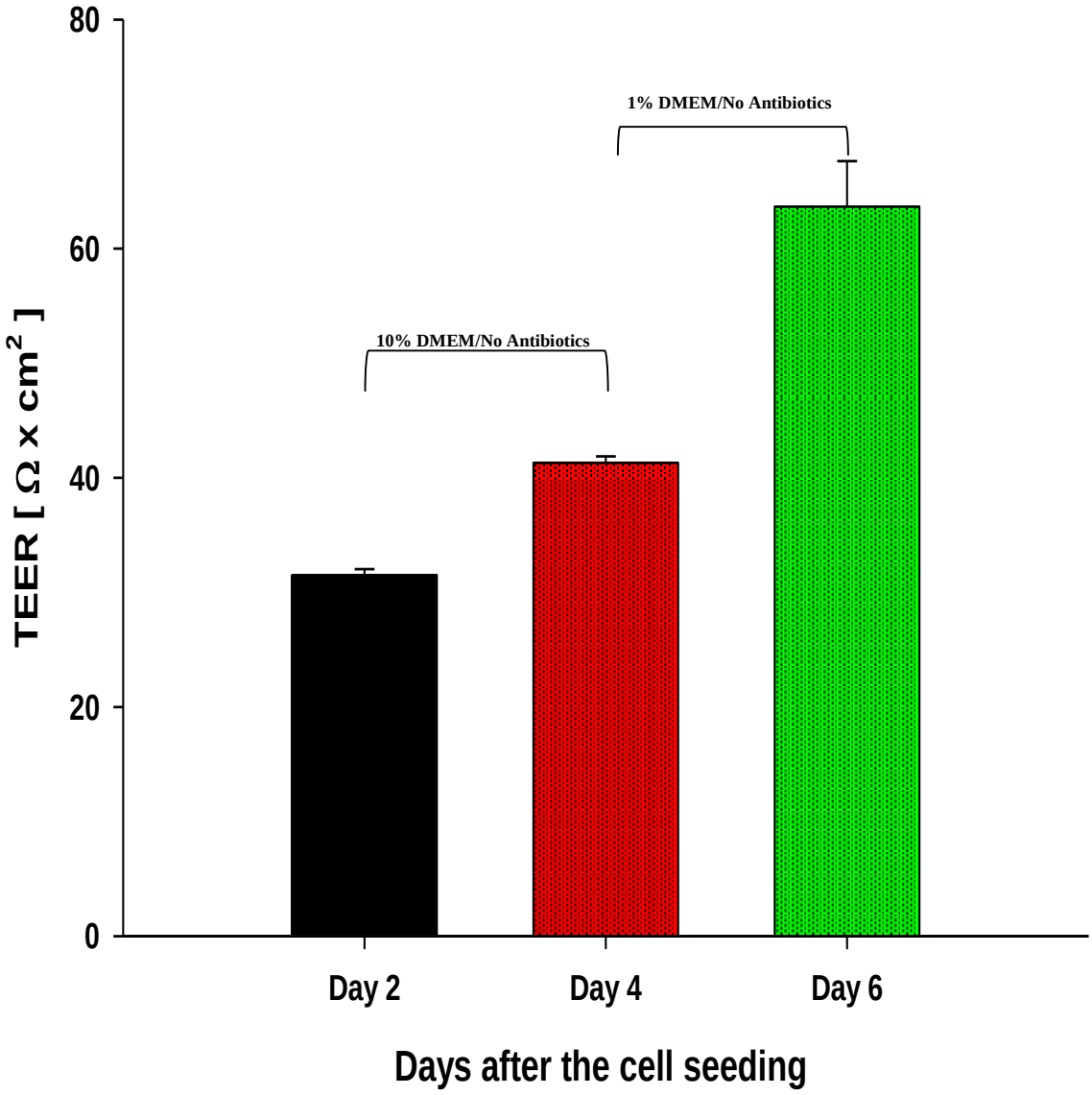

Figure 49| TEER of an antibiotic-free BBB model. Six days after the setup of the model and the different FBS amounts TEER was in a satisfactory level, showing that the model could form a reliable cell monolayer. The final TEER by this model was 63 Ω x cm^2 which was presented as an improvement against the 5-day model (54 Ω x cm^2).

4.6.0 Discussion

Before seeding the cells into the system, bacteria were used in the Transwell® system without the presence of cells in order to evaluate bacterial growth and survival. Serotype 6B successfully grew in both sides of the system, reaching log 8.5 CFU/ml for the top compartment and log 7.3 CFU/ml for the lower compartment respectively. During the BBB model optimization experiments, I observed that approximately 32% of the total cell number used for seeding could migrate to the lower compartment by 24 hours post incubation when following a standard protocol. When the terminal velocity of the cells under creeping flow was calculated, I observed that cells seeded using 500 µl per insert displayed higher velocities in comparison to cells seeded in 150 µl. Hence, I am suggesting that increased flow speed may promote cell migration events. The mass-flow rate of the culture media used in inserts, suggests that the size of the pore allows more media to flow to the lower compartment, which is a contributing factor for cell migration.

4.7.0 Conclusions

In this chapter I established and optimized a BBB model for experiments with *Streptococcus pneumoniae*. This system carried 3.0 μm pore membranes. The terminal velocity of cells under creeping flow and the mass-flow rate showed that the use of 150 μl of cell media increased cell adherence on the membrane and no cell migration was observed. The model was adjusted to an antibiotic-free environment, in order to be used for experiments with the pneumococci.

CHAPTER 5.

Studies Of Pneumococcal Adherence And Invasion In A Human Blood-Brain Barrier Model

5.0 Aims

In the previous chapter, the adherence and invasion of various pneumococcal serotypes to HBEC and HA cells, was investigated. I demonstrated that pneumococcal serotype-1 and -6B adhere better and are more invasive than serotype-2 and that the pneumococcal toxin pneumolysin plays a key role in adherence and invasion. In this chapter, I sought to investigate whether pneumococcal adherence and invasion was altered in a clinically relevant Blood-Brain Barrier model (BBB) (see section 2.3.0 of chapter 2).

I used the same serotypes that I had characterized in monoculture in the optimized BBB model (see chapter 4 of the thesis). Pneumococcal growth, adherence and invasion were monitored to determine whether culture on a semi-permeable membrane would differ from culture in a standard multi-well plate. Measuring the trans-endothelial electrical resistance (TEER) generated by endothelial cells allowed me to monitor the integrity of the model's monolayer. I further sought to investigate the impact of the key pneumococcal toxin pneumolysin on bacterial infection of the BBB system. Generation of a dose response curve with purified toxin enabled me to link toxin concentration to invasiveness of pneumococci. Acquiring samples from the model was part of a multistep process (including but not limited to TEER evaluation, cell lysis for adherence and invasion monitoring, and serial dilutions). Thus, **plating the bacteria on a BAB plate would take ~45 minutes after the time recorded as "time 0"**.

5.1.0 *Streptococcus pneumoniae* serotype 2 (strains D39 and PLN-A), and 6B interactions with a human Blood-Brain Barrier Model

When pneumococci were used in the BBB model, differences in pneumococcal growth were observed. Firstly, serotype 2 CFU declined over time when cultured with the BBB model. In the top compartment of the model, pneumococcal loads dropped to $1x10^4$ CFU/ml by 3 hours post infection (figure 50A). Additionally, no pneumococci were observed in the lower compartment of the model for the duration of the experiment (figure 50B). CFU numbers for the isogenic pneumolysin-deficient mutant of D39, (PLN-A), rapidly declined 3 hours post infection (at ~ $1x10^3$ CFU/ml) (figure 50A). PLN-A was not observed in the lower compartment of the model for the duration of the experiment (figure 50B). By contrast, serotype-6B pneumococci grew in the BBB culture model, with increased CFU counts at 3 hours post incubation, as compared to time 0 (figure 50A). Serotype-6B increased 100-fold in the top compartment 3 hours post infection. Serotype-6B successfully crossed to the lower compartment of the model and was detected at ~ $1x10^6$ CFU/ml 1 hour post infection (figure 50B). The mean CFU for each serotype was significantly different in two-way ANOVA analysis ($p<0.05$).

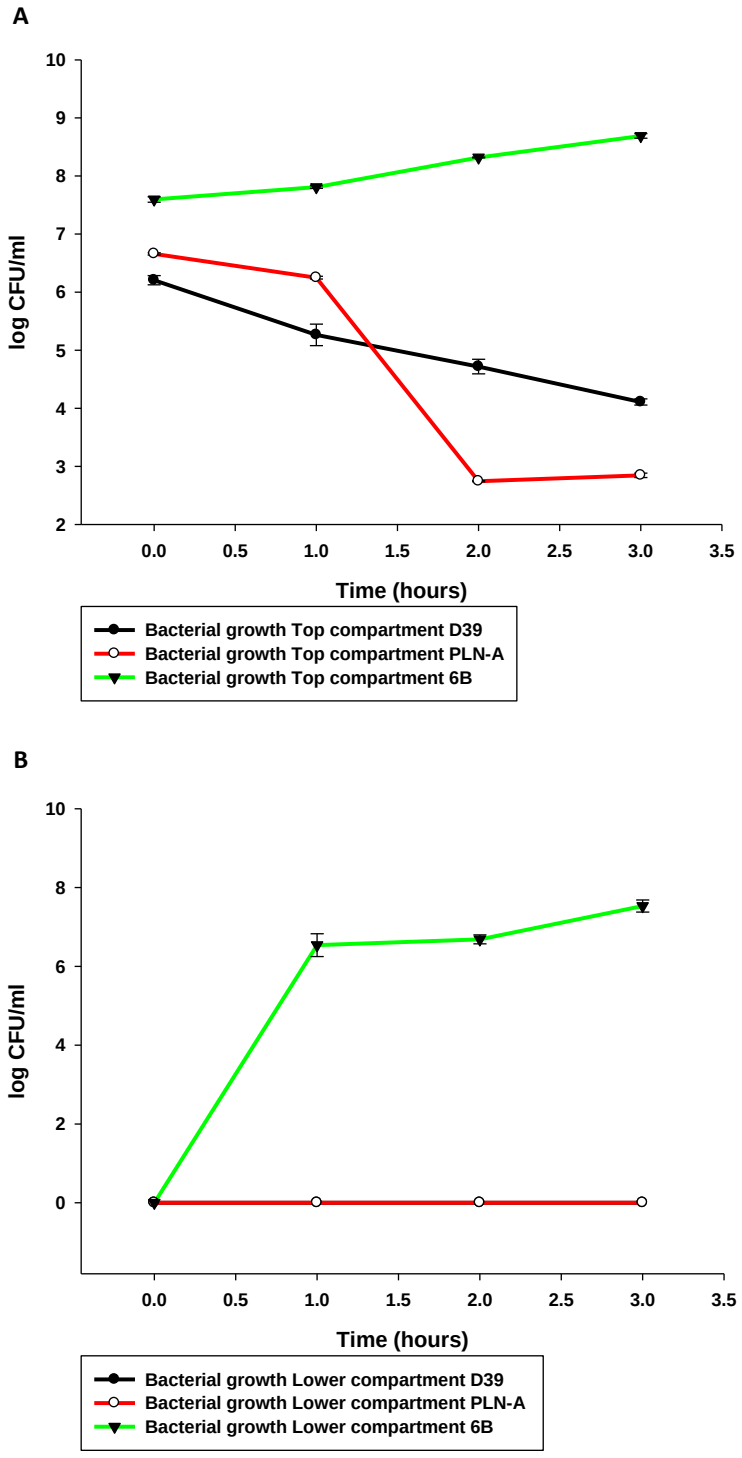

Figure 50| Growth of *Streptococcus pneumoniae* serotype-2 (strains D39 and PLN-A) and 6B in a human BBB model A) *Streptococcus pneumoniae* serotype-2 (strain D39 and PLN-A) and 6B growth in the top compartment of the BBB model. B) *Streptococcus pneumoniae* serotype-2 (strain D39 and PLN-A) and 6B growth in the lower compartment of the BBB model. The pathogen was added in the top side at $1x10^7$ CFU/ml and there was an hourly monitoring of the bacterial growth (by serial dilution of media onto blood agar) on both sides for up to 3 hours post addition of the pathogen. The experiment was repeated 3 times (n=3). The standard error of the mean was calculated (SEM).

5.1.1 *Streptococcus pneumoniae* serotype 2 (strain D39 and PLN-A), and 6B adherence and invasion in a human Blood-Brain Barrier model

Adherent pneumococci in the top compartment of the model were detected for all strains used. Adherent pneumococci in the top compartment declined over time when serotype 2 was used (strain D39 or PLN-A) (figure 51A). Pneumococcal adherence was not observed in the lower compartment of the model when serotype 2 was used (strain D39 or PLN-A) (figure 51B). Adherence in the top compartment of the model was greater for serotype 6B (constant presence of ~$1x10^6$ CFU/ml) than D39 ($1x10^2$ CFU/ml) or PLN-A ($1x10^2$, decreasing to $1x10^1$ CFU/ml). This difference was significant versus D39 at 2 and 3 hours post infection (*$p<0.05$ for both time points) and versus PLN-A at 0, 2 and 3 hours post infection ($^{\$}p<0.05$ for all 3 time points) (figure 51A).

Adherent serotype-6B was also detected in the lower compartment of the model in this experiment (~$1x10^6$ CFU/ml) (figure 51B). Mean CFU varied significantly according to serotype in two-way ANOVA analysis ($p<0.001$).

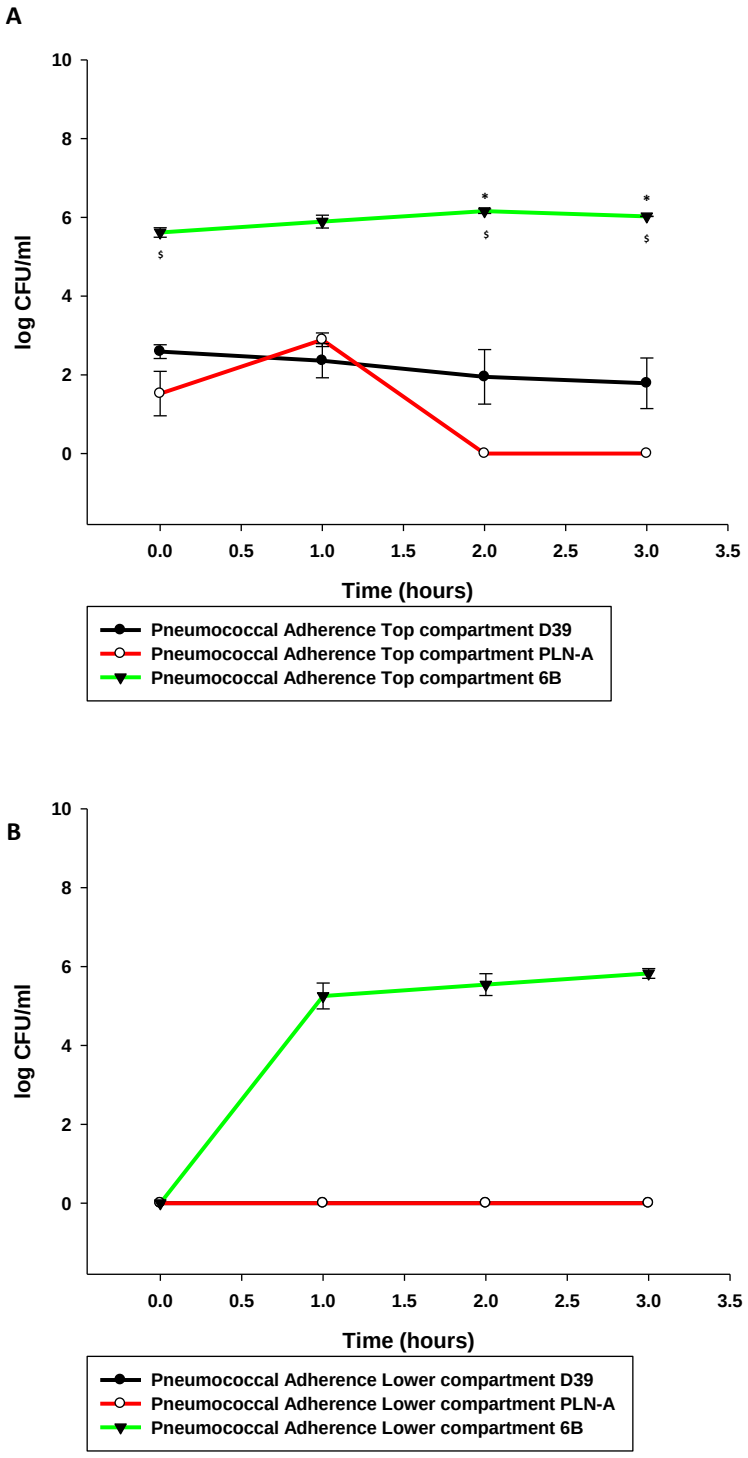

Figure 51| Adherence of *Streptococcus pneumoniae* serotype-2 (strain D39 and PLN-A) and 6B in a human BBB model A) *Streptococcus pneumoniae* serotype-2 (strain D39 and PLN-A) and 6B adherence in the top compartment of the BBB model. B) *Streptococcus pneumoniae* serotype-2 (strain D39 and PLN-A) and 6B adherence in the lower compartment of the BBB model. The pathogen was added in the top compartment at $1x10^7$ CFU/ml and there was an hourly monitoring of pneumococcal adherence in both sides for up to 3 hours post addition of the pathogen. The experiment was repeated 3 times (n=3). The standard error of the mean was calculated (SEM). Significant differences are determined using a two-way ANOVA. *P<0.05, $^{\$}$P<0.05.

Amongst the different serotypes used, 6B was the only serotype that successfully invaded cells in both compartments whereas serotype 2 (strain D39) invaded only the cells found in the top compartment (HBECs) (figure 52A+B); the invaded serotype-2 pneumococci were detected on the first sampling of the pneumococci and not at later time points. PLN-A did not invade cells during the course of this experiment (figure 52A+B). Serotype-6B successfully invaded both cell types in the model 3 hours post infection (figure 52A+B). Mean CFU varied significantly by serotype in two-way ANOVA analysis ($p<0.001$).

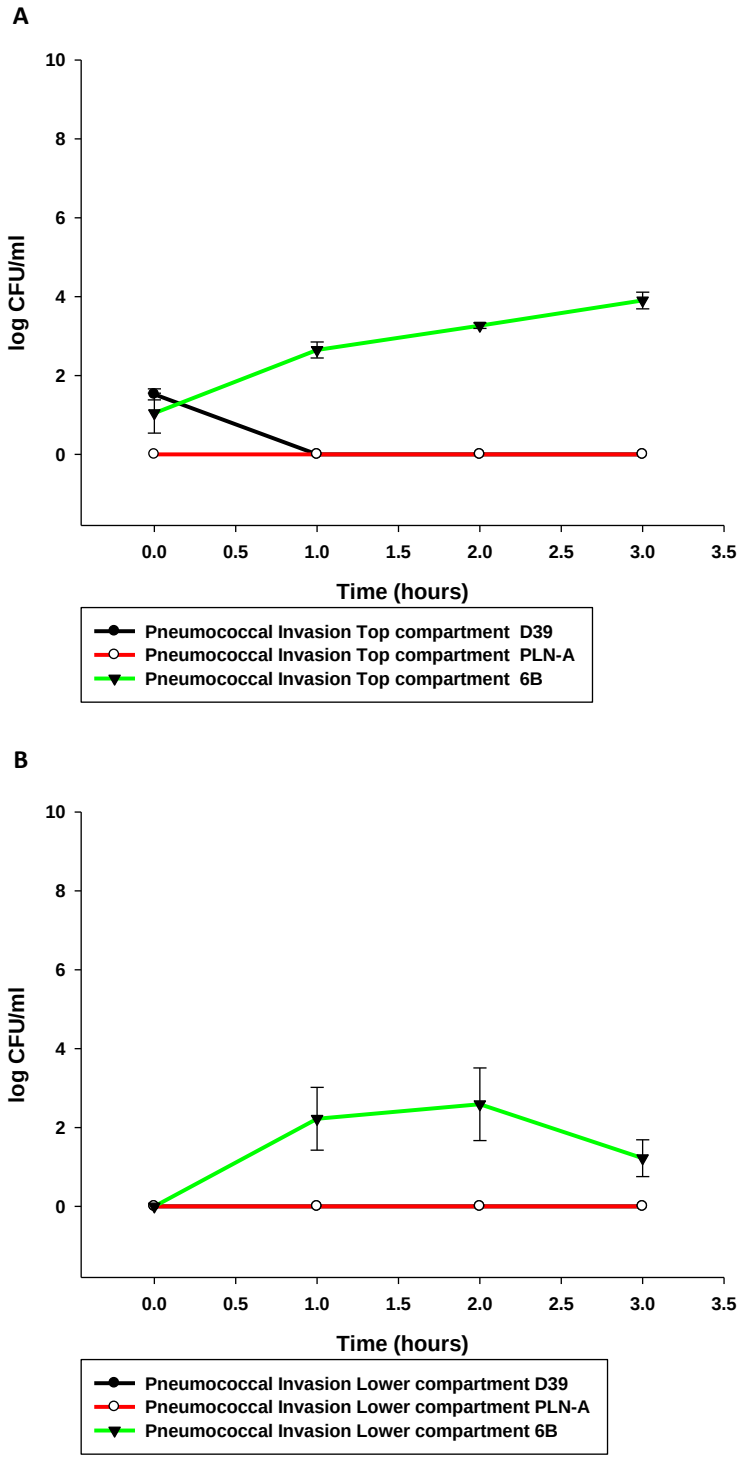

Figure 52| Invasion of *Streptococcus pneumoniae* serotype-2 (strain D39 and PLN-A) and 6B in a human BBB model A) *Streptococcus pneumoniae* serotype-2 (strain D39 and PLN-A) and 6B invasion in the top compartment of the BBB model. B) *Streptococcus pneumoniae* serotype-2 (strain D39 and PLN-A) and 6B invasion in the lower compartment of the BBB model. The pathogen was added in the top compartment at $1x10^7$ CFU/ml and there was an hourly monitoring of pneumococcal invasion in both sides for up to 3 hours post addition of the pathogen. The experiment was repeated 3 times (n=3). The standard error of the mean was calculated (SEM).

5.2.0 Trans-Endothelial Electrical Resistance

The integrity of the HBEC monolayer was monitored hourly by acquiring the TEER values pre and post infection. Use of electrodes in the untreated wells does not significantly alter the TEER value over time. TEER values in the untreated wells had dropped by 10 Ω x cm^2 by 3 hours post infection (figure 53A). TEER values for wells treated with serotype-2 (strain D39 and PLN-A) showed a similar pattern of reduction to the untreated (figure 53A). TEER loss relative to untreated wells at 3 hours post infection was 11% for D39 and 4% for PLN-A (figure 53B).

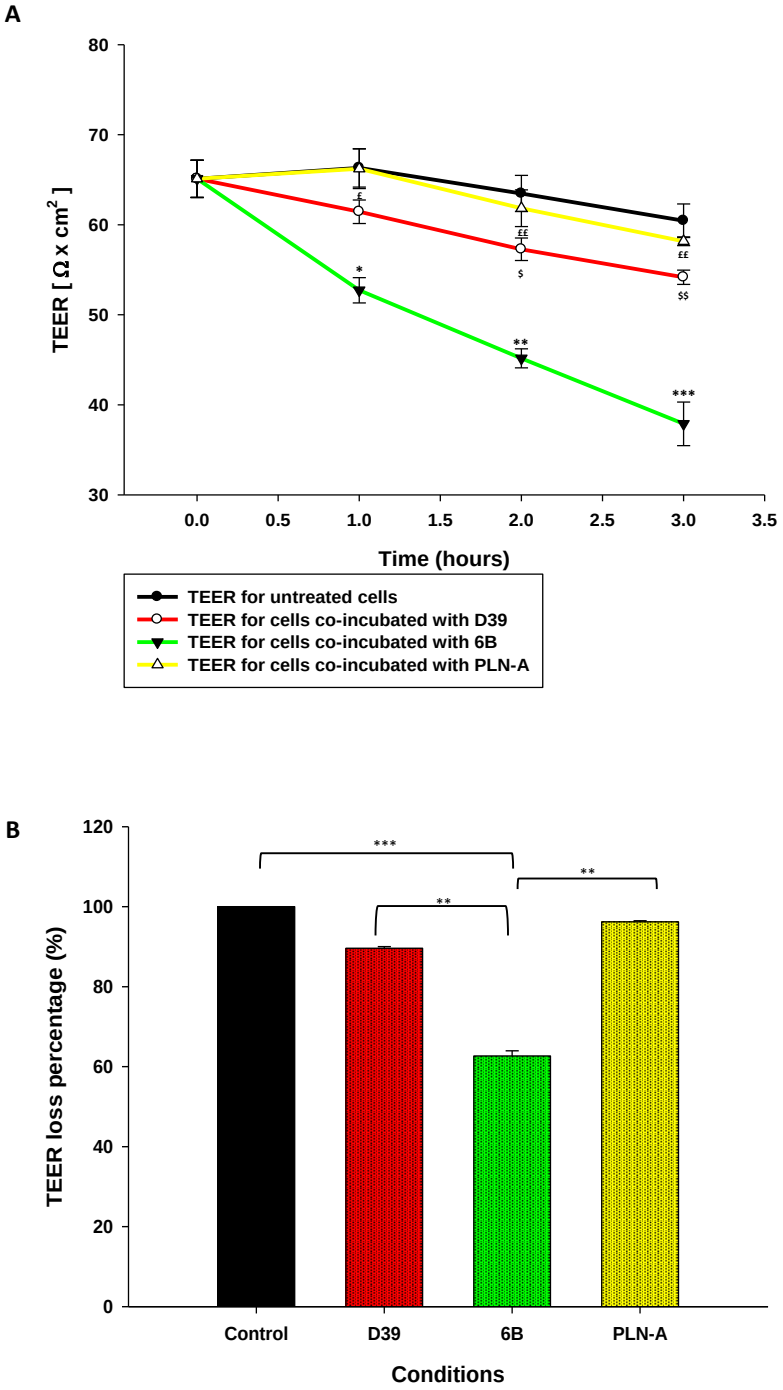

Figure 53|| Trans-endothelial electrical resistance of cells challenged with *Streptococcus Pneumoniae* serotype-2 (strain D39 and PLN-A) and 6B A) Trans-endothelial electrical resistance of cells co-incubated with D39, PLN-A and 6B, during bacterial growth, adherence and invasion for up to 3 hours. B) Trans-endothelial electrical resistance loss of cells co-incubated with D39, PLN-A and 6B, during bacterial growth, adherence and invasion 2 hours post infection. The average TEER value at all 0 hour conditions was use to determine significant differences. The experiment was repeated 3 times (n=3). The standard error of the mean was calculated (SEM). Significant differences are determined using a two-way ANOVA (A) and a Mann-Whitney U test (B) and relate to differences as compared to the type of pneumococcal serotype over the course of time. *P<0.05, **P<0.01, ***P<0.001/$^{\$}$P<0.05, $^{\$\$}$P<0.01/$^{£}$P<0.05, $^{££}$P<0.01.

Serotype-6B severely compromised the model's monolayer, decreasing TEER by 37% relative to untreated wells by the end of the experiment (figure 53B). TEER values acquired when 6B was co-cultured with the model were significantly different to the untreated wells at 1, 2 and 3 hours post infection (*$p<0.05$, **$P<0.01$ and ***$P<0.001$ respectively). TEER values for the serotype-6B infected cells were significantly different when compared against D39 infected cells at 2 and 3 hours post infection ($^{\$}p<0.05$ and $^{\$\$}p<0.01$ respectively) and against PLN-A infected cells at 1, 2 and 3 hours post incubation ($^{£}p<0.05$ after 1 hour of incubation, $^{ff}p<0.01$ for 2 and 3 hours of incubation). Mean TEER values varied significantly between serotypes in two-way ANOVA analysis ($p<0.001$). TEER also varied significantly over time ($p<0.01$).

5.3.0 Interactions of pneumolysin with Human Brain Endothelial Cells

To further examine the causes of loss of TEER, and serotype specific effects on adherence and invasion, the role of pneumolysin was investigated. Serotype invasiveness was correlated with pneumococcal pneumolysin concentrations. In order to do this, I first tested a range of purified pneumolysin concentrations and identified a dose where viability of cells was not significantly affected by the toxin, but significant TEER loss was observed.

Firstly, the toxin was used in a monoculture of HBECs. The dose ranged from 0 to 1000 ng/ml. Cell viability assays were performed using 3-(4,5-dimethylthiazol-2-yl)-2,5-diphenyl-2H-tetrazol-3-ium bromide (MTT). My findings were supported by an additional cell viability test, the Bicinchoninic acid assay (BCA). The cells were incubated

with the toxin for 2 hours and later time points were avoided in order to avoid the confounder of toxin degradation (figure 54).

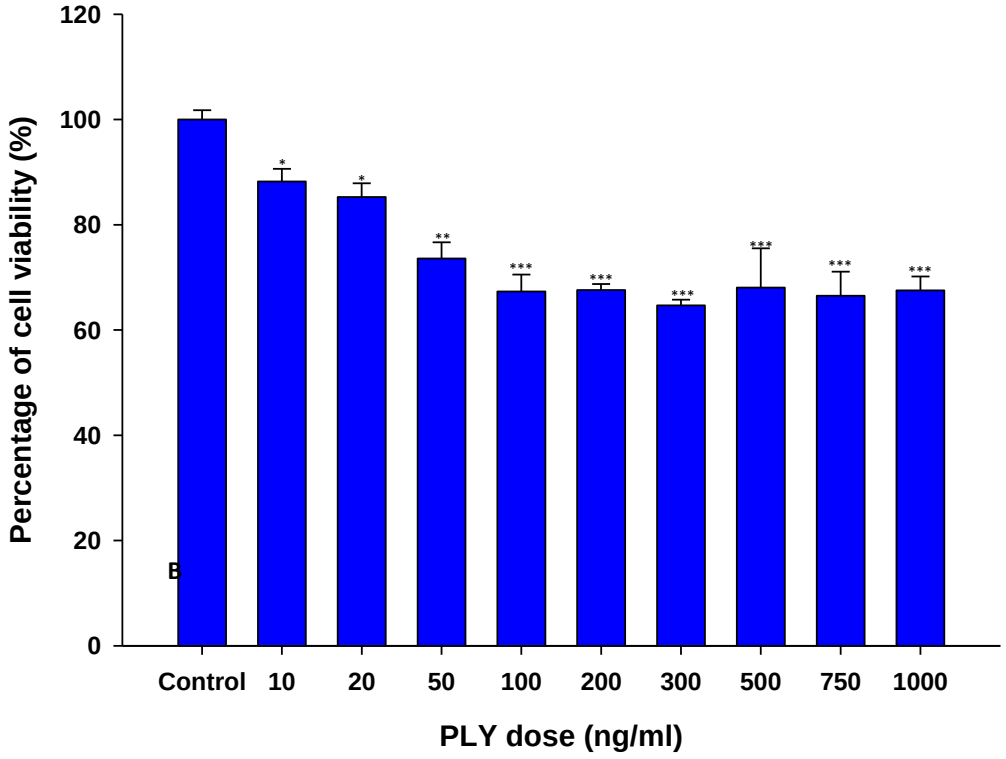

Figure 54| HBEC viability assay of cells co-cultured for 2 hours with pneumolysin The percentage of viability was calculated when all dosages were compared against the untreated cells for a total of 2 hours. The assays were performed using 3-(4,5-dimethylthiazol-2-yl)-2,5-diphenyl-2H-tetrazol-3-ium bromide (MTT) and Bicinchoninic acid. The experiment was repeated 3 times (n=3). The standard error of the mean was calculated (SEM). Significant differences are determined using a Mann-Whitney U test and relate to differences as compared to the concentration of pneumolysin used for co-incubation with HBECs. *P<0.05, **P<0.01, ***P<0.001.

Cells incubated with doses of 100 ng/ml or greater, showed similar cell viability. At the dose of 10 ng/ml, there was a significant 12% loss in viability (*$p<0.05$). Cell viability decreased further, with a 33%-decrease when 100ng/ml were used (***$p<0.001$). Mean percentage viability varied significantly between doses in a one-way ANOVA test ($p<0.001$).

5.3.1 Interactions of pneumolysin with a human Blood-Brain Barrier model

In the previous experiment I demonstrated that maximal reduction of HBEC viability was observed in doses of toxin between 100 – 300 ng/ml. Thus,, dose-ranging experiments performed in the BBB model were confined to concentrations of less than 100ng/ml to avoid significant reductions in cell viability. As in monoculture experiments, the toxin was incubated with the BBB model for 2 hours. Additionally, during the 2-hour incubation, TEER was recorded in order to monitor the integrity of the model monolayer.

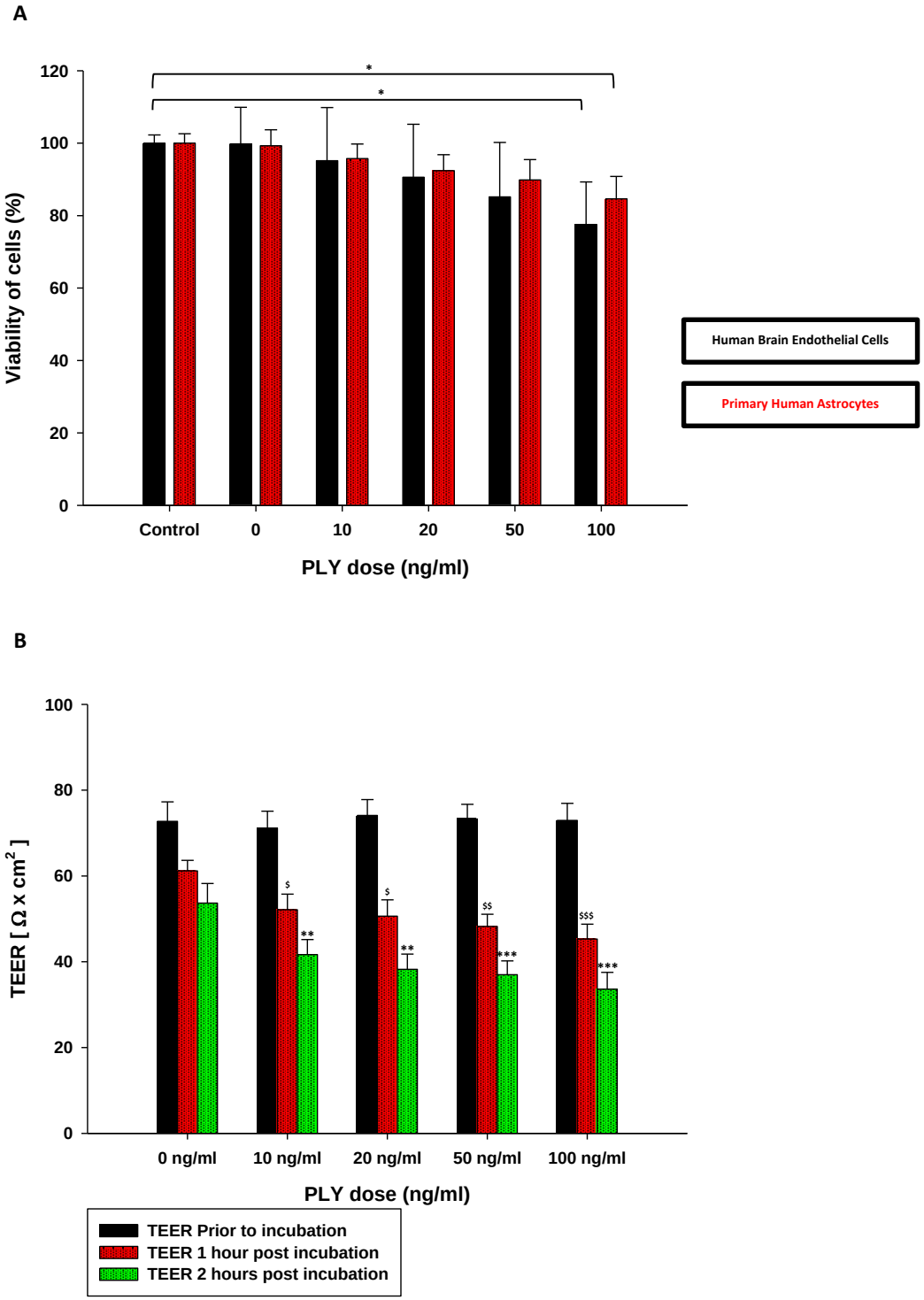

Figure 55| Trans-endothelial electrical resistance and cell viability of HBECs and HA co-cultured with pneumolysin A) Cell viability was assessed using 3-(4,5-dimethylthiazol-2-yl)-2,5-diphenyl-2H-tetrazol-3-ium bromide (MTT) and Bicinchoninic acid. The percentage of viability was calculated when all dosages were compared against the untreated cells for a total of 2 hours. B) Trans-endothelial electrical resistance of cells incubated with pneumolysin for 2 hours. The experiment was repeated 3 times (n=3). The standard error of the mean was calculated (SEM). Significant differences are determined using A) a Mann-Whitney U test and B) a two-way ANOVA test, and relate to differences as compared to the concentration of pneumolysin used for co-incubation with HBECs and the effect of the toxin on electrical resistance. **P<0.01, ***P<0.001/$^{\$}$P<0.05, $^{\$\$}$P<0.01/$^{\$\$\$}$P<0.001.

At two hours, cell viability was reduced at all toxin concentrations at and above 10 ng/ml (figure 55A). The drop in viability relative to untreated wells was 5% for both HBECs and HA at 10 ng/ml, 10% loss for HBECs and 8% for HA at 20 ng/ml, 15% loss for HBECs and 10% for HA at 50 ng/ml and 20% loss for HBECs and 15% for HA at 100 ng/ml (*$p<0.05$). TEER was significantly reduced at both 1 and 2 hours post incubation with all doses of pneumolysin, as compared to untreated wells (figure 55B).

5.3.2 Interactions of the genetically detoxified variant of pneumolysin (PdB) with a human Blood-Brain Barrier model

The genetically detoxified variant of pneumolysin; PdB has only 0.01% hemolytic activity in comparison to wildtype native pneumolysin [337]. PdB was used to determine whether the effects of pneumolysin on cell viability and TEER derived from the toxin pore forming hemolytic activity or another undetermined function. As previously with pneumolysin, PdB was used in a range of doses (0-100 ng/ml) and incubated for 2 hours. Cell viability was not significantly reduced at 2 hours post incubation for any dose of PdB (figure 56A), nor was significant TEER loss observed, suggesting that pore formation is a key factor in loss of TEER (figure 56B).

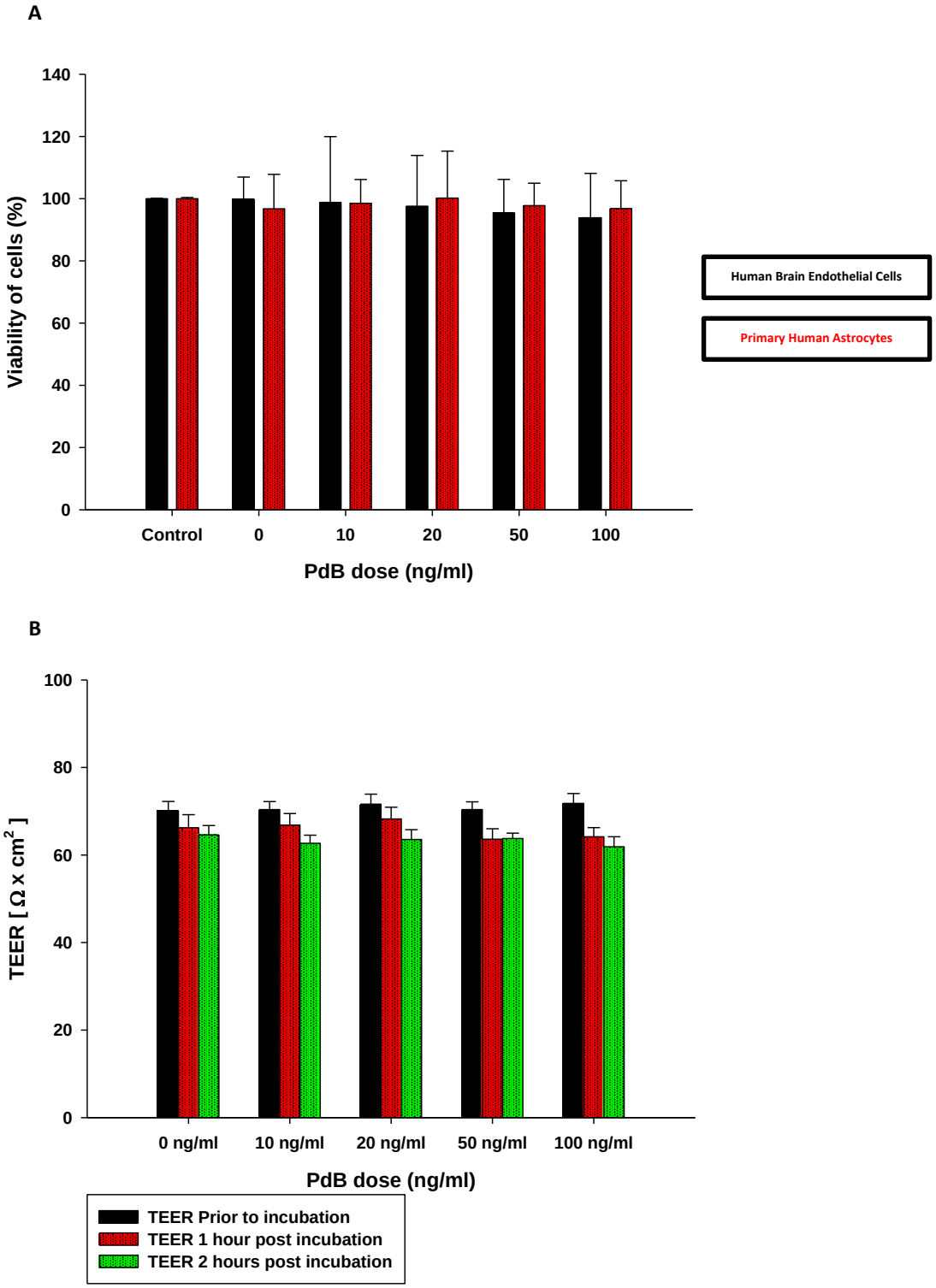

Figure 56| Trans-endothelial electrical resistance and cell viability of HBECs and HA co-cultured with PdB A) Cell viability was assessed using 3-(4,5-dimethylthiazol-2-yl)-2,5-diphenyl-2H-tetrazol-3-ium bromide (MTT) and Bicinchoninic acid. The percentage of viability was calculated when all dosages were compared against the untreated cells for a total of 2 hours. B) Trans-endothelial electrical resistance of cells incubated with PdB for 2 hours. The experiment was repeated 3 times (n=3). The standard error of the mean was calculated (SEM).

5.3.3 Interactions of pneumolysin or the genetically detoxified variant of pneumolysin (PdB) when co-cultured with *Streptococcus pneumoniae* serotype-2 isogenic pneumolysin deficient mutant (PLN-A)

In this experiment, 100 ng/ml of purified pneumolysin or PdB were co-incubated with $1x10^7$ CFU/ml PLN-A in the BBB model**.** CFU counts of PLN-A increased in the top compartment of the model when co-incubated with pneumolysin but decreased when co-incubated with PdB (figure 57A). Two-way ANOVA analysis confirmed that the type of toxin used in the experiment was significant in determining its outcome ($p<0.01$).

Pneumococci co-incubated with pneumolysin successfully crossed to the lower compartment of the model and CFUs were recoverable up to 3 hours post infection (~3.0 log CFU/ml). Pneumococci co-incubated with PdB did not cross to lower compartment of the model (figure 57B).

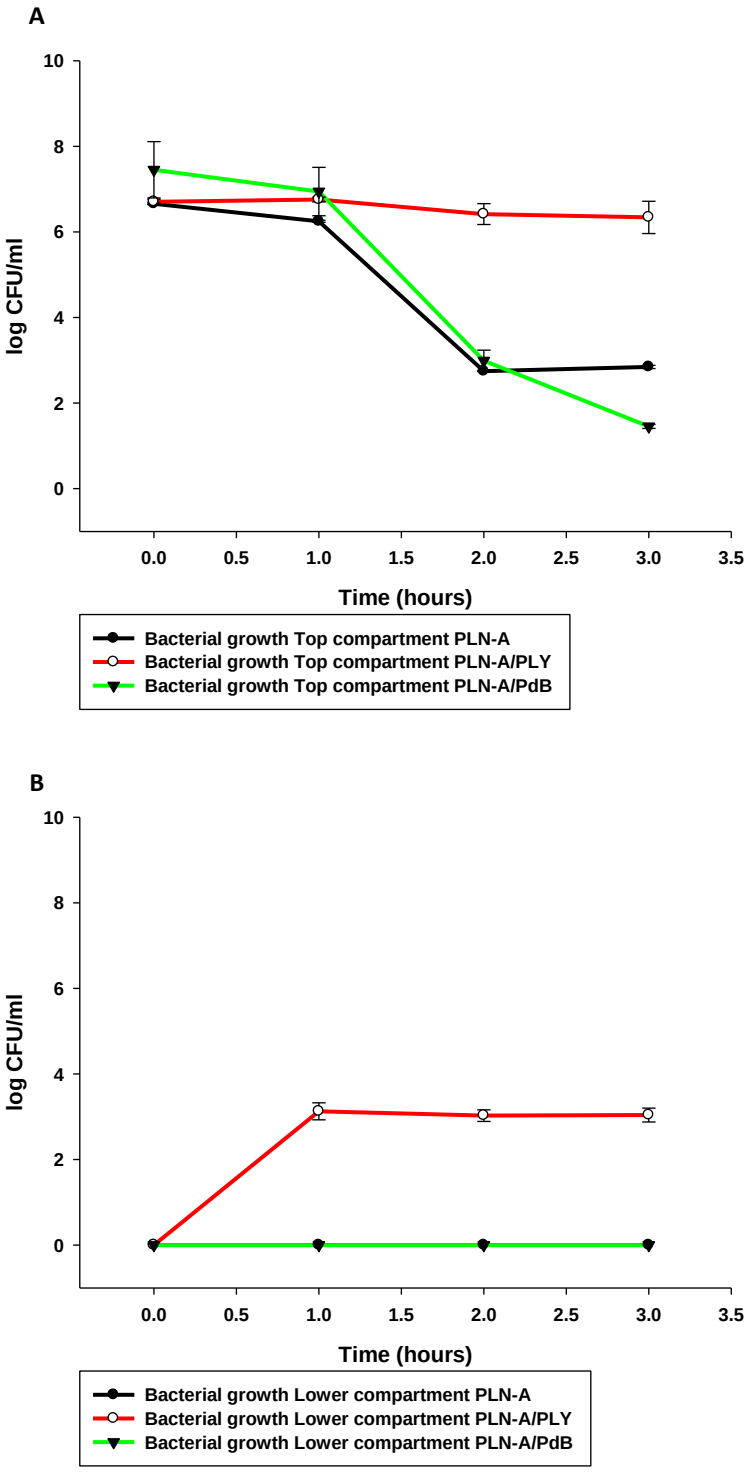

Figure 57| Growth of *Streptococcus pneumoniae* serotype-2 (PLN-A) in co-culture with PLY or PdB A) *Streptococcus pneumoniae* PLN-A/PLY^{+} & PLN-A/PdB growth in the top compartment of the BBB model. B) *Streptococcus pneumoniae* PLN-A/PLY^{+} & PLN-A/PdB growth in the lower compartment of the BBB model. Before the addition of the pathogen in the model, 100 ng/ml of pneumolysin or PdB were introduced to the top side of the model. Immediately after, the pathogen was also added in the top side at $1x10^{7}$ CFU/ml with an hourly monitoring of bacterial growth on both sides for up to 3 hours. The experiment was repeated 3 times (n=3). The standard error of the mean was calculated (SEM).

5.4.0 *Streptococcus pneumoniae* PLN-A adherence when co-cultured with pneumolysin or PdB

Pneumococcal adherence in the upper compartment was significantly increased when PLN-A was co-cultured with pneumolysin, as compared to co-culture with PdB. Significant differences were observed immediately after the addition of the pneumococcus (*$p<0.05$), at 2 hours (*$p<0.05$) and at 3 hours post incubation (**$p<0.01$). Pneumococcal adherence in co-culture with PdB declined over time (figure 58A). No adherence to cells in the lower compartment was observed under any condition or at any time point (figure 58B). A two-way ANOVA test confirmed that the type of toxin used was significant in determining the outcome of the experiment ($p<0.001$).

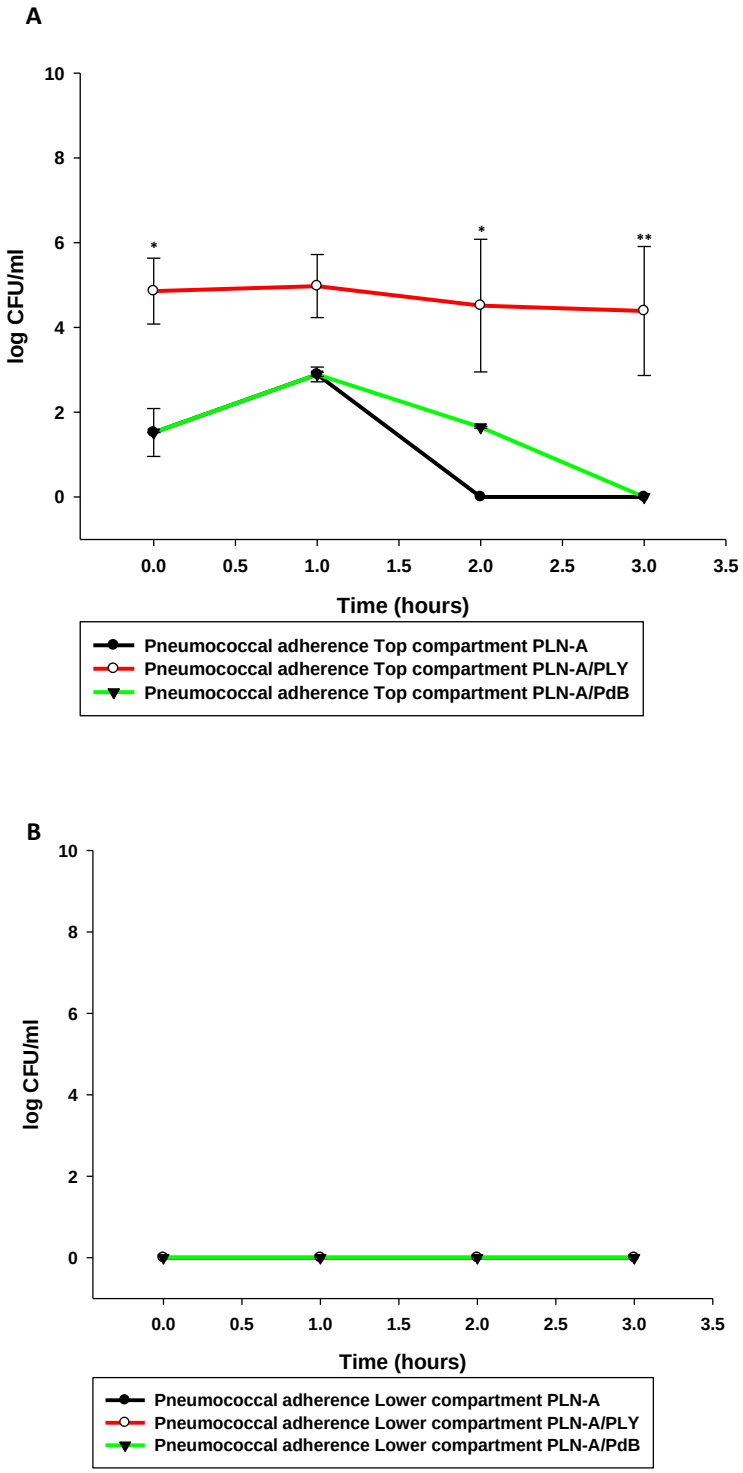

Figure 58| Adherence of *Streptococcus pneumoniae* serotype-2 (PLN-A) in co-culture with PLY or PdB A) Adherence of PLN-A/PLY & PLN-A/PdB to cells in the top compartment of the BBB model. B) Adherence of PLN-A/PLY & PLN-A/PdB to cells in the lower compartment of the BBB model. Before the addition of the pathogen in the model, 100 ng/ml of pneumolysin or PdB were introduced to the top side. Immediately after, the pathogen was also added in the top side at $1x10^7$ CFU/ml with an hourly monitoring of pneumococcal adherence in both sides for up to 3 hours. The experiment was repeated 3 times (n=3). The standard error of the mean was calculated (SEM). Significant differences are determined using a two-way ANOVA and relate to comparisons of pneumococcal adherence of PLN-A over the course of time when using two different forms of pneumolysin. *P<0.05, **P<0.01.

5.4.1 *Streptococcus pneumoniae* PLN-A invasion when co-cultured with pneumolysin or PdB

Pneumococci co-cultured with pneumolysin invaded HBECs in the top compartment of the model by 1, 2 and 3 hours post incubation (**$p<0.01$ for 1 and 2 hours post incubation, *$p<0.05$ 3 hours post incubation) (figure 59A). Pneumococci co-cultured with PdB did not invade cells during the course of this experiment (figure 59A+B). A two-way ANOVA test showed that the type of toxin used, was significant in determining invasion ($p<0.001$).

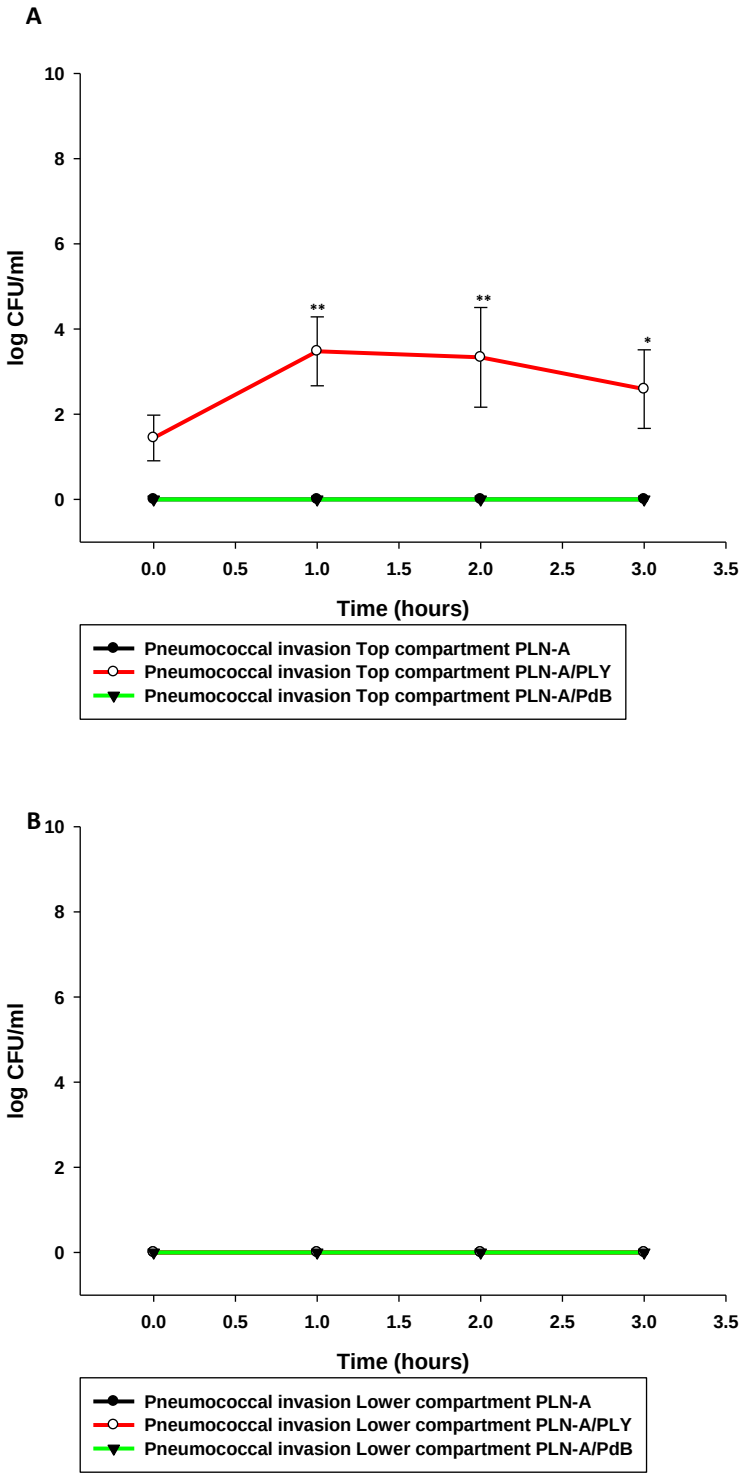

Figure 59| Invasion of *Streptococcus pneumoniae* serotype-2 (PLN-A) in co-culture with PLY or PdB A) Invasion of PLN-A/PLY & PLN-A/PdB to the cells in the top compartment of the BBB model. B) Invasion of PLN-A/PLY & PLN-A/PdB to the cells in the lower compartment of the BBB model. Before the addition of the pathogen in the model, 100 ng/ml of pneumolysin or PdB were introduced to the top side. Immediately after, the pathogen was also added in the top side at $1x10^7$ CFU/ml with an hourly monitoring of pneumococcal invasion in both sides for up to 3 hours. The experiment was repeated 3 times (n=3). The standard error of the mean was calculated (SEM). Significant differences are determined using a two-way ANOVA and relate to comparisons of pneumococcal adherence of PLN-A over the course of time when using two different forms of pneumolysin. *P<0.05, **P<0.01.

5.5.0 Trans-endothelial electrical resistance of BBB cells co-cultured with PLN-A and pneumolysin or PdB

The BBB model infected with PLN-A and co-incubated with pneumolysin showed a significant drop in TEER over time in comparison to the untreated model (**$p<0.01$ for 1, 2, and 3 hours post incubation) (figure 60A). By contrast, the TEER of the BBB model infected with PLN-A and co-incubated with PdB did not differ significantly from uninfected controls (figure 60B). A two-way ANOVA test showed that the type of toxin used, as well as the duration of the experiment were significant factors determining outcome ($p<0.05$ for both comparisons).

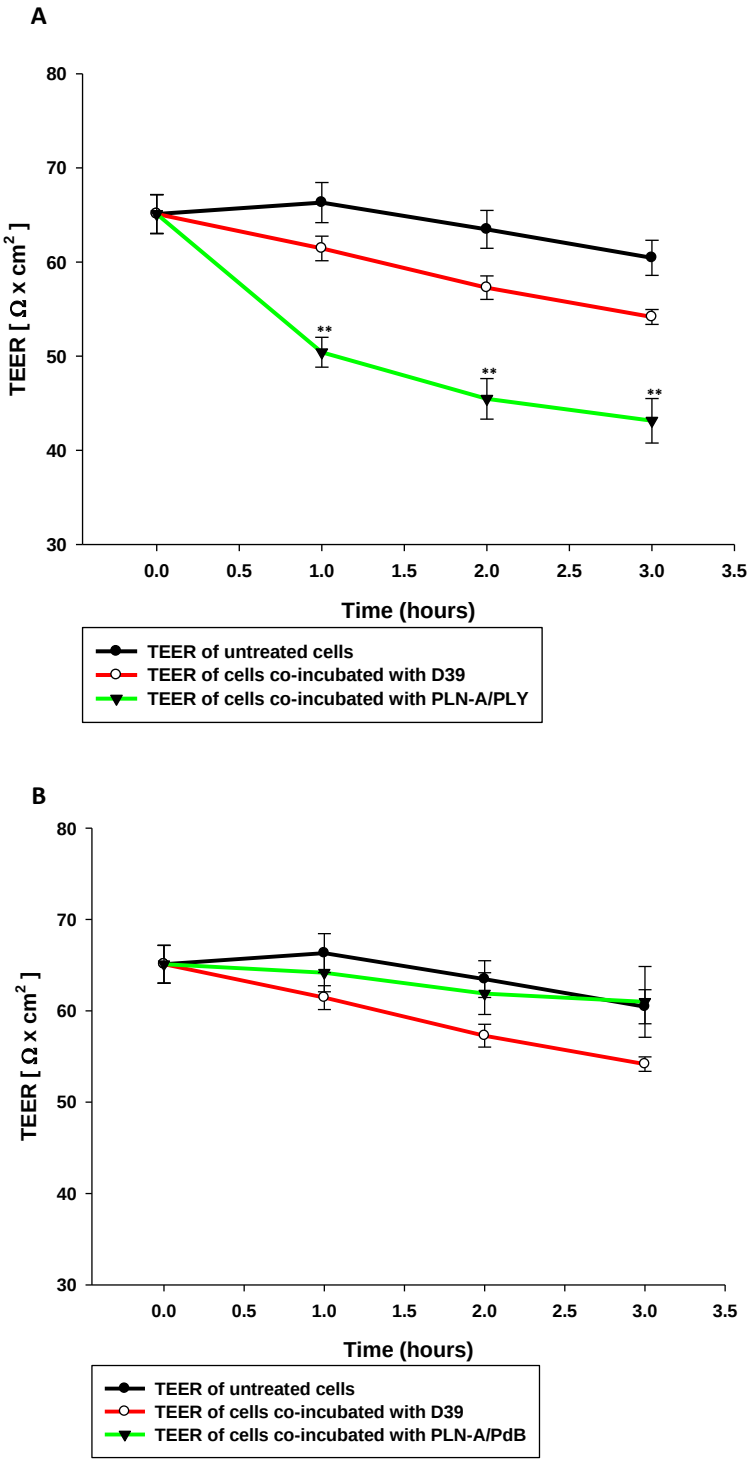

Figure 60| Trans-endothelial electrical resistance of HBECs co-cultured with *Streptococcus pneumoniae* serotype-2 (PLNA) and pneumolysin or PdB A) Trans-endothelial electrical of cells challenged with PLN-A/PLY during bacterial growth, adherence and invasion for up to 3 hours. B) Trans-endothelial electrical resistance of cells challenged with PLN-A/PdB during bacterial growth, adherence and invasion for up to 3 hours. The experiment was repeated 3 times (n=3). The standard error of the mean was calculated (SEM). Significant differences are determined using a two-way ANOVA test, and relate to differences on electrical resistance as compared to the use of pneumolysin or PdB for co-incubation with PLN-A. **P<0.01.

5.6.0 Detection and quantification of pneumolysin levels

The concentration of pneumolysin was measured via a custom ELISA (see materials and methods –section 2.11.1). Initially, samples (supernatant) were collected at 2 hours post agent exposure from the top compartment, containing the endothelial cell layer, of the model. Replicate experiments (n=3) were measured per condition. In order to determine the amount of pneumolysin carried by each serotype, the pneumococci were lysed at the initial infection dose ($1x10^7$ CFU/ml) and the concentration of pneumolysin was measured. Median concentration of pneumolysin among unexposed cells and following exposure to each agent is presented in figure 61 where D39 released significantly higher concentration of the toxin in comparison to 6B and PLN-A (**$p<0.01$ for both comparisons). Serotype 6B released 8 times less pneumolysin than D39. At 2 hours the concentration of pneumolysin in the supernatant was reduced (to almost half) compared to the initial concentration applied to the cells (100 ng/ml).

At the initial infection dose, the concentration for pneumolysin carried from D39 was significantly higher in comparison to 6B and PLN-A (**$p<0.01$ for both comparisons). A 10-fold difference was observed when comparing D39 against 6B. S1 exhibited the highest pneumolysin concentrations among the compared strains (***$p<0.001$ for comparisons with PLN-A and 6B/**$p<0.01$ for comparisons with D39). No pneumolysin was detected in unexposed cells or cells exposed to the isogenic mutant of serotype-2, PLN-A, which was used as a negative control in this assay (figure 62A).

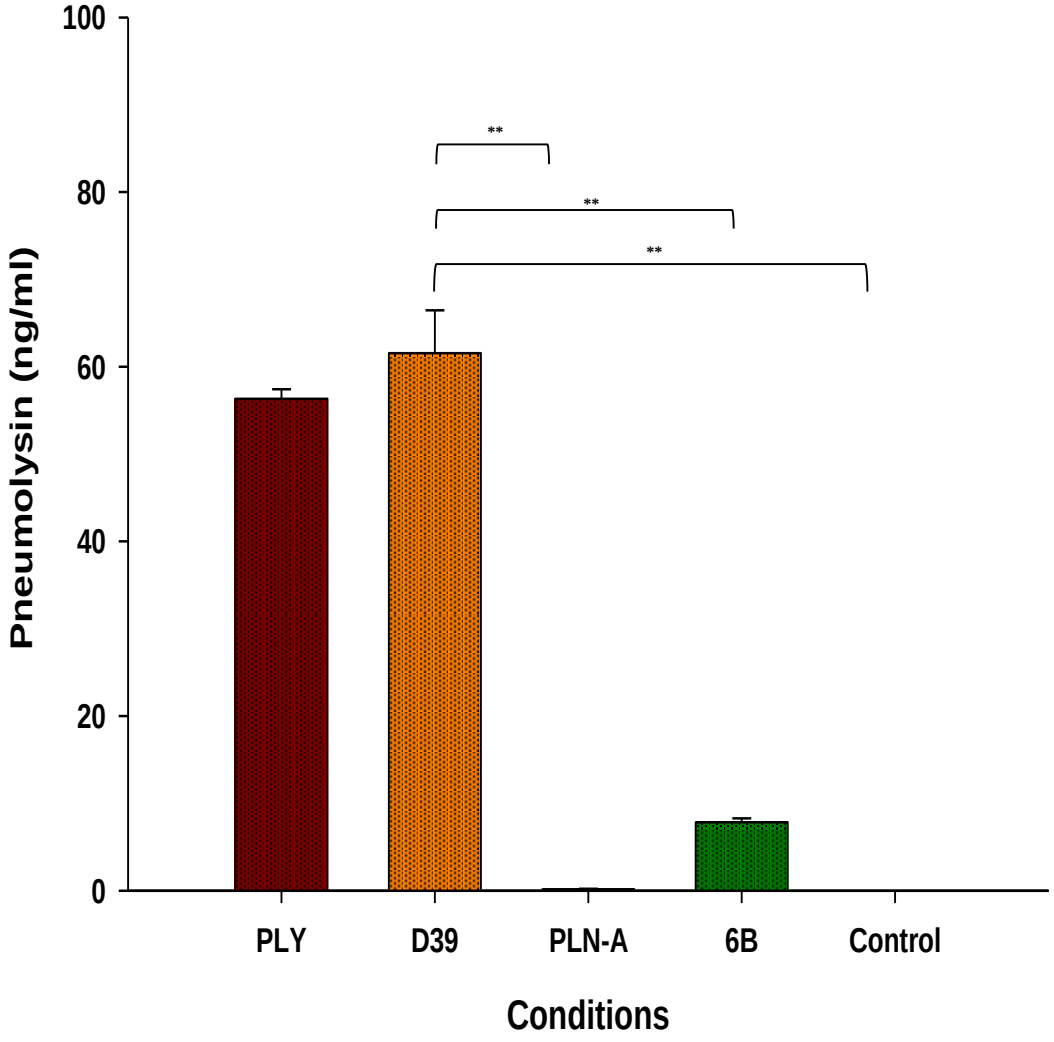

Figure 61| Level of pneumolysin released from *Streptococcus pneumoniae* serotype-2, and 6B 2 hours post infection The recombinant pneumolysin isolated during this experiment derived from the supernatant of the model 2 hours post infection (100 ng/ml). The PLN-A was used as the negative control for this experiment. The experiment was repeated 3 times (n=3). The standard error of the mean was calculated (SEM). Significant differences are determined using a Mann-Whitney U test and relate to differences in pneumolysin concentration as compared to the type of pneumococcal serotype used. **P<0.01.The median concentration of pneumolysin carried within each initial bacterial inoculum and per bacterium is presented in figure 7B. D39 carried the highest average amount of toxin, 8.00 fg/bacterium. In contrast, 6B carried relatively small amounts of toxin, 0.65/bacterium.

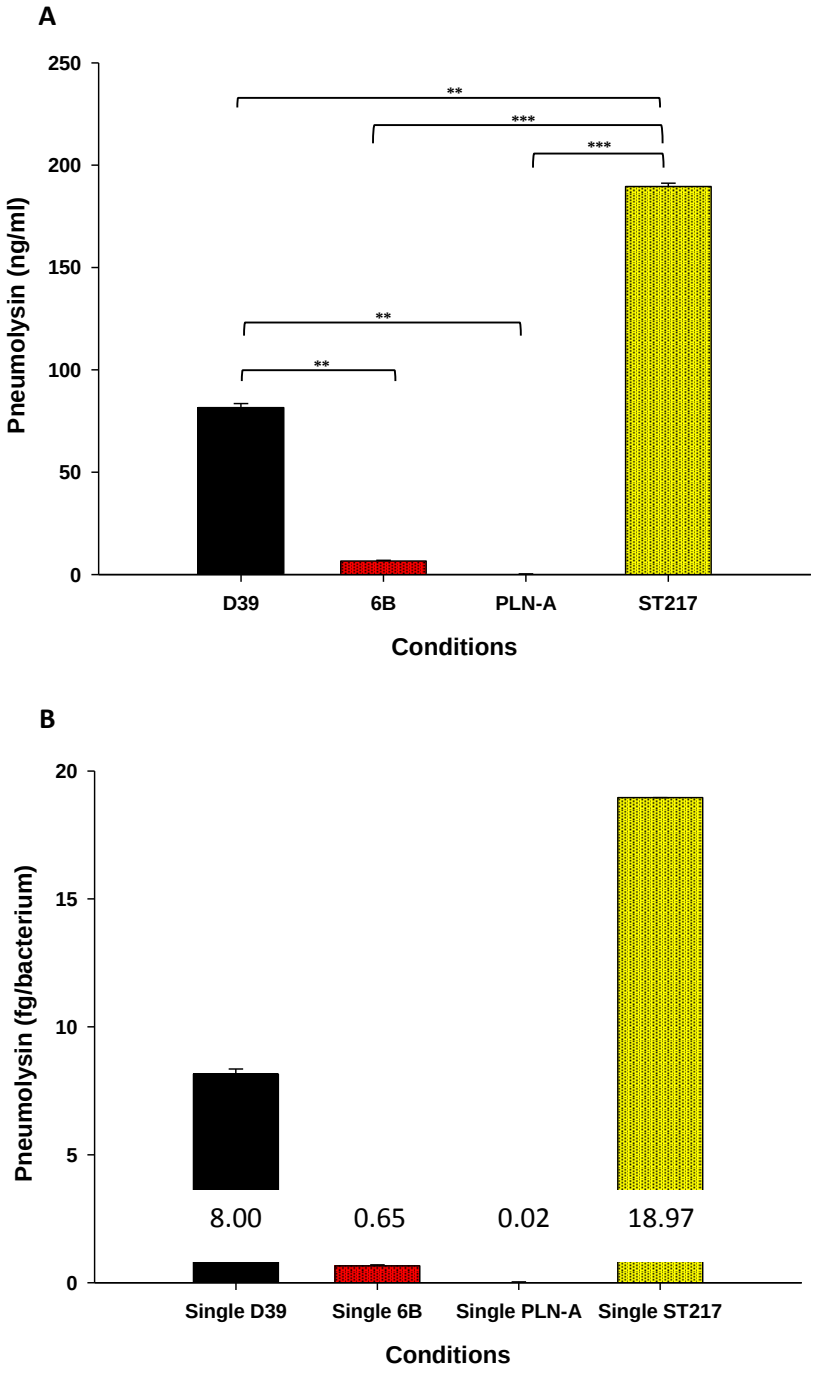

Figure 62| Levels of pneumolysin carried from pneumococcal serotype-1, -2 and 6B at the initial dose of infection A) Pneumolysin levels of each serotype at the infection dose of $1x10^7$ CFU/ml. B) Pneumolysin carried by a single bacterium. The PLN-A was used as the negative control. The experiment was repeated 3 times (n=3). The standard error of the mean was calculated (SEM). Significant differences are determined using Mann-Whitney U test and relate to differences in pneumolysin concentration as compared to the type of pneumococcal serotype used. **P<0.01, ***P<0.001.

5.7.0 Size determination of serotype 2 (strain D39, and PLN-A) and 6B

The capsular size of each pneumococcal serotype was measured using a FITC-Dextran exclusion assay. The median value was acquired by averaging the number of the mono-coccid population (see materials and methods – section 2.13.0). The bacteria were visualized on a Nikon Eclipse 80i fluorescence microscope with 100x objective lens and photographed by a Hamamatsu C4742-95 camera. Pixel number was used as a proxy marker for bacterium size (total area).

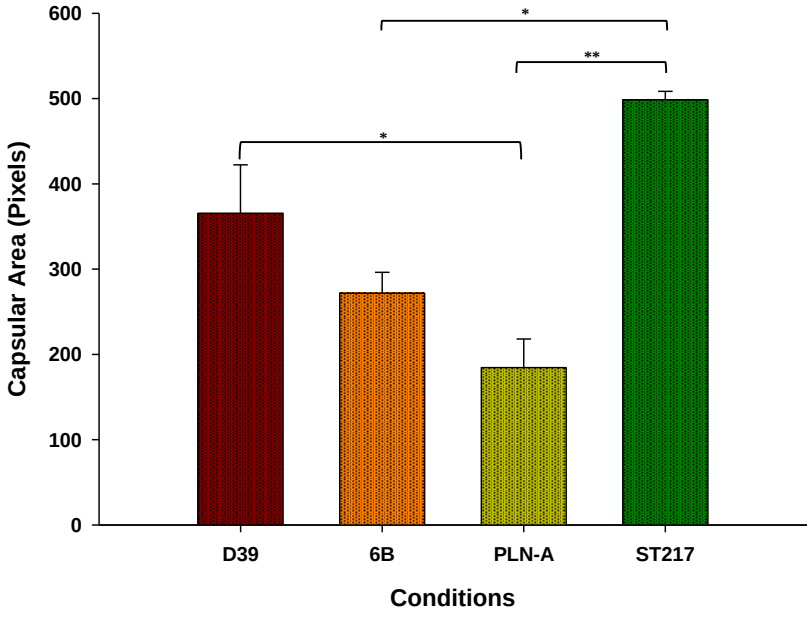

Figure 63| Pneumococcal surface determination of serotype-2 and 6B Average capsular surface area of D39, 6B, PLN-A and ST217. All the single coccids from each serotype were averaged in order to acquire the median value. The values were calculated in square pixels. The experiment was repeated 3 times (n=3). The standard error of the mean was calculated (SEM). Significant differences are determined using Mann-Whitney U test and relate to differences in capsular size as compared to the type of pneumococcal serotype used. *P<0.05, **P<0.01.

Total area per bacterium, as measured by mean pixel number, was 365, 265, 184 and 498 pixels for D39, 6B, PLN-A and S1 respectively (figure 63) where D39 significantly differed from PLN-A in capsular size (*$p<0.05$). Additionally S1 exhibited the highest pixel value, which significantly differed from PLN-A and 6B (**$p<0.01$ and *$p<0.05$ respectively).

******* *Serotype 1 (ST217) was not used with the BBB model. Its presence in figures 62&63 is to enable me to compare between2 clinical isolates.*

5.8.0 Discussion

In this chapter, the growth, adherence and invasion of various *Streptococcus pneumoniae* serotypes in a BBB model was evaluated. Serotype-2 (D39 and its pneumolysin negative mutant PLN-A) was found to behave differently in comparison to monoculture incubations. Serotype-6B adhered, invaded and crossed to the lower compartment of the BBB model.

The contribution of pneumolysin to bacterial growth and junctional breakdown was evaluated. TEER significantly declined over time due to presence of the toxin. When co-incubated with PLN-A, pneumolysin enhanced pneumococcal growth, adherence and invasion of this pneumolysin deficient mutant. A new element was revealed in regards to virulence and pneumolysin, since serotype 6B (the virulent isolate in this study) contained the least pneumolysin concentrations at the infection dose of $1x10^7$ CFU/ml.

It was evident that co-incubation of pneumolysin with PLN-A significantly increased adherent and invaded bacteria in the BBB model. During CFU monitoring I observed:

- When pneumococcal adherence reached or exceeded 50% of the initial infection dose, pneumococcal invasion was present.
- When pneumococcal invasion reached or exceeded 50% of the adherent pneumococci, transfer to the lower compartment of the model was observed.

I postulate, therefore, that a specific CFU threshold needs to be met by the pneumococcus in order for infection to progress.

For the serotypes that produce active toxin, two different scenarios were observed:

1) Serotype-2 strain D39 exhibited declining CFUs over time. Adherent and invaded pneumococci were observed for a short period of time. Pneumococci did not cross to the lower compartment of the model.
2) Serotype-6B exhibited increasing CFUs over time. Adherent and invaded pneumococci were observed in high numbers during the course of the experiment. Serotype-6B successfully crosses to the lower compartment of the model, and continues with adherence and invasion.

Initial observations lead to the hypothesis that pneumolysin could be increasing bacterial replication or providing an environment conducive to replication and growth. When PLN-A was co-incubated with pneumolysin, pneumococcal CFUs increased. Figure 63-ex shows a proposed mechanism of action, which is designed in line with the data acquired so far.

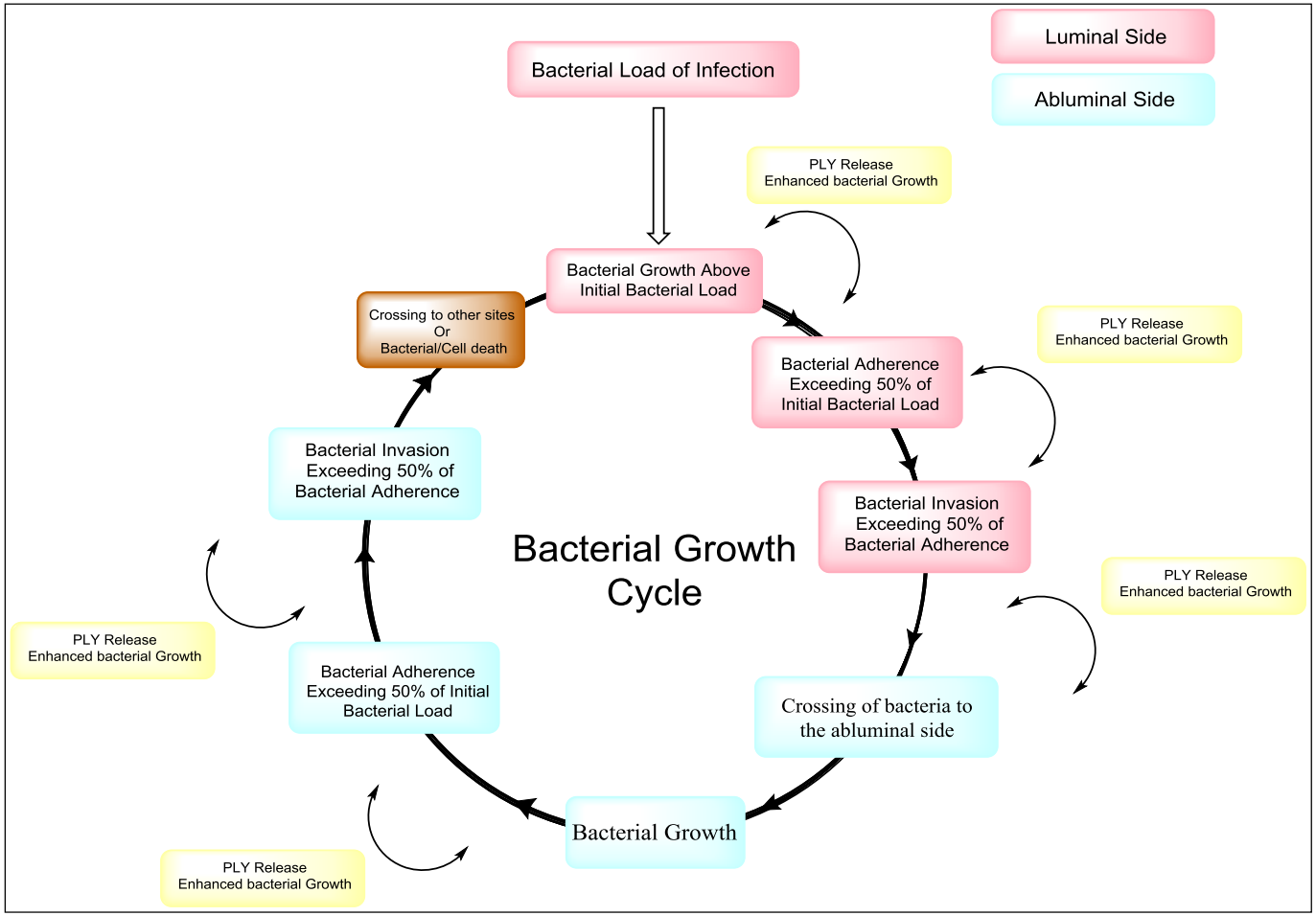

Figure 63-ex| Bacterial growth and its relationship to pneumolysin a) Proposed mechanism of Bacterial growth: The presence of PLY enhances bacterial growth, which allows the bacteria to surpass their initial numbers. Adherence exceeding 50% of the initial bacterial load, leads to bacterial invasion. Invasion exceeding 50% of the adhered bacteria leads to successful crossing of the bacteria to the abluminal side. b) Absence or low presence of PLY is associated with reduced bacterial growth. Adherence occurs but does not exceed the 50% threshold. Little or no bacterial invasion is observed leading eventually to bacterial depletion.

5.9.0 Conclusions

Since pneumolysin is essential for pneumococcal survival in the BBB infection model, my initial hypothesis was that D39 releases pneumolysin at lower concentrations than serotype-6B. Surprisingly the opposite was true, and D39 exhibited the highest concentrations of pneumolysin, whereas 6B showed significantly lower amounts of the toxin. This observation was based on the same CFUs. The concentration of pneumolysin released in the supernatant during infection correlated with the concentrations of pneumolysin in the initial infection dose.

In conclusion, hemolytically active pneumolysin is key in driving pathogenesis and the variations in virulence amongst different pneumococcal serotypes need to be taken into account in order to secure efficacy in future therapeutics.

CHAPTER 6.

Gene Expression Studies Of Human Brain Endothelial Cells Under Pneumococcal Infection

6.0 Aim

To use the gene library available for identifying significant genes related to host immune responses. Identification of genes that have not been previously associated to pneumococcal infection, could allow me to link the existing information with my findings, and increase my knowledge around pathways related to pneumococcal infections in the BBB.

6.1.0 Selection of a time point for microarray analysis

To assess the impact of the pneumococci used previously and the host's response due to infection, the second hour of the experiment was selected. The reason of my selection was that serotype-6B and PLN-A co-cultured with pneumolysin showed better survival, adherence and invasiveness 2 hours after incubation, without compromising cell viability (see chapter 5 of the thesis).

PLN-A exhibited less invasiveness in comparison to D39 and serotype-6B; I sought to investigate gene expression of cells infected with PLN-A in order to identify cell-repair mechanisms. Having a strain with its isogenic mutant was ideal for identifying cell responses that occur exclusively from serotype-2 and are not related to pneumolysin. Additionally, challenging cells with recombinant pneumolysin would allow me to investigate gene expression that relates exclusively to the toxin. The ability to explore multiple variables would enable me to identify if TEER of cells treated with 6B and pneumolysin exhibited similar gene expression patterns (figure 64).

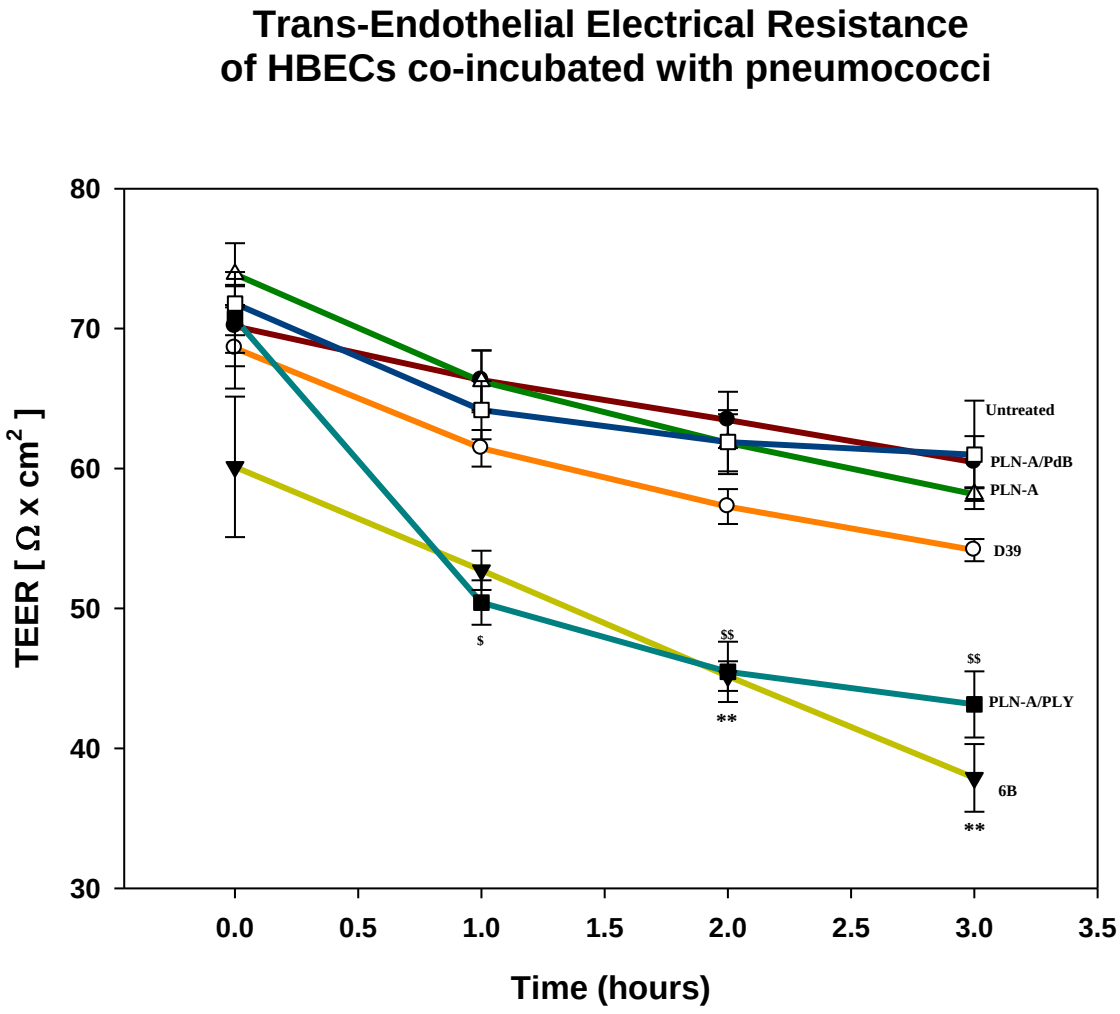

Figure 64| Trans-endothelial electrical resistance of HBECs co-cultured with *Streptococcus Pneumoniae* serotype-2, -6B, the toxin pneumolysin and the toxin mutant PdB A) Trans-endothelial electrical resistance values of the model when challenged with the strains D39, 6B, PLN-A, PLN-A/PLY, PLN-A/PdB and untreated during bacterial growth, adherence and invasion in a total of 3 hours. Significant differences are determined using a two-way ANOVA. **P<0.01 / $P<0.05, $$P<0.01.

The untreated cells associated with these experiments were embedded in the microarray analysis as the background expression, whereas cells infected with D39, PLN-A, 6B and pneumolysin (at 100 ng/ml), were used as the different comparison groups.

6.2.0 Isolation of Human Brain Endothelial Cells RNA

RNA extracted from untreated cells used was used as the baseline of the microarrays. RNA extracted from cells infected with pneumococci or pneumolysin derived from the same experiment as the untreated cells. **Several RNA samples of the same condition (replicates) were pooled to achieve stronger gene signal and higher diversity**. RNA purity was considered of high standards since the reading ratios from the RNA evaluation (A260/280 and A260/230) ranged around the recommended values (~1.6 – 2.0) (Table 4).

Table 4 RNA content of Human Brain Endothelial Cells isolated from a BBB model at t = 2h

Strains/Conditions	Isolated RNA (ng/ul)	A 260/280 ratio	A 260/230 ratio	Cy3/Cy5 (pmol/ul)
Control	224.92	1.75	2.22	n/a
PLY	196.58	1.76	2.34	n/a
PLNA$^-$	253.38	1.77	2.33	n/a
D39	221.85	1.74	2.34	n/a
6B	192.46	1.78	2.23	n/a
Control - Cy3	116.97	n/a	n/a	1.93
PLY - Cy5	41.98	n/a	n/a	0.51
PLNA$^-$ - Cy5	67.65	n/a	n/a	0.94
D39 - Cy5	58.78	n/a	n/a	0.91
6B - Cy5	76.90	n/a	n/a	1.21

Table 4| RNA content isolated from Human Brain Endothelial Cells 2 hours post infection a) The cells used during the experiments (both treated and untreated) were isolated and purified accordingly (see methodology chapter). The content exceeded the minimum requirements and the A260/280 – A260/230 readings revealed that the RNA isolated from the cells was of high purity. The collected RNA was tagged with cyanine florescent dye 3 (untreated) & cyanine florescent dye 5 (treated), and amplified to increase its content. Further purification of the RNA occurred and the amplified RNA exceeded the minimum requirements of amplified RNA (min. Of ~20ng/µl of RNA and 0.50 pmol/µl of the dye tagged to the RNA).

RNA extracted from cells was labeled with florescent detection dyes (Cy3 & Cy5). The labeled RNA was amplified and purified. The average value of RNA labeled with Cy3 was 61 ng/µl (for all comparison groups). The average value of RNA labeled with CY5 was 64 ng/µl.

6.3.0 RNA hybridization and two-color microarray

62966 genes embedded in a custom designed microarray chips were screened for expression. The initial analysis which was carried through the Agilent Scanner®, presented the up- and down-regulated genes in a generic form. The significantly up-regulated genes are presented as red scatters, the significantly down-regulated genes are presented as green scatters; the not-differentially expressed genes are presented as yellow scatters, and the genes used to normalize the data are presented as blue scatters (figure 65A-D).

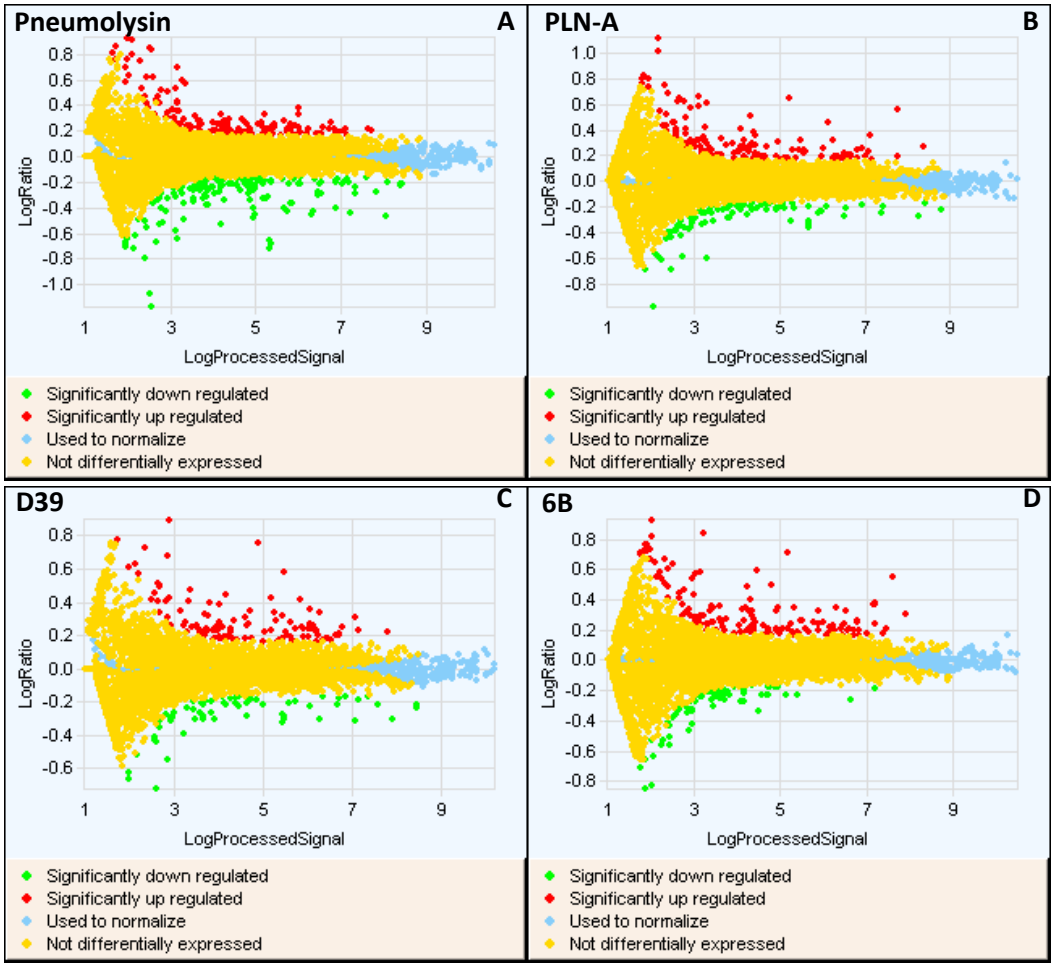

Figure 65| Gene expression array initial analysis of the RNA isolated during treatment of Human Brain Endothelial Cells in a BBB model Two-color microarray graphical representation of Human Brain Endothelial cells when challenged with A) 100 ng/ml pneumolysin, B) PLN-A, C) D39 and D) 6B. Red dots show the up-regulated genes, green dots show down-regulated genes, yellow dots show the not- differentially expressed genes, and the blue dots are the genes which were used to normalize the data presented in these images during infection. All the acquired results are in a Log Ratio scale and range from -1.2 to 1.2.

When observing the different images in figure 65, an obvious variation between results that were acquired from different conditions was observed. Up- and down regulation of genes was presented in a log ratio form which extends from log -1.2 to 1.2. Further statistical analysis was required in order to identify the specific genes, which were positively or negatively expressed.

6.4.0 Gene classification of the two-color microarray expressed genes

After initial presentation of the significantly expressed genes, it was considered important to further analyze the data, in order to acquire information about the genes separately.

The first step was to introduce the acquired data in the Collapser® software which identified the replicates of the same gene. Further on, the software combined the replicates of each gene and calculated the average value. Post calculation, the database contained only one of each gene. From the 62966 genes, 20429 genes were found to be replicates of the same gene. The remaining 42537 genes were loaded in the Cluster 3.0® software. The Cluster 3.0® assigned each gene to a gene family. In the form of a dendrogram, the genes were further classified into specific sub-families where interactions between them could occur (part of a specific mechanistic pathway). The outcome of the gene clustering was subject to the parameters set for the calculations. For example the gene vector removed all genes that had standard deviations of observed values less than X. For example, if the gene vector was set at the value of 0.25 then the genes, which had a standard deviation of 0.25 or higher, accounted to 2513. If the gene vector was set at the value of 0.15, then the genes, which had a standard deviation of 0.15 or more, increased to 14482. With more genes assigned to sub-families, the processing of the data became more complex for the computer during the analysis. The simultaneous calculations prevented the software from functioning correctly when the gene vector was set below 0.15. Thus, I decided not to set the gene vector value below 0.15.

One type of analysis was to investigate how gene expression differed when the cells were challenged with various serotypes. A strategy was formed where the 14482 genes would

go under significant analysis of microarray (SAM). The SAM® software was specifically designed for microarray data. It can measure the gene expression of the data, but it can also measure how the condition, which was set in the experiment, affects this expression. The computation of a statistic Xj for each gene j is the function of SAM. This computation showed how strong the relationship between the gene and the condition was. The ability of the software to use repeated permutations of the data, allowed the determination of the significance for expressed genes in relation to the condition used. The decision on how significant each gene was, lied with the user of the software. The tuning parameter delta (d) allowed the user to choose the false positive rate of the genes. A greater delta value would reduce the rate of false positive genes whereas a reduced delta value would increase the rate of the false positive genes. All 14482 genes isolated from the initial clustering were either up- or down-regulated. The SAM software assumed which genes were significant according to what the delta value given by the user was. That immediately excluded genes, which mathematically may not be considered significant, but *in vita* they might have contributed into a cascade of a protein-protein reaction. A **fixed false discovery rate of 5%** will be used to identify the significant genes calculated by the SAM software. The 5% false discovery rate indicates that there is a 5% chance that the total gene number analysed appears as a false positive. This also indicates that the p value of these genes will not exceed 0.05, thus, achieving statistical significant. All compared conditions were used under the same values and ratios in order to identify different up- and down-regulated genes.

When a condition was analyzed against the other conditions, it was always named as "group 2". All genes deriving from the analysis, showed how much more, over or under-

expressed the same genes are, for the specific condition. This type of analysis generated 4 combinations:

- Pneumolysin vs. PLN-A, D39, 6B
- PLN-A vs. Pneumolysin, D39, 6B
- D39 vs. Pneumolysin, PLN-A, 6B
- 6B vs. Pneumolysin, PLN-A, D39

6.5.0 Significant Analysis of Microarrays for a false discovery rate of 5%

Firstly the 14482 genes were filtered through the assigned false discovery rate. The 4 conditions revealed different amounts of significant genes. When pneumolysin was compared against the other three conditions it displayed the highest amount of significantly expressed genes (Table 5).

5 Table B Significant Analysis of Microarrays (SAM) calculations for all four conditions used

Conditions	False Discovery Cut-Off Rate	Number of Significant genes
PLY *vs.* PLNA$^-$, D39, 6B	5.00%	790
PLNA$^-$ *vs.* PLY, D39, 6B	5.00%	39
D39 *vs.* PLNA$^-$, PLY, 6B	5.00%	4
6B *vs.* PLY, PLNA$^-$, D39	5.00%	289

Table 5| Significant Analysis of Microarrays for all conditions used All 4 conditions of infection used in the bc-BBB model presented different false discovery rates and different d-values. The reason behind this is the different amount of genes falling in the importance threshold set, in an effort to define these genes as statistically significant. With an FDR of 4.93% and a d-value of 0.55 the pneumolysin condition revealed 788 significant genes. The PLN-A condition with an FDR of 3.02% and d-value of 0.78 showed 31 significant genes. The D39 condition showed only four genes with no FDR value and a d-value of 0.58. The 6B condition with an FDR value of 4.88% and a d-value of 0.61 showed that 289 genes were considered significant. All these genes were used further for a pathway analysis.

Through SAM analysis for the pneumolysin condition, 790 genes were considered significantly up- or down-regulated (figure 66A). Only 39 genes were significantly up- or down-regulated when PLN-A challenged endothelial cells (figure 66B).

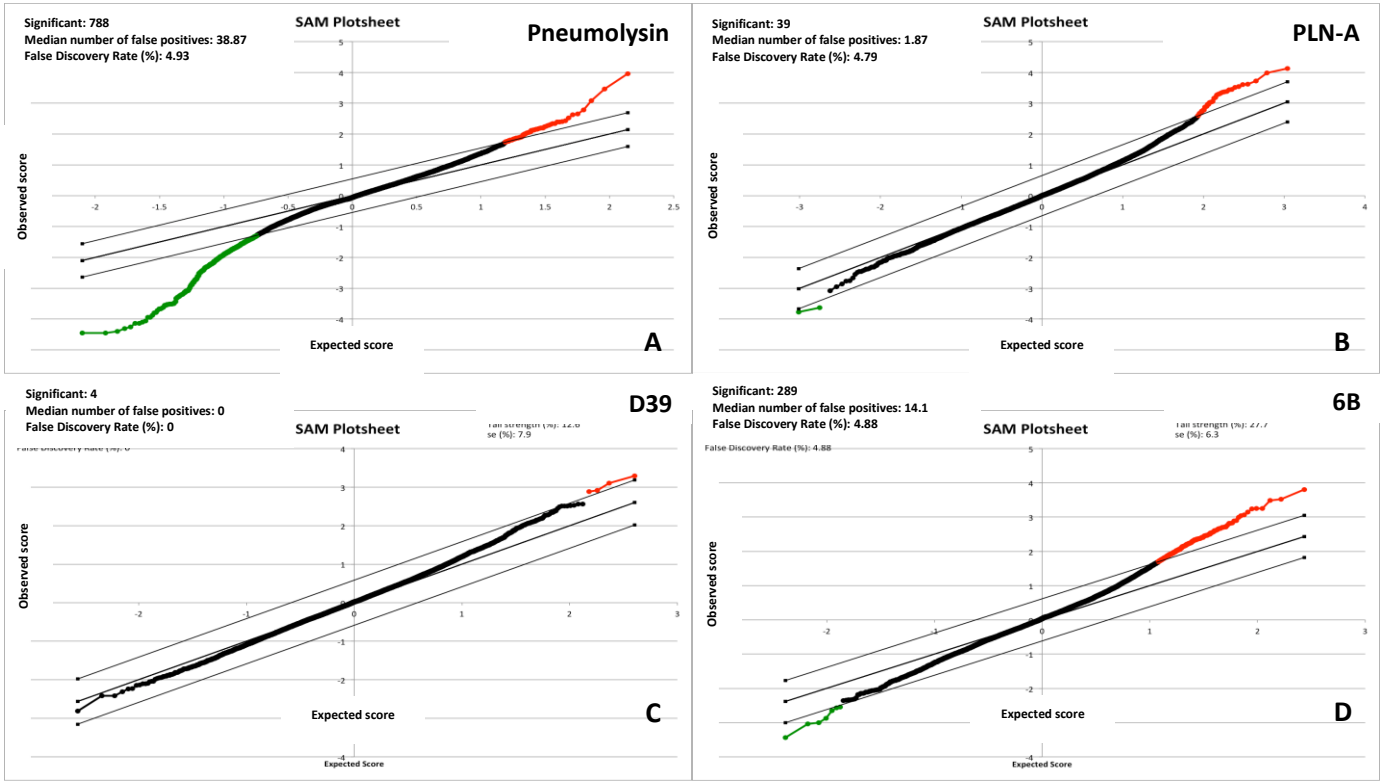

Figure 66| SAM genes analysis from the RNA isolated during treatment of Human Brain Endothelial Cells in a BBB model. The plots presented are significant genes with a false discovery rate of 5%. The Red and Green scatters in the plot represent the genes that match or exceed the delta value threshold (either positively or negatively). The black scatters in the plot are all the up- or down-regulated genes, which are not considered significant by SAM. The conditions shown in the graph are from cells that were challenged with a) 100 ng/ml pneumolysin, b) PLN-A, c) D39 and d) 6B. All the acquired results are in a Log (base2) scale.

Serotype-2 strain D39 displayed only 4 significantly up- or down-regulated genes (figure 66C). Serotype 6B displayed 289 genes significantly expressed genes (figure 66D).

The TreeView® software was used for the visualization of the clustered genes in the form of heat maps. The TreeView® software presented the expressed genes as colored squares. According to the gene's state the square took the color red (up-regulated), green (down-regulated) or black (not differentially expressed).

Hierarchically clustered genes that were in close proximity and were expressed in the same way, displayed a firm band on the heat map. These genes could be compared against different conditions in order to identify if pneumolysin or a pathogen affects a gene by driving its expression. Selection of a band through all conditions used for the experiment allowed for individual gene identification. Since the majority of genes for cells challenged with either D39 or PLN-A did not significantly deviated from untreated cells, I decided to focus my analysis specifically to genes that were expressed when pneumolysin or 6B were used. Figure 67A shows genes that were up-regulated due to exposure of the cells to pneumolysin, whereas figure 67B shows genes that were down-regulated because of pneumolysin.

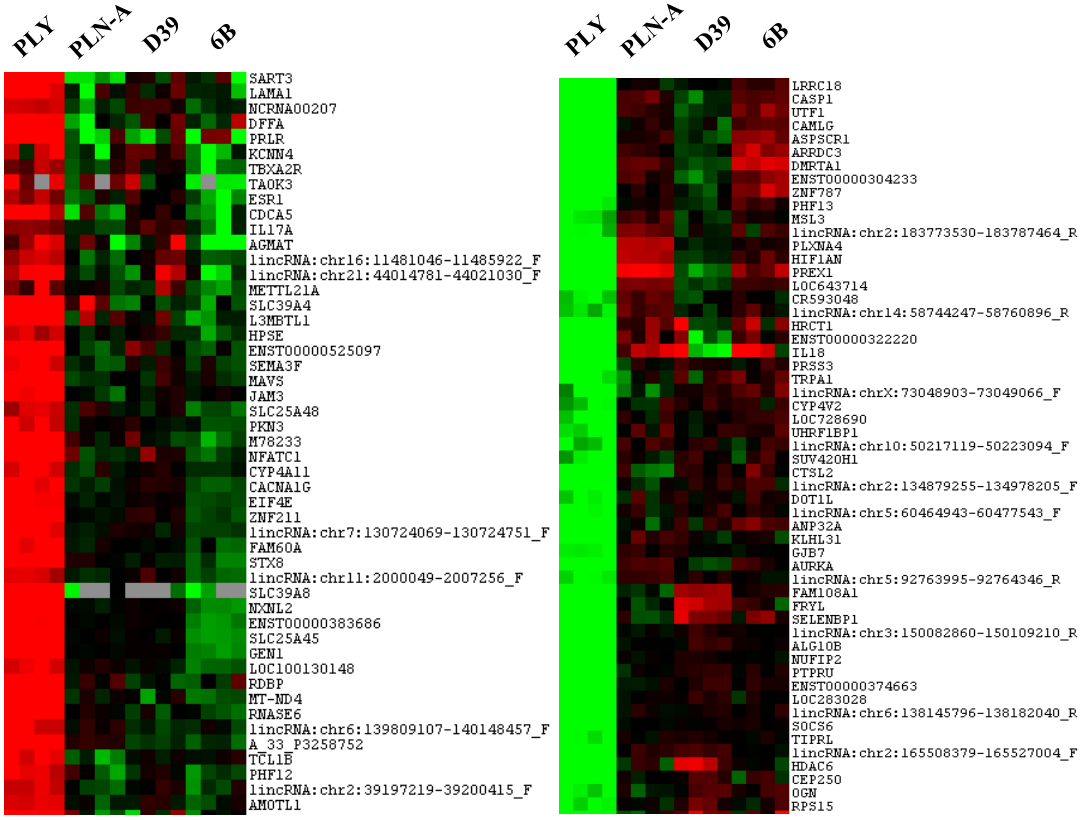

Figure 67| Clustered genes analysis from RNA isolated during infection of Human Brain Endothelial Cells with pneumolysin in a BBB model - presentation in the form of a heat-map Heat map-like representation of Human Brain Endothelial cells at 100% magnification when A) pneumolysin drives specific genes to up-regulate their processes and B) when the toxin down-regulate the process of specific genes. The red squares show up-regulated genes, green squares show down-regulated genes whereas black squares show genes that did not deviated from the expected expression. Different intensity in colour shows different expression levels (intense color shows strong expression – weak color shows less expression). All the acquired results are in a Log (base2) scale.

In the same manner, figure 68A shows the genes that were up-regulated due to exposure of cells to serotype 6B, whereas figure 68B shows genes that were down-regulated due exposure to the specific pneumococci. During my heat-map analysis, I observed that when a gene was up-regulated due to pneumolysin, the same gene would be found to be down-regulated when serotype 6B was used and *vice versa*.

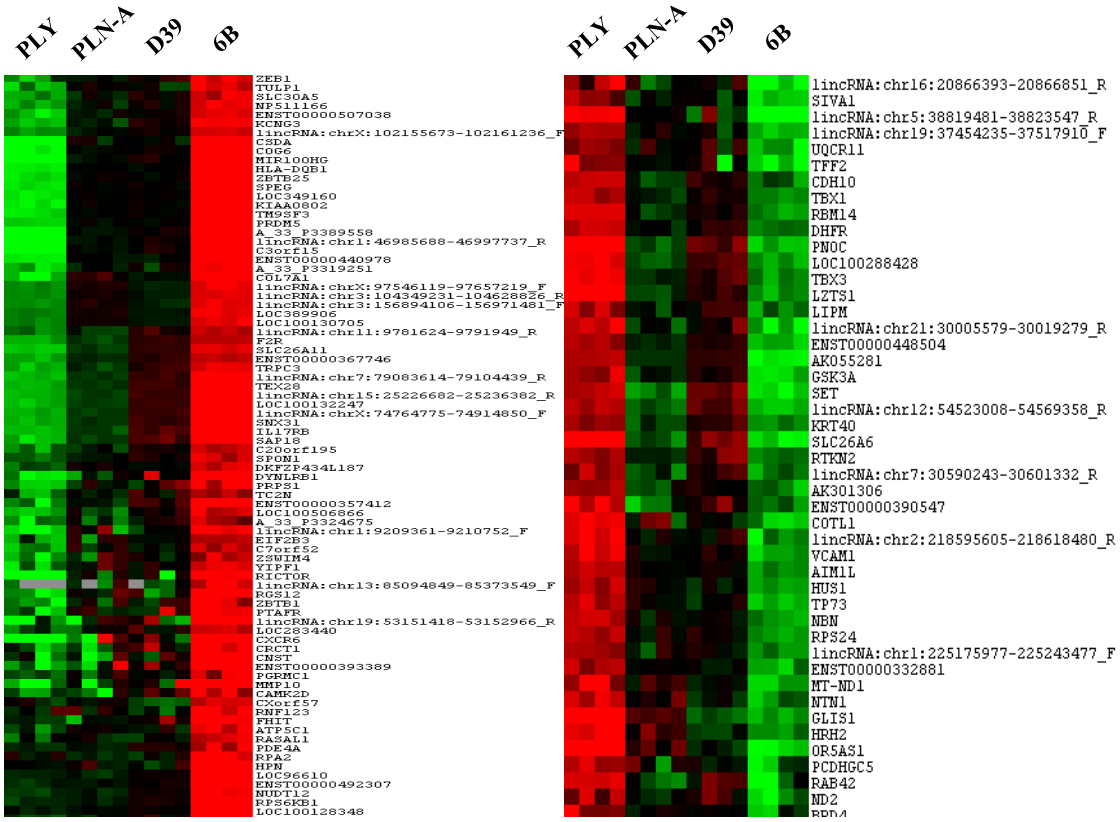

Figure 68| Reverse effects on gene expression when Human Brain Endothelial Cells were challenged with pneumolysin or 6B in a BBB model - presentation in the form of a heat-map Heat map-like representation of Human Brain Endothelial cells at 100% magnification. When pneumolysin drives specific genes to down-regulate their processes (left heat-map), the same genes are down-regulated when 6B is used. In contrast when the toxin up-regulates the processes of specific genes, 6B is found to do the exact opposite to those same genes (right heat-map). The red squares show up-regulated genes, green squares show down-regulated genes whereas black squares show genes that did not deviated from the expected expression. Different intensity in colour shows different expression levels (intense colour shows strong expression – weak colour shows less expression). All the acquired results are in a Log (base2) scale.

I sought to further analyze the data in order to see how these genes contributed in pathways that relate to immune responses, cell-cell interactions as well as infectious diseases.

6.6.0 Gene pathway analysis of the significantly expressed genes during infection with pneumolysin and serotype 6B

The gene ontology (GO) is a project that was created in order to enhance knowledge about the contribution of genes in molecular functions, biological processes, as well as cellular components. This information has 3 different categories (ontologies). The use of GO terms is fortified with the combination of various gene databases. Shared information allows the unification of the databases, but even more effort is now put to this project in order to keep up with the change in knowledge and find a way to smooth information of gene acquired from different databases. An additional analysis, which derives from the GO analysis, is a Gene Ontology (GO) over-representation analysis (ORA). The ORA analysis can show a list of genes or proteins for GO terms, which appear more frequent in the dataset than expected by chance. The accumulation of this frequency, distinguishes the significance of the genes in regards to important biological processes, cellular components or molecular functions.

6.6.1 Infection with pneumolysin

The 6 most significant pathways were selected (3 up-regulated pathways and 3 down-regulated pathways). The sources of the generated pathways were KEGG and REACTOME (Table 6).

Table 6 Pathway over-representation of statistically significant genes: Infection with PLY

Pathway	Source	Genes involved in pathway	p-value	p-value (corrected)	
Regulation of Actin Cytoskeleton	KEGG	ARPC2/GNA13/ITGB2/MAPK3	0.0076	0.0243	↑
Leukocyte trans-endothelial migration	KEGG	CXCR4/ITGB2/JAM3	0.0092	0.0283	↑
Gap Junction	KEGG	MAPK3/PBLC2	0.0421	0.0607	↑
Collagen degradation	REACTOME	COL4A2/COL7A1/MMP10 MMP2/MMP3	0.0266	0.4175	↓
Degradation of the extracellular matrix	REACTOME	ADAMTS1/COL4A2/COL7A1/CTSL2 MMP10/MMP2/MMP3/SPP1	0.0152	0.3538	↓
Activation of MMPs	REACTOME	CTSL2/MMP10/MMP2/MMP3	0.0113	0.3046	↓

Table 6| Pathway over-representation analysis when the bc-BBB is infected with pneumolysin During the analysis of the significant genes, six pathways were selected and a total of 15 genes were involved in these pathways. The values with an upright direction arrow show the p-values of pathways that are up-regulated whereas the values with an downright direction arrow show down-regulated p-values of the pathways. Many pathway information providers can be found online, but KEGG and REACTOME were selected as the providers with the most information in regards to pathways.

In total, 15 genes generated these 6 pathways of which 7 were down-regulated and 8 were up-regulated (Table 7).

Table 7 Significant Analysis of Microarrays (SAM) up- & down-regulated genes: Infection with PLY

Organism	Gene name	Regulation	Score (d)	q-value (%)
Homo Sapiens	ARPC2	↑	+1.9971	2.8600
Homo Sapiens	GNA13	↑	+1.8007	4.4435
Homo Sapiens	ITGB2	↑	+1.8506	3.8074
Homo Sapiens	MAPK3	↑	+1.8393	3.8074
Homo Sapiens	CXCR4	↑	+1.8877	3.8074
Homo Sapiens	JAM3	↑	+2.1126	2.1172
Homo Sapiens	PLCB2	↑	+2.0816	2.1172
Homo Sapiens	COL4A2	↓	-1.4968	2.4490
Homo Sapiens	COL7A1	↓	-1.7437	0.8235
Homo Sapiens	MMP10	↓	-1.4382	3.1569
Homo Sapiens	MMP2	↓	-1.3086	4.9329
Homo Sapiens	MMP3	↓	-2.3017	0.0000
Homo Sapiens	ADAMTS1	↓	-1.4133	3.1569
Homo Sapiens	CTSL2	↓	-2.4806	0.0000
Homo Sapiens	SPP1	↓	-1.3929	3.8074

Table 7| Significant analysis of microarrays (SAM) calculations of the genes involved in pathways when the bc-BBB was infected with pneumolysin From these 15 significant genes, 6 pathways were generated. Seven genes showed up-regulated activities whereas the other 8 genes showed significantly down-regulated activity. The score (d) signifies the correlation of the compared groups (pneumolysin *vs.* PLN-A, D39, 6B) q-value represents the chance of the specific genes to be considered as false positives.

6.6.2 Significantly expressed genes when the BBB model is challenged with pneumolysin

A detailed description of the genes' function and relationship to pneumolysin infection is presented below.

- ACTIN-RELATED PROTEIN 2/3 COMPLEX, SUBUNIT 2 - **ARPC2 gene**:

  It has been demonstrated that localisation of the Arp2/3 protein complex occurs due to pneumolysin interactions with the specific complex [346], which confirms previous work performed with the toxin. The ARPC2 gene is part of the Arp2/3 protein complex found in humans. It has 7 subunits and ARPC2 encodes one of them. This protein complex was found to be involved in the polymerization of actin in cells [347, 348].

- GUANINE NUCLEOTIDE-BINDING PROTEIN, ALPHA-13 - **GNA13 gene**:

  Iliev *et al.*, demonstrated that binding of pneumolysin on the cell membrane activates GTPases [84]. Migration of fibroblasts and endothelial cells is induced by the activation of a tyrosine kinase receptor, which is believed to be associated with the presence of GNA13 [349]. The GNA13 gene encodes G proteins, which regulate correct transfer of information from the receptors found on a cell's surface to the internal components of the cell. G proteins are trimeric and upon their activation GTP is exchanged for GDP [350]. GNA13 was found to interact with Hax1, which favours GNA13 cell migration [351]. The activation of GNA13 due to toxin infection is a novelty in this thesis and it was not previously described in the literature.

- INTEGRIN, BETA-2 - **ITGB2 gene**:

  It has been shown that pneumolysin up-regulates β2 integrins in epithelial cells [352]. The activation of ITGB2 in endothelial cells is considered a novelty and

verification that epithelial and endothelial cells share similar functional characteristics. Activation of endothelial cells with various inflammatory cytokines increases T-cell transendothelial migration suggesting that cytokines may create a binding complex of ITGB2-JAM1 enabling leukocyte migration past the endothelium [45].

- MITOGEN-ACTIVATED PROTEIN KINASE 3 - **MAPK3 gene**:

  It has been demonstrated that pneumococci and pneumolysin are capable of inducing phosphorylation of ERK [353] something that was verified by my findings during this experiment. MAPKs are also characterized as ERK1/ERK2. Upon expression of epidermal growth factor, ribosomal transcription is activated through the ERK1/ERK2 complex whereas blockage of the complex leads to ribosomal transcription being deactivated, suggesting that MAPK3 have a key role in ribosome biogenesis in regards to growth regulation [354].

- CHEMOKINE, CXC MOTIF, RECEPTOR 4 - **CXCR4 gene**:

  Down-regulation of CXCR4 was observed when endothelial cells were treated with TNF-α, INF-γ, or IL1β. The levels of CXCR4 expression remain low for 48 hours during inflammatory responses [355, 356]. The CXC cytokines function through the G protein-coupled receptors such as interleukin-8 receptors IL8RA and IL8RB [357]. In the pathway of figure 7, CXCR4 is shown to be acting outside of the cells. Nevertheless it has been demonstrated that CXCR4 is also found in endothelial cells and is responsible for cellular processes as well as a receptor to

infectious agents [358]. The activation of this gene proves the existence of CXCR4 in endothelial cells and confirms its contribution towards infection.

- JUNCTIONAL ADHESION MOLECULE 3 - **JAM3 gene**:

  The up-regulation of this gene in my experiments confirms previous studies, where adhesion molecules showed up-regulation of their expression when exposed to pneumolysin [91]. M JAM3 strongly interacts with JAM2. Blocking the C domain of the protein increased transmigration of monocytes through the endothelial cell monolayer. Mutation of the JAM3 gene leads to brain injury by hemorrhage [359, 360].

- PHOSPHOLIPASE C, BETA-2 - **PLCB2 gene**:

  Instabilities of calcium levels due to pneumolysin have previously been observed when calcium influx driven by the activation of GTPases [84]. The specific up-regulation of PLCB2 shows the significance of this gene in calcium influx processes. Deficiency or absence of the PLCB2 gene promotes instabilities in cytoplasmic calcium levels [361-365].

- MATRIX METALLOPROTEINASE 10 - **MMP10 gene**:

  MMP10 has been previously shown to be down-regulated upon use of cytolysins [366], but not specifically due to pneumolysin, which is considered to be a novelty. MMP10 is closely associated with the HISTONE DEACETYLASE 7A gene (HDAC7A). Down-regulation of MMP10 by HDAC7A was crucial for the correct

function of MMP10 whereas deletion of the HDAC7A gene significantly up-regulated MMP10 concentrations, resulting in vascular damage in mouse endothelium [367]. MMP10 is part of the MMPs family and is capable of degrading most components of the extracellular matrix as well as the basal membrane in order to progress to tissue remodelling. MMP10 can specifically degrade laminin, elastin, proteoglycan core protein, fibronectin, gelatins, as well as various types of collagen [368].

- MATRIX METALLOPROTEINASE 2 - **MMP2 gene**:

  Similarly to MMP10, MMP2 was also down-regulated when cytolysins were used on cells [366] but no previous experiments were performed to prove the impact of pneumolysin specifically. The MMP2 proteinase is associated with integrin alpha-V and integrin beta-3 which are predominantly expressed on the surface of blood vessels. These two integrins are responsible for the suppressed activity of MMP2 in order to maintain correct vascular function and prevent inflammation [369, 370]. MMP2 is widely known as type IV collagenase since it specifically cleaves type IV collagen, which is fundamental to the creation of basement membranes.

- MATRIX METALLOPROTEINASE 3 - **MMP3 gene**:

  MMP3 expression was activated when neonatal rats suffered from bacterial meningitis [371]. MMP3 is produced upon activation of IL1B as well as the epidermal growth factor [372, 373] MMP3 is produced predominantly by cells that have connective tissue characteristics. It can degrade fibronectin, laminin,

proteoglycan as well as type IV collagen but not type I collagen. My findings have shown deactivation of this gene which contradicts the findings supported by the literature.

- CATHEPSIN L2 - **CTSL2 gene**:

  Instability of cathepsins levels leads to hydrogen peroxide production. Oxidative stress has been previously associated with bacterial meningitis in humans [285], which may progress to tissue degradation (matrix degradation) [374]. Although the down-regulation of this gene confirms the general knowledge around oxidative stress, it was not previously described to be directly associated with the BBB. Cathepsins are papain cysteine proteinases and are involved in many cellular processes.

- COLLAGEN, TYPE IV, ALPHA-2 - **COL4A2 gene**:

  Interactions of the pneumococci with the extracellular matrix have shown type IV collagen binding by the bacteria [375]. Down-regulation of COL4A2 leads to neuronal inflammation and parenchymal hemorrhage [376]. The use of the toxin alone during this experiment shows that COL4A2 is directly interacting with pneumolysin during adherence processes with the pneumococci, something that was not previously characterized. COL4A2 is related to proteoglycans, which form the membrane layer between the epithelium or between the endothelium. Entactin, laminin and heparin sulphate are proteoglycans directly associated to type IV collagen [377-379].

- COLLAGEN, TYPE VII, ALPHA-1 - **COL7A1 gene**:

  Down-regulation of COL7A1 can lead to the dissociation of some extracellular matrix components [380]. Down-regulation of COL7A1 has never been associated to pneumolysin. The COL7A1 gene is responsible for the expression of the alpha-1 chain in type VII collagens. The basal lamina consists of fibrils, which have as a main component collagen type VII [381].

- A DISINTEGRIN-LIKE AND METALLOPROTEINASE WITH THROMBOSPONDIN TYPE 1 MOTIF, 1 - **ADAMTS1 gene**:

  Absence of ADAMTS1 due to pneumococcal infection leads to improper cleavage of multimers released by the brain endothelium and causes microangiopathy [382]. These innovative findings show that the ADAMTS gene can be independently silenced by pneumolysin during pneumococcal infection. The ADAMTS proteins are found on the extracellular matrix and interact with other matrix components. Activation of ADAMTS1 leads to angiogenesis disruption [383].

- SPHINGOSINE-1-PHOSPHATE PHOSPHATASE 1 - **SPP1 gene**:

  The SPP1 gene encodes the enzyme that catalyses the dephosphorylation of sphingosine-1-phosphate, a lipid that has an important role in cell proliferation, angiogenesis and apoptosis [384]. With SP1 usually found in relatively low concentrations, it is believed that recycling of the SP1 lipid distorts normal SP1 quantities and leads to increased vascular permeability and cytoskeletal instability [384, 385]. The deactivation of this gene due to toxin infection is a novel finding,

since instabilities of its expression have never been associated with infection before.

6.6.2 Infection with *Streptococcus pneumoniae* serotype-6B

The 3 most significant pathways (only 3 available) were selected (3 up-regulated pathways). The sources of the generated pathways were KEGG and REACTOME (Table 8).

Table 8 Pathway over-represantattion analysis of statistically significant genes: Infection with 6B

Pathway	Source	Genes involved in pathway	p-value	p-value (corrected)
Type I diabetes Melitus	KEGG	HLA-DPA1/HLA-DQB1/IL12A IL12B/PTPRN	0.0001	0.0134 ↑
Cytokine-cytokine interactions	KEGG	CXCR6/EGFR/IL12A/IL12B IL17RB/IL1RAP/IL6ST	0.0160	0.1114 ↑
T-cell receptor signalling pathway	KEGG	CBLB/FYN/PAK7/VAV3	0.0235	0.1193 ↑

Table 8| Pathway over-representation analysis when the bc-BBB is infected with 6B During the analysis of the significant genes, three pathways were selected and a total of 14 genes were involved in these pathways. No down-regulated pathways could be detected. The values with an upright direction arrow show the p-values of pathways that are up-regulated. Many pathway information providers can be found online, but KEGG was selected as the provider with the most information in regards to pathways.

A total of 14 genes contributed to the generation of the 3 pathways and all these genes were significantly up-regulated (Table 9).

Table 9 Significant Analysis of Microarrays (SAM) up- & down-regulated genes: Infection with 6B

Organism	Gene name	Regulation	Score (d)	q-value (%)
Homo Sapiens	HLA-DQB1	↑	+2.3735	1.3378
Homo Sapiens	HLA-DPA1	↑	+1.9945	2.6584
Homo Sapiens	IL12A	↑	+1.9160	2.6584
Homo Sapiens	IL12B	↑	+2.0326	2.3364
Homo Sapiens	PTPRN	↑	+1.8210	3.5906
Homo Sapiens	CXCR6	↑	+2.6150	0.0000
Homo Sapiens	EGFR	↑	+1.8679	2.9928
Homo Sapiens	IL17RB	↑	+2.4873	0.0000
Homo Sapiens	IL1RAP	↑	+1.8340	3.1749
Homo Sapiens	IL6ST	↑	+1.8392	3.1749
Homo Sapiens	CBLB	↑	+2.3314	1.3378
Homo Sapiens	FYN	↑	+1.8082	3.5906
Homo Sapiens	PAK7	↑	+1.7506	3.9186
Homo Sapiens	VAV3	↑	+1.7311	4.4915

Table 9| Significant analysis of microarrays (SAM) calculations of the genes involved in pathways when the bc-BBB was infected with 6B All 14 were involved in the generation of three pathways. The score (d) signifies the correlation of the compared groups (6B *vs.* pneumolysin, PLN-A, D39) q-value represents the chance of the specific genes to be considered as false positives.

6.6.3 Significantly expressed genes when the BBB model is challenged with 6B

A detailed description of the genes' function and relationship to pneumococcal infection is presented below.

- CHEMOKINE, CXC MOTIF, RECEPTOR 6 - **CXCR6 gene**:

  It has been previously shown that CXCR6 is expressed on microvascular endothelial cells and its expression is dependent on IL-1β concentrations [386]. The presence of IL-12 leads to the up-regulation of CXCR6 whereas the chemokine was reduced in the presence of IL-4. CXCR6 may also have a key role in effector T-cell trafficking, which facilitates inflammation [387]. The activation of this gene in the BBB due to serotype 6B was not previously described.

- EPIDERMAL GROWTH FACTOR RECEPTOR - **EGFR gene**:

  It has previously been shown that phosphorylation and up-regulation of EGFR during bacterial infection lead to increased bacterial invasion [388] which was confirmed in my findings during this experiment.

  The EGFR is a receptor assigned as a cell-signalling molecule. This receptor is responsible for cell proliferation, development and survival [389]. The EGF receptor binds to the EGF, which is associated with signalling of the previously mentioned Rho family.

- INTERLEUKIN 17, RECEPTOR B - **IL17RB gene**:

  Expression of IL17RB is critical since inhibition of expression of this receptor leads to higher uptake of pneumococci [390]. The activation of this gene confirms the need of the BBB to reduce the uptake of pneumococci during infection. Overexpression of IL17RB showed increased production of IL8, suggesting that the protein is associated with proinflammatory processes [391]. IL17RB is

member of a group of proteins relating to structure and cell assembly and interacts with a homolog member called IL17BR.

- INTERLEUKIN 1 RECEPTOR ACCESSORY PROTEIN - **IL1RAP gene**:

  IL1RAP is directly associated with toll-interleukin 1 receptor accessory protein (TIRAP) which was activated in individuals suffering from severe pneumococcal infection [392]. This is also found during my experiments with serotype 6B. Activation of IL1 in an in vitro model showed the formation of the IL1RAP:ILIRA complex initiating a signalling cascade for IL1B production. Overexpression of IL1RAP leads to the inability of Interleukin 1 Receptor Associated Kinase (IRAK) to form the IL1RAP:IL1RA complex. Lack of the IRAK protein was shown to reduce production of INF-γ [393]. This gene encodes a transmembrane protein, which is important for IL1 signalling during infection [394].

- INTERLEUKIN 6 SIGNAL TRANSDUCER - **IL6ST gene**:

  The IL6ST gene encodes the glycoprotein 130 (gp130), which is a signal transducer for IL6, IL11, oncostatin M (OSM), leukaemia inhibitory factor (LIF) and ciliary neurotrophic factor (CNTF) [395]. The gp130 receptor was shown to trigger the activation of YES –Associated Protein (YAP) and the transmembrane receptor Notch. IL6ST is involved in brain barrier immune responses as well as brain development [396]. These two proteins are responsible for the regeneration as well the growth of tissue. The coexistence of YAP-Notch-gp130, stimulates the epithelial/endothelial proliferation, and aids in the preservation of mucus in

epithelial cells [397]. This is an innovative finding since the IL6ST gene was not previously associated with pneumococcal infection.

- CAS-BR-M MURINE ECOTROPIC RETROVIRAL TRANSFORMING SEQUENCE B - **CBLB gene**:

  Absence of the CBLB gene leads to the release of cytokines and chemokines involved in sepsis. CBLB is also responsible for toll-like receptor-4 regulation (TLR4) during a septic episode [398]. The CBLB gene controls the tolerance of peripheral immunity by reducing T-cell activity [399]. CBLB thus, has the ability to prevent chronic inflammation and autoimmunity. In the current experiments the activation of the gene proves its importance in regulating inflammatory responses during infection.

- FYN ONCOGENE RELATED TO SRC, FGR, YES - **FYN gene**:

  In the absence of the gene, function of nuclear factor kappa-B (NFKB) pathways and B-cell development is impaired [400]. The FYN gene is part of the protein-tyrosine kinase family and it was shown to be essential for successful cell growth. The activation of this gene is another confirmation of the BBB ability to respond to infection in an effort to maintain stability in the system.

- PROTEIN-ACTIVATED KINASE 7 - **PAK7 gene**:

  This kinase is abundantly expressed in the brain and was found to regulate the dynamics of the cell cytoskeleton, cell death, cell cycle, and cell signaling. It

promotes neurite development (end-feet of neuronal cells) [401, 402]. Although the above were also seen in my model it was not previously shown that PAK7 gene is activated due to pneumococcal infection.

- VAV 3 ONCOGENE - **VAV3 gene**:

  The VAV3 protein is closely linked with receptors related to tyrosine kinases. Mutated versions of the VAV3 gene lead to malformation of cells and impairment in cytokinesis [403]. The gene was previously investigated and it was shown to be up-regulated in patients with colorectal cancer [404] but it was never associated with pneumococcal infection.

- MAJOR HISTOCOMPATIBILITY COMPLEX, CLASS II, DP ALPHA-1 - **HLA-DPA1 gene**:

  The HLA-DPA1 gene is one of the three major isotypes of the human class II major histocompatibility complex (MHC) molecules [405]. The HDLA-DPA1 gene was shown to be an essential regulator of normal immune responses in humans [406]. The HLA-DPA1 was not previously associated with pneumococcal infection.

- MAJOR HISTOCOMPATIBILITY COMPLEX, CLASS II, DQ BETA-1 - **HLA-DQB1 gene**:

  HLA-DQB1 is expressed on the surface of endothelial cells and drives immunity via interactions with T-cells of the circulatory system [407]. It was previously shown that the HLA class II molecules could determine the immune reaction against invasive pneumococcal disease [408] and my data confirm these findings. Patients expressing the HLA-DQB1 gene were less likely to develop severe systemic disease [408]. The HLA-DQB1 gene encodes parts of the MHC class II complex and is found anchored in the cell membrane.

- INTERLEUKIN 12A - **IL12A gene**:

  IL12, a proinflammatory cytokine associated with type 1 immune responses has been previously detected in patients suffering with pneumococcal meningitis [409]. The activation of these genes during my experiments confirms the previous findings. Interestingly, IL12A also forms a component (together with EBI3) of the cytokine IL35 that has been associated with T regulatory cell function. Both IL12A and EBI3 showed increased expression in GFP+ cells from fork-head box p3 (FOXP3) eGFP transgenic mice. Furthermore, immuno-precipitation of EBI3 and IL12A occurs in T-regulatory cells (Tregs) but not in effector T-cells. EBI3 is a downstream target of FOXP3 and it has been demonstrated that Treg cells produce IL35, which enhances their suppressive abilities [410].

- INTERLEUKIN 12B **IL12B gene**:

  During a gene expression analysis of European American and African American patients, it was shown that IL12B was highly expressed in people suffering from invasive pneumococcal disease [411]. Activation of IL12B was also observed during my experiments with serotype 6B IL12B is one subunit of IL23 (together with p19) (IL23A) [412]. Disruption of the normal functions of IL12B leads to impaired production of interferon-γ (INF- γ) [413].

- PROTEIN-TYROSINE PHOSPHATASE, RECEPTOR-TYPE, N - **PTPRN gene**:

  It has been demonstrated that activation of the PTPR complex leads to increased endothelial cell permeability [414]. The PTPRN gene was found to interact with spectrin beta non-erythrocytic 4 (SPTBN4), which encodes a protein responsible for the organization of cell transmembranes and organelles [339]. The PTPRN gene encodes proteins from the tyrosine phosphatase family (PTP). These proteins are responsible for the regulation of processes such as cell growth, cell differentiation as well as cell mitosis [339]. The PTRPN gene was not previously associated with pneumococcal infection.

6.7.0 Discussion

6.7.1 Generation of pathways when the BBB model was incubated with pneumolysin

**** It is important to point out that all comparisons for up- or down-regulated genes relate to gene expression that deviates from untreated cells. As previously mentioned, the RNA collected from untreated cells was used as the background during the microarray analysis. Figures of these pathways are in the appendix of the thesis marked as "Ap".*

6.7.2 Up-regulation of Actin Cytoskeleton

Cell movement is a crucial process and the actin cytoskeleton contributes to embryonic morphogenesis, angiogenesis, monitoring of the immune system, and regeneration of damaged or dead tissue. Preserving the correct dynamics in the actin cytoskeleton allows these processes to be executed correctly [415]. The four protein products of genes related to these pathways that were up-regulated during infection were extracellular signal-regulated kinase (ERK), G_{12}/G_{13} alpha subunits ($G\alpha_{12/13}$), integrin (ITG) and the actin-related complex 2/3 (Arp2/3) (figure Ap1). A recent report demonstrated that upon pore formation of pneumolysin, actin polymerization was enhanced suggesting that actin co-localizes with pneumolysin [346].

6.7.3 Up-regulation of Leukocyte trans-endothelial migration pathways

Leukocyte migration from blood into tissues is a key process in the fight against infection and in inflammation. The leukocytes bind to endothelial cell adhesion molecules (CAM) and further on migrate across the vascular endothelium. During the migration process, alpha/beta2 integrin activates RhoA (through VAV), which subsequently activates the kinase p160ROCK. ROCK activation leads to the retraction of the actin cytoskeleton. Leukocytes are also responsible for the endothelial cell retraction during localized dissociation of the endothelial cell junctions [341]. The protein products of the three genes related to this pathway up-regulated were JAM3, ITGB2 and CXCR4. Although the pathway shows up-regulation of genes that are not directly found on endothelial cells, an immediate relationship of those genes is observed with the receptors found on the endothelial cells (figure Ap2). ROCK activation was also present when cells were co-infected with pneumolysin [84].

6.7.4 Up-regulation of Gap Junction genes

Gap junctions contain intercellular channels that allow direct contact between the cytosol of adjacent cells. These channels enable small molecules such as amino acids, nucleotides and ions to be transferred between adjacent cells. This internal communication is crucial for many biological processes, such as homeostasis of tissue, transport of metabolites, cell apoptosis, electrical coupling or even embryonic development. Applying voltage between the junctions, changing the pH or the level of calcium cations in the cell (Ca^{2+}) is something that would initiate gap junction communication in order to preserve equilibrium in the cells [341]. Pneumolysin has been shown to dissociate gap junctions in

a rat pneumococcal meningitis model [416]. The two protein products of genes associated with this pathway that were up-regulated were Phospholipase C (PLC), and the extracellular signal-regulated kinases complex 1&2 (ERK 1/2) (Figure Ap3).

6.7.5 Down-regulation of MMP activation pathway

MMPs play key roles in the remodeling of tissue, homeostasis and morphogenesis. MMP expression is associated with several diseases, such as cancer, atherosclerosis and encephalitis [417]. Four genes involved in this pathway were found to be down-regulated during infection. These encode the proteinases MMP2, MMP3, and MMP10 (figure Ap4). It has been previously shown that MMPs degrade pore-forming toxins [366]. Down-regulation of MMPs could void protection of neutrophils against the pneumococci and allow them to progress in the tissue [418], thus, the process of MMP down-regulation may be pathogen-driven. Most MMPs are bound on the membrane of the cell but others can be found to have interactions with proteins intracellularly [419]. Usually the MMPs are not activated unless they are released. The degree of their activation is dependent on cellular transcription, other associated MMPs or the tissue inhibitors of metalloproteinases (TIMPs). When activated, MMPs degrade the extracellular matrix (ECM) and remove its components.

6.7.6 Down-regulation of Collagen degradation pathway

Matrix metalloproteinases (MMPs) have a crucial role in collagen degradation as well as degradation of other macromolecules found on the extracellular matrix. Degradation of collagen leads to the dissociation of the endothelial monolayer and eventually the BBB

breakdown [420]. Five genes related to this pathway were down-regulated in infection, and these encode MMP2, MMP3, MMP10, COL4A2 and COL7A1 (figure Ap5).

6.7.7 Down-regulation of extracellular matrix degradation pathway

Decomposition of the ECM releases growth factors, which are connected to the ECM [421]. Eight genes involved in this pathway were down-regulated (figure Ap6). Inhibition of MMPs was observed when interacting with pore-forming cytolysins [418].

6.7.8 Generation of pathways when the BBB model is challenged with 6B

6.7.9 Up-regulation of cytokine-cytokine interaction pathways

Cytokine expression has been shown to be associated with pneumococcal meningitis, causing inflammation and tissue damage [259]. They are very important regulators of the host immune response and their role extends to both innate and adaptive responses. Cytokines have a role in cell repair, homeostasis, and angiogenesis and in cell development. Released by various types of cells, cytokines are part of many activating cascades and according to their receptors and target cells, can be divided into different families [341]. The protein products of the 7 genes involved in these pathways that were significantly upregulated during 6B infection are shown in figure Ap7.

6.7.10 Up-regulation of T-cell receptor signalling pathway

Although no T-cells were used in the model, it has been demonstrated that endothelial cells have class I and II MHC-peptide complexes on their surface, which regularly interact with T-cells in the circulatory system [407]. Various phosphatases, GTP-binding proteins and tyrosine kinases contribute to the initiation of a cascade where T-cells and cytokines

interact to drive inflammatory response [341]. Four genes involved in this pathway encode were up-regulated in serotype 6B infection (figure Ap8).

6.7.11 Up-regulation of Type I Diabetes Mellitus pathway

Although the pathway relates to type I diabetes mellitus, the immunological responses of this pathway could be applied to other cell types and conditions. The online software generates the pathways according to which genes are linked by interactions and what diseases are often associated with these genes [341]. As previously mentioned, endothelial cells have class I and II MHC-peptide complexes on their surface [407]. Additionally it was shown that endothelial cells could affect the function of B cells, a process driven by laminins [422]. Five genes related to this pathway were up-regulated (figure Ap9).

6.8.0 Conclusions

In this chapter I investigated gene expression of endothelial cells when different pneumococcal serotypes or pneumolysin are used in the BBB model. High numbers of significant genes were observed when the BBB was challenged either with pneumolysin or 6B. A very low number of significant genes were identified when the BBB model was challenged with D39 or its isogenic mutant PLN-A thus, my studies were focused on serotype-6B and the recombinant pneumolysin used with the model.

CHAPTER 7.

Investigation Of Host Factors That Influence Blood-Brain Barrier Integrity During Pneumococcal Infection

7.0 Aims

To investigate host factors that may influence BBB integrity during pneumococcal infection. I have demonstrated that TEER of cells declines during pneumococcal infection *in-vitro*. TEER loss has been linked to damage to the host cells and inter-cellular junctions of the BBB [423].

7.1.0 Host inflammatory cytokine release

Human cells release inflammatory cytokines following bacterial infection [424]. Pro-inflammatory cytokines have been reported to cause host and tissue damage [425]. Advancing on from my transcript abundance analyses, I decided to measure cytokine protein abundance (i.e. the translational products) following exposure to each agent (bacterial serotype or pneumolysin), and relate cytokine abundance to TEER among each infection experiment. I focused on three key cytokines, IL-1β, IL-6 and IL-8 previously reported to be upregulated during pneumococcal infection [241, 261, 278]. I also examined transcript abundance (using my previous results) within the signaling pathways for each of these cytokines.

7.2.0 Tight Junction Integrity

The adjacent endothelial cells composing the BBB are held closely together via the 'tight junction' [9]. Loss of integrity within the tight junction has been reported to cause a drop in TEER [426]. Zonula occludens 1 (ZO-1) is a critical component of the tight junction [427]. An indirect marker of junction integrity is observation of ZO-1 in the walls of the

endothelial cells forming the BBB [428]. I examined the presence, the location and relative amount of ZO-1 protein in the endothelial cell monolayer, following agent exposure in each experiment.

7.3.0 Host inflammatory cytokine measurement

The concentration of each secreted cytokine (IL-6, IL-1β and IL-8) was measured via enzyme-linked immunosorbent assay (ELISA). Samples (supernatant) were collected at 2 hours post agent exposure from the top compartment, containing the endothelial cell layer, of the model. Replicate experiments (n=3) were measured per condition.

7.3.1 Interleukin 6 secretion using an ELISA assay

The median concentration for IL-6 in the supernatant from 3 replicate experiments per condition was 808.60, 635.20, 92.45 and 27.57 pg/ml for 6B, PLN-A, pneumolysin and D39 respectively (figure 69). The concentration for IL-6 was significantly higher following exposure to 6B compared to either D39 or pneumolysin ($p<0.001$ and $p<0.01$ respectively). Similarly, the concentration for IL-6 was significantly higher following exposure to PLN-A compared with either D39 or pneumolysin ($p<0.01$ and $p<0.01$ respectively). Significant differences were determined using a Mann-Whitney U test.

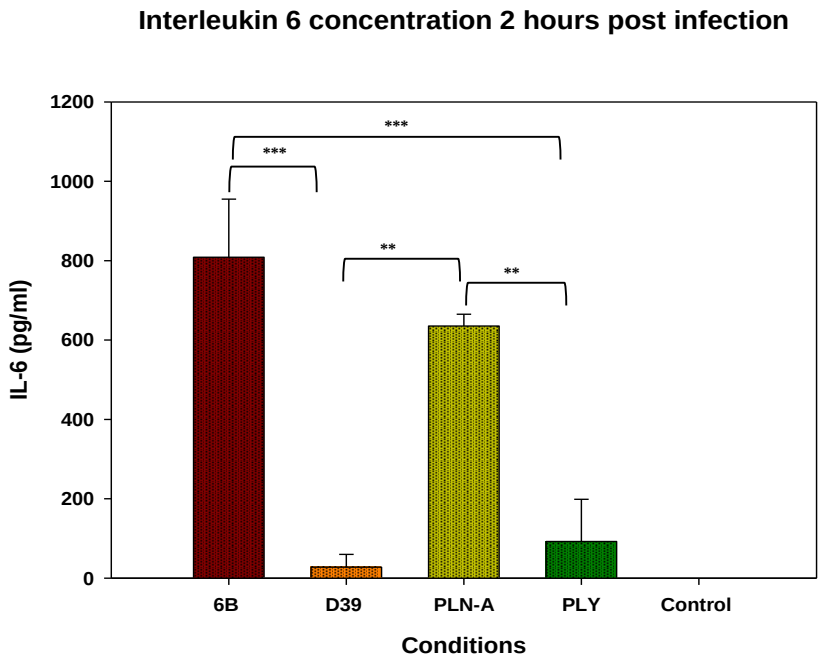

Figure 69|Interleukin 6 levels when the BBB model was challenged with *Streptococcus pneumoniae* serotype-2, -6B and the toxin pneumolysin During an ELISA assay, high concentrations of IL-6 were observed when the model was challenged with 6B or PLN-A. Challenging cells with 6B revealed a significant difference between the current serotype and D39 or pneumolysin (***p<0.01). PLN-A was also significantly different from D39 and pneumolysin, (**p<0.01). Significant differences are determined using a Mann-Whitney U test and relate to differences of interleukin 6 concentrations as compared to the type of pneumococcal strain. **P<0.01, ***P<0.001 at 95% confidence interval.

7.3.2 Interleukin 1β secretion using an ELISA assay

The median concentration for IL-1β in the supernatant from 3 replicate experiments per condition was 2.14, 13.07, 28.75 and 26.01 pg/ml for 6B, PLN-A, pneumolysin and D39 respectively (figure 70). The concentration for IL-1β was significantly higher following exposure to PLN-A compared to 6B ($p<0.05$). Significant differences were determined using a Mann-Whitney U test.

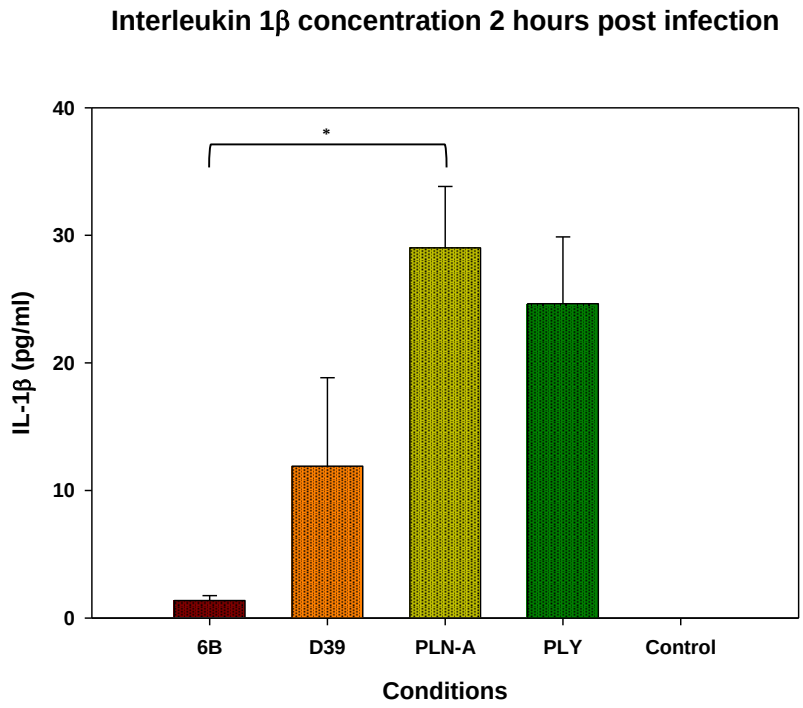

Figure 70|Interleukin 1β levels when the BBB model was challenged with *Streptococcus pneumoniae* serotype-2, -6B and the toxin pneumolysin During an ELISA assay, high concentrations of IL-1β were observed when the model was challenged with PLN-A or pneumolysin. Challenging cells with PLN-A revealed a significant difference when compared to serotype-6B (*p<0.05). Significant differences are determined using a Mann-Whitney U test and relate to differences of interleukin 1β concentrations as compared to the type of pneumococcal strain. *P<0.05 at 95% confidence interval.

7.3.3 Interleukin 8 secretion using an ELISA assay

The median concentration for IL-8 in the supernatant from 3 replicate experiments per condition was 1129.11, 226.28, 1068.93 and 175.78 pg/ml for 6B, PLN-A, pneumolysin and D39 respectively (figure 71). The concentration for IL-8 was significantly higher following exposure to 6B compared to either D39 or pneumolysin ($p<0.001$ and $p<0.01$ respectively). Similarly, the concentration for IL-8 was significantly higher following exposure to PLN-A compared with either D39 or pneumolysin ($p<0.01$ and $p<0.01$ respectively). Significant differences were determined using a Mann-Whitney U test.

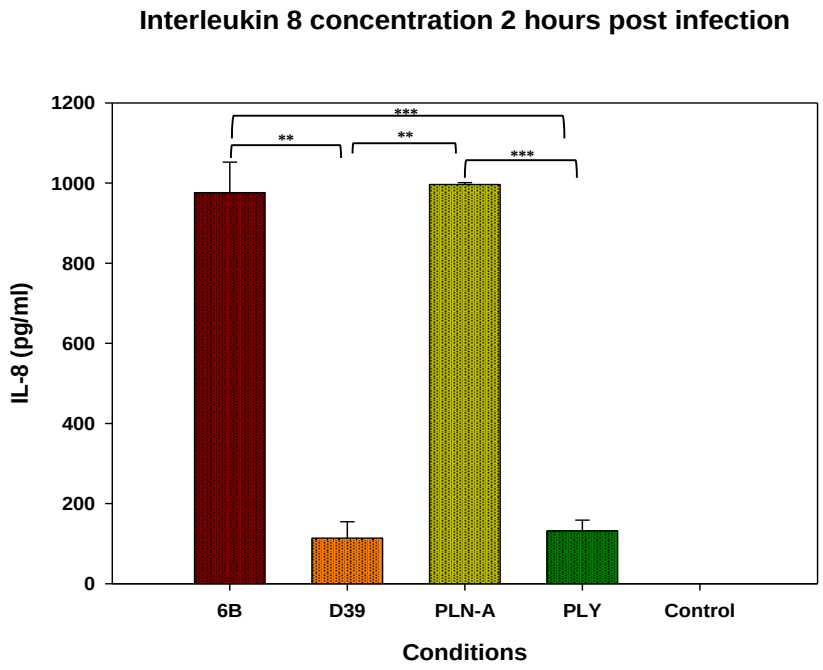

Figure 71|Interleukin 8 levels when the BBB model was challenged with *Streptococcus pneumoniae* serotype-2, -6B and the toxin pneumolysin During an ELISA assay, high concentrations of IL-8 were observed when the model was challenged with 6B or PLN-A. Challenging cells with 6B revealed a significant difference when compared to D39 or pneumolysin (**p<0.01). PLN-A was also significantly different from D39 and pneumolysin, (**p<0.01). Significant differences are determined using a Mann-Whitney U test and relate to differences of interleukin 8 concentrations as compared to the type of pneumococcal strain. **P<0.01, ***P<0.001 at 95% confidence interval.

7.4.0 Interleukin 6 gene expression and its contribution towards the Interleukin 6 pathway

As seen in the data acquired from the microarray experiment, up-regulation of IL-6 was observed when 6B or PLN-A (figure 72). When the total gene population was uploaded to the REACTOME database, over-representation of specific transcripts appeared in the analysis. There was a major difference in expression when the pathway was either visualized with data acquired from 6B or PLN-A (pathway 1A+C). Specifically the IL6R-2 gene was activated only when the cells were challenged with 6B or PLN-A. An overall reduction in expression was observed when the cells were challenged with D39 or pneumolysin (pathway1B+D).

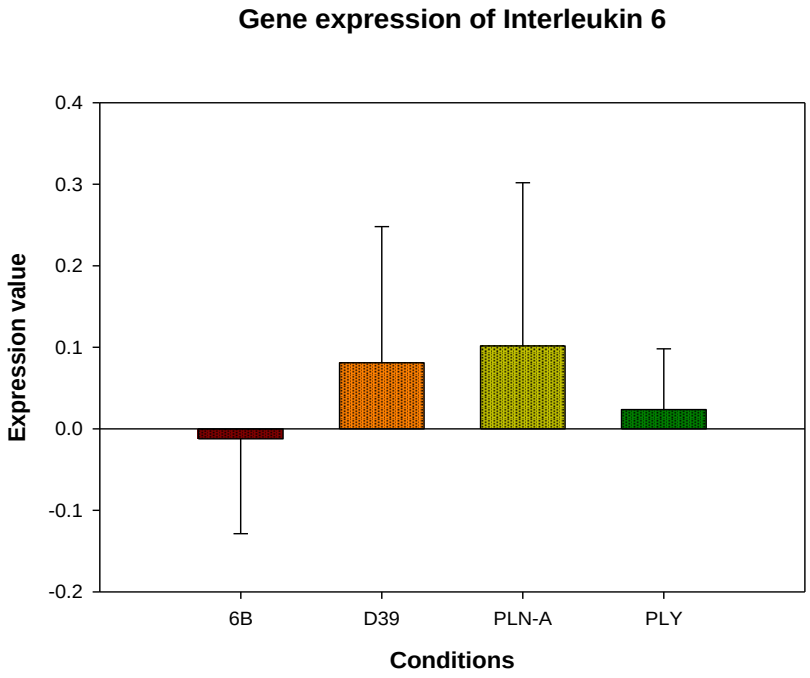

Figure 72|Interleukin 6 gene expression when the BBB model was challenged with *Streptococcus pneumoniae* serotype-2, -6B and the toxin pneumolysin Interleukin 6 exhibited more expression when 6B or PLN-A were co-cultured with the model. The data are shown in expression values, as acquired post calculation with the SAM® software.

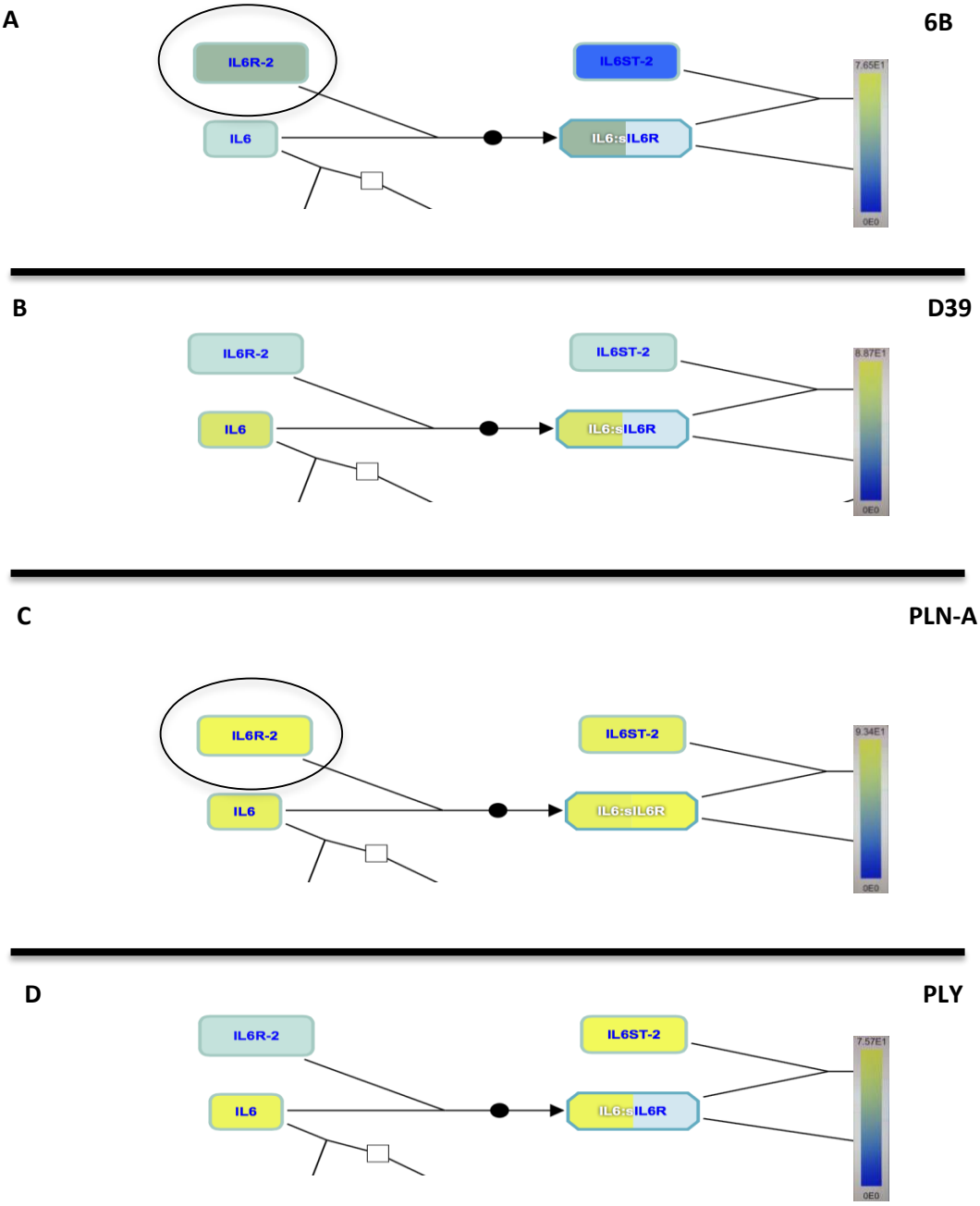

Pathway 1| Interleukin 6 signalling when the BBB model was challenged with *Streptococcus pneumoniae* serotype-2, -6B and the toxin pneumolysin The pathway was generated without setting a threshold of significance. No activation of the IL-6 transcript was observed during infection with pneumococcal 6B. Relevant transcripts to IL-6 were activated. The IL6R-2 transcript (in circle) was activated only when the cells were challenged with 6B or PLN-A (more expression observed with 6B – dark grey color). The pathway was generated using **only** the positively regulated genes from the gene expression assay. The pathway was generated using the REACTOME Pathway Database. The colored ladder designates differences in expression in the form of the q-value (dark blue = highest expression – grey = moderate expression - yellow = least expression – light blue = gene not present for this transcript). One or more genes can contribute in the activation of a complex, and this is illustrated with different colored bars (variation in expression) inside the complex. Although multiple complexes were activated during the generation of this pathway, I only highlighted the transcript relevant to my observations in previous experiments.

7.4.1 Interleukin 1β gene expression and its contribution towards the Interleukin 1β pathway

As seen in the data acquired from the microarray experiment, up regulation of IL-1β was observed when D39, PLN-A and pneumolysin were used (figure 73). The gene expression for the IL1 pathway revealed that the interleukin 1 transcript showed maximal activation for cells challenged with PLN-A (pathway 2C). Similar activation of transcripts was observed for D39 and pneumolysin (pathway 2B+D) whereas the least activation of transcripts in the pathway was observed for cells challenged with 6B (pathway 2A).

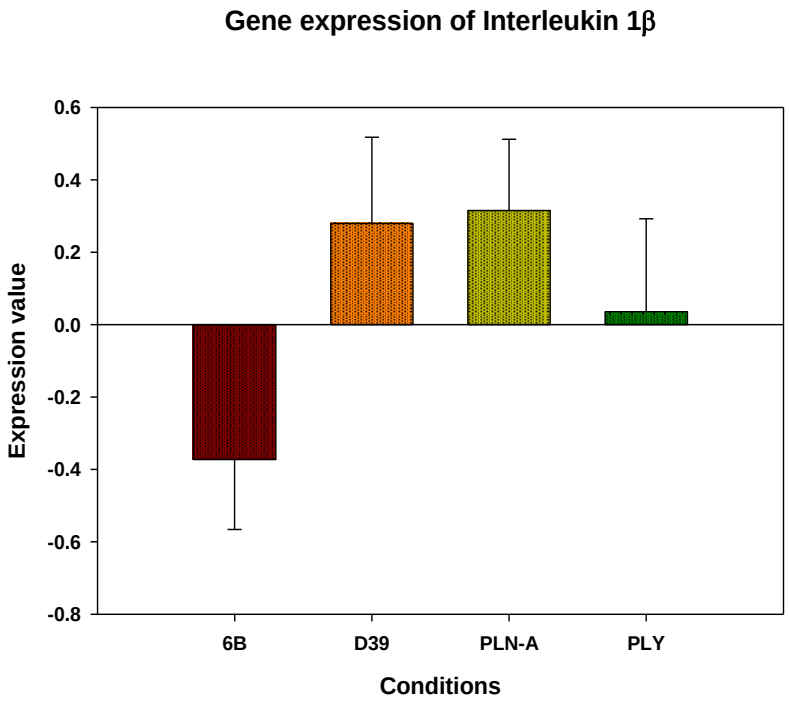

Figure 73|Interleukin 1β gene expression when the BBB model was challenged with *Streptococcus pneumoniae* serotype-2, -6B and the toxin pneumolysin Interleukin 1β exhibited more expression when PLN-A or pneumolysin were co-cultured with the model. The data are shown in expression values, as acquired post calculation with the SAM® software.

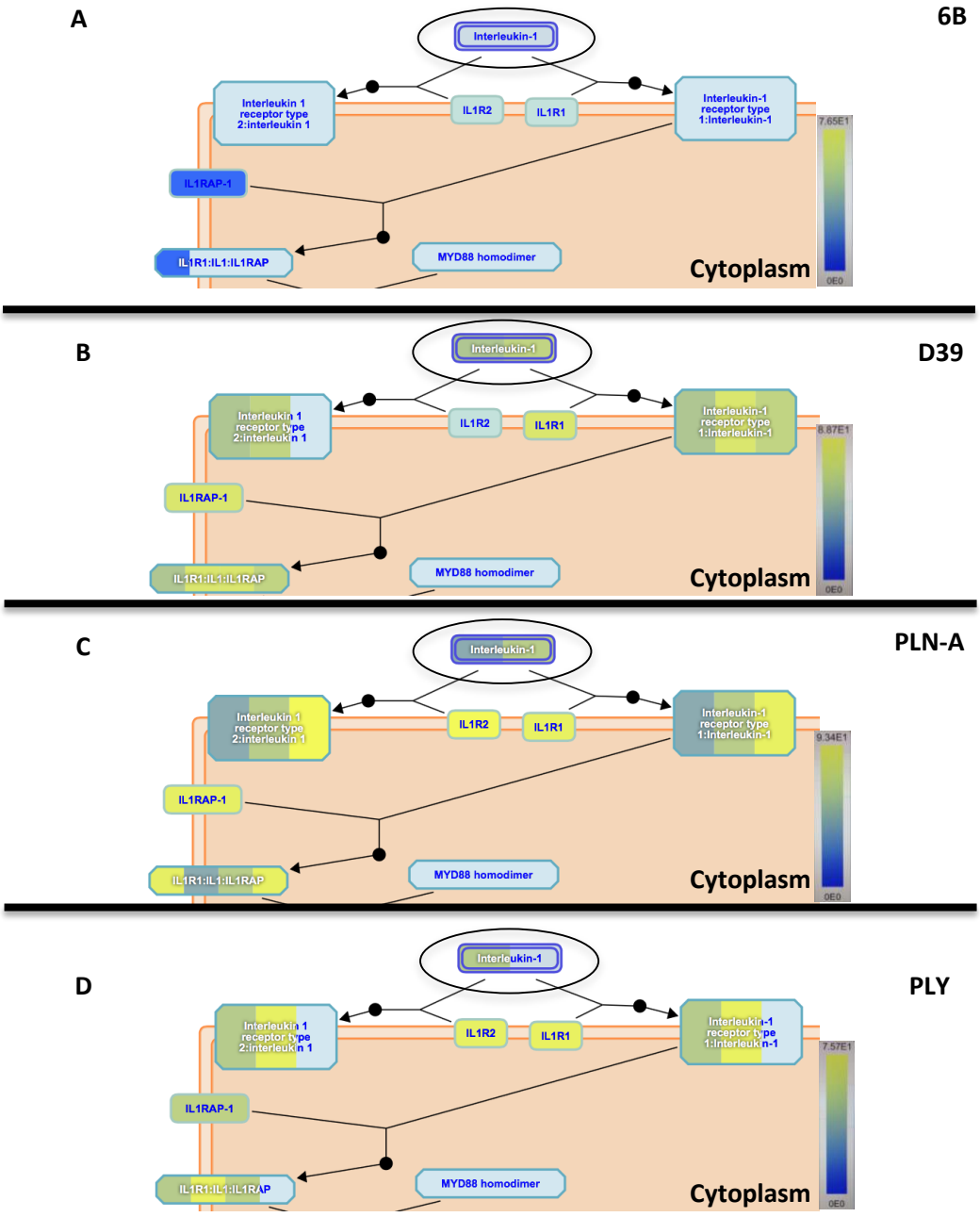

Pathway 2| Interleukin 1β signalling when the BBB model was challenged with *Streptococcus pneumoniae* serotype-2, -6B and the toxin pneumolysin The pathway was generated without setting a threshold of significance. It was observed that the Interleukin 1 transcript (in circle) more expression when PLN-A was used as the infecting agent. The pathway was generated using **only** the positively regulated genes from the gene expression assay. The pathway was generated using the REACTOME Pathway Database. The colored ladder designates differences in expression in the form of the q-value (dark blue = highest expression – grey = moderate expression - yellow = least expression – light blue = gene not present for this transcript). One or more genes can contribute in the activation of a complex, and this is illustrated with different colored bars (variation in expression) inside the complex. Although multiple complexes were activated during the generation of this pathway, I only highlighted the transcript relevant to my observations in previous experiments.

7.4.2 Interleukin 8 gene expression and its contribution towards the Interleukin 8 pathway

As seen in the data acquired from the microarray experiment, up-regulation of IL-8 was observed when 6B or PLN-A (figure 74). Using the total gene population through the REACTOME database, it was observed that the IL-8 transcript from the pathway was activated only when cells were challenged by 6B or PLN-A (pathway 3A+C).

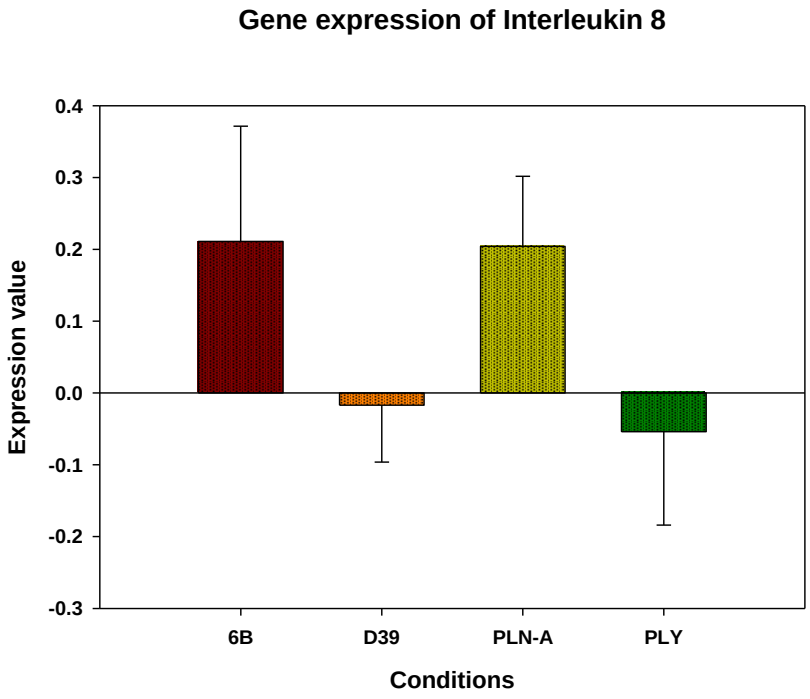

Figure 74|Interleukin 8 gene expression when the BBB model was challenged with *Streptococcus pneumoniae* serotype-2, -6B and the toxin pneumolysin Interleukin 8 exhibited more expression when 6B or PLN-A were co-cultured with the model. The data are shown in expression values, as acquired post calculation with the SAM® software.

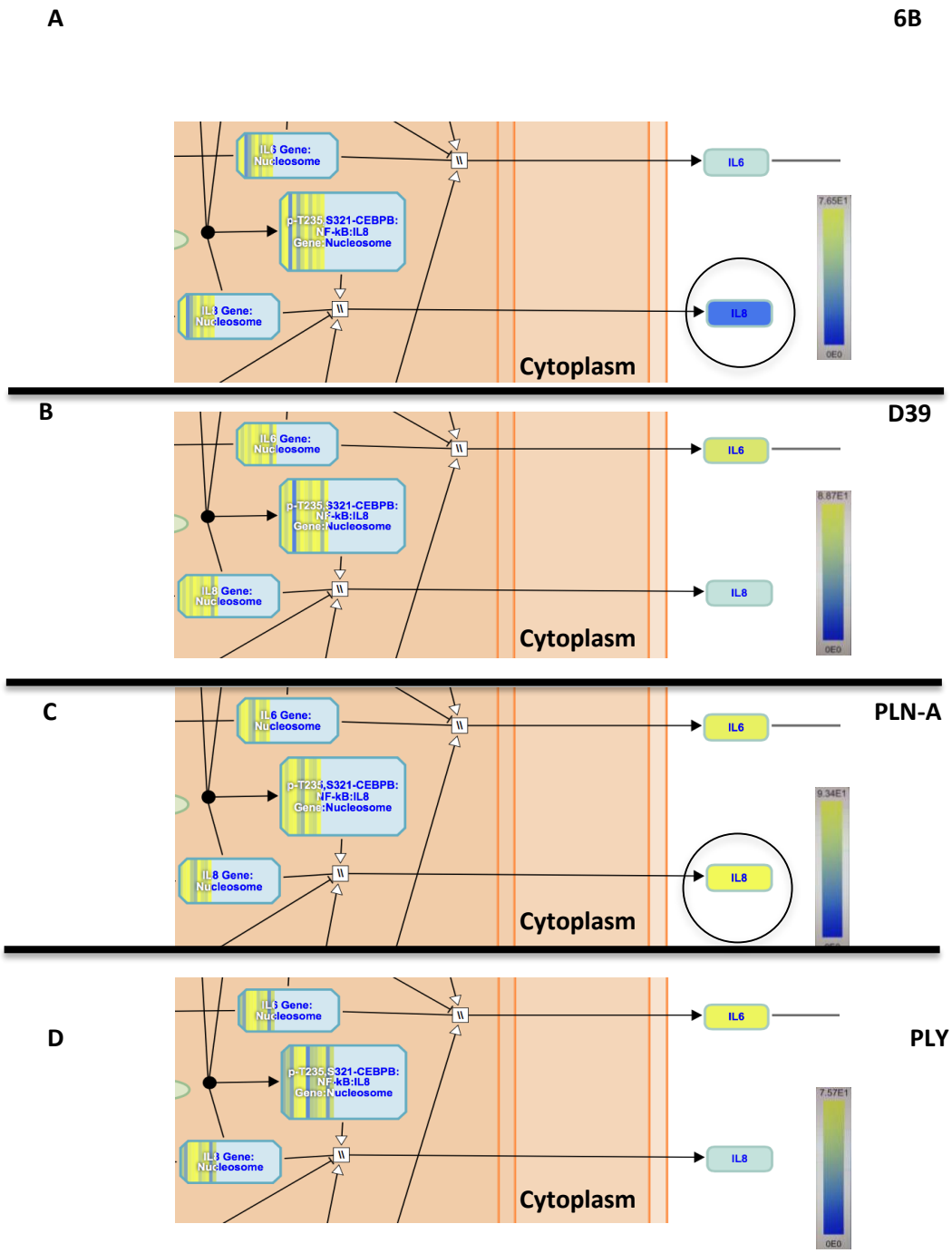

Pathway 3| Interleukin 8 when the BBB model was challenged with *Streptococcus pneumoniae* serotype-2, -6B and the toxin pneumolysin The pathway was generated without setting a threshold of significance. It was observed that the IL-8 (in circle) was activated only when 6B or PLN-A challenged the cells (IL-8 expressed more with 6B). The pathway was generated using **only** the positively regulated genes from the gene expression assay. The pathway was generated using the REACTOME Pathway Database. The colored ladder designates differences in expression in the form of the q-value (dark blue = highest expression – grey = moderate expression - yellow = least expression – light blue = gene not present for this transcript). One or more genes can contribute in the activation of a complex, and this is illustrated with different colored bars (variation in expression) inside the complex. Although multiple complexes were activated during the generation of this pathway, I only highlighted the transcript relevant to my observations in previous experiments.

7.5.0 Detection of zonula occludens 1 (ZO-1)

Endothelial cell ZO-1 was fluorescent labeled using a fluorescent antibody. ZO-1 fluorescence intensity was measured at two hours post exposure and among unexposed cell monolayers (n = 3 replicates per condition). During the ZO-1 fluorescent cell labeling, nuclei were stained blue via 4',6-diamidino-2-phenylindole (DAPI - see chapter 2, section 2.12.0). In an effort to maximize visibility of cells under the microscope the assay was done on cells cultured in a conventional 12-well plate. Among unexposed cells, ZO-1 diffusely stained the cytoplasm, with a relatively higher intensity of fluorescence at the cell margins (figure 75A).

The intensity of ZO-1 staining was higher in the cytoplasm and lower at the cell margins following exposure to either pneumolysin or D39. In contrast, intensity of ZO-1 staining was lower following exposure to 6B compared to unexposed cells. Similarly, intensity of ZO-1 staining was significantly lowest following exposure to 6B compared to pneumolysin or D39.

When using the gene expression data against ZO-1 fluorescence it was observed that cells challenged with pneumolysin and 6B showed up-regulation of important tight junction genes 2 hours post exposure. Cells from all conditions exhibited claudin activation with serotype 2 having more genes contributing towards claudin activation (in circle) (pathway 4B+C). Additionally, the JAM-A:PAR-aKPC is activated only when cells are exposed to pneumolysin or 6B (in circle) (pathway 4A+D). It has been demonstrated that this complex regulates the formation of cell-to-cell interaction and the formation of tight junctions [429]. The F11 receptor (F11R) is also activated only when cells are exposed to

pneumolysin or 6B (in circle) (pathway 4A+D). F11R encodes the JAM-A protein, which is crucial in the formation of tight junctions. Additionally it has been demonstrated that F11R interacts with ZO-1 [51, 430].

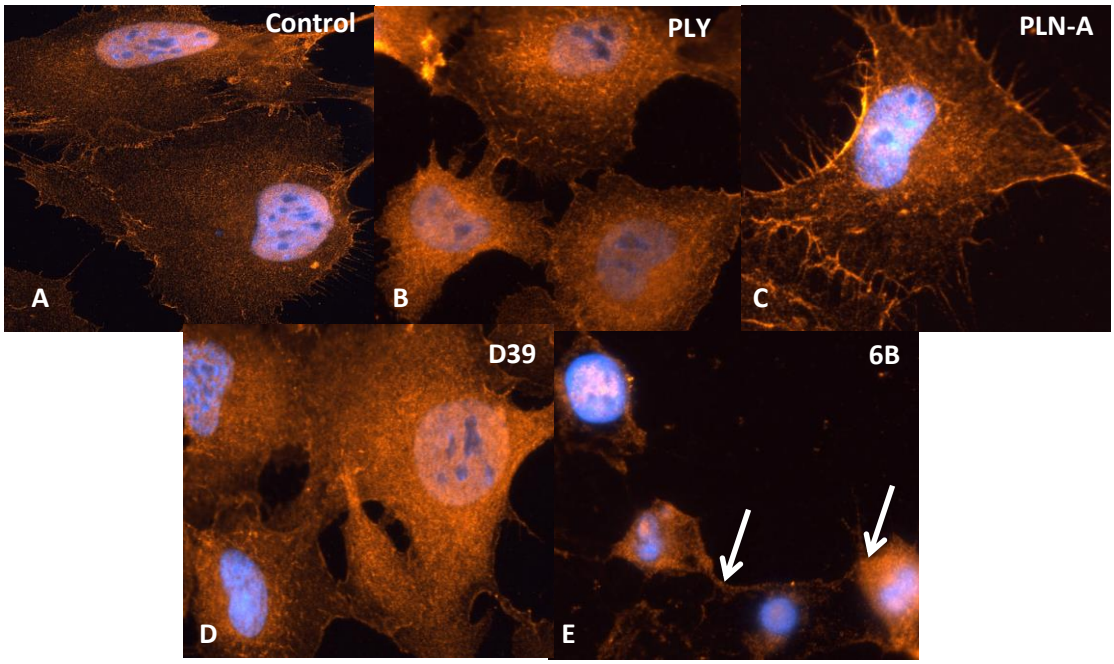

Figure 75|The effect of pneumococcal serotype-2, -6B, and the toxin pneumolysin on the Zonula Occludens protein 1 (ZO-1) Endothelial cell ZO-1 was fluorescent labeled using a fluorescent antibody. ZO-1 fluorescence intensity was measured at two hours post exposure and among unexposed cell monolayers (n = 3 replicates per condition). During the ZO-1 fluorescent cell labeling, nuclei were stained blue via 4',6-diamidino-2-phenylindole (DAPI). A) Among unexposed cells, ZO-1 diffusely stained the cytoplasm, with a relatively higher intensity of fluorescence at the cell margins. B) Cells exposed to pneumolysin exhibited more ZO-1 protein in the cytoplasm and less protein at the cell margins. E) Cells exposed to 6B also showed change in ZO-1 levels. Reduction of ZO-1 intensity at the cell margins (arrows in panel E) derives from reduction in cell viability due to exposure of the monoculture to the pneumococci.

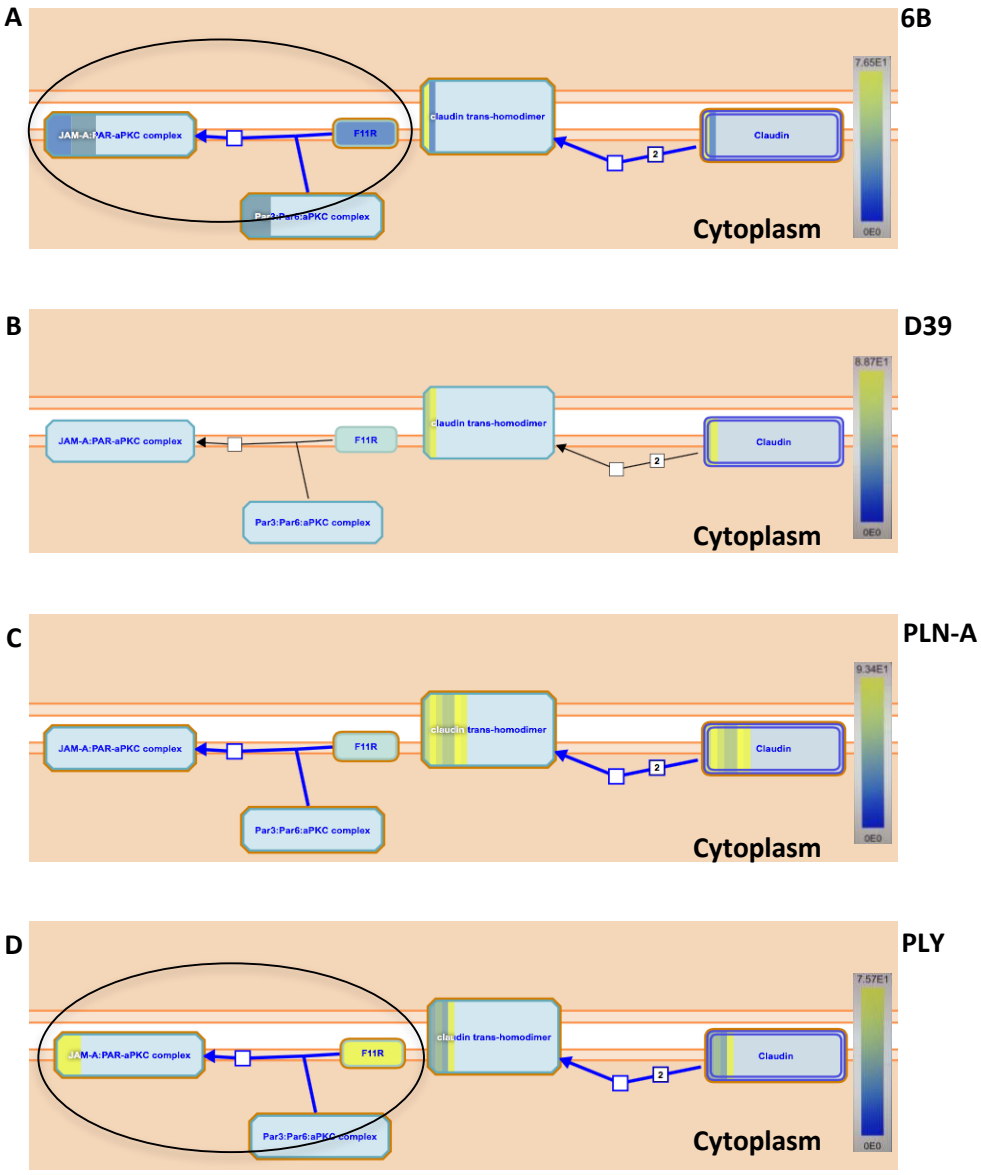

Pathway 4| Tight junction signalling pathway when the BBB model was challenged with *Streptococcus pneumoniae* serotype-2, -6B and the toxin pneumolysin The pathway was generated without setting a threshold of significance. It was observed that the JAM-A:PAR-aKPC was activated only when cells were exposed to pneumolysin or 6B (in circle) (panel A and D). Similarly the F11 receptor was activated when cells were exposed to pneumolysin or 6B (in circle) (panel A and D). Cells challenged with serotype-2 exhibited higher expression in regards to occludin proteins (panel B and C). The pathway was generated using the REACTOME Pathway Database. The colored ladder designates genes of different significance in the form of the q-value (dark blue = 0% = significant - yellow = over 75.7% = not significant). Different colors found in the same transcript or complex, show the contribution of more than one gene to activate the transcript or complex, in different significant values.

7.6.0 Discussion

In this chapter I observed that the concentration of IL-6 was significantly higher when the model was infected with 6B, and PLN-A. This suggests that activation of IL-6 is not associated with pneumolysin since the toxin did not significantly activate the cytokine. Although the IL-6 transcript was not present in the gene expression assay for 6B, the concentrations of the cytokine in the supernatant were significantly elevated. Interleukin 6 also binds to the glycoprotein 130 (gp130 or IL6ST), which forms a complex with IL-6 receptor (IL6R). I also observed that the IL6R-2 gene was up-regulated only when 6B or PLN-A challenged the cells. This signifies that pneumolysin could be an inhibitor to the specific gene, as pneumolysin and D39-derived pneumolysin were observed in high concentrations 2 hours post infection.

When cells were challenged with 6B, almost no IL-1β was present. Although not significantly different, IL-1β detection was higher for PLN-A and pneumolysin whereas D39 showed lower concentrations of the cytokine. Confirmation of the findings derived from the IL-1 pathway, where the interleukin 1 transcript showed higher expression for PLN-A whereas no activation was observed for serotype-6B. Highest expression of IL-1β derived from a strain that did not express the toxin. This suggests that the capsule might activate other inflammasomes or early activation of the cytokine (prior to 24 hours of exposure to the toxin) may not be associated to the toxin.

Cells challenged with 6B and PLN-A showed high concentrations of the cytokine, suggesting that a thin bacterial capsule is related to the activation of the cytokine. Additionally, as in the case of IL-6, pneumolysin may not be contributing to the activation

of IL-8. The pathway of cellular senescence (deterioration of cellular functions) was selected to investigate IL-8 contribution to infection. It was observed that during this pathway, the IL-8 transcript was activated only when 6B and PLN-A were used.

Interestingly when cells were challenged with pneumolysin or 6B, the majority of the ZO-1 protein was found in the cytosol, especially near the nuclei. On the contrary, cells challenged with D39 or PLN-A showed expression of the ZO-1 protein at the junctions and the nuclei, similarly to the untreated cells.

As seen in the tight junction pathway, cells challenged with D39 or PLN-A exhibited higher activation of claudins in comparison to pneumolysin and 6B. Additionally, the JAM-A:PAR-aKPC complex was activated only when cells are exposed to pneumolysin or 6B. The F11 receptor (F11R) was also activated only when cells are exposed to pneumolysin or 6B. Both transcripts are crucial for the formation of tight junctions and their interactions with ZO-1.

7.7.0 Conclusions

In this chapter I demonstrated that using all the genes (without setting a threshold of significance) to generate pathways, revealed direct and indirect expression of IL-6, IL-1β and IL-8. Tight junction proteins, which have been previously associated to bacterial meningitis and BBB dissociation were also expressed during this analysis. The virulence of serotype 6B was in coherence to the results seen in all other chapters.

CHAPTER 8.

Discussion

8.0 Discussion

8.1.0 *Streptococcus pneumoniae* serotype-1, -2, -6B, survive and grow when in co-culture with human brain endothelial cells and primary human astrocytes

Endothelial cells and astrocytes have been previously used in monoculture to assess invasion and toxicity of pneumococcal infection of neuronal cells [431, 432].

The findings suggest that serotypes 1 and 6B are highly virulent and this is supported by epidemiological data demonstrating that serotype 1 is a major cause of meningitis in sub-Saharan Africa [433], whereas 6B is a highly invasive serotype in Europe and is particularly associated with empyema [434]. Serotype-2 has not been considered a major cause of invasive disease since the 1960's, but a recent outbreak of serotype 2 in Bangladeshi children suggests it retains the capacity for virulence under the right conditions [435]. My findings are in accordance with the work of Chuck et al., who observed that pathogens behave like particles in solution and that flow enhances their adherence capabilities [436]. I therefore, reasoned that gravitational flow in a BBB model could be significant in accelerating pneumococcal adherence to and invasion of host cells.

8.2.0 Cell migration in a Transwell® system, terminal velocity and mass-flow rate

Transwell® systems have previously been used by others [214]; Rat brain microvascular endothelial cells adhering on the pore membrane were significantly larger than the ones I used in my project (cells would remain on membrane with 12 μm pores whereas I saw cell migration using 3.0 μm pore membranes). Corning® classifies all inserts with 3.0 μm pores or greater, as systems suitable for cell migration studies [331]. Thus, I sought to determine

how the pores size of this semipermeable membrane affected particle (in my example cells) flow as well as media translocation from the upper compartment to the lower compartment of the system.

8.3.0 *Streptococcus pneumoniae* serotype-2 are rapidly eliminated from a Blood-Brain Barrier model

When serotype-2 pneumococci are cultured in the BBB model, CFUs decline over time; this is a result that is the opposite to that observed in monoculture incubations. However, serotype-2 adherence was greater in the BBB model than in monoculture incubations. Similarly, serotype-2 successfully invaded HBEC cells in the BBB model but not in monoculture, which may suggest acceleration of adherence and invasion due to gravitational flow. Despite the increased adherence of pneumococci and successful invasion, no pneumococci were observed in the lower compartment of the model at any point during the course of the experiment.

The pneumolysin-deficient PLN-A strain successfully adhered to HBEC cells in the BBB model immediately after pneumococcal infection, as well as at 1-hour post incubation. Again, gravitational flow is likely to be important in accelerating pneumococcal adherence. However, no invasion was observed with PLN-A, suggesting that pneumolysin plays an important role in this process.

8.3.1 *Streptococcus pneumoniae* serotype-6B is invasive in a Blood-Brain Barrier model

Serotype-6B was the only pneumococcal serotype that displayed consistently high levels of adherence and invasion in the BBB model. The high levels of adherence to and invasion of HBEC cells in the top compartment of the model likely contributed to traversing of serotype-6B to the lower compartment of the model. Additionally, adherent and invaded pneumococci were also observed in the lower compartment.

8.3.2 Loss of Trans-endothelial electrical resistance when *Streptococcus pneumoniae* serotype-2 and -6B is incubated in a BBB model

The integrity of the model's monolayer was significantly compromised when serotype-6B was cultured in the BBB model. TEER loss was 37% in comparison to untreated wells, a loss that was not observed during infection with D39 or PLN-A (11% and 4% loss respectively). Some of the reasons for the loss of TEER during 6B infection could include:

- The total number of pneumococci in the BBB model.
- The quantity of adherent or invaded pneumococci.
- The amount of pneumolysin released upon pneumococcal lysis.
- Differences in the host immune response to infection.
- Differences in bacterial virulence factors between serotypes. These may include but are not limited to adhesion molecules (e.g. Pav-A), and pneumococcal enzymes (e.g. neuraminidases).

According to what is known in the literature serotype 6B is mostly observed having a transparent capsule rather than an opaque one [437]. As mentioned previously a

transparent capsule allows more pneumococcal binding sites to initiate adhesion on the mucosal epithelial layer. Thus, I am postulating that 6B is an excellent adhesive serotype, which allows it to communicate with both the endothelial and epithelial barriers in humans, enabling it to traverse to the bloodstream initially and then further into the BBB.

8.3.3 Use of pneumolysin or PdB in co-culture with *Streptococcus pneumoniae* PLN-A

When PLN-A was co-incubated with purified pneumolysin in the BBB model, a significant decline in TEER was observed when compared to untreated cells, suggesting that pneumolysin has a direct effect on the tight junctions of the cell monolayer. Along with significant TEER loss, PLN-A proliferation was observed when co-incubated with purified pneumolysin, suggesting that pneumolysin either enhances pneumococcal growth directly (or by instigating the release of factors from host cells upon damage, which sustain bacterial growth) or else allows pneumococci to thrive by inhibition of host defence mechanisms. Pneumococcal adherence was significantly increased relative to PLN-A infection alone and invasion was also observed. This was striking, as invasion had not been observed in any previous experiment where PLN-A was used alone. PLN-A co-cultured with pneumolysin successfully crossed to the lower compartment of the model.

PLN-A co-incubation with the non-hemolytic pneumolysin toxoid PdB did not significantly influence bacterial growth, adherence, invasion or translocation to the lower compartment. This suggests that the pore forming activity of pneumolysin is key to driving pneumococcal infection.

8.3.4 Pneumococcal growth cycle and its association with pneumolysin

I suggest that rapid release of pneumolysin leads to its immediate use or degradation rendering the toxin ineffective in promoting pneumococcal growth. My speculation is supported by the declining CFUs of serotype-2 during the experiment. On the contrary, 6B exhibits low pneumolysin levels, but its constant presence in the supernatant was essential for pneumococcal survival and growth. Hence, the balanced ratio of live to lysed pneumococci [219] in 6B infection promotes pneumococcal growth, adherence and invasion. Toxin added to the supernatant (100ng/ml) increased CFUs for PLN-A. Eventually PLN-A adhered, invaded and crossed to the lower compartment of the model. Despite the increase, PLN-A did not adhere or invade astrocytes in the lower compartment. This is because the toxin irreversibly adheres to cholesterol on host cell surfaces and is used for pore formation on endothelial cells and as such remains in the supernatant and is unable to go through. Without the presence of pneumolysin in the lower compartment, PLN-A exhibited similar invasiveness to its levels prior to pneumolysin co-incubation.

8.4.0 Previous bacterial work with the Blood-Brain Barrier, common findings and novelties

The first published results relating to bacterial work in BBB models was in 1998 by Ring, A. et al. where immortalised rat and human brain microvascular endothelial cells (BMECs) were used to investigate transcytosis of pneumococci. Transcytosis was facilitated by the choline-binging protein A (CbpA) found on the pneumococcal surface and the platelet-activating factor receptor (PAF) found on BMECs [214]. Opaque and

transparent variants of serotype-6B were used during these experiments, but no significant adherence or invasion was observed. This is in contrast to my findings where I saw high levels of adherent and invaded pneumococci when using serotype-6B. Ring et al., used a serotype-6B isolate, but it was not a meningitis CSF isolate like the one used in my studies. It is possible that increased virulence is associated with meningitis isolates or that the Ring et al., study used a non-invasive 6B carriage isolate. This idea is supported by data generated Fuchs et al., who demonstrated that serotype 7F meningitis isolates exhibited a higher rate of transmigration in comparison to non-invasive clinical isolates of the same serotype. In this model, hBMECs and murine astrocytes were used in co-culture [438]. A meningitis isolate (serotype 4) was also used in a BBB model carrying immortalised hBMECs to investigate pneumococcal adherence over the course of time [439]. Having a serotype-6B in my model from a meningitis isolate, I also observed increased adherence and invasion of bacteria; the high virulence potential of this strain emphasises the importance of its inclusion in commercially available vaccines [146].

Serotype-2 (strains D39 and PLN-A) were also used in the BBB model. I observed less adherence and minimum levels of invasion from this serotype. Nevertheless, when PLN-A was co-incubated with purified pneumolysin, I observed a substantial increase of adherence and invasion in the BBB model. Pneumolysin expression is strongly associated with virulence [87, 201, 337, 440, 441]. Absence of the toxin has been associated with reduced infection in the lung [442] whereas increased levels of the toxin were associated with prolonged colonization [93] and high mortality [94]. In order to identify the importance of hemolysis by pneumolysin, I used the genetically detoxified variant PdB. In co-culture with PLN-A, PdB did not enhance pneumococcal adherence or invasion, nor

alter the resistance generated by cellular tight junctions. In concordance with my results, it has been previously demonstrated that a pneumococcal serotype 1 of sequence type (ST)306 expresses a non-hemolytic pneumolysin and is rarely found associated with invasive disease [443]. ST306 carries more virulence factors in its genome in comparison to serotype 1 of ST217; nevertheless ST217 is the leading cause of meningitis in sub-Saharan Africa (meningitis belt), emphasising the importance of pneumolysin for virulence [433]. A partially reduced immune response is also observed when ST306 is compared to different serotypes that express WT pneumolysin, highlighting the antigenic and immunostimulatory nature of pneumolysin [433, 441].

In comparison to other infection models, my BBB model exclusively uses human cells in co-culture, which enables me to look at pneumococcal interactions with the model and relate them directly to human immune responses or cellular processes. Additionally, I constantly monitored TEER whilst infecting my model with different pneumococcal serotypes, something not previously attempted. However, *in vitro* models are limited in the number of cell types they can accommodate. For example, it has been previously demonstrated that bacterial injury in the BBB mediated leukocyte migration [444], a factor not covered by my model. Similarly, *in vivo* meningitis models allow for a broader spectrum of experimental variables to be considered [420]. Nonetheless, my findings suggest that a significant reason for observing increased invasiveness with serotype-6B is the presence of pneumolysin. Although significant in pathogenesis progression, pneumolysin is not the only virulence factor required for infection. Garnier et al., identified a serotype 1 isolate which was unable to express pneumolysin, yet caused acute infection in the upper pulmonary lobe to a woman suffering from pneumonia [445].

Many important pneumococcal factors contribute to infection and disease progression. One of those factors is pneumococcal protein CbpA. This pneumococcal surface protein was the first recognised to adhere to host tissues. This is achieved through interactions of the choline of teichoic acid or lipoteichoic acid with human cell glycoconjugates. This process may be the way that the pneumococci advance from colonization to invasion [446]. Neuraminidase (NanA) is another significant pneumococcal virulence factor. Its function involves cleavage of sialic acid deriving from glycans such as glycoproteins, mucin or glycolipids. Removal of glycans from the host cell surface allows the pneumococci to adhere and interact with cellular surface receptors [447]. NanA has been previously associated with brain endothelial cell activation through promotion of secretion of chemoattractants such as IL-8, CXCL-1 and CXCL-2 [448]. Contributions of these factors to virulence (along with pneumolysin) likely determine the ability of pneumococci to adhere and invade the host.

During my project, the ability to use different serotypes but also purified pneumolysin proteins with various haemolytic activities allowed me to correlate virulence and invasiveness with haemolysis, and tight junction alternations. The tight junctions formed by endothelial cells were significantly affected when cells were co-incubated with recombinant pneumolysin or serotype-6B. My initial assumption was that the amount of toxin is what defines the severity of infection. Interestingly, serotype-6B did not release high concentrations of the toxin. When comparing the 2 conditions, readings for TEER were similar up to 3 hours post infection. It was evident that multiple factors contribute to tight junction imbalances and thus, secure pneumococcal survival and progression in the BBB. Serotype-2 D39 produced substantially more pneumolysin than 6B and yet no

significant disruption in the junctions was observed. When determining the capsular thickness of the pneumococci, serotype-2 capsule was significantly thicker than serotype-6B. To compare 2 clinical isolates, S1 was also investigated for capsule thickness and pneumolysin concentration. It was observed that S1 exceeded all other serotypes both in capsule thickness as well as pneumolysin concentrations. I suggest that the amount of pneumolysin carried pneumococci is proportional to its capsule thickness. It has been previously shown that a small or thin capsule increases adherence, thus, capsule differences may have accounted for the increased adhesion of serotype-6B in my model relative to D39 [449]. This could explain why S1 is a bad coloniser bad lethal when infection is establish in the host [152]. Although both the toxin and the capsule have a significant role in pathogenesis, their co-existence in defined proportions is key to allow the pneumococci to traverse through the BBB and cause further inflammation. Another possible reason underpinning differences in invasiveness is the different structure of pneumolysin carried by different serotypes. Crystallization of pneumococcal-derived (rather than recombinant) pneumolysin has not been attempted so far and it would be a significant step forward in determining toxin contribution to relative virulence of different serotypes.

8.5.0 Interpretation of the up-regulated pathways when using pneumolysin

Increases in intracellular Ca^{2+} is one of the mechanisms that CNS cells use to communicate with neighbouring cells [450]. Calcium efflux is a natural process for the BBB where signalling to neuronal cells is initiated in order for the BBB to restore its role as a nutrient controller and a metabolism regulator [451, 452]. Pneumolysin seems to

trigger calcium efflux from endothelial cells upon pore formation [453]. Whilst the BBB is trying to re-establish its integrity and regulate function, pneumococci can traverse through the barrier not only by endocytosis, but also between the junctions, which have been dissociated due to cytoskeletal rearrangements. Hyperpolarization of the cells can also affect the gap junctions, which could be why the pathway is up-regulated in my experimental conditions. The up-regulation of gap junctions might be indirectly because of pneumolysin, but it is more likely to be due to the calcium efflux.

8.5.1 Interpretation of the down-regulated pathways when using pneumolysin

All the down-regulated pathways identified in my analysis are related to each other since cleavage of collagen occurs following the activation of MMPs. This eventually leads to ECM degradation. ECM degradation is part of a remodelling process that cells undergo [454]. During the remodelling process, MMP levels are kept low in order to maintain a controlled degradation of the matrix [455]. If degradation of ECM reaches a point where a system (such as the BBB) is under threat, then MMP inhibitors are activated in order to regulate ECM breakdown [456]. I identified MMP down-regulation following pneumolysin exposure and this may have reflected cellular attempts to control the degradation occurring during infection. Interestingly though, ADAMTS1, one of the MMPs inhibitors was also down-regulated due to pneumolysin. This may suggest that pneumolysin is interrupting the inhibition process, in order to promote pneumococcal progression through the BBB.

8.5.2 Interpretation of the down-regulated pathways when pneumococcal serotype-6B

As mentioned in the introduction of this thesis, pathogenesis progression involves simultaneous steps both from the pathogen as well as the host. During infection of the BBB model, cytokines as well as MHC-peptide complexes are activated in order to initiate T-cell trafficking in the infected area. T-regulatory cells are also stimulated by the up-regulation of IL12A. Simultaneously, activation of the EGFR gene leads to increased invasiveness of the pneumococci whereas the IL17RB contributes to increased pneumococcal uptake. Different inflammasomes must be activated when serotype-6B is used, as TLR4 was activated due to the CBLB gene. TLR4 production leads to the activation of IL1RAP gene in order to induce production of IL-1β. The IL6ST gene is activated, and is a signal transducer for IL6. As IL6 increases permeability [262], pneumococci begin to traverse through the BBB paracellularly. Remodeling and increased permeability of the barrier occurs through the activations of the PTPRN gene. This further allows the pneumococci to traverse paracellularly, but also initiate activation of B cells due to the up-regulation of laminins.

8.6.0 Further gene analysis using the total gene population of the microarray experiment

In my project I have emphasized the statistically significant results of the gene expression assay. Through these results, host immune elements were identified such as the IL6ST, IL17RB, and IL1RAP. It has been previously shown that these genes are associated with IL-6, IL-8 and IL-1B, which are present during pneumococcal infection and cause tissue inflammation in pneumococcal meningitis cases. The decline in TEER, as well as the up-regulation of important junctional proteins revealed possible tight junction activity. Thus, I sought necessary to perform some immunological assays in order to determine the concentrations of IL-6, IL-8, and IL1β secreted from the cells during infection. Additionally, I performed a fluorescent detection assay to observe the levels of ZO-1 protein in the cell cytoplasm and the cell walls.

8.6.1 Interleukin 6, 1B and 8 when the BBB model was challenged with the pneumococcal serotypes 2 (stains D39 and PLN-A), 6B and the toxin pneumolysin

It has been previously shown that up-regulation of IL-6 leads to tissue damage and an immediate increase in vascular permeability [261]. It has also been shown that IL-6 disrupts the normal function of many proinflammatory and anti-inflammatory cytokines [263]. Although the IL-6 transcript was not present in the gene expression assay for 6B, the concentrations of the cytokine in the supernatant were significantly elevated. Interleukin 6 also binds to the glycoprotein 130 (gp130 or IL6ST), which forms a complex with IL-6 receptor (IL6R). This was expressed specifically when 6B or PLN-A were co-cultured with the BBB model, suggesting that IL6R may serve as a marker for IL-6

activation [457]. It has been previously demonstrated that IL-6 release was suppressed when using serotype-6B in a human *ex vivo sepsis* model [458]. It was also shown that IL-6 was kept in low concentrations when pneumococcal serotype 6B was present [459]. Absence of IL-6 or suppression of the cytokine increases inflammatory response in pneumococcal infection [262]. Although gene expression and cytokine secretion do not match in the case of IL-6, it is known that expression of a gene is not always in accordance to protein secretion [460].

I also observed that the IL6R-2 gene was up-regulated only when 6B or PLN-A challenged the cells. Specifically IL6R-2 was shown to increase susceptibility to respiratory tract infections when up-regulated [461].

The IL-1β proinflammatory cytokine is readily secreted from meningeal macrophages [241]. Although present during bacterial meningitis, the cytokine does not seem to be associated with BBB disruption [217]. Leukocyte entry to the infected area is dependent from the presence of IL-1β [259]. The IL1 receptor is also crucial for the survival of organisms with meningitis [260]. It has been previously demonstrated that suppression of IL-1β occurs in a human ex vivo sepsis model [458]. My result contradict the dogma existing arount IL-1β and pneumolysin, since pneumolysin activates the NLRP3 inflammasome which is the main source of IL-1β [88]. In my case, highest expression of IL-1β derived from a strain that did not express the toxin. This suggests that the capsule might activate other inflammasomes or early activation of the cytokine (prior to 24 hours of exposure to the toxin) may not be associated to the toxin.

The IL-8 chemokine (CXCL8) is known to be associated with bacterial meningitis since it induces neutrophil chemotaxis when patients suffer with meningitis [278]. Leukocyte migration is related to IL-8 levels, resulting in the secretion of chemotactic cytokines [444]. Increased levels of IL-8 result in increased pleocytosis [462]. The pathway of cellular senescence (deterioration of cellular functions) was selected to investigate IL-8 contribution to infection. It was observed that during this pathway, the IL-8 transcript was activated only when 6B and PLN-A were used.

8.6.2 Fluorescent detection of the zonula occludens 1 (ZO-1)

It has been previously shown that when there is dissociation of the tight junction connecting the endothelial cells, ZO-1 and ZO-2 translocate to the nuclei; this suggest that they act as messengers in regards to cell-cell signalling [463].

The F11 receptor (F11R) was also activated only when cells are exposed to pneumolysin or 6B. Both transcripts are crucial for the formation of tight junctions and their interactions with ZO-1. It is important to clarify that the fluorescent detection assay was done in monoculture (in an effort to resolve issues of visibility under the microscope) whereas the cells isolated for gene expression where isolated from a BBB model. The fluorescent detection assay was an additional experiment performed to acquire preliminary data on the interactions of pathogens with the tight junction proteins of endothelial cells. Additional tight junction proteins are going to be used in a future fluorescent detection assay, in order to investigate in detail tight junction protein interactions during pneumococcal infection.

8.7.0 Limitations of gene and pathway analysis

All experiments that involve microarrays are user dependent. That is because the user is the one setting the threshold of significance in the microarray analysis. Thus, the array experiment has a lot of bias interpretations when performed. It is usually suggested to verify the findings of a microarray experiment by either protein detection assays (such as ELISAs) or q-PCR. As seen in the pathway analysis, there is a clear contribution of more than one gene in proteins and cytokines of the investigated pathways. This makes the analysis more complex, since each gene contributes to the specific cytokine in different levels of significance. By not taking into account the statistical significance of each gene, then more genes appear in the pathway, which makes the analysis even more difficult to interpret. Additionally the amount of proteins contributing to a pathway is vast; thus, it is advisable to focus on a single protein and its contributing genes, rather than try to identify all genes from all pathways.

8.8.0 General conclusions – novelties of this thesis

During this project, I have assessed the growth, adherence and invasion of various *Streptococcus pneumoniae* serotypes and strains. Each serotype was found to behave differently during co-incubation with either HBECs or HA. Serotype-6B grew, adhered and invaded these cells in greater numbers and efficiency than the other serotypes tested. The pneumolysin deficient strain was unable to adhere to or invade HBEC or HA cells, suggesting that the toxin pneumolysin has a crucial role in pneumococcal adherence and invasion to host cells. The comparison of multiple serotypes with multiple cells constituting the BBB system is a novelty in the studies around infectious diseases and was not previously attempted.

To progress my research in BBB studies, I established and optimised a novel BBB model for experiments with *Streptococcus pneumoniae*. This system utilised 3.0 μm pore membranes. The terminal velocity of cells under creeping flow and the mass-flow rate showed that the use of 150 μl of cell media increased cell adherence on the membrane and no cell migration was observed. The model was adjusted to an antibiotic-free environment, in order to be used for experiments with the pneumococci, and consisted of human brain cells (endothelial cells and astrocytes).

The growth, adherence and invasion of various *Streptococcus pneumoniae* serotypes in a BBB model were evaluated. Serotype-2 (D39 and PLN-A) was found to behave differently in comparison to monoculture incubations. Serotype-6B adhered, invaded and crossed to the lower compartment of the BBB model. The investigation of pneumococcal

processes such as adhesion and invasion using various pneumococcal serotypes is considered a novelty in the field.

The contribution of pneumolysin to bacterial survival, growth and junctional breakdown was evaluated. TEER significantly declined over time due to presence of the toxin. When co-incubated with PLN-A, pneumolysin enhanced pneumococcal growth, adherence and invasion of the specific mutant. A pneumococcal CFU cycle was proposed, where pneumococci reaching or exceeding the 50% threshold could adhere, invade and cross to the lower compartment of the model. A hemolytically active pneumolysin is key in driving pathogenesis and the variations in virulence amongst different pneumococcal serotypes need to be taken into account in order to secure efficacy in future therapeutics. Pneumolysin was not directly associated with BBB breakdown previously and the ability to directly assess the endothelial resistance produced by the tight junctions was a science gap in this area. To initiate the importance of investigating the tight junctions during pneumococcal infection, I assessed ZO-1 at the junctions of brain endothelial cells,

Looking at the immunological aspects of the project, I investigated gene expression of endothelial cells when different pneumococcal serotypes or pneumolysin are used in the BBB model. The dominance of serotype-6B and pneumolysin was confirmed by the amount of significant genes identified during various statistical tests. A very low number of significant genes were observed when the BBB model was challenged with D39 or its isogenic mutant PLN-A. Studying the host as well as the pathogen in equal proportions is a time consuming task. I decided to investigate both in order to establish a library of pathogen and host mechanistic pathways; this will allow me in the future to drive my

research in specific interactions between the pneumococci and the cells of the BBB, allowing for a more targeted approach in regards to possible therapeutics.

Gathering all data from this project I am suggesting a novel role of pneumolysin, where pneumococcal survival, adherence and invasion are regulated by the toxins presence, concentration and time of release. Cytoskeletal remodelling of cells due to pneumolysin allows the pneumococci to invade the blood-brain barrier through multiple mechanisms (transcellularly as well as paracellularly). Pneumolysin might also be associated with pneumococcal capsule thickness as thin capsule with little or no pneumolysin exhibited higher levels of IL-6 and IL-8 and higher numbers of adherent bacteria [449]. A detailed pathogenesis pathway was designed, showing all interactions identified in this project between the pneumococci and the host (figure 76).

From all the novelties mentioned previously, I aim to take forward and expand the following:

- **Elaborate and explain further the adhesion/invasion mechanisms of the different pneumococci strains used in a BBB model**

  I will achieve this by culturing astrocyte/neuronal cells in a novel 3D petri dish (http://www.microtissues.com/3d-cell-culture-products.html), and cover them with endothelial cells to form a "nano-brain". This will allow me to infect the 3D cell structure with pneumococci, and perform an X, Y, Z imaging to follow the pneumococci's route of infection throughout the system.

- **Expand on the mechanisms that pneumolysin uses to sustain as well as promote pneumococcal growth**

  As seen previously in chapter 5, PLN-A showed improved survival when co-incubated with pneumolysin. I plan to repeat those experiments and during co-incubation, inhibit pneumolysin's action in order to see how pneumococcal viability is affected. This experiment will be performed for all serotypes used during my PhD thesis.

- **Investigate more about the role of Sphingosine-1 phosphate phosphatase in the Blood-Brain Barrier during infection**

  SPP1 has been previously associated with autoimmune diseases but never with infectious diseases. I aim to use the recombinant form of the lipid cleaved by this phosphatase, block the receptor engaging with SP1 as well as inhibit the enzyme cleaving this lipid. This will allow me to observe variations in permeability of the BBB model and identify possible biomarkers that could lead to therapeutics.

- **Establish a novel human *in vitro* dynamic Blood-Brain Barrier model**

  I aim to apply for pump priming funding (pilot / seed corn funding) to acquire a novel technology, which allows for automated TEER readings of cells under flow. Then I will develop the model and perform preliminary experiments to prove its efficacy.

- **Use the novel Blood-Brain Barrier model to elucidate more around pneumococcal meningitis**

  It is well evident (as previously discussed) that the introduction of flow in a static system, models the brain better. This will allow me to investigate leukocyte migration during infection, pharmacokinetics, as well as differences of pneumococcal infection between a static model and a flow model.

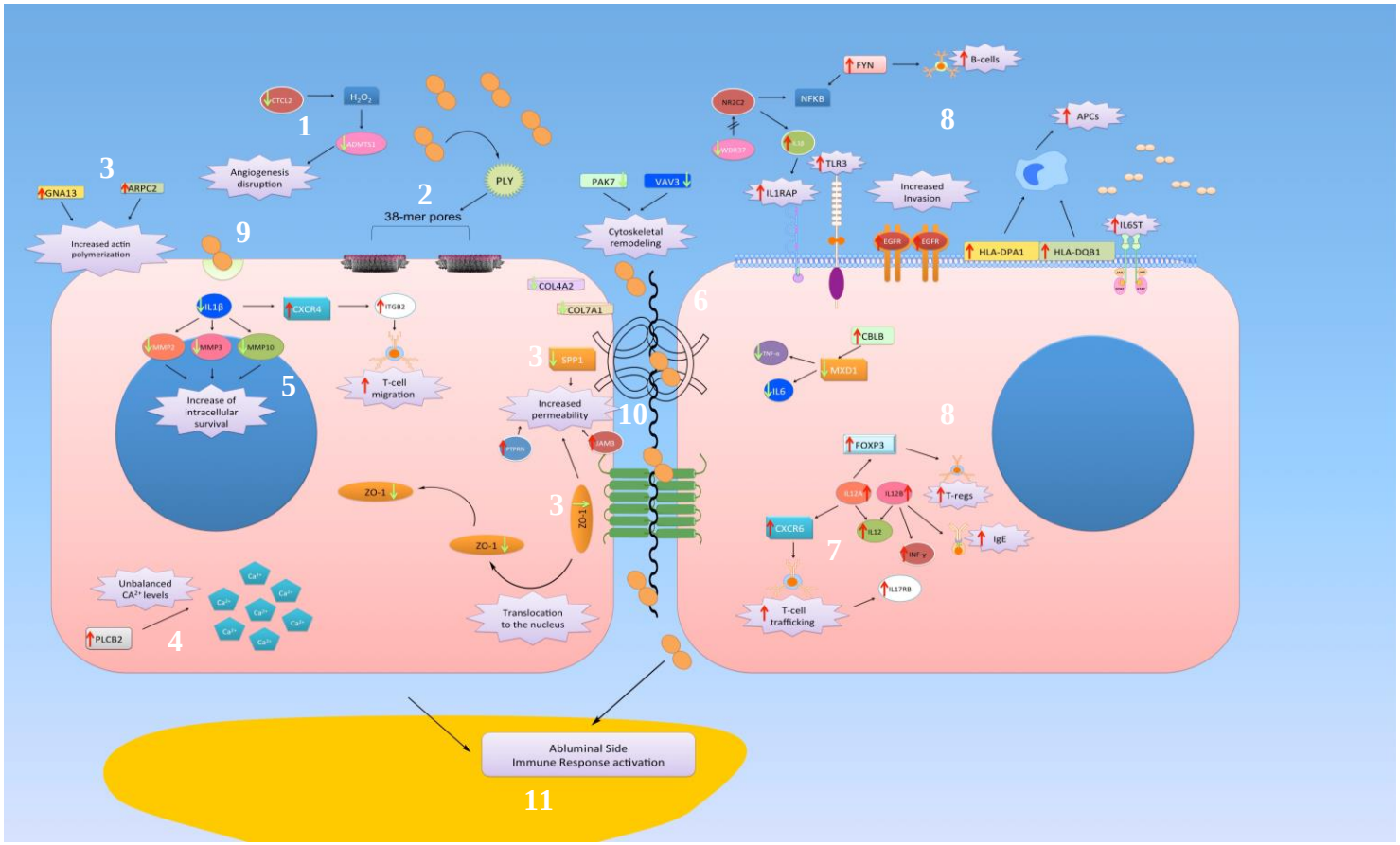

Figure 76| Pathogenesis mechanisms for interactions of Streptococcus pneumoniae with the Blood-Brain Barrier During pneumococcal infection and exposure of the cells to pneumolysin, concurrent events take place. Angiogenesis disruption is taking place due to oxidative stress initiated by the pneumococci (1). Pneumolysin forms pores (2) and promotes cytoskeletal remodeling through tight junction lipids and proteins (3). An aftereffect of this event is calcium influx (4) and inhibition of MMPs (5), which subsequently leads to the inhibition of extracellular matrix degradation (6). This allows the pneumococci to extend their presence around a cellular environment. Leukocyte migration is activated (7) and strong immune responses are initiated involving cytokines and chemokines (8). The presence of pneumolysin as well as the increased numbers of pneumococci, allow the pathogen to traverse through the Blood-Brain Barrier using the transcellular (9) and paracellular (10) routes. Dissociation of the Blood-Brain Barrier and invasion of leukocytes and cytokines in the brain, trigger a new immune response within the brain, which leads to neuronal inflammation and neurological sequelae (11).

Finally it is important to state that my study gives an overview of the interactions between the pathogen and the host. Thus, it is important to expand on the findings and the novelties of this thesis by testing each separately. With a library of elevated genes against pneumococcal infection, many genes can be tested as biomarkers of disease or targets for therapeutic intervention in order to contribute to translational medicine (a more bench to bedside research). The new role of pneumolysin may be informative for the current efforts in producing a vaccine. The speculation that pneumolysin might be promoting the interruption of cation-channels in the cell to supply the pneumococci with nutrients, gives a new insight into the importance of pneumolysin in virulence of the bacteria.

To conclude, I have shown that disease progression is dependent both on the host and the pathogen. The ability of the pneumococci to avoid or neutralise parts of the immune system and the damage occurring from the host inflammatory response leads to increased severity of disease.

I would like to close the thesis by referring to a saying from my grandfather, which I will always have as a beacon throughout my life:

‘’With a good heart you always achieve your goals’’

«Πάντα καλή καρδιά και έτσι κάνεις ότι θέλεις.»

Καλλής Κουλουμή Καρακώστα

9.0 Appendix

9.1.0 Chapter 3 - Terminal Velocity in creeping flow calculations

In mathematical terms, a terminal velocity without the effects of buoyancy is given by

$$V_t = \sqrt{\frac{2mg}{\rho A C_d}}$$

where

- V_t is terminal velocity,
- m is the mass of the falling object
- g is the acceleration due to gravity ($9.81 m/s^2$)
- C_d is the drag coefficient of the object (resistance force applied on an object found in a fluid)
- ρ is the density of the fluid through which the object is executing a fall, and
- A is the surface area of the object.

When the fluid itself has a very slow motion, the inertia forces related to the fluid are not taken into account, hence providing the assumption that the fluid has no mass. That is called terminal velocity in creeping flow and is given by

$$V_t = \frac{gd^2}{18\mu}(\rho_s - \rho)$$

where

- d is the diameter of the spherical object
- g is the acceleration due to gravity ($9.81 m/s^2$)
- μ is the fluid viscosity
- ρ is the density of the fluid through which the object is executing a fall, and
- ρ_s is the density of the object itself.

All the variables in the equation mention above are known, where the density of both the object and the fluid can be calculated by the formula

$$\rho = \frac{m}{V}$$

where

- m is the mass of the object calculated (cell or fluid)
- V is the volume of the where the object is found in

Variables and calculations

1) When acquiring the weight of the endothelial cells it was found that $1x10^5$ cells accounts to 1.114 g which accounts to 11.14 μg per cell.
2) The density of the endothelial cells used in the specific experiment ($1x10^5$ cells/ml) accounted to 1.114 g/ml (ρ_s).
3) When acquiring the weight of the DMEM used to culture endothelial cells, it was found that 1ml of DMEM weighs 0.992 g at 37^oC hence the density was found to be 0.992 g/ml (ρ).

4) According to the literature the viscosity of a DMEM at 37ºC is 0.77 cP (centipoise).
5) The average diameter of endothelial cells before adhering on a surface was acquired by images taken from a phase microscope at 4x, (see appendix for calculations) and it accounts to 41.72μm per cell.

For cells seeded in a total volume of 500 μl, the terminal velocity in creeping flow is:

$$V_t = \frac{gd^2}{18\mu}(\rho_s - \rho) = \frac{9.81 m/s^2 x(41.72x10^{-6}m)^2}{18x(0.77x10^{-3}Pa\cdot s)} x([557-496]Kg/m^3)$$
$$= \frac{1.7075x10^{-8}\frac{\cancel{m}^3}{s^2}}{1.386x10^{-2}Pa\cdot s} x(81\frac{Kg}{\cancel{m}^3}) = 9.978x10^{-5}\frac{Kg}{Pa\cdot s^3} = 9.978x10^{-5}\frac{\cancel{Kg}}{\frac{\cancel{Kg}}{m\cdot \cancel{s}^2}xs^{\cancel{3}}} = 9.978x10^{-5} m/s$$

where for cells seeded in a total volume of 150 μl, the terminal velocity in creeping flow is:

$$V_t = \frac{gd^2}{18\mu}(\rho_s - \rho) = \frac{9.81 m/s^2 x(41.72x10^{-6}m)^2}{18x(0.77x10^{-3}Pa\cdot s)} x([167.1-148.8]Kg/m^3)$$
$$= \frac{1.7075x10^{-8}\frac{\cancel{m}^3}{s^2}}{1.386x10^{-2}Pa\cdot s} x(18.3\frac{Kg}{\cancel{m}^3}) = 2.254x10^{-5}\frac{Kg}{Pa\cdot s^3} = 2.254x10^{-5}\frac{\cancel{Kg}}{\frac{\cancel{Kg}}{m\cdot \cancel{s}^2}xs^{\cancel{3}}} = 2.254x10^{-5} m/s$$

9.1.1 Chapter 3 – Mass-flow rate calculations

Darcy's law describes the kinetics of fluid flow through a porous membrane in relation to the driving force as well as the permeability of the media.

The flow rate is given by the formula

$$Q = \frac{K}{\mu}\frac{\Delta P}{\Delta L}A$$

where

- Q is the flow rate (m^3/s),
- K is the permeability coefficient (m^2),
- L is flow length or thickness of test sample (m),
- A is the area of cross-sectional area to flow (m^2), and
- μ is the fluid viscosity (Pa·s).

In order to emphasise on the role that the size of the pore has, it was assumed that the permeability coefficient (K) and the flow length (L) where both valued as one.

Having in mind from previous calculations that the DMEM viscosity is 0.77cP, the equation is solved as followed:

For an endothelial cell media found in inserts of 3.0 μm pores, the flow rate is calculated as:

$$Q = \frac{K}{\mu}\frac{\Delta P}{\Delta L}A = \frac{1N\cdot m^2\cdot s}{0.77x10^{-3}Pa\cdot s}x\frac{1}{1}m\ x[\frac{3.14x(3x10^{-6}m)^2}{2}] =$$
$$1298.7\frac{N\cdot m^3\cdot s}{Pa\cdot s}x\ 0.1413x10^{-10}m^2 = 1.835x10^{-8}\frac{\cancel{N}\cdot m^5\cdot \cancel{s}}{\frac{\cancel{N}\cdot s^{\cancel{2}}}{m^2}} = 1.835x10^{-4}\frac{m^3}{s}$$

where for an endothelial cell media found in inserts of 0.4 μm pores, the flow rate is calculated as:

$$Q = \frac{K}{\mu}\frac{\Delta P}{\Delta L}A = \frac{1N \cdot m^2 \cdot s}{0.77x10^{-3}Pa \cdot s}x\frac{1}{1}m\ x[\frac{3.14x(0.4x10^{-6}m)^2}{2}] =$$

$$1298.7\frac{N \cdot m^3 \cdot s}{Pa \cdot s}x\ 0.2512x10^{-12}m^2 = 3.262x10^{-10}\frac{\cancel{N} \cdot m^5 \cdot \cancel{s}}{\frac{\cancel{N} \cdot s^{\cancel{2}}}{m^2}} = 3.262x10^{-6}\frac{m^3}{s}$$

The mass-flow rate can be calculated according to the formula

$$\dot{m} = \rho \cdot Q$$

where

- ρ is the density of the fluid through which the object is executing a fall, and
- Q is the flow rate (m^3/s).

According to the values of flow rate and density calculated above, the mass-flow rate for an endothelial cell media found in inserts of 3.0 μm pores is

$$\dot{m} = \rho \cdot Q = 496\frac{Kg}{\cancel{m}^3}x1.835x10^{-4}\frac{\cancel{m}^3}{s} = 9.1016x10^{-2}\frac{Kg}{s}$$

where the mass-flow rate for an a media found in inserts of 0.4 μm pores is

$$\dot{m} = \rho \cdot Q = 148.8\frac{Kg}{\cancel{m}^3}x3.262x10^{-6}\frac{\cancel{m}^3}{s} = 4.8538x10^{-4}\frac{Kg}{s}$$

9.2.0 Chapter 6 – Graphical representation of pathways generated during incubation of the model with pneumolysin or pneumococcal serotype 6B

9.2.1 Figure Ap1: Up-regulation of Actin Cytoskeleton pathway

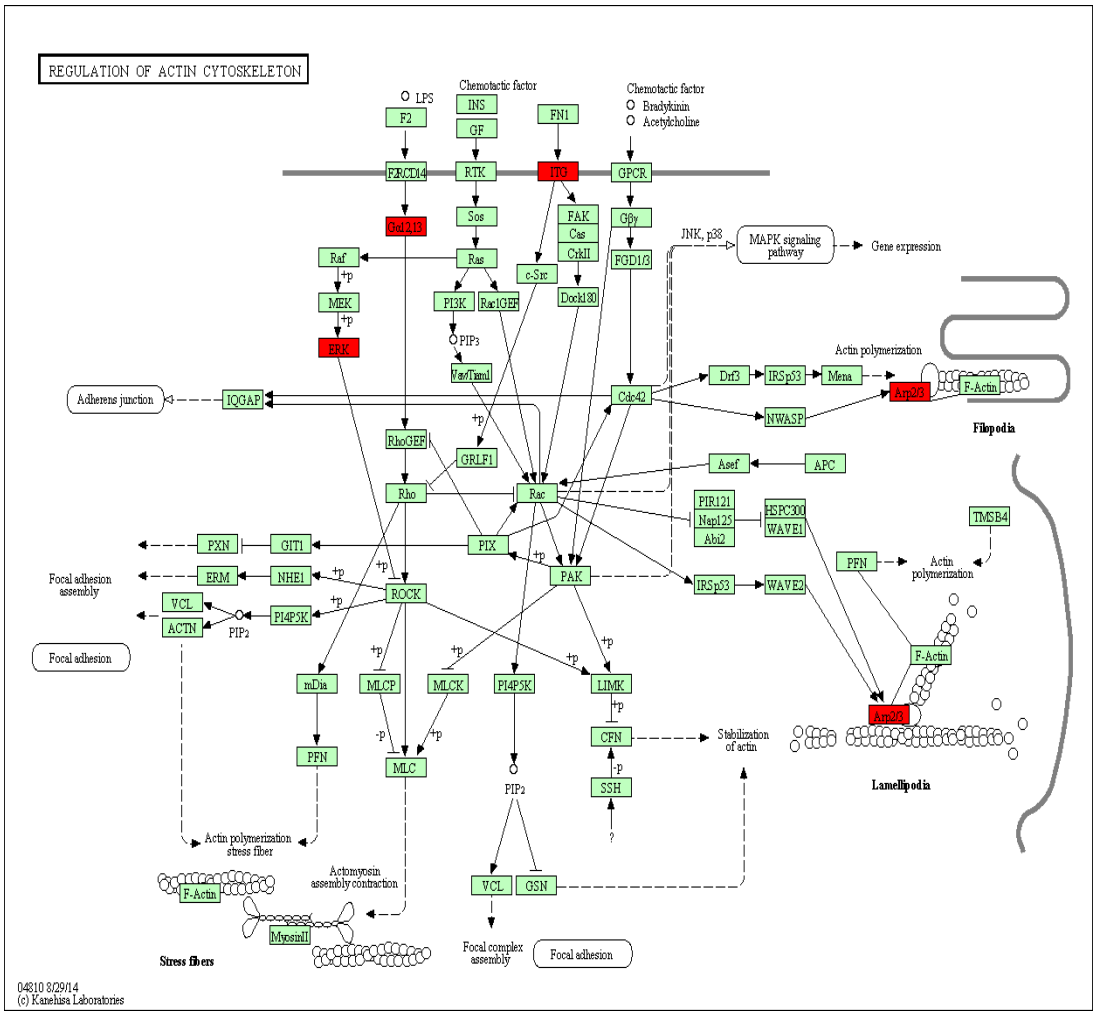

Figure Ap1| Up-regulation of Actin Cytoskeleton during infection with pneumolysin With the use of significant analysis of microarrays (SAM) and the online software InnateDB, it was observed that 4 genes were responsible for the up-regulation of this pathway (ARPC2, GNA13, ITGB2, MAPK3). These genes encode ERK, Gα12/13, ITG and Arp2/3. The pathway was generated using the Kyoto Encyclopedia of Genes and Genomes (KEGG). The red transcripts are genes found to be significantly up-regulated. The intense-green transcripts (not present in this pathway) show the genes, which down-regulate the transcript, whereas pale-green boxes are transcripts, which are not activated due to the absence of the relevant genes. Pathway p-value and p-value (corrected) ***p<0.0076, *p<0.0243.

9.2.2 Figure Ap2: Up-regulation of Leukocyte trans-endothelial migration pathway

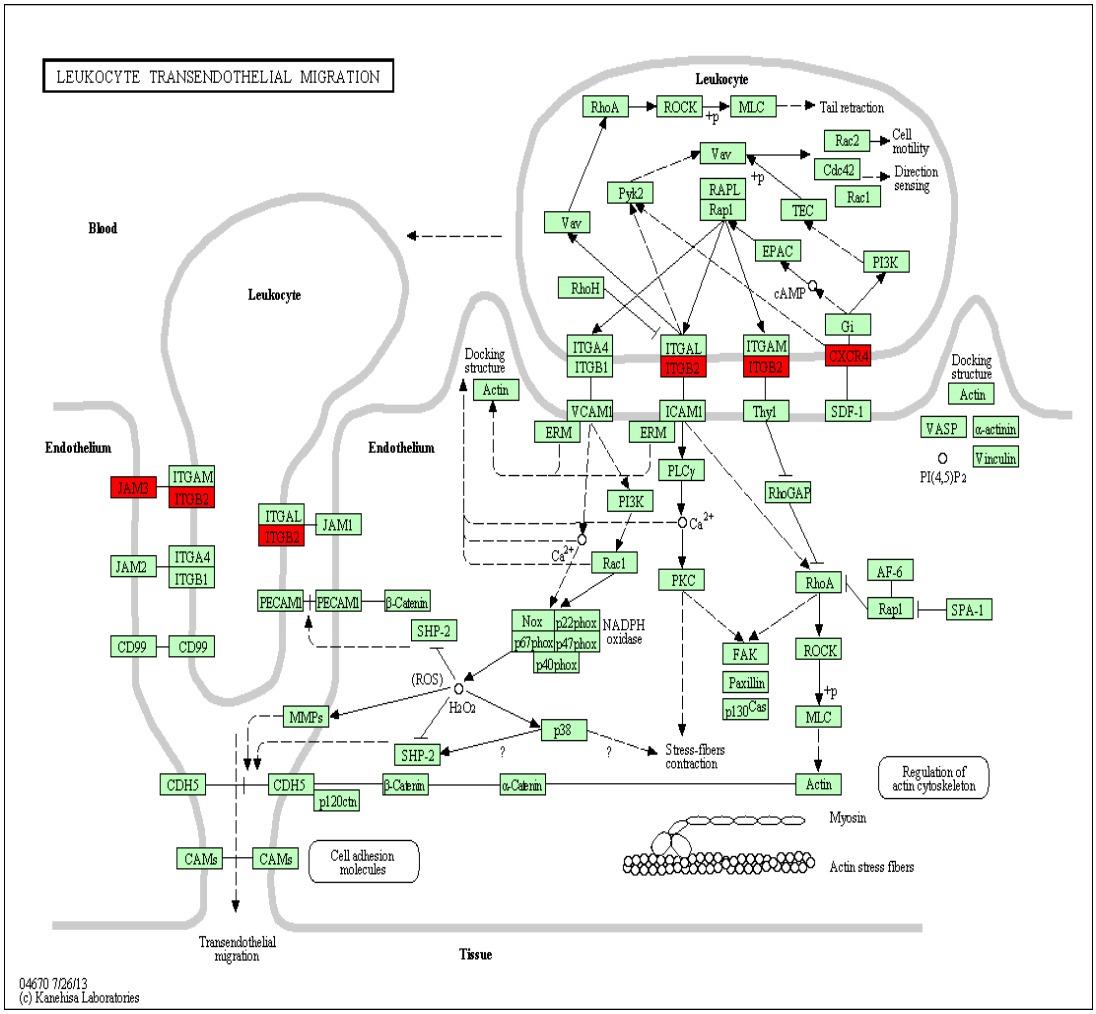

Figure Ap2| Up-regulation of Leukocyte trans-endothelial migration during infection with pneumolysin With the use of significant analysis of microarrays (SAM) and the online software InnateDB, it was observed that 3 genes were responsible for the up-regulation of this pathway (CXCR4, ITGB2, JAM3). These genes encode and up-regulate JAM3, ITGB2, and CXCR4. The pathway was generated using the Kyoto Encyclopedia of Genes and Genomes (KEGG). The red transcripts are genes found to be significantly up-regulated. The intense-green transcripts (not present in this pathway) show the genes, which down-regulate the transcript, whereas pale-green boxes are transcripts, which are not activated due to the absence of the relevant genes. Pathway p-value and p-value (corrected) ***p<0.0092, *p<0.0283.

9.2.3 Figure Ap3: Up-regulation of Gap Junction pathway

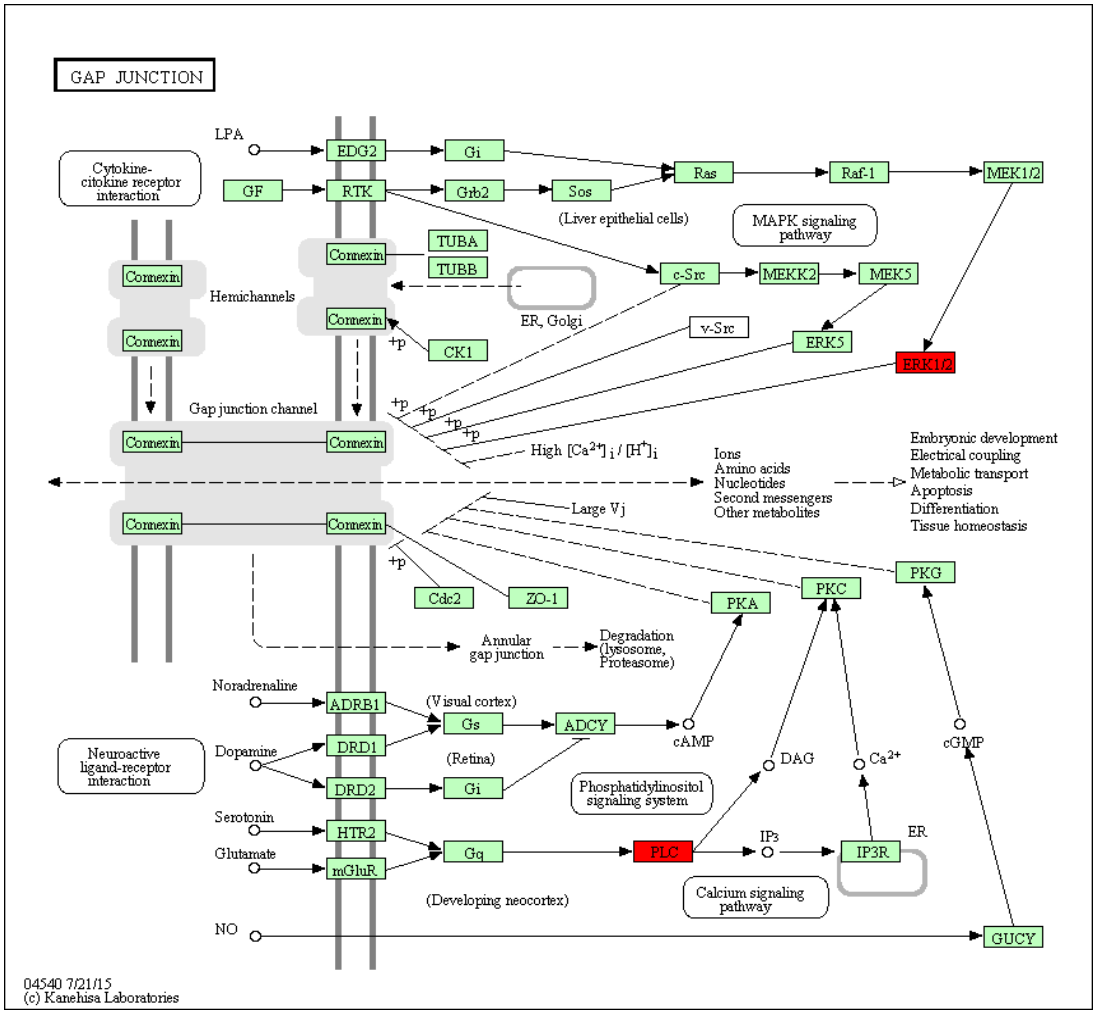

Figure Ap3| Up-regulation of Gap Junction during infection with pneumolysin With the use of significant analysis of microarrays (SAM) and the online software InnateDB, it was observed that 2 genes were responsible for the up-regulation of this pathway (MAPK3, PBLC2). These genes encode and up-regulate ERK1/2, and PLC. The pathway was generated using the Kyoto Encyclopedia of Genes and Genomes (KEGG). The red transcripts are genes found to be significantly up-regulated. The intense-green transcripts (not present in this pathway) show the genes, which down-regulate the transcript, whereas pale-green boxes are transcripts, which are not activated due to the absence of the relevant genes. Pathway p-value and p-value (corrected) *$p<0.0421$, $p<0.0607$.

9.2.4 Figure Ap4: Down-regulation of MMP activation pathway

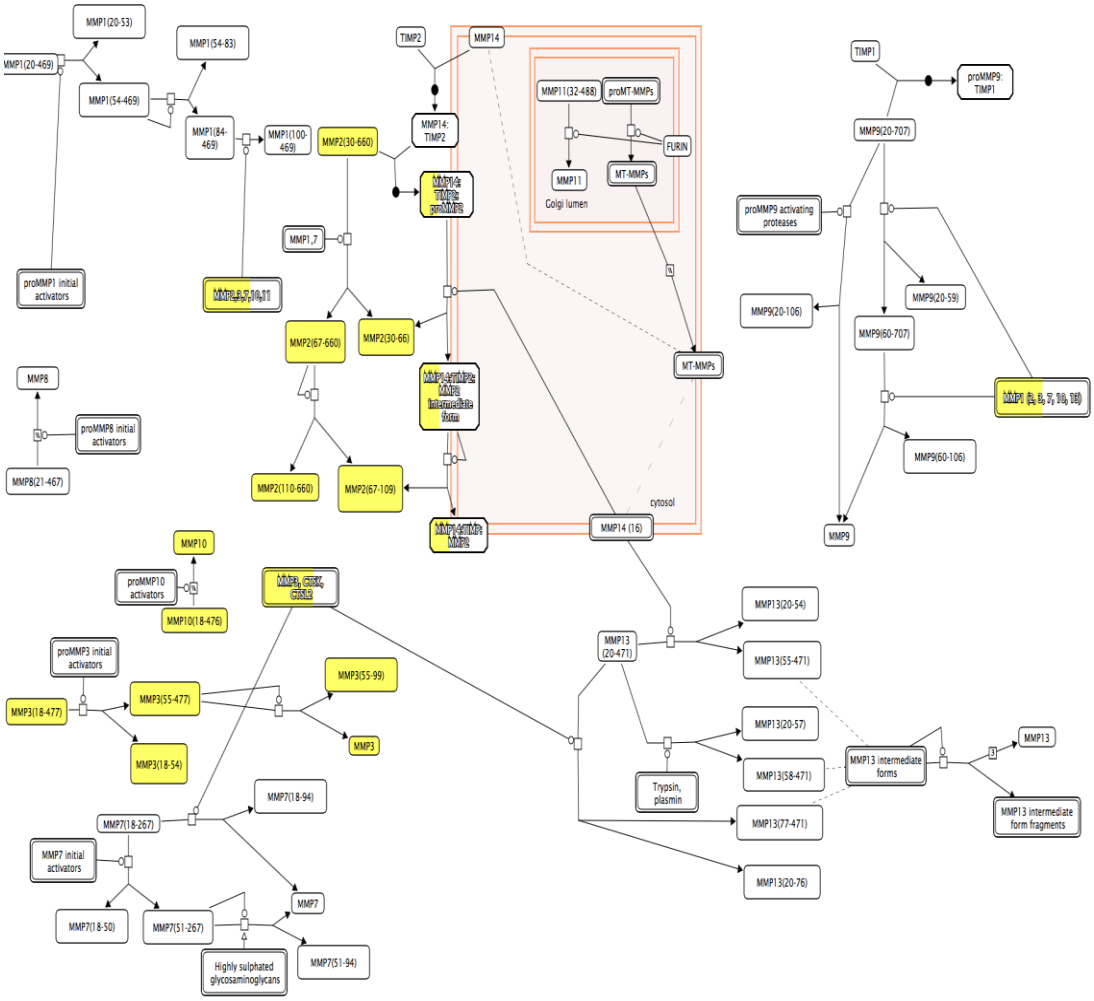

Figure Ap4| Down-regulation of MMPs activation during infection with pneumolysin With the use of significant analysis of microarrays (SAM) and the online software InnateDB, it was observed that 4 genes were responsible for the down-regulation of this pathway (CTSL2, MMP2, MMP3, MMP10). These genes encode and down-regulate MMP2, MMP3, and MMP10. The pathway was generated using only the significantly expressed genes. The generation of the pathway was achieved by using the REACTOME Pathway Database. The yellow colour in the transcripts designates genes contributing to the transcript's expression. Transcripts without any colour are not activated due to the absence of the relevant genes. Pathway p-value and p-value (corrected) **p<0.0113, p<0.3046.

9.2.5 Figure Ap5: Down-regulation of Collagen degradation pathway

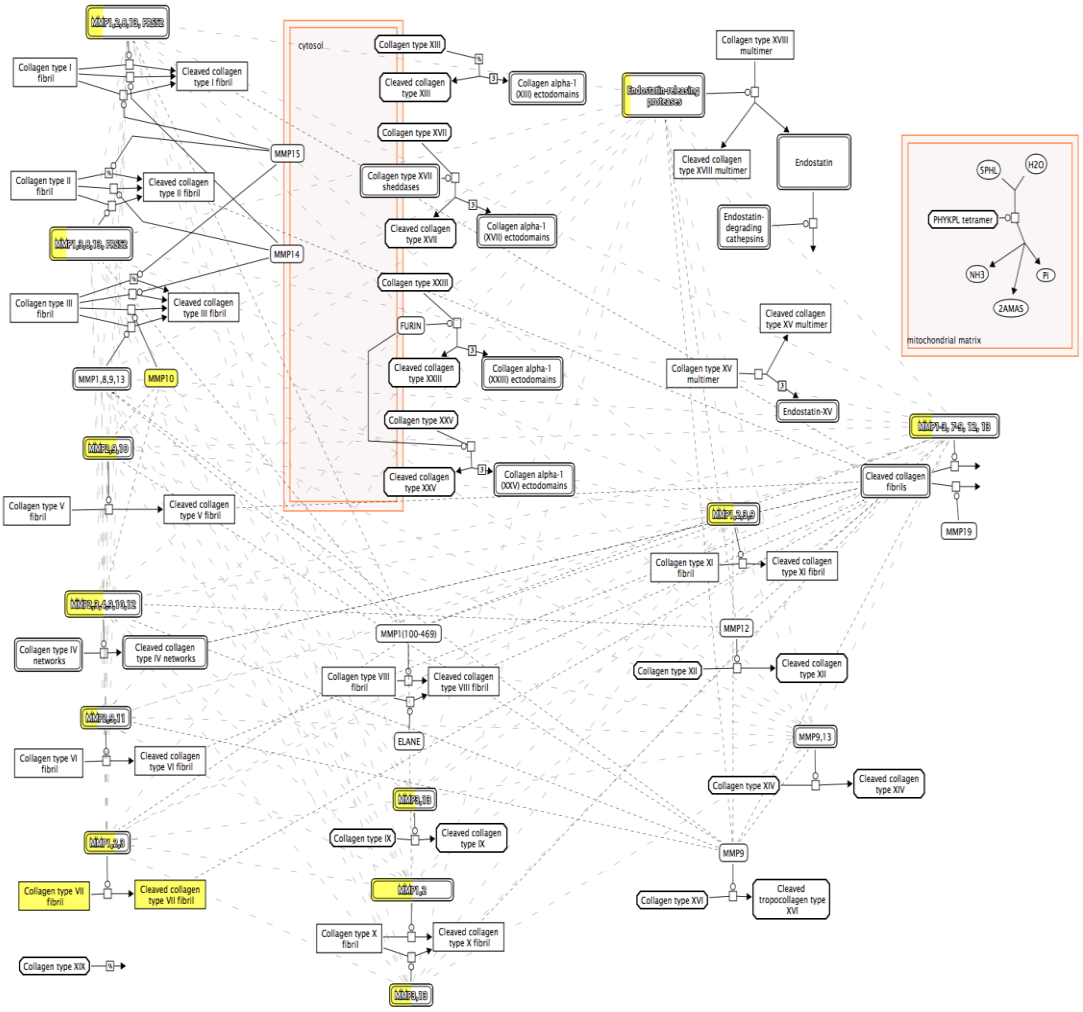

Figure Ap5| Down-regulation of Collagen Degradation during infection with pneumolysin With the use of significant analysis of microarrays (SAM) and the online software InnateDB, it was observed that 5 genes were responsible for the down-regulation of this pathway (COL4A2, COL7A1, MMP2, MMP3, MMP10). These genes encode and down-regulate MMP2, MMP3, and MMP10, Collagen type VII fibril and cleaved Collagen type VII fibril. The pathway was generated using only the significantly expressed genes. The generation of the pathway was achieved by using the REACTOME Pathway Database. The yellow colour in the transcripts designates genes contributing to the transcript's expression. Transcripts without any colour are not activated due to the absence of the relevant genes. Pathway p-value and p-value (corrected) **p<0.0266, p<0.4175.

9.2.6 Figure Ap6: Down-regulation of extracellular matrix degradation pathway

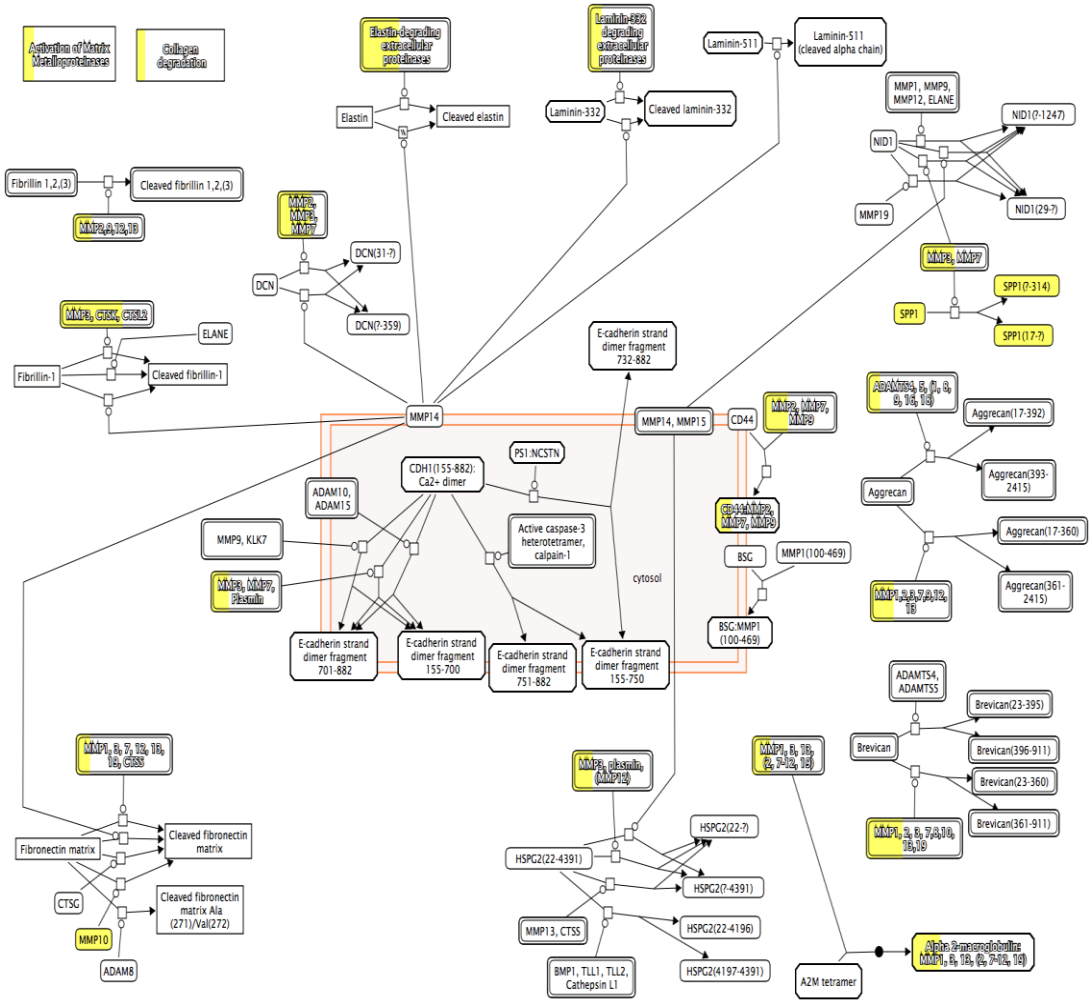

Figure Ap6| Down-regulation of the degradation of the Extracellular Matrix during infection with pneumolysin With the use of significant analysis of microarrays (SAM) and the online software InnateDB, it was observed that 8 genes were responsible for the down-regulation of this pathway (ADAMTS1, COL4A2, COL7A1, CTSL2, MMP2, MMP3, MMP10, SPP1). These genes encode and down-regulate MMP2, MMP3, MMP10, collagen degradation, elastin, laminin-332, ADAMTS1 and SPP1. The pathway was generated using only the significantly expressed genes. The generation of the pathway was achieved by using the REACTOME Pathway Database. The yellow colour in the transcripts designates genes contributing to the transcript's expression. Transcripts without any colour are not activated due to the absence of the relevant genes. Pathway p-value and p-value (corrected) **p<0.0152, p<0.3538.

9.2.7 Figure Ap7: Up-regulation of cytokine-cytokine interaction pathway

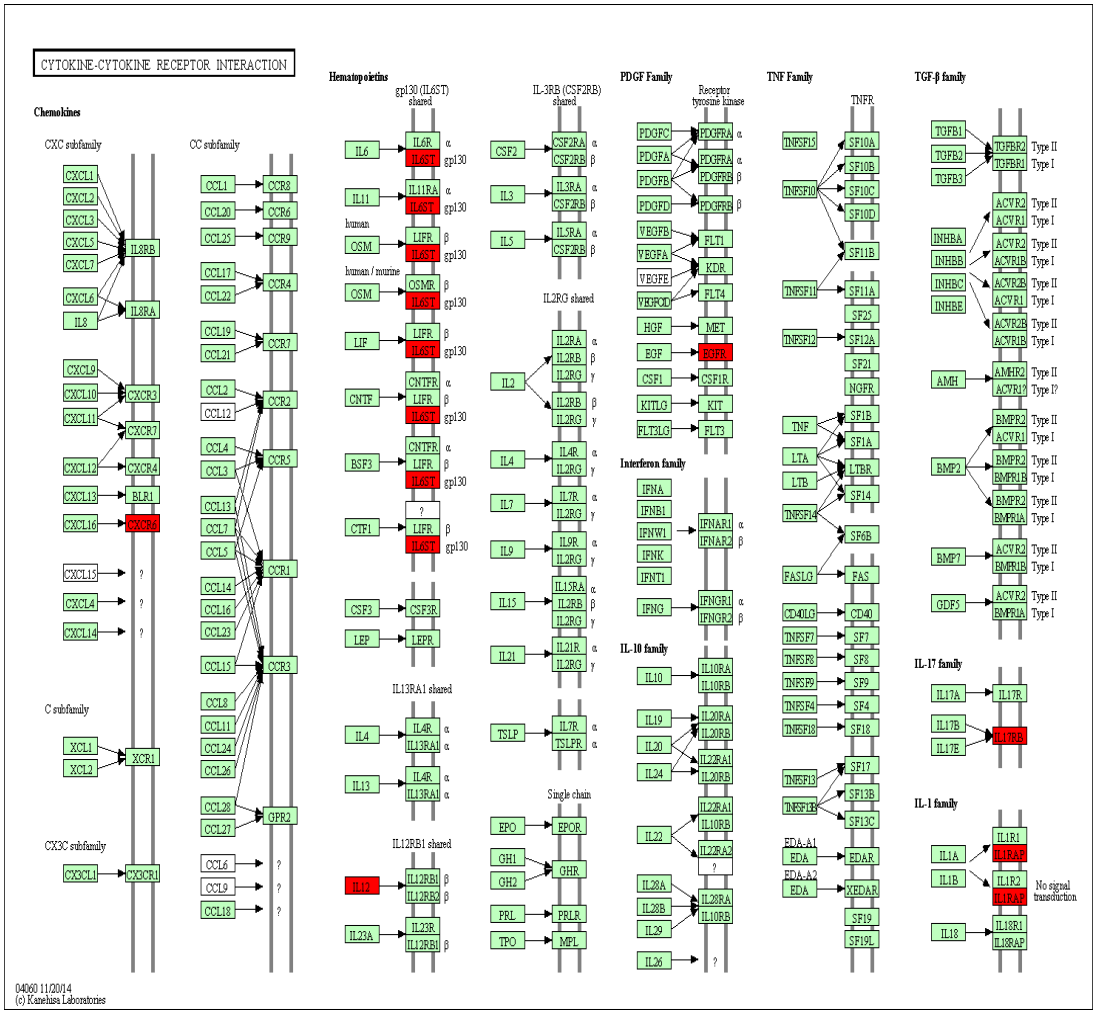

Figure Ap7| Up-regulation of Cytokine-Cytokine interactions during infection with 6B With the use of significant analysis of microarrays (SAM) and the online software InnateDB, it was observed that 7 genes were responsible for the up-regulation of this pathway (CXCR6, EGFR, IL12A, IL12B, IL17RB, IL1RAP, IL6ST). These genes encode and up-regulate CXCR6, IL12, IL6ST, EGFR, IL1RAP and IL17RB. The pathway was generated using the Kyoto Encyclopedia of Genes and Genomes (KEGG). The red transcripts are genes found to be significantly up-regulated. The intense-green transcripts (not present in this pathway) show the genes, which down-regulate the transcript, whereas pale-green boxes are transcripts, which are not activated due to the absence of the relevant genes. Pathway p-value and p-value (corrected) **p<0.0160, p<0.1114.

9.2.8 Figure Ap8: Up-regulation of T-cell receptor signalling pathway

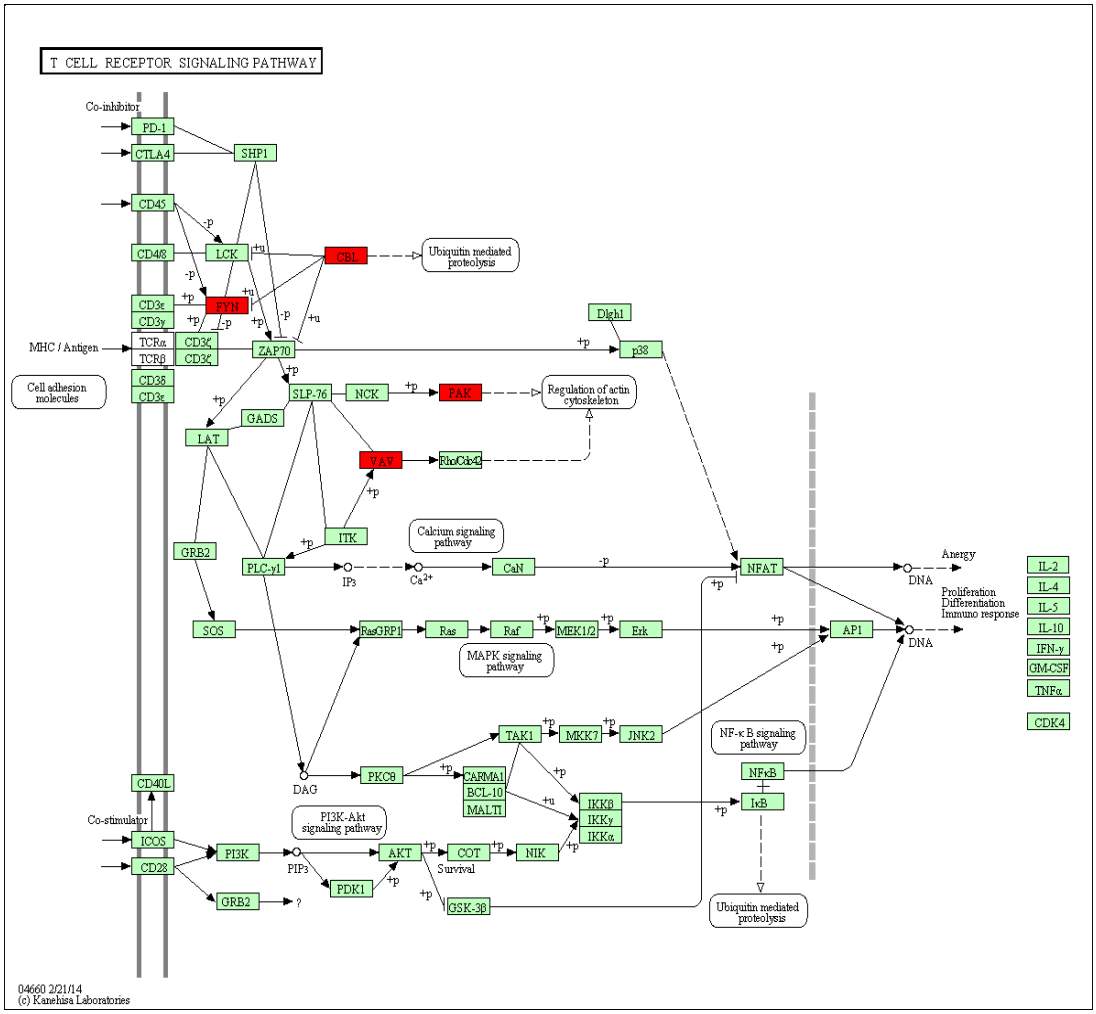

Figure 14| Up-regulation of the T-cell receptor signalling pathway during infection with 6B With the use of significant analysis of microarrays (SAM) and the online software InnateDB, it was observed that 4 genes were responsible for the up-regulation of this pathway (CBLB, FYN, PAK7, VAV3). These genes encode and up-regulate FYN, CBL, VAV and PAK. These genes encode and up-regulate CXCR6, IL12, IL6ST, EGFR, IL1RAP and IL17RB. The pathway was generated using the Kyoto Encyclopedia of Genes and Genomes (KEGG). The red transcripts are genes found to be significantly up-regulated. The intense-green transcripts (not present in this pathway) show the genes, which down-regulate the transcript, whereas pale-green boxes are transcripts, which are not activated due to the absence of the relevant genes. Pathway p-value and p-value (corrected) **p<0.0235, p<0.1193.

9.2.9 Figure Ap9: Up-regulation of Type I Diabetes Mellitus pathway

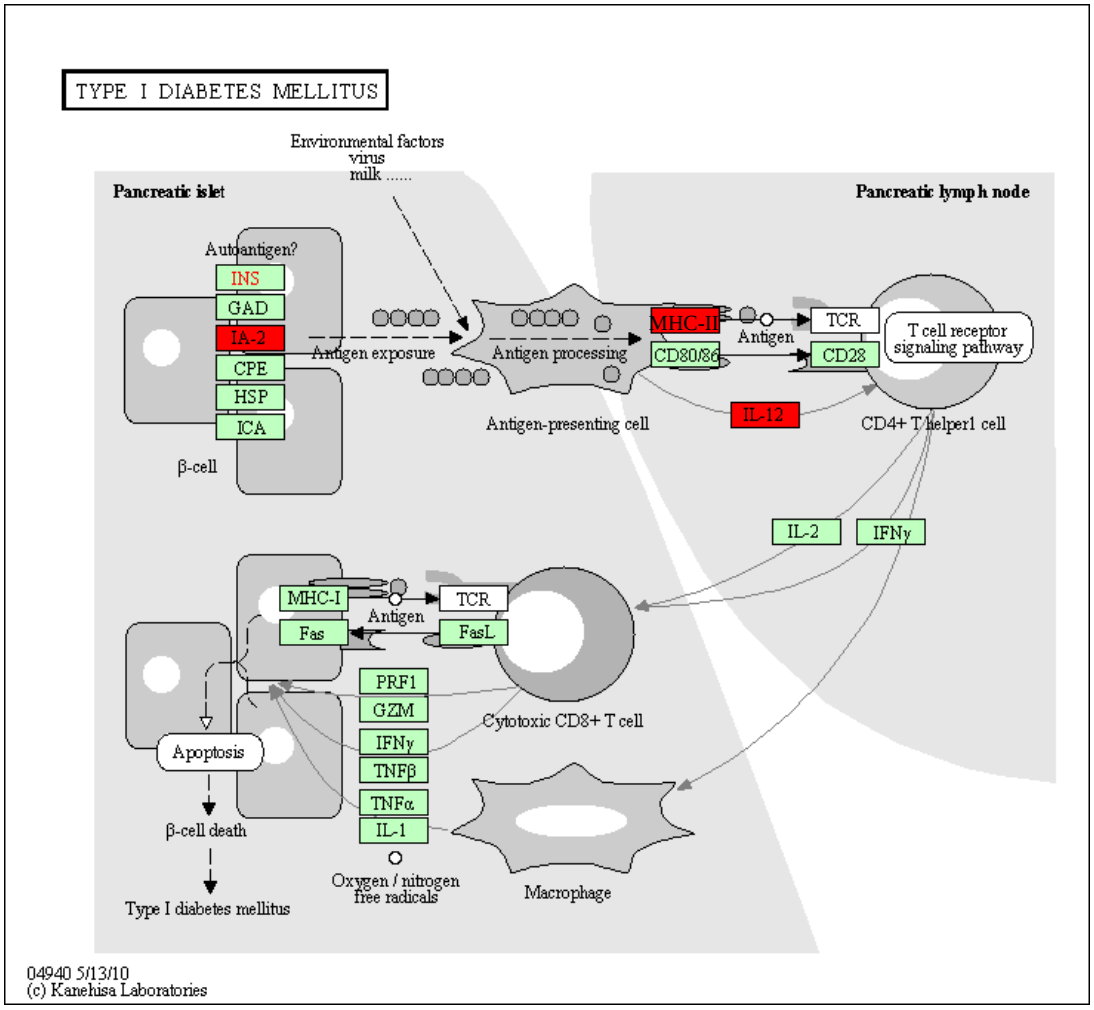

Figure Ap9| Up-regulation of Type I Diabetes Mellitus pathway during infection with 6B With the use of significant analysis of microarrays (SAM) and the online software InnateDB, it was observed that 5 genes were responsible for the up-regulation of this pathway (HLA-DPA1, HLA-DQB1, IL12A, IL12B, PTPRN). These genes encode and up-regulate IA-2, INF-γ, MHCII and IL12. The pathway was generated using the Kyoto Encyclopedia of Genes and Genomes (KEGG). The red transcripts are genes found to be significantly up-regulated. The intense-green transcripts (not present in this pathway) show the genes, which down-regulate the transcript, whereas pale-green boxes are transcripts, which are not activated due to the absence of the relevant genes. Pathway p-value and p-value (corrected) ****$p<0.0001$, **$p<0.0134$.

10.0 References

1. (WHO), W.H.O., *THE GLOBAL BURDEN OF DISEASE 2004 UPDATE*. 2004.
2. Agency, H.P., *Health Protection in the 21st Century - Understanding the Burden of Disease; preparing for the future.* 2005: p. 124.
3. (WHO), W.H.O. 2015 14 September]; Available from: http://www.who.int/.
4. Solomon, T., et al., *Japanese encephalitis.* Journal of Neurology, Neurosurgery, and Psychiatry, 2000. **68**: p. 405-15.
5. Bell, J.D., et al., *Management of suspected herpes simplex virus encephalitis in adults in a UK teaching hospital.* Clinical Medicine, 2009. **9**(3): p. 231-35.
6. Society, T.E. 2014 22 October]; Available from: http://www.encephalitis.info.
7. Brouwer, M.C., A.R. Tunkel, and D. van de Beek, *Epidemiology, diagnosis, and antimicrobial treatment of acute bacterial meningitis.* Clin Microbiol Rev, 2010. **23**(3): p. 467-92.
8. van de Beek, D., et al., *Community-Acquired Bacterial Meningitis in Adults.* The New England Journal of Medicine, 2006. **354**(1): p. 44-53.
9. Abbott, N.J., et al., *Structure and function of the blood-brain barrier*. Neurobiol Dis, 2010. **37**(1): p. 13-25.
10. Lo, E.H., T. Dalkara, and M.A. Moskowitz, *Mechanisms, challenges and opportunities in stroke.* Nat Rev Neurosci, 2003. **4**(5): p. 399-415.
11. Lok, J., et al., *Cell-cell signaling in the neurovascular unit.* Neurochem Res, 2007. **32**(12): p. 2032-45.
12. Liddelow, S.A., *Fluids and barriers of the CNS: a historical viewpoint.* Fluids and barriers of the CNS, 2011. **8**(2): p. 01-16.
13. Ehrlich, P., *Das Sauerstoff-Bedürfnis des Organismus:Eine farbenanalytische studie*. 1885: August Hirschwald. 01-165.
14. Saunders, N.R., et al., *The rights and wrongs of blood-brain barrier permeability studies: a walk through 100 years of history*. Front Neurosci, 2014. **8**: p. 404.
15. Frank, P.G., et al., *Caveolin, caveolae, and endothelial cell function.* Arterioscler Thromb Vasc Biol, 2003. **23**(7): p. 1161-8.
16. Simionescu, M., N. Simionescu, and E.G. Palade, *MORPHOMETRIC DATA ON THE ENDOTHELIUM OF BLOOD CAPILLARIES.* The Journal of Cell Biology, 1974. **60**: p. 128-52.
17. Liu, P. and W.G.R. Anderson, *Compartmentalized Production of Ceramide at the Cell Surface*. The Journal of Biological Chemistry, 1995. **270**(45): p. 27179-85.
18. Virgintino, D., et al., *EXPRESSION OF CAVEOLIN-1 IN HUMAN BRAIN MICROVESSELS*. Neuroscience, 2002. **115**(1): p. 145-52.
19. Ikezu, T., et al., *Affinity-purification and characterization of caveolins from the brain: Differential expression of caveolin-1, -2, and -3 in brain endothelial and astroglial cell types.* Brain Research, 1998. **804**: p. 177-192.
20. Nag, S., R. Venugopalan, and D.J. Stewart, *Increased caveolin-1 expression precedes decreased expression of occludin and claudin-5 during blood-brain barrier breakdown.* Acta Neuropathol, 2007. **114**(5): p. 459-69.

21. Shin, T., et al., *Expression of caveolin-1, -2, and -3 in the spinal cords of Lewis rats with experimental autoimmune encephalomyelitis.* J Neuroimmunol, 2005. **165**(1-2): p. 11-20.
22. Scherer, E.P., et al., *Identification, sequence, and expression of caveolin-2 defines a caveolin gene family.* Cell Biology, 1996. **93**: p. 131-35.
23. Reese, S.T. and J.M. Karnovsky, *FINE STRUCTURAL LOCALIZATION OF A*

BLOOD-BRAIN BARRIER TO EXOGENOUS PEROXIDASE. The Journal of Cell Biology, 1967. **34**: p. 207-17.
24. Nagy, Z., H. Peters, and I. Hüttner, *Fracture Faces of Cell Junctions in Cerebral Endothelium during Normal and Hyperosmotic Conditions.* Laboratory Investigation, 1984. **50**(3): p. 313-22.
25. Crone, C. and P.S. Olesen, *Electrical Resistance of Brain Microvascular Endothelium.* Brain Research, 1982. **24**: p. 49-55.
26. Smith, R.Q. and I.S. Rapoport, *Cerebrovascular Permeability Coefficients to Sodium, Potassium, and Chloride.* Journal of Neurochemistry, 1986. **46**(6): p. 1732-42.
27. Krause, D., et al., *Correlation of zonula occludens ZO-1 antigen expression and transendothelial resistance in porcine and rat cultured cerebral endothelial cells.* Neuroscience Letters, 1991. **128**: p. 301-04.
28. Morita, K., et al., *Claudin multigene family encoding four-transmembrane domain protein components of tight junction strands.* Cell Biology, 1999. **96**: p. 511-16.
29. Tsukita, S., M. Furuse, and M. Itoh, *MULTIFUNCTIONAL STRANDS IN TIGHT JUNCTIONS.* Molecular Cell Biology, 2001. **2**: p. 285-93.
30. Turksen, K. and T.C. Troy, *Barriers built on claudins.* J Cell Sci, 2004. **117**(Pt 12): p. 2435-47.
31. Van Itallie, C.M. and J.M. Anderson, *Claudins and epithelial paracellular transport.* Annu Rev Physiol, 2006. **68**: p. 403-29.
32. Hamazaki, Y., et al., *Multi-PDZ domain protein 1 (MUPP1) is concentrated at tight junctions through its possible interaction with claudin-1 and junctional adhesion molecule.* J Biol Chem, 2002. **277**(1): p. 455-61.
33. Furuse, M. and S. Tsukita, *Claudins in occluding junctions of humans and flies.* Trends Cell Biol, 2006. **16**(4): p. 181-8.
34. Saitou, M., et al., *Complex Phenotype of Mice Lacking Occludin, a Component of Tight Junction Strands.* Molecular Biology of the Cell, 2000. **11**: p. 4131-42.
35. Gow, A., et al., *CNS Myelin and Sertoli Cell Tight Junction Strands Are Absent in Osp/Claudin-11 Null Mice.* Cell, 1999. **99**: p. 649-59.
36. Krause, G., et al., *Structure and function of extracellular claudin domains.* Ann N Y Acad Sci, 2009. **1165**: p. 34-43.
37. Hirase, T., et al., *Occludin as a possible determinant of tight junction permeability in endothelial cells.* Journal of Cell Science, 1997. **110**: p. 1603-13.
38. Furuse, M., et al., *Occludin: A Novel Integral Membrane Protein Localizing at Tight Junctions.* The Journal of Cell Biology, 1993. **123**(6): p. 1777-88.
39. Balda, M.S. and K. Matter, *Tight junctions at a glance.* Journal of Cell Science, 2008. **121**(22): p. 3677-3682.

40. Barrios-Rodiles, M., et al., *High-Throughput Mapping of a Dynamic Signaling Network in Mammalian Cells.* Science, 2005. **307**: p. 1621-25.

41. Wang, Z., et al., *The second loop of occludin is required for suppression of Raf1-induced tumor growth.* Oncogene, 2005. **24**(27): p. 4412-4420.
42. Bazzoni, G., *The JAM family of junctional adhesion molecules.* Current Opinion in Cell Biology, 2003. **15**(5): p. 525-530.
43. Palmeri, D., et al., *Vascular endothelial junction-associated molecule, a novel member of the immunoglobulin superfamily, is localized to intercellular boundaries of endothelial cells.* J Biol Chem, 2000. **275**(25): p. 19139-45.
44. Martìn-Padura, I., et al., *Junctional Adhesion Molecule, a Novel Member of the Immunoglobulin Superfamily That Distributes at Intercellular Junctions and Modulates Monocyte Transmigration.* The Journal of Cell Biology, 1998. **142**(1): p. 117-27.

45. Ostermann, G., et al., *JAM-1 is a ligand of the beta(2) integrin LFA-1 involved in transendothelial migration of leukocytes.* Nat Immunol, 2002. **3**(2): p. 151-8.
46. Naik, M.U., et al., *Signaling through JAM-1 and alphavbeta3 is required for the angiogenic action of bFGF: dissociation of the JAM-1 and alphavbeta3 complex.* Blood, 2003. **102**(6): p. 2108-14.
47. Kornecki, E., et al., *Activation of Human Platelets by a Stimulatory Monoclonal Antibody.* The Journal of Biological Chemistry, 1990. **265**(17): p. 10042-48.
48. Ozaki, H., et al., *Junctional adhesion molecule (JAM) is phosphorylated by protein kinase C upon platelet activation.* Biochem Biophys Res Commun, 2000. **276**(3): p. 873-8.
49. Barton, S.E., et al., *Junction Adhesion Molecule Is a Receptor for Reovirus.* Cell, 2001. **104**: p. 441-51.
50. Forrest, J.C., et al., *Structure-function analysis of reovirus binding to junctional adhesion molecule 1. Implications for the mechanism of reovirus attachment.* J Biol Chem, 2003. **278**(48): p. 48434-44.
51. Ebnet, K., et al., *The junctional adhesion molecule (JAM) family members JAM-2 and JAM-3 associate with the cell polarity protein PAR-3: a possible role for JAMs in endothelial cell polarity.* J Cell Sci, 2003. **116**(Pt 19): p. 3879-91.
52. Bradfield, P.F., et al., *JAM family and related proteins in leukocyte migration (Vestweber series).* Arterioscler Thromb Vasc Biol, 2007. **27**(10): p. 2104-12.
53. Weber, C., L. Fraemohs, and E. Dejana, *The role of junctional adhesion molecules in vascular inflammation.* Nat Rev Immunol, 2007. **7**(6): p. 467-77.
54. Nag, S., *Role of the endothelial cytoskeleton in blood-brain-barrier permeability to protein.* Acta Neuropathol, 1995. **90**: p. 454-60.
55. Nag, S., M.D. Robertson, and B.H. Dinsdale, *Cytoplasmic Filaments in Intracerebral Cortical Vessels.* Annals of Neurology, 1978. **13**(6): p. 555-59.
56. Itoh, M., et al., *Direct Binding of Three Tight Junction-associated MAGUKs, ZO-1, ZO-2, and ZO-3, with the COOH Termini of Claudins.* The Journal of Cell Biology, 1999. **147**(6): p. 1351-63.
57. Guillemot, L., et al., *The cytoplasmic plaque of tight junctions: a scaffolding and signalling center.* Biochim Biophys Acta, 2008. **1778**(3): p. 601-13.

58. Matter, K. and M.S. Balda, *Epithelial tight junctions, gene expression and nucleo-junctional interplay.* J Cell Sci, 2007. **120**(Pt 9): p. 1505-11.
59. Paris, L., et al., *Structural organization of the tight junctions.* Biochim Biophys Acta, 2008. **1778**(3): p. 646-59.
60. Hartsock, A. and W.J. Nelson, *Adherens and tight junctions: structure, function and connections to the actin cytoskeleton.* Biochim Biophys Acta, 2008. **1778**(3): p. 660-9.
61. Staddon, M.J. and L.L. Rubin, *Cell adhesion, cell junctions and the blood-brain barrier.* Current Opinion in Neurobiology, 1996. **6**: p. 622-27.
62. Furuse, M., et al., *Direct Association of Occludin with ZO-1 and Its Possible Involvement in the Localization of Occludin at Tight Junctions.* The Journal of Cell Biology, 1994. **127**(6): p. 1617-26.
63. Itoh, M., K. Morita, and S. Tsukita, *Characterization of ZO-2 as a MAGUK Family Member Associated with Tight as well as Adherens Junctions.* The Journal of Biological Chemistry, 1999. **274**(9): p. 5981-86.
64. Kale, G., et al., *Tyrosine phosphorylation of occludin attenuates its interactions with ZO-1, ZO-2, and ZO-3.* Biochemical and Biophysical Research Communications, 2003. **302**(2): p. 324-329.
65. Chiba, H., et al., *Transmembrane proteins of tight junctions.* Biochimica et Biophysica Acta (BBA) - Biomembranes, 2008. **1778**(3): p. 588-600.
66. Forster, C., *Tight junctions and the modulation of barrier function in disease.* Histochem Cell Biol, 2008. **130**(1): p. 55-70.
67. Zlokovic, B.V., *The blood-brain barrier in health and chronic neurodegenerative disorders.* Neuron, 2008. **57**(2): p. 178-201.
68. Gray, J.K., et al., *Invasive Group B Streptococcal Infection in Infants, Malawi.* Emerging Infectious Diseases, 2007. **13**(2): p. 223-29.
69. Heyderman, R.S., et al., *Group B streptococcus vaccination in pregnant women with or without HIV in Africa: a non-randomised phase 2, open-label, multicentre trial.* The Lancet Infectious Diseases, 2016.
70. Kalin, M., *Pneumococcal serotypes and their clinical relevance.* Thorax, 1998. **53**: p. 159-62.
71. Eagle, K., *Streptococcus pneumoniae.* Images in Clinical Medicine, 1993. **329**(7): p. 477.
72. Champoux, J.J., et al., *Sherris Medical Microbiology*, ed. J.K. Ryan and G.C. Ray. 2004: MCGRAW-HILL. 937.
73. Libman, E., *A PNEUMOCOCCUS PRODUCING A PECULIAR FORM OF HEMOLYSIS.* Proceedings of the New York Pathological Society, 1905. **5**: p. 168.
74. Billington, J.S., H.B. Jost, and G.J. Songer, *Thiol-activated cytolysins: structure, function and role in pathogenesis.* FEMS Microbiology Letters, 2000. **182**(2): p. 197-205.
75. Shumway, N.C. and J.S. Klebanoff, *Purification of Pneumolysin.* Infect Immun, 1971. **4**(4): p. 388-92.
76. Johnson, K.M., *Properties of Purified Pneumococcal Hemolysin.* Infect Immun, 1972. **6**(5): p. 755-60.
77. Price, K.E. and A. Camilli, *Pneumolysin localizes to the cell wall of Streptococcus pneumoniae.* J Bacteriol, 2009. **191**(7): p. 2163-8.

78. Price, K.E., N.G. Greene, and A. Camilli, *Export requirements of pneumolysin in Streptococcus pneumoniae.* J Bacteriol, 2012. **194**(14): p. 3651-60.
79. Kadioglu, A., et al., *The role of Streptococcus pneumoniae virulence factors in host respiratory colonization and disease.* Nat Rev Microbiol, 2008. **6**(4): p. 288-301.
80. Walker, A.J., et al., *Molecular Cloning, Characterization, and Complete Nucleotide Sequence of the Gene for Pneumolysin, the Sulfhydryl-Activated Toxin of Streptococcus pneumoniae*. 55, 1987. **5**: p. 1184-89.
81. Marshall, E.J., et al., *The Crystal Structure of Pneumolysin at 2.0 Å Resolution Reveals the Molecular Packing of the Pre-pore Complex.* Scientific Reports, 2015. **5**: p. 13293-04.
82. Lawrence, L.S., et al., *Crystal structure of Streptococcus pneumoniae pneumolysin provides key insights into early steps of pore formation.* Sci Rep, 2015. **5**(14352): p. 01-13.
83. Tilley, S.J., et al., *Structural basis of pore formation by the bacterial toxin pneumolysin.* Cell, 2005. **121**(2): p. 247-56.
84. Iliev, I.A., et al., *Cholesterol-dependent actin remodeling via RhoA and Rac1 activation by the Streptococcus pneumoniae toxin pneumolysin.* PNAS, 2007. **104**(8): p. 2897-902.
85. Witzenrath, M., et al., *Role of pneumolysin for the development of acute lung injury in pneumococcal pneumonia.* Crit Care Med, 2006. **34**(7): p. 1947-54.
86. Lucas, R., et al., *Protein kinase C-alpha and arginase I mediate pneumolysin-induced pulmonary endothelial hyperpermeability.* Am J Respir Cell Mol Biol, 2012. **47**(4): p. 445-53.
87. Hirst, R.A., et al., *The role of pneumolysin in pneumococcal pneumonia and meningitis.* Clin Exp Immunol, 2004. **138**(2): p. 195-201.
88. McNeela, E.A., et al., *Pneumolysin activates the NLRP3 inflammasome and promotes proinflammatory cytokines independently of TLR4.* PLoS Pathog, 2010. **6**(11): p. e1001191.
89. Kung, E., et al., *The pneumococcal polysaccharide capsule and pneumolysin differentially affect CXCL8 and IL-6 release from cells of the upper and lower respiratory tract.* PLoS One, 2014. **9**(3): p. e92355.
90. Kadioglu, A., *Upper and Lower Respiratory Tract Infection by Streptococcus pneumoniae Is Affected by Pneumolysin Deficiency and Differences in Capsule Type.* Infection and Immunity, 2002. **70**(6): p. 2886-2890.
91. Thornton, J. and L.S. McDaniel, *THP-1 monocytes up-regulate intercellular adhesion molecule 1 in response to pneumolysin from Streptococcus pneumoniae.* Infect Immun, 2005. **73**(10): p. 6493-8.
92. Canvin, R.J., et al., *The Role of Pneumolysin and Autolysin in the Pathology of Pneumonia and Septicemia in Mice Infected with a Type 2 Pneumococcus.* The Journal of Infectious Diseases, 1995. **172**(1): p. 119-23.
93. Richards, L., et al., *The immunising effect of pneumococcal nasopharyngeal colonisation; protection against future colonisation and fatal invasive disease.* Immunobiology, 2010. **215**(4): p. 251-63.

94. Wall, E.C., et al., *Persistence of pneumolysin in the cerebrospinal fluid of patients with pneumococcal meningitis is associated with mortality.* Clin Infect Dis, 2012. **54**(5): p. 701-5.
95. Pasteur, L., *Oeuvres De Pasteur*. 1881, Paris: Masson et CIE Editeurs. 360.
96. (U.S.), N.B.o.H., *Annual report of the National Board of Health.* 1881.
97. Watson, A.D., et al., *A Brief History of the Pneumococcus in Biomedical Research: A Panoply of Scientific Discovery.* Clinical Infectious Diseases, 1993. **17**: p. 913-24.
98. van Dam, G.E.J., A. Fleer, and S. Harm, *Immunogenicity and immunochemistry of Streptococcuspneumoniae capsular polysaccharides.* Antonie van Leeuwenhoek, 1990. **58**: p. 01-47.
99. Henrichsen, J., *Six Newly Recognized Types of Streptococcus pneumoniae.* Journal of Clinical Microbiology, 1995. **33**(10): p. 2759-62.
100. Robbins, B.J., et al., *Considerations for Formulating the Second-Generation Pneumococcal Capsular Polysaccharide Vaccine with Emphasis on the Cross-Reactive 'Iypes Within Groups.* The Journal of Infectious Diseases, 1983. **148**(6): p. 1136-59.
101. Salyers, A.A. and D.D. Whitt, *Bacterial Pathogenesis: A Molecular Approach*. 1994: ASM Press.
102. Austrian, R., *Some Observations on the Pneumococcus and on the Current Status of Pneumococcal Disease and Its Prevention.* Reviews of Infectious Diseases, 1981. **3**: p. S01-S17.
103. Austrian, R., *The Pneumococcus at the Millennium: Not Down, Not Out.* J Infect Dis, 1999. **179**(Suppl 2): p. S338-S341.
104. Monto, S.A., *Acute Respiratory Infection in Children of Developing Countries: Challenge of the 1990s.* Reviews of Infectious Diseases, 1989. **11**(3): p. 498-505.
105. Hussain, M., et al., *A longitudinal household study of Streptococcus pneumoniae nasopharyngeal carriage in a UK setting.* Epidemiol Infect, 2005. **133**(5): p. 891-8.
106. Melegaro, A., et al., *The current burden of pneumococcal disease in England and Wales.* J Infect, 2006. **52**(1): p. 37-48.
107. Lindberg, A.A. and M. Kalin, *Diagnosis of Pneumococcal Pneumonia: A Comparison between Microscopic Examination of Expectorate, Antigen Detection and Cultural Procedures.* Scand. J. Dis., 1983. **15**(3): p. 247-55.
108. Burnman, Å.L., R. Norrby, and B. Trollfors, *Invasive Pneumococcal Infections: Incidence, Predisposing Factors, and Prognosis.* Reviews of Infectious Diseases, 1985. **7**(2): p. 133-42.
109. Örtqvist, Å., et al., *Aetiology, outcome and prognostic factors in community-acquired pneumonia requiring hospitalization.* Eur. Resp. J., 1990. **3**: p. 1105-13.
110. Fang, G.-D., et al., *New and Emerging Etiologies for Community-Acquired Pneumonia with Implications for Therapy.* Medicine, 1990. **69**(5): p. 307-16.
111. Ruiz-González, A., et al., *Is Streptococcus Pneumoniae the Leading Cause of Pneumonia of Unknown Etiology? A Microbiologic Study of Lung Aspirates in Consecutive Patients with Community-acquired Pneumonia.* The American Journal of Medicine, 1999. **106**(4): p. 385-390.

112. Jokinen, C., et al., *Incidence of Community-Acquired Pneumonia in the Population of Four Municipalities in Eastern Finland.* American Journal of Epidemiology, 1993. **137**(9): p. 977-88.
113. Scott, G.A.J., et al., *Serogroup-Specific Epidemiology of Streptococcus pneumoniae: Associations with Age, Sex, and Geography in 7,000 Episodes of Invasive Disease.* Clinical Infectious Diseases, 1996. **22**(6): p. 973-81.
114. Mufson, M.A. and R.J. Stanek, *Epidemiology of Invasive Streptococcus Pneumoniae Infections and Vaccine Implications among Children in a West Virginia Community, 1978-2003.* The Pediatric Infectious Disease Journal, 2004. **23**(8): p. 779-781.
115. O'Brien, L.K., et al., *Severe Pneumococcal Pneumonia in Previously Healthy Children: The Role of Preceding Influenza Infection.* Clin Infect Dis, 2000. **30**(5): p. 784-89.
116. Madhi, S.A., K.P. Klugman, and G. Vaccine Trialist, *A role for Streptococcus pneumoniae in virus-associated pneumonia.* Nat Med, 2004. **10**(8): p. 811-3.
117. Hodges, G.R. and M.C. Macleod, *EPIDEMIC PNEUMOCOCCAL PNEUMONIA V. FINAL CONSIDERATION OP THE FACTORS UNDERLYING THE EPIDEMIC.* Am. J. Epidemiol., 1946. **44**(2): p. 237-43.
118. Musher, M.D., et al., *Emergence of Antibody to Capsular Polysaccharides of Streptococcus pneumoniae During Outbreaks of Pneumonia: Association with Nasopharyngeal Colonization.* Clin Infect Dis, 1997. **24**(3): p. 441-46.
119. Dillard, P.J., W.M. Vandersea, and J. Yother, *Characterization of the Cassette Containing Genes for Type 3 Capsular Polysaccharide Biosynthesis in Streptococcus pneumoniae.* J. Exp. Med., 1995. **181**: p. 973-83.
120. García, E., et al., *A Functional Analysis of the Streptococcus pneumoniae Genes Involved in the Synthesis of Type 1 and Type 3 Capsular Polysaccharides.* Microb Drug Resist, 1997. **3**(1): p. 73-88.
121. Coffey, J.T., et al., *Recombinational exchanges at the capsular polysaccharide biosynthetic locus lead to frequent serotype changes among natural isolates of Streptococcus pneumoniae.* Mol Microbiol, 1998. **27**(1): p. 73-83.
122. Hermans, M.W.P., et al., *Molecular Epidemiology of Drug-Resistant Pneumococci: Toward an International Approach.* Microb Drug Resist, 1997. **3**(3): p. 243-51.
123. Nesin, M., M. Ramirez, and A. Tomasz, *Capsular Transformation of a Multidrug-Resistant Streptococcus pneumoniae In Vivo.* J Infect Dis, 1998. **177**(3): p. 707-13.
124. Nielsen, V.S. and J. Henrichsen, *Capsular Types of Streptococcus pneumoniae Isolated from Blood and CSF During 1982-1987.* Clin Infect Dis, 1992. **15**(5): p. 794-808.
125. Verhaegen, J., et al., *Capsular Types and Antibiotic Susceptibility of Pneumococci Isolated from Patients in Belgium with Serious Infections, 1980-1993.* Clin Infect Dis, 1995. **20**(5): p. 1339-45.
126. Peltola, H., R. Booy, and H.J. Schmitt, *What can children gain from pneumococcal conjugate vaccines?* Eur J Pediatr, 2004. **163**(9): p. 509-16.

127. Yochay-Regev, G., et al., *Association Between Carriage of Streptococcus pneumoniae and Staphylococcus aureus in Children.* The Journal of the American Medical Association, 2004. **292**(6): p. 716-20.
128. Adetifa, I.M., et al., *Pre-vaccination nasopharyngeal pneumococcal carriage in a Nigerian population: epidemiology and population biology.* PLoS One, 2012. **7**(1): p. e30548.
129. Jafri, Z.R., et al., *Global epidemiology of invasive meningococcal disease.* Population Health Metrics, 2013. **11**(17): p. 02-09.
130. Scarborough, M., et al., *Corticosteroids for Bacterial Meningitis in Adults in Sub-Saharan Africa.* The New England Journal of Medicine, 2007. **357**(24): p. 2441-50.
131. Scarborough, M. and E.G. Twaites, *The diagnosis and management of acute bacterial meningitis in resource-poor settings.* Lancet Neurology, 2008. **7**(7): p. 637-48.
132. Campagne, G., et al., *Epidemiology of bacterial meningitis in Niamey, Niger, 1981-96.* Bulletin of the World Health Organization, 1999. **77**(6): p. 499-508.
133. de Gans, J. and D. van de Beek, *DEXAMETHASONE IN ADULTS WITH BACTERIAL MENINGITIS.* The New England Journal of Medicine, 2002. **347**(20): p. 1549-56.
134. Arda, B., et al., *Pooled analysis of 2,408 cases of acute adult purulent meningitis from Turkey.* Med Princ Pract, 2008. **17**(1): p. 76-9.
135. Thigpen, C.M., et al., *Bacterial Meningitis in the United States, 1998–2007.* The New England Journal of Medicine, 2011. **364**(21): p. 2016-25.
136. van de Beek, D., et al., *Clinical Features and Prognostic Factors in Adults with Bacterial Meningitis.* The New England Journal of Medicine, 2004. **351**(18): p. 1849-59.
137. Bolan, G., et al., *Pneumococcal Vaccine Efficacy in Selected Populations in the United States.* Annals of Internal Medicine, 1986. **104**(1): p. 01-06.
138. Butler, C.J., et al., *Pnemococcal Polysaccharide Vaccine Efficacy.* JAMA, 1993. **270**(15): p. 1826-31.
139. Laban, T.J. and K. O'Neil, *CNS infections.* Neurosurgery, 2009. **27**(3): p. 125-29.
140. Sellner, J., G.M. Täuber, and L.S. Leib, *Pathogenesis and pathophysiology of bacterial CNS infections.* Handbook of Clinical Neurology, 2010. **96**(3): p. 01-16.
141. Bleck, P.T., *Bacterial and fungal infections of the nervous system.* Neurobiol Dis, 2007. **40**: p. 446-51.
142. Ghanem, K.G., *REVIEW: Neurosyphilis: A historical perspective and review.* CNS Neurosci Ther, 2010. **16**(5): p. e157-68.
143. Hollingsworth, R., et al., *Serotype Distribution of S. pneumoniae Community Acquired Pneumonia (CAP) in Adults in the Netherlands in the CAPiTA (Community-Acquired Pneumonia Immunization Trial In Adults).* IDWeek, 2014.
144. Ho, P.L., et al., *Serotypes and antimicrobial susceptibilities of invasive Streptococcus pneumoniae before and after introduction of 7-valent pneumococcal conjugate vaccine, Hong Kong, 1995-2009.* Vaccine, 2011. **29**(17): p. 3270-5.
145. Shibl, A.M., Z.A. Memish, and K.M. Al-Kattan, *Antibiotic resistance and serotype distribution of invasive pneumococcal diseases before and after*

introduction of pneumococcal conjugate vaccine in the Kingdom of Saudi Arabia (KSA). Vaccine, 2012. **30 Suppl 6**: p. G32-6.
146. Chiba, N., et al., *Rapid decrease of 7-valent conjugate vaccine coverage for invasive pneumococcal diseases in pediatric patients in Japan.* Microb Drug Resist, 2013. **19**(4): p. 308-15.
147. Parra, E.L., et al., *Changes in Streptococcus pneumoniae serotype distribution in invasive disease and nasopharyngeal carriage after the heptavalent pneumococcal conjugate vaccine introduction in Bogota, Colombia.* Vaccine, 2013. **31**(37): p. 4033-8.
148. Weinberger, M.D., R. Malley, and M. Lipsitch, *Serotype replacement in disease after pneumococcal vaccination.* Lancet, 2011. **378**: p. 1962-73.
149. Gladstone, R.A., et al., *Five winters of pneumococcal serotype replacement in UK carriage following PCV introduction.* Vaccine, 2015. **33**(17): p. 2015-21.
150. Kamtchoua, T., et al., *Safety and immunogenicity of the pneumococcal pneumolysin derivative PlyD1 in a single-antigen protein vaccine candidate in adults.* Vaccine, 2013. **31**(2): p. 327-33.
151. Amaya-Villar, R., et al., *Three-year multicenter surveillance of community-acquired listeria monocytogenes meningitis in adults.* BMC Infectious Diseases 2010. **10**(324): p. 01-08.
152. Gessner, D.B., E.J. Mueller, and S. Yaro, *African meningitis belt pneumococcal disease epidemiology indicates a need for an effective serotype 1 containing vaccine, including for older children and adults.* BMC Infect Dis, 2010. **10**(22): p. 01-10.
153. Moon, S.Y., et al., *Changing etiology of community-acquired bacterial meningitis in adults: a nationwide multicenter study in Korea.* Eur J Clin Microbiol Infect Dis, 2010. **29**(7): p. 793-800.
154. Domingo, P., et al., *The changing pattern of bacterial meningitis in adult patients at a large tertiary university hospital in Barcelona, Spain (1982-2010).* J Infect, 2013. **66**(2): p. 147-54.
155. Castelblanco, L.R., M. Lee, and R. Hasbun, *Epidemiology of bacterial meningitis in the USA from 1997 to 2010: a population-based observational study.* Lancet Infectious Diseases, 2014. **14**(9): p. 813-19.
156. Okike, O.I., et al., *Trends in bacterial, mycobacterial, and fungal meningitis in England and Wales 2004–11: an observational study.* Lancet Infectious Diseases, 2014. **14**(4): p. 301-07.
157. Kastenbauer, S. and H.W. Pfister, *Pneumococcal meningitis in adults: Spectrum of complications and prognostic factors in a series of 87 cases.* Brain, 2003. **126**(5): p. 1015-1025.
158. van de Beek, D., et al., *Cognitive Impairment in Adults with Good Recovery after Bacterial Meningitis.* The Journal of Infectious Diseases, 2002. **186**: p. 1047-52.
159. Weisfelt, M., et al., *Clinical features, complications, and outcome in adults with pneumococcal meningitis: a prospective case series.* Lancet Neurology, 2006. **5**: p. 123-29.
160. Coonrod, D.J., R. Varble, and K. Yoneda, *Mechanism of Killing of Pneumococci by Lysozyme.* The Journal of Infectious Diseases, 1991. **164**: p. 527-32.
161. Nelson, A.L., et al., *Capsule enhances pneumococcal colonization by limiting mucus-mediated clearance.* Infect Immun, 2007. **75**(1): p. 83-90.

162. Shimada, J., et al., *Lysozyme M deficiency leads to an increased susceptibility to Streptococcus pneumoniae-induced otitis media.* BMC Infect Dis, 2008. **8**: p. 134.
163. Janoff, N.E., et al., *Killing of Streptococcus pneumoniae by capsular polysaccharide–specific polymeric IgA, complement, and phagocytes.* The Journal of Clinical Investigation, 1999. **104**(8): p. 1139-47.
164. Shaper, M., et al., *PspA protects Streptococcus pneumoniae from killing by apolactoferrin, and antibody to PspA enhances killing of pneumococci by apolactoferrin [corrected]*. Infect Immun, 2004. **72**(9): p. 5031-40.
165. Bogaert, D., et al., *The role of complement in innate and adaptive immunity to pneumococcal colonization and sepsis in a murine model.* Vaccine, 2010. **28**(3): p. 681-5.
166. Kaetzel, S.C., *Polymeric Ig receptor: Defender of the fort or Trojan Horse?* Current Biology, 2001. **11**(1): p. 35-38.
167. Kurono, Y., et al., *INHIBITION OF BACTERIAL ADHERENCE BY NASOPHARYNGEAL SECRETIONS.* Annals, of Otology, Rhinology & Laryngology, 1991. **100**(6): p. 455-58.
168. Raphael, G.D., E.Z. Jeney, and J.N. Baraniuk, *Pathophysiology of rhinitis.* American Journal of Otolaryngology, 1989. **11**(6): p. 1528-35.
169. Murphy, K., *Janeway's immunobiology*. 8 ed. 2012, U.S.A: Garland Science, Taylor & Francis Group, LLC. 892.
170. Cundell, D.R., et al., *Streptococcus pneumoniae anchor to activated human cells by the receptor for platelet-activating factor.* 1995. **377**(6548): p. 435-38.
171. Li-Korotky, H.S., et al., *Interaction of pneumococcal phase variation and middle ear pressure/gas composition: an in vitro model of simulated otitis media.* Microb Pathog, 2008. **45**(3): p. 201-6.
172. Weiser, N.J., et al., *Phase Variation in Pneumococcal Opacity: Relationship between Colonial Morphology and Nasopharyngeal Colonization.* Infect Immun, 1994. **62**(6): p. 2582-89.
173. Chaguza, C., J.E. Cornick, and D.B. Everett, *Mechanisms and impact of genetic recombination in the evolution of Streptococcus pneumoniae.* Comput Struct Biotechnol J, 2015. **13**: p. 241-7.
174. Goldenberg, B.H., L.T. McCool, and J.N. Weiser, *Cross-Reactivity of Human Immunoglobulin G2 Recognizing Phosphorylcholine and Evidence for Protection against Major Bacterial Pathogens of the Human Respiratory Tract.* The Journal of Infectious Diseases, 2004. **190**: p. 1254-63.
175. Hyams, C., et al., *Streptococcus pneumoniae resistance to complement-mediated immunity is dependent on the capsular serotype.* Infect Immun, 2010. **78**(2): p. 716-25.
176. Kim, O.J., et al., *Relationship between Cell Surface Carbohydrates and Intrastrain Variation on Opsonophagocytosis of Streptococcus pneumoniae.* Infect Immun, 1999. **67**(5): p. 2327-33.
177. Burnaugh, A.M., L.J. Frantz, and S.J. King, *Growth of Streptococcus pneumoniae on human glycoconjugates is dependent upon the sequential activity of bacterial exoglycosidases.* J Bacteriol, 2008. **190**(1): p. 221-30.
178. King, S.J., K.R. Hippe, and J.N. Weiser, *Deglycosylation of human glycoconjugates by the sequential activities of exoglycosidases expressed by Streptococcus pneumoniae.* Mol Microbiol, 2006. **59**(3): p. 961-74.

179. Tong, H.H., et al., *Comparison of structural changes of cell surface carbohydrates in the eustachian tube epithelium of chinchillas infected with a Streptococcus pneumoniae neuraminidase-deficient mutant or its isogenic parent strain.* Microb Pathog, 2001. **31**(6): p. 309-17.
180. Feldman, C., et al., *The effects of pneumolysin and hydrogen peroxide, alone and in combination, on human ciliated epithelium in vitro.* Respiratory Medicine, 2002. **96**(8): p. 580-585.
181. Feldman, C., et al., *The effect of Streptococcus pneumoniae pneumolysin on human respiratory epithelium in vitro.* Microbial Pathogenesis, 1990. **9**: p. 275-84.
182. Weiser, J.N., et al., *Antibody-enhanced pneumococcal adherence requires IgA1 protease.* PNAS, 2003. **100**(7): p. 4215-20.
183. Aas, J.A., et al., *Defining the normal bacterial flora of the oral cavity.* J Clin Microbiol, 2005. **43**(11): p. 5721-32.
184. Brugger, S.D., L.J. Hathaway, and K. Muhlemann, *Detection of Streptococcus pneumoniae strain cocolonization in the nasopharynx.* J Clin Microbiol, 2009. **47**(6): p. 1750-6.
185. McCullers, J.A., *Insights into the interaction between influenza virus and pneumococcus.* Clin Microbiol Rev, 2006. **19**(3): p. 571-82.
186. Bogaert, D., et al., *Colonisation by Streptococcus pneumoniae and Staphylococcus aureus in healthy children.* Lancet, 2004. **363**: p. 1871-72.
187. Yochay-Regev, G., et al., *Nasopharyngeal Carriage of Streptococcus pneumoniae by Adults and Children in Community and Family Settings.* Clinical Infectious Diseases, 2004. **38**: p. 632-9.
188. Lux, T., et al., *Diversity of bacteriocins and activity spectrum in Streptococcus pneumoniae.* J Bacteriol, 2007. **189**(21): p. 7741-51.
189. Cundell, R.D., et al., *Relationship between Colonial Morphology and Adherence of Streptococcus pneumoniae.* Infect Immun, 1995. **63**(3): p. 757-61.
190. Radin, J.N., et al., *beta-Arrestin 1 participates in platelet-activating factor receptor-mediated endocytosis of Streptococcus pneumoniae.* Infect Immun, 2005. **73**(12): p. 7827-35.
191. Elm, C., et al., *Ectodomains 3 and 4 of human polymeric Immunoglobulin receptor (hpIgR) mediate invasion of Streptococcus pneumoniae into the epithelium.* J Biol Chem, 2004. **279**(8): p. 6296-304.
192. Zhang, J.-R., et al., *The Polymeric Immunoglobulin Receptor Translocates Pneumococci across Human Nasopharyngeal Epithelial Cells.* Cell, 2000. **102**: p. 827-37.
193. Abeyta, M., G.G. Hardy, and J. Yother, *Genetic Alteration of Capsule Type but Not PspA Type Affects Accessibility of Surface-Bound Complement and Surface Antigens of Streptococcus pneumoniae.* Infection and Immunity, 2003. **71**(1): p. 218-225.
194. Alcantara, R.B., L.C. Preheim, and M.J. Gentry-Nielsen, *Pneumolysin-induced complement depletion during experimental pneumococcal bacteremia.* Infect Immun, 2001. **69**(6): p. 3569-75.

195. Han, F., et al., *Role for Toll-like receptor 2 in the immune response to Streptococcus pneumoniae infection in mouse otitis media.* Infect Immun, 2009. **77**(7): p. 3100-8.
196. Letiembre, M., et al., *Toll-like receptor 2 deficiency delays pneumococcal phagocytosis and impairs oxidative killing by granulocytes.* Infect Immun, 2005. **73**(12): p. 8397-401.
197. Mogensen, T.H., et al., *Live Streptococcus pneumoniae, Haemophilus influenzae, and Neisseria meningitidis activate the inflammatory response through Toll-like receptors 2, 4, and 9 in species-specific patterns.* J Leukoc Biol, 2006. **80**(2): p. 267-77.
198. Yoshimura, A., et al., *Cutting Edge: Recognition of Gram- Positive Bacterial Cell Wall Components by the Innate Immune System Occurs Via Toll-Like Receptor 21.* The Journal of Immunology, 1999. **163**: p. 01-05.
199. Branger, J., et al., *Role of Toll-Like Receptor 4 in Gram-Positive and Gram-Negative Pneumonia in Mice.* Infection and Immunity, 2004. **72**(2): p. 788-794.
200. Lee, K.S., et al., *TLR2 synergizes with both TLR4 and TLR9 for induction of the MyD88-dependent splenic cytokine and chemokine response to Streptococcus pneumoniae.* Cell Immunol, 2007. **245**(2): p. 103-10.
201. Malley, R., et al., *Recognition of pneumolysin by Toll-like receptor 4 confers resistance to pneumococcal infection.* Proc Natl Acad Sci U S A, 2003. **100**(4): p. 1966-71.
202. Albiger, B., et al., *Toll-like receptor 9 acts at an early stage in host defence against pneumococcal infection.* Cell Microbiol, 2007. **9**(3): p. 633-44.
203. Zola, T.A., E.S. Lysenko, and J.N. Weiser, *Mucosal Clearance of Capsule-Expressing Bacteria Requires Both TLR and Nucleotide-Binding Oligomerization Domain 1 Signaling.* The Journal of Immunology, 2008. **181**(11): p. 7909-7916.
204. Roche, A.M., S.J. King, and J.N. Weiser, *Live attenuated Streptococcus pneumoniae strains induce serotype-independent mucosal and systemic protection in mice.* Infect Immun, 2007. **75**(5): p. 2469-75.
205. Fassbender, K., et al., *Endothelial-derived adhesion molecules in bacterial meningitis: association to cytokine release and intrathecal leukocyte-recruitment.* Journal of Neuroimmunology, 1997. **74**: p. 130-34.
206. Tang, T., et al., *Cytokine-induced meningitis is dramatically attenuated in mice deficient in endothelial selectins.* J Clin Invest, 1996. **97**(11): p. 2485-90.
207. O'Neil, K. and A. Parker, *Infection of the CNS.* Neurosurgery, 2004. **22**(3): p. 57-59.
208. Bennett, E.J., R. Dolin, and J.M. Blaser, *PRINCIPLES AND PRACTICE OF INFECTIOUS DISEASES, EIGHTH EDITION*. Vol. 1. 2015: Elsevier Saunders. 4909.
209. Scheld, M.W., J.R. Whitley, and M.C. Marra, *Infections of the Central Nervous System*. 2014, Philadelphia: Wolters Kluwer Health. 1684.
210. van der Flier, M., et al., *Reprogramming the Host Response in Bacterial Meningitis: How Best To Improve Outcome?* Clinical Microbiology Reviews, 2003. **16**(3): p. 415-429.
211. Pfister, H.-W., W. Feiden, and K.-M. Einh, *Spectrum of Complications During Bacterial Meningitis in Adults.* Archives of Neurology, 1993. **50**: p. 575-81.

212. Ziai, W.C. and J.J. Lewin, 3rd, *Advances in the management of central nervous system infections in the ICU.* Crit Care Clin, 2006. **22**(4): p. 661-94; abstract viii-ix.
213. Quagliarello, V.J., W.J. Long, and W.M. Scheld, *Morphologic alterations of the blood-brain barrier with experimental meningitis in the rat. Temporal sequence and role of encapsulation.* J Clin Invest, 1986. **77**(4): p. 1084-95.
214. Ring, A., J.N. Weiser, and E.I. Tuomanen, *Pneumococcal trafficking across the blood-brain barrier. Molecular analysis of a novel bidirectional pathway.* J Clin Invest, 1998. **102**(2): p. 347-60.
215. Rijneveld, W.A., et al., *Improved Host Defense against Pneumococcal Pneumonia in Platelet-Activating Factor Receptor–Deficient Mice.* The Journal of Infectious Diseases, 2004. **189**: p. 711-16.
216. Freyer, D., et al., *Cerebral Endothelial Cells Release TNF-α After Stimulation with Cell Walls of Streptococcus pneumoniae and Regulate Inducible Nitric Oxide Synthase and ICAM-1 Expression Via Autocrine Loops.* The Journal of Immunology, 1999. **163**: p. 4308-14.
217. Sharief, K.M., M. Ciardi, and J.E. Thompson, *Blood-Brain Barrier Damage in Patients with Bacterial Meningitis: Association with Tumor Necrosis Factor-α but not Interleukin-1β.* The Journal of Infectious Diseases, 1992. **166**: p. 350-58.
218. Zysk, G., et al., *Pneumolysin is the main inducer of cytotoxicity to brain microvascular endothelial cells caused by Streptococcus pneumoniae.* Infect Immun, 2001. **69**(2): p. 845-52.
219. Tomasz, A., P. Moreillon, and G. Pozzi, *Insertional Inactivation of the Major Autolysin Gene of Streptococcus pneumoniae.* J Bacteriol, 1988. **170**(12): p. 5931-34.
220. Tuomanen, E., et al., *The Induction of Meningeal Inflammation by Components of the Pneumococcal Cell Wall.* The Journal of Infectious Diseases, 1985. **11**(5): p. 859-68.
221. Wellmer, A., et al., *Decreased Virulence of a Pneumolysin-Deficient Strain of Streptococcus pneumoniae in Murine Meningitis.* Infection and Immunity, 2002. **70**(11): p. 6504-6508.
222. Trostdorf, F., et al., *Reduction of meningeal macrophages does not decrease migration of granulocytes into the CSF and brain parenchyma in experimental pneumococcal meningitis.* Journal of Neuroimmunology, 1999. **99**: p. 205-10.
223. Volterra, A. and J. Meldolesi, *Astrocytes, from brain glue to communication elements: the revolution continues.* Nat Rev Neurosci, 2005. **6**(8): p. 626-40.
224. Liu, W., Y. Tang, and J. Feng, *Cross talk between activation of microglia and astrocytes in pathological conditions in the central nervous system.* Life Sci, 2011. **89**(5-6): p. 141-6.
225. Chinnery, R.H., J.M. Ruitenberg, and G.P. McMenamin, *Novel Characterization of Monocyte-Derived Cell Populations in the Meninges and Choroid Plexus and Their Rates of Replenishment in Bone Marrow Chimeric Mice.* Journal of neuropathology and experimental neurology, 2010. **69**(9): p. 896-09.
226. de Graaf, M.T., et al., *Central memory CD4+ T cells dominate the normal cerebrospinal fluid.* Cytometry B Clin Cytom, 2011. **80**(1): p. 43-50.
227. Gehrmann, J., Y. Matsumoto, and W.G. Kreutzberg, *Microglia: intrinsic immuneffector cell of the brain.* Brain Research Reviews, 1995. **20**: p. 269-87.

228. Echchannaoui, H., et al., *Toll-Like Receptor 2–Deficient Mice Are Highly Susceptible to Streptococcus pneumoniae Meningitis because of Reduced Bacterial Clearing and Enhanced Inflammation.* The Journal of Infectious Diseases, 2002. **186**: p. 798-806.
229. Klein, M., et al., *Morphological Correlates of Acute and Permanent Hearing Loss During Experimental Pneumococcal Meningitis.* Brain Pathology, 2003. **13**(2): p. 123-32.
230. Koedel, U., et al., *Toll-Like Receptor 2 Participates in Mediation of Immune Response in Experimental Pneumococcal Meningitis.* The Journal of Immunology, 2003. **170**(1): p. 438-444.
231. Liu, X., et al., *NOD2 mediates inflammatory responses of primary murine glia to Streptococcus pneumoniae.* Glia, 2010. **58**(7): p. 839-47.
232. Klein, M., et al., *Innate immunity to pneumococcal infection of the central nervous system depends on toll-like receptor (TLR) 2 and TLR4.* J Infect Dis, 2008. **198**(7): p. 1028-36.
233. Opitz, B., et al., *Nucleotide-binding oligomerization domain proteins are innate immune receptors for internalized Streptococcus pneumoniae.* J Biol Chem, 2004. **279**(35): p. 36426-32.
234. Picard, C., et al., *Clinical features and outcome of patients with IRAK-4 and MyD88 deficiency.* Medicine (Baltimore), 2010. **89**(6): p. 403-25.
235. Rock, L.F., et al., *A family of human receptors structurally related to Drosophila Toll.* Proc Natl Acad Sci U S A, 1998. **95**: p. 588-93.
236. Zhang, X.F., et al., *Bacterial Lipopolysaccharide Activates Nuclear Factor- B through Interleukin-1 Signaling Mediators in Cultured Human Dermal Endothelial Cells and Mononuclear Phagocytes.* J Biol Chem, 1999. **274**(12): p. 7611-14.
237. Ku, C.L., et al., *Selective predisposition to bacterial infections in IRAK-4-deficient children: IRAK-4-dependent TLRs are otherwise redundant in protective immunity.* J Exp Med, 2007. **204**(10): p. 2407-22.
238. McDonald, D.R., et al., *Interleukin receptor-associated kinase-4 deficiency impairs Toll-like receptor-dependent innate antiviral immune responses.* J Allergy Clin Immunol, 2006. **118**(6): p. 1357-62.
239. von Bernuth, H., et al., *Pyogenic Bacterial Infections in Humans with MyD88 Deficiency.* Science, 2008. **321**: p. 691-96.
240. Ku, C.L., et al., *IRAK4 and NEMO mutations in otherwise healthy children with recurrent invasive pneumococcal disease.* J Med Genet, 2007. **44**(1): p. 16-23.
241. Zysk, G., et al., *Elimination of blood-derived macrophages inhibits the release of interleukin-1 and the entry of leukocytes into the cerebrospinal fluid in experimental pneumococcal meningitis.* Journal of Neuroimmunology, 1997. **73**: p. 77-80.
242. Ribes, S., et al., *Toll-like receptor stimulation enhances phagocytosis and intracellular killing of nonencapsulated and encapsulated Streptococcus pneumoniae by murine microglia.* Infect Immun, 2010. **78**(2): p. 865-71.
243. Polfliet, M.M.J., et al., *Meningeal and Perivascular Macrophages of the Central Nervous System Play a Protective Role During Bacterial Meningitis.* The Journal of Immunology, 2001. **167**(8): p. 4644-4650.

244. Hanisch, U.-K., et al., *The protein tyrosine kinase inhibitor AG126 prevents the massive microglial cytokine induction by pneumococcal cell walls.* Eur J Immunol, 2001. **31**: p. 2104-15.
245. Freyer, D., et al., *Pneumococcal Cell Wall Components Induce Nitric Oxide Synthase and TNF-a in Astroglial-EnrichedCultures.* Glia, 1996. **6**(1): p. 01-06.
246. Taüber, G.M. and B. Moser, *Cytokines and Chemokines in Meningeal Inflammation: Biology and Clinical Implications.* Clinical Infectious Diseases, 1999. **28**(1): p. 01-11.
247. van Furth, A.M., J.J. Roord, and R. van Furth, *Roles of Proinflammatory and Anti-Inflammatory Cytokines in Pathophysiology of Bacterial Meningitis and Effect of Adjunctive Therapy.* Infect Immun, 1996. **64**(12): p. 4883-90.
248. Schultz, M.J., E.K. Wolthuis, and P.E. Spronk, *Need for Critical Appraisal of Implementation of Use of Lower Tidal Volumes.* Critical Care Medicine, 2005. **33**(11): p. 2718.
249. Leppert, D., et al., *Matrix Metalloproteinase (MMP)-8 and MMP-9 in Cerebrospinal Fluid during Bacterial Meningitis: Association with Blood-Brain Barrier Damage and Neurological Sequelae.* Clinical Infectious Diseases, 2000. **31**(1): p. 80-84.
250. Glimåker, M., P. Kragsbjerg, and M. Forsgren, *Tumor Necrosis Factor-a (TNFa) in Cerebrospinal Fluid from Patients with Meningitis of Different Etiologies: High Levels of TNFa Indicate Bacterial Meningitis.* J Infect Dis, 1993. **167**(4): p. 882-89.
251. Ubenauf, K.M., et al., *Lipopolysaccharide binding protein is a potential marker for invasive bacterial infections in children.* Pediatr Infect Dis J, 2007. **26**(2): p. 159-62.
252. Barichello, T., et al., *Tumor necrosis factor alpha (TNF-alpha) levels in the brain and cerebrospinal fluid after meningitis induced by Streptococcus pneumoniae.* Neurosci Lett, 2009. **467**(3): p. 217-9.
253. Østergaard, C., et al., *Differences in Survival, Brain Damage, and Cerebrospinal Fluid Cytokine Kinetics Due to Meningitis Caused by 3 Different Streptococcus pneumoniae Serotypes: Evaluation in Humans and in 2 Experimental Models.* J Infect Dis, 2004. **190**(7): p. 1212-20.
254. Gerber, J., et al., *Increased mortality and spatial memory deficits in TNF-alpha-deficient mice in ceftriaxone-treated experimental pneumococcal meningitis.* Neurobiol Dis, 2004. **16**(1): p. 133-8.
255. Tsao, N., et al., *Development of hematogenous pneumococcal meningitis in adult mice: the role of TNF-a.* FEMS Immunology and Medical Microbiology, 2002. **32**(2): p. 133-40.
256. Schmidt, H., et al., *Intravenous Granulocyte Colony-Stimulating Factor Increases the Release of Tumour Necrosis Factor and Interleukin-1 into the Cerebrospinal Fluid, But Does Not Inhibit the Growth of Streptococcus pneumoniae in Experimental Meningitis.* Scand. J. Immunol, 1999. **49**(5): p. 481-486.
257. Ray, A.C., et al., *Viral Inhibition of Inflammation: Cowpox Virus Encodes an Inhibitor of the Interleukin-1 p Converting Enzyme.* Cell, 1992. **69**(4): p. 597-604.

258. Koedel, U., et al., *Role of Caspase-1 in experimental pneumococcal meningitis: Evidence from pharmacologic Caspase inhibition and Caspase-1-deficient mice.* Ann Neurol, 2002. **51**(3): p. 319-29.
259. Saukkonen, K., et al., *THE ROLE OF CYTOKINES IN THE GENERATION OF INFLAMMATION AND TISSUE DAMAGE IN EXPERIMENTAL GRAM-POSITIVE MENINGITIS.* The Journal of Experimental Medicine, 1990. **171**: p. 439-48.
260. Zwijnenburg, P.J.G., et al., *IL-1 Receptor Type 1 Gene-Deficient Mice Demonstrate an Impaired Host Defense Against Pneumococcal Meningitis.* The Journal of Immunology, 2003. **170**(9): p. 4724-4730.
261. Gadient, A.R. and H.P. Patterson, *Leukemia Inhibitory Factor, Interleukin 6, and Other Cytokines Using the GP130 Transducing Receptor: Roles in Inflammation and Injury.* STEM CELLS, 1999. **17**: p. 127-37.
262. Paul, R., et al., *Lack of IL-6 augments inflammatory response but decreases vascular permeability in bacterial meningitis.* Brain, 2003. **126**(Pt 8): p. 1873-82.
263. van der Poll, T., et al., *Interleukin-6 Gene Deficient Mice Show Impaired Defense against Pneumococcal Pneumonia.* The Journal of Infectious Diseases, 1997. **176**: p. 439-44.
264. Glimåker, M., P. Olcén, and B. Andersson, *Interferon-y in Cerebrospinal Fluid from Patients with Viral and Bacterial Meningitis.* Scand. J. Infect Dis, 1994. **26**(2): p. 141-47.
265. Kornelisse, F.R., et al., *Intrathecal Production of Interleukin-12 and Gamma Interferon in Patients with Bacterial Meningitis.* Infect Immun, 1997. **65**(3): p. 887-81.
266. Diab, A., et al., *Haemophilus influenzae and Streptococcus pneumoniae induce different intracerebral mRNA cytokine patterns during the course of experimental bacterial meningitis.* Clin Exp Immunol, 1997. **109**(2): p. 233-41.
267. Ostergaard, C. and T. Benfield, *Macrophage migration inhibitory factor in cerebrospinal fluid from patients with central nervous system infection.* Crit Care, 2009. **13**(3): p. R101.
268. de Waal Malefyt, R., et al., *Interleukin 10(IL-10)Inhibits Cytokine Synthesis by Human Monocytes: An Autoregulatory Role of IL-10 Produced by Monocytes.* The Journal of Experimental Medicine, 1991. **174**: p. 1209-20.
269. Thomssen, H., M. Kahan, and M. Londei, *Differential effects of interleukin-10 on the expression of HLA class I1 and CD1 molecules induced by granulocyte/macrophage colony- stimulating factor/interleukin-4.* European Journal of Immunology, 1995. **25**(9): p. 2465-70.
270. Zwijnenburg, P.J.G., et al., *Interleukin-10 Negatively Regulates Local Cytokine and Chemokine Production but Does Not Influence Antibacterial Host Defense during Murine Pneumococcal Meningitis.* Infection and Immunity, 2003. **71**(4): p. 2276-2279.
271. Orihuela, C.J., et al., *Cell wall-mediated neuronal damage in early sepsis.* Infect Immun, 2006. **74**(7): p. 3783-9.
272. Koedel, U., et al., *Systemically (but Not Intrathecally) Administered IL-10 Attenuates Pathophysiologic Alterations in Experimental*

Pneumococcal Meningitis. J Immunol, 1996. **157**(11): p. 5185-91.
273. Li, M.O. and R.A. Flavell, *Contextual regulation of inflammation: a duet by transforming growth factor-beta and interleukin-10.* Immunity, 2008. **28**(4): p. 468-76.
274. Ledeboer, A., et al., *Interleukin-10, Interleukin-4, and Transforming Growth Factor Differentially Regulate Lipopolysaccharide-Induced Production of Pro-Inflammatory Cytokines and Nitric Oxide in Co-Cultures of Rat Astroglial and Microglial Cells.* Glia, 2000. **30**(2): p. 134-42.
275. Suzumura, A., et al., *Transforming Growth Factor-b Suppresses Activation and Proliferation of Microglia in Vitro.* J Immunol, 1993. **151**(4): p. 2150-58.
276. Malipiero, U., et al., *Bacterial meningitis: the role of transforming growth factor-Beta in innate immunity and secondary brain damage.* Neurodegener Dis, 2007. **4**(1): p. 43-50.
277. Pfister, H.-W., et al., *Transforming Growth Factor b2 Inhibits Cerebrovascular Changes and Brain Edema Formation in the Tumor Necrosis Factor a-Independent Early Phase of Experimental Pneumococcal Meningitis.* J. Exp. Med., 1992. **176**(1): p. 265-68.
278. Spanaus, K.-S., et al., *C-X-C and C-C Chemokines Are Expressed in the Cerebrospinal Fluid in Bacterial Meningitis and Mediate Chemotactic Activity on Peripheral Blood-Derived Polymorphonuclear and Mononuclear Cells In Vitro.* The Journal of Immunology, 1997. **158**: p. 1956-64.
279. Østergaard, C., et al., *Treatment with a monoclonal antibody to IL-8 attenuates the pleocytosis in experimental pneumococcal meningitis in rabbits when given intravenously, but not intracisternally.* Clinical and Experimental Immunology, 2000. **122**(2): p. 207-11.
280. Rosenberg, G.A., *Matrix metalloproteinases in neuroinflammation.* Glia, 2002. **39**(3): p. 279-91.
281. Yong, W.V., et al., *Metalloproteinases in Biology and Pathology of The Nervous System.* Nat Rev Neurosci, 2001. **2**: p. 502-13.
282. McCawley, J.L. and M.L. Matrisian, *Matrix metalloproteinases: they're not just for matrix anymore!* Current Opinion in Cell Biology, 2001. **13**(5): p. 534-540.
283. Van Lint, P. and C. Libert, *Chemokine and cytokine processing by matrix metalloproteinases and its effect on leukocyte migration and inflammation.* J Leukoc Biol, 2007. **82**(6): p. 1375-81.
284. Aycicek, A., et al., *Oxidant and antioxidant parameters in the treatment of meningitis.* Pediatr Neurol, 2007. **37**(2): p. 117-20.
285. Kastenbauer, S., et al., *Oxidative stress in bacterial meningitis in humans.* Neurology, 2002. **58**(2): p. 186-91.
286. de Menezes, C.C., et al., *Oxidative stress in cerebrospinal fluid of patients with aseptic and bacterial meningitis.* Neurochem Res, 2009. **34**(7): p. 1255-60.
287. Leib, S.L., et al., *Reactive oxygen intermediates contribute to necrotic and apoptotic neuronal injury in an infant rat model of bacterial meningitis due to group B streptococci.* J Clin Invest, 1996. **98**(11): p. 2632-9.
288. Joó, F., *The Cerebral Microvessels in Culture, an Update.* Journal of Neurochemistry, 1992. **58**(1): p. 01-17.

289. Li, G., et al., *Permeability of endothelial and astrocyte cocultures: in vitro blood-brain barrier models for drug delivery studies.* Ann Biomed Eng, 2010. **38**(8): p. 2499-511.
290. Tontsch, U. and H.-C. Bauer, *Glial cells and neurons induce blood-brain barrier related enzymes in cultured cerebral endothelial cells.* Brain Res, 1991. **539**: p. 247-53.
291. Nakagawa, S., et al., *Pericytes from brain microvessels strengthen the barrier integrity in primary cultures of rat brain endothelial cells.* Cell Mol Neurobiol, 2007. **27**(6): p. 687-94.
292. Thanabalasundaram, G., et al., *Regulation of the blood-brain barrier integrity by pericytes via matrix metalloproteinases mediated activation of vascular endothelial growth factor in vitro.* Brain Res, 2010. **1347**: p. 1-10.
293. Schiera, G., et al., *Synergistic effects of neurons and astrocytes on the differentiation of brain capillary endothelial cells in culture.* Journal of Cellular and Molecular Medicine, 2003. **7**(2): p. 165-70.
294. de Boer, A.G. and W. Sutanto, *Drug Transport Across the Blood-brain Barrier: In vitro and In vivo Techniques*. 1997: Hardwood Academic Publishers, Amsterdam. 220.
295. Joó, F. and I. Karnushina, *A procedure for the isolation of capillaries from rat brain.* Cytobios, 1973. **8**(29): p. 41-48.
296. Mršulja, B.B., et al., *Isolation of brain capillaries: a simplified technique.* Brain Research, 1976. **110**: p. 361-65.
297. Ohtsuki, S., et al., *Establishing a method to isolate rat brain capillary endothelial cells by magnetic cell sorting and dominant mRNA expression of multidrug resistance-associated protein 1 and 4 in highly purified rat brain capillary endothelial cells.* Pharm Res, 2007. **24**(4): p. 688-94.
298. Boado, J.R. and M.W. Pardridge, *A One-Step Procedure for Isolation of Poly(A)+ mRNA from Isolated Brain Capillaries and Endothelial Cells in Culture.* Journal of Neurochemistry, 1991. **57**(6): p. 2136-39.
299. Yousif, S., et al., *Expression of drug transporters at the blood-brain barrier using an optimized isolated rat brain microvessel strategy.* Brain Res, 2007. **1134**(1): p. 1-11.
300. Weber, J.S., et al., *Assessment of an In Vitro Blood-Brain Several [Met5] Enkephalin Opioid Analog.* The Journal of Pharmacology and Exprerimental Therapeutics, 1993. **266**(3): p. 1649-55.
301. Abbruscato, J.T. and P.T. Davis, *Combination of Hypoxia/Aglycemia Compromises In Vitro Blood-Brain Barrier Integrity.* The Journal of Pharmacology and Exprerimental Therapeutics, 1999. **289**(2): p. 668-75.
302. Abbruscato, T.J., et al., *Regulation of blood-brain barrier Na,K,2Cl-cotransporter through phosphorylation during in vitro stroke conditions and nicotine exposure.* J Pharmacol Exp Ther, 2004. **310**(2): p. 459-68.
303. Vemula, S., et al., *A functional role for sodium-dependent glucose transport across the blood-brain barrier during oxygen glucose deprivation.* J Pharmacol Exp Ther, 2009. **328**(2): p. 487-95.
304. Yang, T., et al., *Protein kinase C family members as a target for regulation of blood-brain barrier Na,K,2Cl-cotransporter during in vitro stroke conditions and nicotine exposure.* Pharm Res, 2006. **23**(2): p. 291-302.

305. Brillault, J., et al., *Hypoxia effects on cell volume and ion uptake of cerebral microvascular endothelial cells.* Am J Physiol Cell Physiol, 2008. **294**(1): p. C88-96.
306. Janzer, R. and C.M. Raff, *Astrocytes induce blood-brain barrier properties in endothelial cells.* Letters to Nature, 1987. **325**: p. 253-57.
307. Gaillard, J.P., et al., *Establishment and functional characterization of an in vitro model of the blood–brain barrier, comprising a co-culture of brain capillary endothelial cells and astrocytes.* European Journal of Pharmaceutical Sciences, 2001. **12**: p. 215-22.
308. Isobe, I., et al., *ASTROCYTIC CONTRIBUTIONS TO BLOOD-BRAIN BARRIER (BBB) FORMA TION BY ENDOTHELIAL CELLS" A POSSIBLE USE OF AORTIC ENDOTHELIAL CELL FOR IN VITRO BBB MODEL.* Neurochemistry International, 1996. **28**(5/6): p. 523-33.
309. Mukhtar, M. and J.R. Pomerantz, *Developement of an In Vitro Blood-Brain Barrier Model to Study Molecular Neuropathogenesis and Neurovirologic Disorders Induced by Human Immunodeficiency Virus Type 1 Infection.* Journal of Human Virology, 2000. **3**: p. 324-34.
310. Brown, R.C., A.P. Morris, and R.G. O'Neil, *Tight junction protein expression and barrier properties of immortalized mouse brain microvessel endothelial cells.* Brain Res, 2007. **1130**(1): p. 17-30.
311. Franke, H., H.-J. Galla, and T.-C. Beuckmann, *An improved low-permeability in vitro-model of the blood–brain barrier: transport studies on retinoids, sucrose, haloperidol, caffeine and mannitol.* Brain Res, 1999. **818**: p. 65-71.
312. Colgan, O.C., et al., *Influence of basolateral condition on the regulation of brain microvascular endothelial tight junction properties and barrier function.* Brain Res, 2008. **1193**: p. 84-92.
313. Hoheisel, D., et al., *Hydrocortisone Reinforces the Blood–Brain Barrier Properties in a Serum Free Cell Culture System.* Biochem Biophys Res Commun, 1998. **244**: p. 312-16.
314. El Hafny, B., J.-M. Bourre, and F. Roux, *Synergistic Stimulation of Gamma-Glutamyl Transpeptidase and Alkaline Phosphatase Activities by Retinoic Acid and Astroglial Factors in Immortalized Rat Brain Microvessel Endothelial Cells.* Journal of Cellular Physiology, 1996. **167**: p. 451-60.
315. El Hafny, B., et al., *Modulation of P-glycoprotein activity by glial factors and retinoic acid in an immortalized rat brain microvessel endothelial cell line.* Neuroscience Letters, 1997. **236**: p. 107-11.
316. Roux, F., et al., *Regulation of Gamma-Clutamyl Transpeptidase and Alkaline Phosphatase Activities in Immortalized Rat Brain Microvessel Endothelial Cells.* Journal of Cellular Physiology, 1994. **159**: p. 101-113.
317. Obinata, M., *Conditionally immortalized cell lines with differentiated functions established from temperature-sensitive T-antigen transgenic mice.* Genes to Cells, 1997. **2**(4): p. 235-44.
318. Muruganandam, A., et al., *Development of immortalized human cerebromicrovascular endothelial cell line as an in vitro model of the human blood-brain barrier.* The FASEB Journal, 1997. **11**(13): p. 1187-97.

319. Duvar, S., et al., *Glycosphingolipid Composition of a New Immortalized Human Cerebromicrovascular Endothelial Cell Line.* Journal of Neurochemistry, 2000. **75**(5): p. 1970-76.
320. Kannan, R., et al., *GSH transport in human cerebrovascular endothelial cells and human astrocytes: evidence for luminal localization of Na+ -dependent GSH transport in HCEC.* Brain Res, 2000. **852**(2): p. 374-82.
321. Xiao, L., et al., *Plasmodium falciparum: Involvement of Additional Receptors in the Cytoadherence of Infected Erythrocytes to Microvascular Endothelial Cells.* Experimental Parasitology, 1996. **84**(1): p. 42-55.
322. Prudhomme, G.J., et al., *Studies of Plasmodium falciparum Cytoadherence Using Immortalized Human Brain Capillary Endothelial Cells.* International Journal of Parasitology, 1996. **26**(6): p. 647-655.
323. Sano, Y., et al., *Establishment of a new conditionally immortalized human brain microvascular endothelial cell line retaining an in vivo blood-brain barrier function.* J Cell Physiol, 2010. **225**(2): p. 519-28.
324. Patabendige, A., et al., *A detailed method for preparation of a functional and flexible blood-brain barrier model using porcine brain endothelial cells.* Brain Res, 2013. **1521**: p. 16-30.
325. Urich, E., et al., *Multicellular self-assembled spheroidal model of the blood brain barrier.* Sci Rep, 2013. **3**: p. 1500.
326. Ogunshola, O., *Development of a Novel Multicellular 3-Dimensional Blood Brain Barrier In Vitro Model.* Projects in Progress, 2007. **24**: p. 95-96.
327. Cucullo, L., et al., *Immortalized human brain endothelial cells and flow-based vascular modeling: a marriage of convenience for rational neurovascular studies.* J Cereb Blood Flow Metab, 2008. **28**(2): p. 312-28.
328. Ruck, T., S. Bittner, and G.S. Meuth, *Blood-brain barrier modeling: challenges and perspectives.* Neural Regeneration Research, 2015. **10**(6): p. 889-91.
329. Huntley, M.A., et al., *Dissecting gene expression at the blood-brain barrier.* Front Neurosci, 2014. **8**: p. 355.
330. Seo, M.-S., et al., *Isolation and characterization of canine umbilical cord blood-derived mesenchymal stem cells.* Journal of Veterinary Science, 2009. **10**(3): p. 181-87.
331. Corning®, *Transwell® Permeable Supports Selection and Use Guide*. 2015.
332. INSTRUMENTS, W.P., *EVOM & EVOMX Epithelial Voltohmmeters*. 2015, WORLD PRECISION INSTRUMENTS.
333. Mosmann, T., *Rapid Colorimetric Assay for Cellular Growth and Survival: Application to Proliferation and Cytotoxicity Assays.* Journal of lmmunological Methods, 1983. **65**: p. 55-63.
334. Smith, K.P., et al., *Measurement of Protein Using Bicinchoninic Acid.* Analytical Biochemistry, 1985. **150**(1): p. 76-85.
335. Miles, A.A. and S.S. Misra, *THE ESTIMATION OF THE BACTERICIDAL POWER OF THE BLOOD.* Journal of Hygiene, 1938. **38**(6): p. 732-49.
336. Berry, M.A., et al., *Reduced Virulence of a Defined Pneumolysin-Negative Mutant of Streptococcus pneumoniae.* Infect Immun, 1989. **57**(7): p. 2037-42.

337. Paton, J.C., et al., *Purification and Immunogenicity of Genetically Obtained Pneumolysin Toxoids and Their Conjugation to Streptococcus pneumoniae Type 19F Polysaccharide.* Infect Immun, 1991. **59**(7): p. 2297-2304.
338. Chu, G., et al., *SAM "Significance Analysis of Microarrays" Users guide and technical document*. 2015, Standford University.
339. Breuer, K., et al., *InnateDB: systems biology of innate immunity and beyond--recent updates and continuing curation.* Nucleic Acids Res, 2013. **41**(Database issue): p. D1228-33.
340. Stein, L., Gillespie, M., et al., *User Guide for Reactome*. 2015: p. 01-29.
341. Laboratories, K., *Kyoto Encyclopedia of Genes and Genomes*. 2015.
342. Schneider, A.C., S.W. Rasband, and W.K. Eliceiri, *NIH Image to ImageJ: 25 years image analysis.* Nature Methods, 2012. **9**(7): p. 671-75.
343. Nachar, N., *The Mann-Whitney U: A Test for Assessing Whether Two Independent Samples Come from the Same Distribution.* Tutorials in Quantitative Methods for Psychology, 2008. **4**(1): p. 13-20.
344. Lanie, J.A., et al., *Genome sequence of Avery's virulent serotype 2 strain D39 of Streptococcus pneumoniae and comparison with that of unencapsulated laboratory strain R6.* J Bacteriol, 2007. **189**(1): p. 38-51.
345. Batchelor, K.F., *An Introduction to Fluid Dynamics*. 18 ed. 2000, The Edinburgh Building, Cambridge CB2 2RU, UK: Cambridge University Press.
346. Hupp, S., et al., *Direct transmembrane interaction between actin and the pore-competent, cholesterol-dependent cytolysin pneumolysin.* J Mol Biol, 2013. **425**(3): p. 636-46.
347. Volkmann, N., et al., *Structure of Arp2/3 Complex in Its Activated State and in Actin Filament Branch Junctions.* Science, 2001. **293**: p. 2456-60.
348. Medicine, M.-N.I.o.G. and J.H.U.S.o. Medicine, *Online Mendelian Inheritance in Man*. 2015.
349. Shan, D., et al., *The G protein G alpha(13) is required for growth factor-induced cell migration.* Dev Cell, 2006. **10**(6): p. 707-18.
350. Gilman, G.A., *G Proteins: Transducers of Receptor-Generated Signals.* Annual Review of Biochemistry, 1987. **56**: p. 615-49.
351. Radhika, V., et al., *Galpha13 stimulates cell migration through cortactin-interacting protein Hax-1.* J Biol Chem, 2004. **279**(47): p. 49406-13.
352. Maus, U.A., et al., *Pneumolysin-Induced Lung Injury Is Independent of Leukocyte Trafficking into the Alveolar Space.* The Journal of Immunology, 2004. **173**(2): p. 1307-1312.
353. Ha, U., et al., *A Novel Role for I B Kinase (IKK) and IKK in ERK-Dependent Up-Regulation of MUC5AC Mucin Transcription by Streptococcus pneumoniae.* The Journal of Immunology, 2007. **178**(3): p. 1736-1747.
354. Stefanovsky, Y.V., et al., *An Immediate Response of Ribosomal Transcription to Growth Factor Stimulation in Mammals Is Mediated by ERK Phosphorylation of UBF.* Molecular Cell, 2001. **8**: p. 1063-73.
355. Feil, C. and G.H. Augustin, *Endothelial Cells Differentially Express Functional CXC-Chemokine Receptor-4 (CXCR-4/Fusin) under the Control of Autocrine Activity and Exogenous Cytokines.* Biochemical and Biophysical Research Communications, 1998. **247**: p. 38-45.

356. Gupta, K.S., et al., *Chemokine Receptors in Human Endothelial Cells.* The Journal of Biological Chemistry, 1998. **273**(7): p. 4282-87.
357. Loetscher, M., et al., *Cloning of a Human Seven-transmembrane Domain Receptor, LESTR, That Is Highly Expressed in Leukocytes*.* The Journal of Biological Chemistry, 1994. **269**(1): p. 232-37.
358. Molino, M., et al., *CXCR4 on human endothelial cells can serve as both a mediator of biological responses and as a receptor for HIV-2.* Biochimica et Biophysica Acta, 2000. **1500**(2): p. 227-40.
359. Arrate, M.P., et al., *Cloning of human junctional adhesion molecule 3 (JAM3) and its identification as the JAM2 counter-receptor.* J Biol Chem, 2001. **276**(49): p. 45826-32.
360. Bradfield, P.F., et al., *JAM-C regulates unidirectional monocyte transendothelial migration in inflammation.* Blood, 2007. **110**(7): p. 2545-55.
361. Santagata, S., et al., *G-Protein Signaling Through Tubby Proteins.* Science, 2001. **292**: p. 2041-50.
362. Rao, K.A., A.M. Kowalska, and J. Disa, *Impraired Cytoplasmic Ionized Calcium Mobilization in Inherited Platelet Secretion Defects.* Blood, 1989. **74**(2): p. 664-72.
363. Yang, X., et al., *Human Platelet Signaling Defect Characterized by Impaired Production of Inositol-1,4,5-Triphosphateand Phosphatic Acid and Diminished Pleckstrin Phosphorylation: Evidence for Defective Phospholipase C Activation.* Blood, 1996. **88**(5): p. 1676-83.
364. Lee, B.S., et al., *Decreased Expression of Phospholipase C-p2 Isozyme in Human Platelets With Impaired Function.* Blood, 1996. **88**(5): p. 1684-91.
365. Mao, F.G., et al., *Lineage-specific defect in gene expression in human platelet phospholipase C-2 deficiency.* Blood, 2002. **99**(3): p. 905-11.
366. Mamber, S.W., et al., *Effects of streptolysin o on extracellular matrix gene expression in normal human epidermal keratinocytes.* Dose Response, 2011. **9**(4): p. 554-78.
367. Chang, S., et al., *Histone deacetylase 7 maintains vascular integrity by repressing matrix metalloproteinase 10.* Cell, 2006. **126**(2): p. 321-34.
368. Madlener, M. and S. Werner, *cD N A cloning and expression of the gene encoding murine stromelysin-2 (MMP-10).* Gene, 1997. **202**: p. 75-81.
369. Brooks, C.P., et al., *Disruption of Angiogenesis by PEX, a Noncatalytic Metalloproteinase Fragment with Integrin Binding Activity.* Cell, 1998. **92**: p. 391-00.
370. McQuibban, A.G., et al., *Inflammation Dampened by Celatinase A Cleavage of Monocyte Chemoattractant Protein-3.* Science, 2000. **289**: p. 1202-06.
371. Täuber, G.M., et al., *Matrix Metalloproteinases Contribute to Brain Damage in Experimental Pneumococcal Meningitis.* Infection and Immunity, 2000: p. 615-20.
372. Saus, J., et al., *The Complete Primary Structureof Human Matrix Metalloproteinase-3.* The Journal of Biological Chemistry, 1988. **263**(14): p. 6742-45.

373. Quinones, S., et al., *Transcriptional Regulation of Human Stromelysin**. The Journal of Biological Chemistry, 1989. **264**(14): p. 8339-44.
374. Kenney, M.C., et al., *Increased levels of catalase and cathepsin V/L2 but decreased TIMP-1 in keratoconus corneas: evidence that oxidative stress plays a role in this disorder.* Invest Ophthalmol Vis Sci, 2005. **46**(3): p. 823-32.
375. Kostrzynska, M.W., T., *Binding of Laminin, Type IV Collagen, and Vitronectin by Streptococcus pneumoniae.* Zentralblatt für Bakteriologie, 1992. **277**(1): p. 80-83.
376. Debus, O.M., et al., *The factor V G1691A mutation is a risk for porencephaly: A case-control study.* Ann Neurol, 2004. **56**(2): p. 287-90.
377. Kühn, K., et al., *Human basement membrane collagen (type IV) The amino acid sequence of the a2(IV) chain and its comparison with the al(1V) chain reveals deletions in the al(1V) chain.* European Journal of Biochemistry, 1988. **172**: p. 35-42.
378. Favor, J., et al., *Type IV procollagen missense mutations associated with defects of the eye, vascular stability, the brain, kidney function and embryonic or postnatal viability in the mouse, Mus musculus: an extension of the Col4a1 allelic series and the identification of the first two Col4a2 mutant alleles.* Genetics, 2007. **175**(2): p. 725-36.
379. Yoneda, Y., et al., *De novo and inherited mutations in COL4A2, encoding the type IV collagen alpha2 chain cause porencephaly.* Am J Hum Genet, 2012. **90**(1): p. 86-90.
380. Lapiere, J.C., et al., *Epitope mapping of type VII collagen. Identification of discrete peptide sequences recognized by sera from patients with acquired epidermolysis bullosa.* J Clin Invest, 1993. **92**(4): p. 1831-9.
381. Burgeson, E.R., et al., *The Structure of Type VII Collagen.* Annals New York Academy of Sciences, 1990. **580**: p. 32-43.
382. Scully, M., et al., *Guidelines on the diagnosis and management of thrombotic thrombocytopenic purpura and other thrombotic microangiopathies.* Br J Haematol, 2012. **158**(3): p. 323-35.
383. Vázquez, F., et al., *METH-1, a Human Ortholog of ADAMTS-1, and METH-2 Are Members of a New Family of Proteins with Angio-inhibitory Activity**. The Journal of Biological Chemistry, 1999. **274**(33): p. 23349-57.
384. Johnson, K.R., et al., *Role of human sphingosine-1-phosphate phosphatase 1 in the regulation of intra- and extracellular sphingosine-1-phosphate levels and cell viability.* J Biol Chem, 2003. **278**(36): p. 34541-7.
385. Le Stunff, H., et al., *Role of sphingosine-1-phosphate phosphatase 1 in epidermal growth factor-induced chemotaxis.* J Biol Chem, 2004. **279**(33): p. 34290-7.
386. Isozaki, T., et al., *Evidence that CXCL16 is a potent mediator of angiogenesis and is involved in endothelial progenitor cell chemotaxis : studies in mice with K/BxN serum-induced arthritis.* Arthritis Rheum, 2013. **65**(7): p. 1736-46.
387. Kim, C.H., et al., *Bonzo/CXCR6 expression defines type 1-polarized T-cell subsets with extralymphoid tissue homing potential.* J Clin Invest, 2001. **107**(5): p. 595-601.
388. Slanina, H., et al., *Role of Epidermal Growth Factor Receptor Signaling in the Interaction of Neisseria meningitidis with Endothelial Cells.* Infection and Immunity, 2014. **82**(3): p. 1243-55.

389. Wang, K., et al., *Epidermal growth factor receptor-deficient mice have delayed primary endochondral ossification because of defective osteoclast recruitment.* J Biol Chem, 2004. **279**(51): p. 53848-56.
390. Trevejo-Nunez, G., et al., *Ethanol impairs mucosal immunity against Streptococcus pneumoniae infection by disrupting interleukin 17 gene expression.* Infect Immun, 2015. **83**(5): p. 2082-8.
391. Lee, J., et al., *IL-17E, a novel proinflammatory ligand for the IL-17 receptor homolog IL-17Rh1.* J Biol Chem, 2001. **276**(2): p. 1660-4.
392. Khor, C.C., et al., *A Mal functional variant is associated with protection against invasive pneumococcal disease, bacteremia, malaria and tuberculosis.* Nat Genet, 2007. **39**(4): p. 523-8.
393. Kanakaraj, P., et al., *Defective Interleukin (IL)-18–mediated Natural Killer and T Helper Cell Type 1 Responses in IL-1 Receptor–associated Kinase (IRAK)-deficient Mice.* The Journal of Experimental Medicine, 1999. **189**(7): p. 1129-38.
394. Wesche, H., et al., *The Interleukin-1 Receptor Accessory Protein (IL-1RAcP) Is Essential for IL-1-induced Activation of Interleukin-1 Receptor-associated Kinase (IRAK) and Stress-activated Protein Kinases (SAP Kinases)*.* The Journal of Biological Chemistry, 1997. **272**(12): p. 7727-31.
395. Akira, S., T. Taga, and T. Kishimoto, *Cytokine Signal Transduction.* Cell, 1994. **76**: p. 253-62.
396. Stolp, H.B., et al., *Immune responses at brain barriers and implications for brain development and neurological function in later life.* Front Integr Neurosci, 2013. **7**: p. 61.
397. Taniguchi, K., et al., *A gp130-Src-YAP module links inflammation to epithelial regeneration.* Nature, 2015. **519**(7541): p. 57-62.
398. Bachmaier, K., et al., *E3 ubiquitin ligase Cblb regulates the acute inflammatory response underlying lung injury.* Nat Med, 2007. **13**(8): p. 920-6.
399. Sturner, K.H., et al., *A multiple sclerosis-associated variant of CBLB links genetic risk with type I IFN function.* J Immunol, 2014. **193**(9): p. 4439-47.
400. Saijo, K., et al., *Essential role of Src-family protein tyrosine kinases in NF-kappaB activation during B cell development.* Nat Immunol, 2003. **4**(3): p. 274-9.
401. Eswaran, J., et al., *UnPAKing the class differences among p21-activated kinases.* Trends Biochem Sci, 2008. **33**(8): p. 394-403.
402. Dan, C., et al., *PAK5, a New Brain-Specific Kinase, Promotes Neurite Outgrowth in N1E-115 Cells.* Molecular and Cellular Biology, 2002. **22**(2): p. 567-577.
403. Bustelo, R.X. and N. Movilla, *Biological and Regulatory Properties of Vav-3, a New Member of the Vav Family of Oncoproteins.* Molecular and Cellular Biology, 1999: p. 7870-85.
404. Uen, Y.H., et al., *VAV3 oncogene expression in colorectal cancer: clinical aspects and functional characterization.* Sci Rep, 2015. **5**: p. 9360.
405. Dai, S., et al., *The structure of HLA-DR52c: comparison to other HLA-DRB3 alleles.* Proc Natl Acad Sci U S A, 2008. **105**(33): p. 11893-7.
406. Eckels, D.D., et al., *SB-restricted presentation of influenza and herpes simplex virus antigens to human T-lymphocyte clones.* Nature, 1983. **301**: p. 716-18.
407. Choi, J., et al., *T lymphocyte-endothelial cell interactions.* Annu Rev Immunol, 2004. **22**: p. 683-709.

408. Kotb, M., et al., *An immunogenetic and molecular basis for differences in outcomes of invasive group A streptococcal infections.* Nat Med, 2002. **8**(12): p. 1398-404.
409. Mai, N.T., et al., *Immunological and biochemical correlates of adjunctive dexamethasone in Vietnamese adults with bacterial meningitis.* Clin Infect Dis, 2009. **49**(9): p. 1387-92.
410. Collison, L.W., et al., *The inhibitory cytokine IL-35 contributes to regulatory T-cell function.* Nature, 2007. **450**(7169): p. 566-9.
411. Lingappa, J.R., et al., *Identifying host genetic risk factors in the context of public health surveillance for invasive pneumococcal disease.* PLoS One, 2011. **6**(8): p. e23413.
412. Oppmann, B., et al., *Novel p19 Protein Engages IL-12p40 to Form a Cytokine, IL-23, with Biological Activities Similar as Well as Distinct from IL-12.* Immunity, 2000. **13**: p. 715-25.
413. Kondo, N., et al., *RNA editing of interleukin-12 receptor b2, 2451 C-to-U (Ala 604 Val) conversion, associated with atopy.* Clinical and Experimental Allergy, 2004. **34**: p. 363-68.
414. Spring, K., et al., *Phosphorylation of DEP-1/PTPRJ on threonine 1318 regulates Src activation and endothelial cell permeability induced by vascular endothelial growt factor.* Cell Signal, 2014. **26**(6): p. 1283-93.
415. Lee, H.S. and R. Dominguez, *Regulation of Actin Cytoskeleton Dynamics in Cells.* Molecules and Cells, 2010. **29**(4): p. 311-25.
416. Hirst, R.A., et al., *Streptococcus pneumoniae deficient in pneumolysin or autolysin has reduced virulence in meningitis.* J Infect Dis, 2008. **197**(5): p. 744-51.
417. Research, O.I.f.C., E.B. Institute, and N.Y.U.M. Center, *Reactome*. 2015.
418. Arnett, E., et al., *The pore-forming toxin listeriolysin O is degraded by neutrophil metalloproteinase-8 and fails to mediate Listeria monocytogenes intracellular survival in neutrophils.* J Immunol, 2014. **192**(1): p. 234-44.
419. Hadler-Olsen, E., et al., *Regulation of matrix metalloproteinase activity in health and disease.* FEBS J, 2011. **278**(1): p. 28-45.
420. Sellner, J. and S.L. Leib, *In bacterial meningitis cortical brain damage is associated with changes in parenchymal MMP-9/TIMP-1 ratio and increased collagen type IV degradation.* Neurobiol Dis, 2006. **21**(3): p. 647-56.
421. Nagase, H., R. Visse, and G. Murphy, *Structure and function of matrix metalloproteinases and TIMPs.* Cardiovasc Res, 2006. **69**(3): p. 562-73.
422. Johansson, A., et al., *Endothelial cell signalling supports pancreatic beta cell function in the rat.* Diabetologia, 2009. **52**(11): p. 2385-94.
423. Dewi, B.E., T. Takasaki, and I. Kurane, *In vitro assessment of human endothelial cell permeability: effects of inflammatory cytokines and dengue virus infection.* J Virol Methods, 2004. **121**(2): p. 171-80.
424. Kerr, A.R., *Role of Inflammatory Mediators in Resistance and Susceptibility to Pneumococcal Infection.* Infection and Immunity, 2002. **70**(3): p. 1547-1557.
425. Schulte, W., J. Bernhagen, and R. Bucala, *Cytokines in sepsis: potent immunoregulators and potential therapeutic targets--an updated view.* Mediators Inflamm, 2013. **2013**: p. 165974.

426. Deli, M.A., *Potential use of tight junction modulators to reversibly open membranous barriers and improve drug delivery.* Biochim Biophys Acta, 2009. **1788**(4): p. 892-910.
427. Fanning, S.A., et al., *The Tight Junction Protein ZO-1 Establishes a Link between the Transmembrane Protein Occludin and the Actin Cytoskeleton.* J. Biol. Chem., 1998. **273**(45): p. 29745-53.
428. Stamatovic, M.S., F.R. Keep, and V.A. Andjelkovic, *Brain Endothelial Cell-Cell Junctions: How to "Open" the Blood Brain Barrier.* Current Neuropharmacology, 2008. **6**(3): p. 179-92.
429. Iden, S., et al., *aPKC phosphorylates JAM-A at Ser285 to promote cell contact maturation and tight junction formation.* J Cell Biol, 2012. **196**(5): p. 623-39.
430. Ebnet, K., et al., *Junctional adhesion molecule interacts with the PDZ domain-containing proteins AF-6 and ZO-1.* J Biol Chem, 2000. **275**(36): p. 27979-88.
431. Gradstedt, H., F. Iovino, and J.J. Bijlsma, *Streptococcus pneumoniae invades endothelial host cells via multiple pathways and is killed in a lysosome dependent manner.* PLoS One, 2013. **8**(6): p. e65626.
432. Kim, S.Y., S. Kennedy, and G.M. Tauber, *Toxicity of Streptococcus pneumoniae in Neurons, Astrocytes, and Microglia In Vitro.* J Infect Dis, 1995. **171**(5): p. 1363-68.
433. Blumental, S., et al., *Virulence Factors of Streptococcus pneumoniae. Comparison between African and French Invasive Isolates and Implication for Future Vaccines.* PLoS One, 2015. **10**(7): p. e0133885.
434. Fletcher, M.A., et al., *Pneumococcal empyema and complicated pneumonias: global trends in incidence, prevalence, and serotype epidemiology.* Eur J Clin Microbiol Infect Dis, 2014. **33**(6): p. 879-910.
435. Saha, S.K., et al., *Streptococcus pneumoniae serotype-2 childhood meningitis in Bangladesh: a newly recognized pneumococcal infection threat.* PLoS One, 2012. **7**(3): p. e32134.
436. Chuck, S.A. and O.B. Palsson, *Membrane Adsorption Characteristics Determine the Kinetics of Flow-Through Transductions.* Biotechnology and Bioengineering, 1996. **51**: p. 260-70.
437. Hyams, C., et al., *Effects of Streptococcus pneumoniae strain background on complement resistance.* PLoS One, 2011. **6**(10): p. e24581.
438. Fuchs, E., C. Untucht, and M. Rohde, *Capsule Contributes to Transmigration of Streptococcus pneumoniae Serotype 7F Meningitis Isolates through Complex Blood Brain Barrier Models.* Journal of Bacteriology & Parasitology, 2014. **03**(04).
439. Iovino, F., et al., *Interactions between blood-borne Streptococcus pneumoniae and the blood-brain barrier preceding meningitis.* PLoS One, 2013. **8**(7): p. e68408.
440. Paton, J.C., A.R. Lock, and D. Hansman, *Effect of Immunization with Pneumolysin on Survival Time of Mice Challenged with Streptococcus Pneumoniae.* Infect Immun, 1983. **40**(2): p. 548-552.
441. Witzenrath, M., et al., *The NLRP3 inflammasome is differentially activated by pneumolysin variants and contributes to host defense in pneumococcal pneumonia.* J Immunol, 2011. **187**(1): p. 434-40.

442. Rubins, J.B., et al., *Dual function of pneumolysin in the early pathogenesis of murine pneumococcal pneumonia.* J Clin Invest, 1995. **95**(1): p. 142-50.
443. Kirkham, L.A., et al., *Identification of invasive serotype 1 pneumococcal isolates that express nonhemolytic pneumolysin.* J Clin Microbiol, 2006. **44**(1): p. 151-9.
444. Østergaard, C., et al., *Inhibition of Leukocyte Entry into the Brain by the Selectin Blocker Fucoidin Decreases Interleukin-1 (IL-1) Levels but Increases IL-8 Levels in Cerebrospinal Fluid during Experimental Pneumococcal Meningitis in Rabbits.* Infection and Immunity, 2000. **68**(6): p. 3153-57.
445. Garnier, F., et al., *Insertion sequence 1515 in the ply gene of a type 1 clinical isolate of Streptococcus pneumoniae abolishes pneumolysin expression.* J Clin Microbiol, 2007. **45**(7): p. 2296-7.
446. Jedrzejas, M.J., *Pneumococcal virulence factors: structure and function.* Microbiol Mol Biol Rev, 2001. **65**(2): p. 187-207 ; first page, table of contents.
447. Krivan, H., D.D. Roberts, and V. Ginsburg, *Many pulmonary pathogenic bacteria bind specifically to the carbohydrate sequence GalNAc,81-4Gal found in some glycolipids.* Proc Natl Acad Sci U S A, 1988. **85**: p. 6157-61.
448. Banerjee, A., et al., *Activation of brain endothelium by pneumococcal neuraminidase NanA promotes bacterial internalization.* Cell Microbiol, 2010. **12**(11): p. 1576-88.
449. Rukke, H.V., et al., *Capsule expression in Streptococcus mitis modulates interaction with oral keratinocytes and alters susceptibility to human antimicrobial peptides.* Mol Oral Microbiol, 2015.
450. Pasti, L., et al., *Intracellular Calcium Oscillations in Astrocytes: A Highly Plastic, Bidirectional Form of Communication between Neurons and Astrocytes In Situ.* The Journal of Neuroscience, 1997. **17**(20): p. 7817-30.
451. Braet, K., et al., *Calcium signal communication in the central nervous system.* Biol Cell, 2004. **96**(1): p. 79-91.
452. Leybaert, L., *Neurobarrier coupling in the brain: a partner of neurovascular and neurometabolic coupling?* J Cereb Blood Flow Metab, 2005. **25**(1): p. 2-16.
453. Wolfmeier, H., et al., *Ca(2)(+)-dependent repair of pneumolysin pores: A new paradigm for host cellular defense against bacterial pore-forming toxins.* Biochim Biophys Acta, 2015. **1853**(9): p. 2045-54.
454. Gross, J. and M.C. Lapiere, *COLLAGENOLYTIC ACTIVITY IN AMPHIBIAN TISSUES: A TISSUE CULTURE ASSAY.* PNAS, 1962. **48**(6): p. 1014-22.
455. Lu, P., et al., *Extracellular matrix degradation and remodeling in development and disease.* Cold Spring Harb Perspect Biol, 2011. **3**(12).
456. Khokha, R., A. Murthy, and A. Weiss, *Metalloproteinases and their natural inhibitors in inflammation and immunity.* Nat Rev Immunol, 2013. **13**(9): p. 649-65.
457. Hunter, C.A. and S.A. Jones, *IL-6 as a keystone cytokine in health and disease.* Nat Immunol, 2015. **16**(5): p. 448-57.
458. Ertel, W., et al., *Downregulation of Proinflammatory Cytokine Release in Whole Blood From Septic Patients.* The American Society of Hematology, 1995. **85**(5): p. 1341-47.
459. Mohler, J., et al., *Streptococcus pneumoniae strain-dependent lung inflammatory responses in a murine model of pneumococcal pneumonia.* Intensive Care Med, 2003. **29**(5): p. 808-16.

460. Vogel, C. and M.E. Marcotte, *Insights into the regulation of protein abundance from proteomic and transcriptomic analyses.* Nat Rev Gen, 2012. **13**: p. 227-32.
461. Rantala, A., et al., *Association of IL-6 and IL-6R gene polymorphisms with susceptibility to respiratory tract infections in young Finnish men.* Hum Immunol, 2011. **72**(1): p. 63-8.
462. Østergaard, C., et al., *Treatment with a monoclonal antibody to IL-8 attenuates the pleocytosis in experimental pneumococcal meningitis in rabbits when given intravenously, but not intracisternally.* Clinical and Experimental Immunology, 2000. **122**: p. 207-11.
463. Jaramillo, B.E., et al., *Characterization of the tight junction protein ZO-2 localized at the nucleus of epithelial cells.* Exp Cell Res, 2004. **297**(1): p. 247-58.